5-2021

Synthesis, Characterization, and Applications of Nucleobase-Functionalized Conjugated Polymers

Sina Sabury
University of Tennessee, Knoxville, ssabury@vols.utk.edu

To the Graduate Council:

I am submitting herewith a dissertation written by Sina Sabury entitled "Synthesis, Characterization, and Applications of Nucleobase-Functionalized Conjugated Polymers." I have examined the final electronic copy of this dissertation for form and content and recommend that it be accepted in partial fulfillment of the requirements for the degree of Doctor of Philosophy, with a major in Chemistry.

Michael Kilbey, Major Professor

We have read this dissertation and recommend its acceptance:

Brian Long, Gila Stein, John Brantley

Accepted for the Council:

Dixie L. Thompson

Vice Provost and Dean of the Graduate School

(Original signatures are on file with official student records.)

Synthesis, Characterization, and Applications of Nucleobase-Functionalized Conjugated Polymers

A Dissertation Presented for the

Doctor of Philosophy

Degree

The University of Tennessee, Knoxville

Sina Sabury

May 2021

This dissertation is dedicated to my parents, Zhila Rezadoust and Reza Sabury, and to my wife Reyhaneh.

"Sell your cleverness and buy bewilderment. Cleverness is mere opinion. Bewilderment brings intuitive knowledge."

Rumi

Acknowledgments

First, I would like to thank my advisor, Prof. S. Michael Kilbey II, for his for his guidance, inspiration, and unwavering support. I am honored to have had the chance to grow as scientist under his mentorship and learn by following his example of professionalism. I will be forever grateful for the opportunity I had to work in "the Kilbey group". Dr. Kilbey exemplifies clear and concise communication and has taught me its value. He has guided me to improve my communication skills with patience, steady effort, and constant support. His astounding management style has fostered lasting friendships with my group colleagues. His well-balanced commitment to family and work created healthy environment that nurtured my growth and enabled me to overcome problems, both technical and personal. I had to be away from my family for a long time, and without his support I could not have finished my studies. In addition to being my adviser, I am blessed to have him as a friend.

I would like to express my appreciation to my soulmate, best friend, and loving wife, Reyhaneh. Her constant support throughout my graduate studies were essential to my success, as was her deep understanding when I had to be away through the efforts associated with graduate school. I appreciate her sacrifice – it allowed me to achieve my academic and career goals. I would also like to thank my parents. I would not be the person I am today without their guidance and encouragement.

I would also like to acknowledge the contributions of my committee members, Dr. Brian Long, Dr. Gila Stein, and Dr. Johnathan Brantley. I thank all of you for your guidance through my graduate school journey that involved the candidacy research proposal, original research proposal, and classes that helped me become a research scientist.

I would like to thank my collaborators. Dr. Michael Walter, Tyler Adams, and Margaret Kocherga from the University of North Carolina – Charlotte, who helped with fabrication

and characterization of field effect transistor devices. Dr. Ben LaRiviere and Dr. Nance Ericson from Oak Ridge National Laboratory also provided constructive feedback on device fabrication and interpretation of data related to printed electronic devices.

I would like to acknowledge numerous people who aided me throughout my career. I especially thank Dayton Street, Graham Collier, and Zach Seibers. With my background in polymer engineering, I learned a lot of organic chemistry techniques from Graham, who patiently trained me to be a better chemist and was my second mentor, and Zach Seibers, who helped me set up my first polymerization reaction. I would like to thank Dayton Street who inspired me with his enthusiasm about science, helped me adapt to the culture of East Tennessee, and guided me with many constructive comments.

I am also thankful for all of the current and former members of the Kilbey research group at the University of Tennessee, including Dayton, Graham, and Zach, and also Bethany Aden, Jesse Davis, Kamlesh Bornani, Elizabeth O'Connell, Will Ledford, Nia Parker, Dani Chun, Bishal Upadhyay, Natalie Czarnecki, Rachel Ramirez, Evan Boone, Samantha Cahill, and Abigail Allison. I appreciate all of our friendships and I wish the best for each of you in your future endeavors.

Abstract

Understanding the effect of the functional groups at the terminus of the side chains is important for developing conjugated polymers through side chain engineering. Nucleobases, which are known for their multi-functionality, have not been deeply studied as functionality in conjugated polymers due to synthetic challenges. The overarching goal of my dissertation is to design, synthesize, characterize conjugated polymers bearing nucleobase functionality in their side chains and demonstrate their utility in various applications. Stille cross-coupling and direct arylation polymerization are used to synthesize adenine- and thymine-containing conjugated polymers. Monomer design requirements for successful polymerization are studied and conditions that optimize polymerization are identified. Structural, thermal, and photophysical properties of nucleobase-functionalized polymers are studied and compared to non-functionalized homologs to assess the impact of nucleobase functionality. In addition to establishing design-structure-property relationships for these polymers, the ability of nucleobases to chelate metal ions and hydrogen bond were examined. My work highlights that nucleobases in the side chains can help to control thin film properties such as packing, which impacts transport properties, and responsive behaviors and surface assembly. This work shows that the properties of conjugated polymers can be improved and their applicability can be expanded through molecular design that utilizes the functionality and specificity of nucleobases. These outcomes are achieved through careful monomer design and optimization of polymerization conditions.

Table of Contents

List of Tables

List of Figures

xvii

List of Schemes

Chapter 1

Introduction

1.1 Conjugated Polymers: From Discovery to Applications

The field of conjugated polymers, sparked from the discovery of (semi)conductivity of polyacetylene in 1977, has rapidly expanded through many fundamental and applied studies.[1–3] Initially, the structure of conjugated polymers was not well understood because their insolubility made characterization difficult.[3] Later developments in material characterization and synthetic methods provided a better understanding of the chemical structure of conjugated polymers. The delocalized π-molecular orbitals in the structure of conjugated polymers (CPs) give rise to interesting optical and electrical properties compared to conjugated small molecules. The extension of orbital overlap in the electronic structure of the polymer increases the conjugation length and narrows the bandgap between the highest-occupied molecular orbital (HOMO) and the lowest-unoccupied molecular orbital (LUMO). Like many polymer properties, the bandgap of CPs depends on molecular weight, decreasing as more monomeric units are added until it plateaus at moderate molecular weight.[4–6] (See Figure 1.1.) These electrons are delocalized along the backbone, and when photons with enough energy are absorbed, electrons are excited from the HOMO. This excited state may relax by emitting light, and non-radiative relaxations are also possible. Conjugated polymers can also participate in oxidation-reduction processes.[7–9]

In general, polymers benefit from low-cost, scalable solution processing, but this is typically not the case with CPs, which often have low solubility due to their rigid, aromatic structure. These issues with solubility and processability have been addressed by the introduction of solubilizing side chains along the conjugated backbone. This has resulted in the development of the solution processable CPs such as poly(3-alkylthiophene)s and poly(p-phenylene vinylene) derivatives. These CPs with solubilizing side chain are categorized as the "second generation" CPs, and a better understanding of the properties of CPs was gained as a result of the development of these soluble polymers.[10, 11] The next generation of CPs evolved from more complex (hetero)aromatic structures, such as fused ring structures incorporated in the backbone and alternating copolymer designs known as donor-acceptor copolymers. The donor-acceptor concept is known to enable greater control over the bandgap
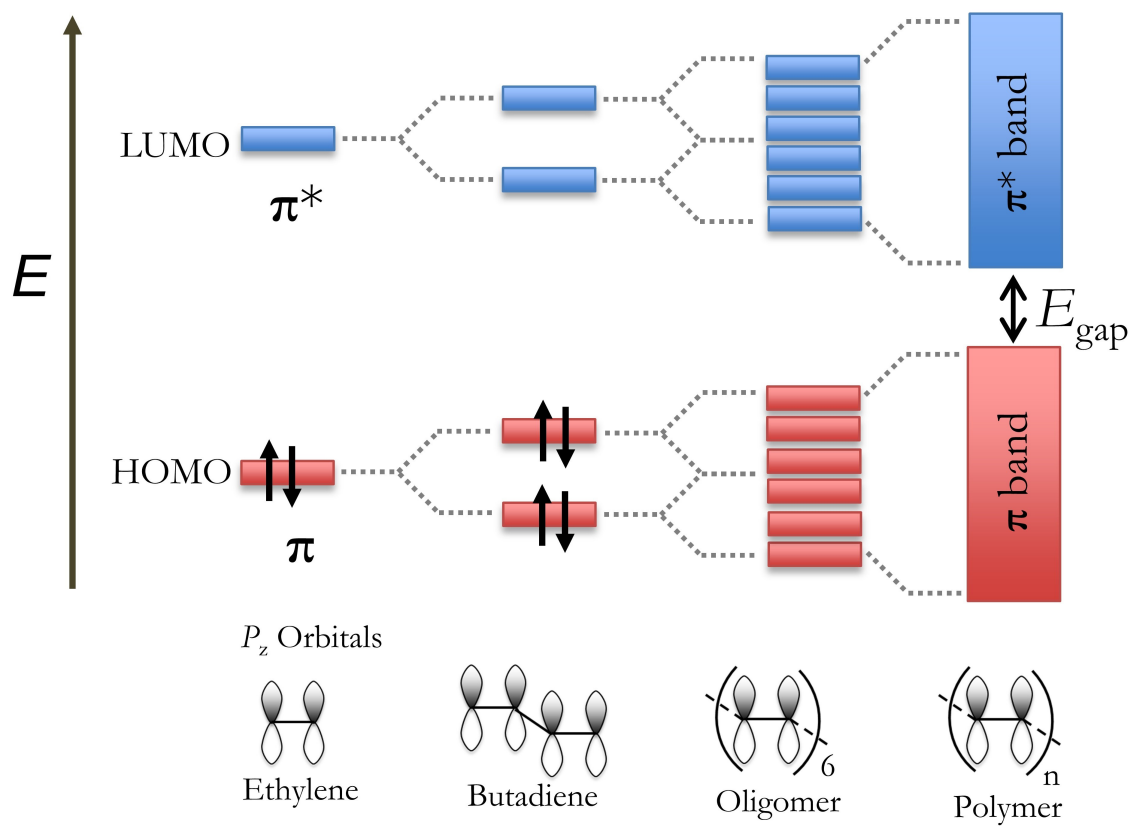
Figure 1.1: Bandgap narrowing by extension of delocalized conjugation length in oligomers and polymers.

of the CP, which also tunes the optical absorbance of the copolymer.[12] Researchers continue to synthesize and study diverse types of CPs, finding additional opportunities to manipulate their bandgap, absorption and emission profiles, solubilities, and stability in air, while also improving processability.[13] As a result of the inherently delocalized electronic structure and the ability to fine-tune their chemical structure and electronic properties, CPs have been utilized in many applications such as bulk heterojunction solar cells,[14–16] perovskite solar cells,[17–19] organic light emitting diode (OLED) devices,[20–22] field effect transistors (FETs),[23–25] supercapacitors,[26, 27], conductive thin film electrodes,[28] water-splitting systems,[29, 30] organic thermoelectrics,[31, 32] wearable sensors,[33, 34] electrochromic glasses,[35, 36] optical sensors,[37, 38] cell imaging,[39, 40] trackable drug delivery,[41, 42] photothermal therapy,[43, 44] tissue engineering,[45, 46] organic dye degradation,[47, 48] and anticorrosion coatings.[49, 50] In most of these applications, the organization in the solid state at different length scales plays an important role governing properties and functionality. Therefore, many works are dedicated to optimizing solid state order for a particular application.

In addition to early efforts focused on the tuning the conjugated backbone, side chain engineering has been utilized recently for purposes beyond improving solubility and processability.[51] Branched alkyl side chains were one of the first structural alterations to the linear alkyl chains that were explored. For instance, Pei and coworkers showed that the branch position in the side chain drastically affected transport properties of conjugated polymer due to changes in the π-stacking and efficiency of main chain packing.[52] In addition to branching, several different side chains, such as fluoroalkyl and ionic groups, have been developed. These improve the properties or expand the scope of conjugated polymers. Approaches and benefits of side chain engineering are discussed in greater detail in the following section.

1.2   Side Chain Engineering in CPs

As mentioned in the previous section, side chains were first introduced to enhance solubility, but they also impact structural organization and properties. Thus, side chain engineering

has been a widely used approach to improve the properties of CPs.[51, 53] For example, the length of simple alkyl chains have a profound effect on crystallization process.[54, 55] This was shown by Causin *et al*, who produced a set of regioregular poly(3-alkylthiophene)s having either butyl, octyl, and dodecyl side chains, yielding poly(3-butylthiophene) (P3BT), poly(3-octylthiophene) (P3OT), and poly(3-dodecylthiophene) (P3DDT), respectively. The melting temperatures ranged from 175 °C for P3DDT to 321 °C for P3BT, which shows the impact of side chain length on crystallization.[54] As an another example of how variation in alkyl side chains impacts behavior, a combination of linear and branched side chains on a naphthalene diimide (NDI) backbone were found to tune the aggregation behavior in solution and packing order in the solid state. Ma *et al.* showed that better packing, controlled by side chain structure, boosted the charge transport properties in a n-type field-effect transistor (FET).[56] Alkoxy side chains, alkyl chains with an ether connection to the backbone, also have been utilized, and their impact also extends beyond simply improving solubility. Alkoxy groups enhance electron donicity, which raises HOMO energy levels without significantly affecting LUMO levels. Thus, they tend to reduce the bandgap. The ether oxygens of alkoxy group also participate in dipolar intramolecular interactions, which tend to increase the planarity of the backbone.[57–59] Oligoether (OE) side chains have also been shown to stabilize the morphology and improve the charge transfer character in OPVs, hydrogen evolution cells, and thermoelectric devices.[60–63] Figure 1.2 shows the design of these basic side chain designs.

Terminally-functionalized side chains are another class of side chains that are widely used in side chain engineering approaches. The functional groups are far enough away from the conjugated backbone to eliminate any direct effect on the bandgap. As a result, the group at the end of side chains typically contributes indirectly to the performance by controlling film morphology and packing order.[51] For example, Swager and coworkers created a series of poly(alkylthiophene)s with polar groups at the terminus of the side chains, and used these as the third component in the active layer of a bulk heterojunction solar cells consisting of a mixture of P3HT and PCBM (donor and acceptor). They showed that a small amount (0.25 wt%) of these side chain functionalized additives increased the power conversion efficiency (PCE) of the ternary blend by ≈ 30%. They hypothesized that the side chain
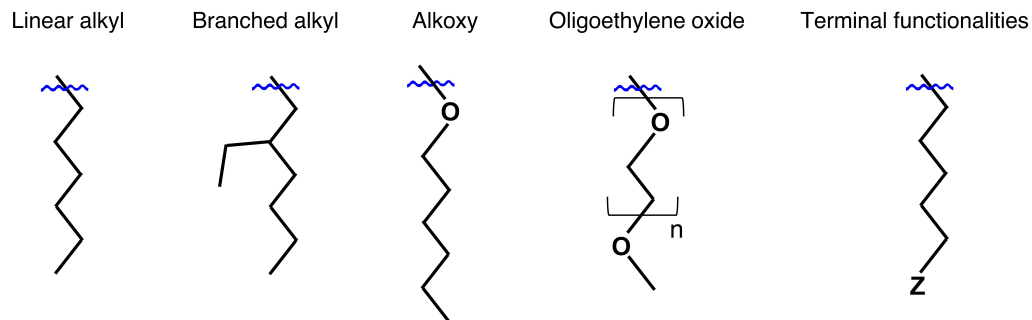
Figure 1.2: Examples of types of side chains frequently used to improve the properties of conjugated polymers.

- ✓ Hydrogen Bonding
- ✓ π-π Stacking
- ✓ Metal-Binding
- ✓ PH responsive
- ✓ High dipole moment
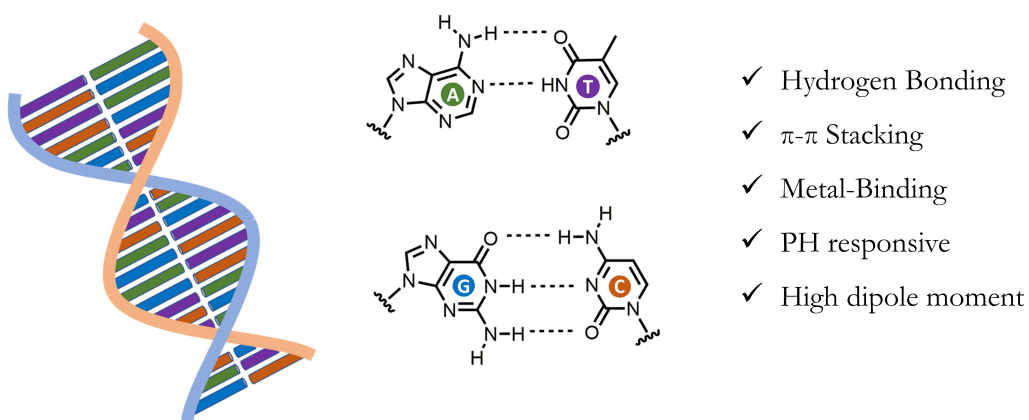
Figure 1.3: Structure and properties of the four primary nucleobases. The specific and directional hydrogen bonding to create complementary base-pairs of adenine-thymine (A···T) and guanine-cytosine (G···C) are also shown.
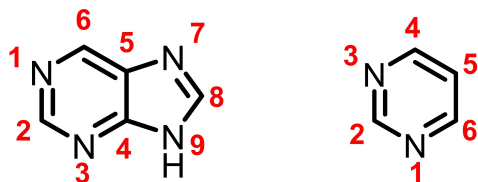
Figure 1.4: Numbering of purine (left) and pyrimidine (right) rings.

functionalized poly(alkylthiophene)s migrated to donor/acceptor interfaces and improved exciton dissociation due to the polar nature of the pendant groups.[64] Bazan and his group incorporated ionic groups at the terminus of side chains to obtain water-soluble conjugated polymers, and demonstrated that these CPs are capable of detecting DNA based on the fluorescence emission of the conjugated backbone.[37, 65, 66] These studies highlight the capability of side chain engineering to improve the properties of CPs in devices, as well as to expand their usage to novel applications. This potential of end-functional side chains to bring new functionality to CPs inspired and motivated my dissertation research.

1.3 Nucleobase Functional Groups

Nucleobases are nitrogen-containing heterocycles that are known to be an essential part of the machinery of life. They also have a unique set of properties such as high dipole moments, specific and directional hydrogen bonding, π-π stacking, and metal ion chelation.[67] (See Figure 1.3.) There are five primary nucleobases—adenine, cytosine, guanine, thymine, and uracil—that form the nucleotides that create the helical structure of deoxyribose nucleic acid (DNA) and ribonucleic acid (RNA). Adenine and guanine are fused ring molecules that belong to the class known as purines, and cytosine, thymine, and uracil are pyrimidines. (See Figure 1.4.) The hydrogen-bonded base pairs, for example the Watson–Crick adenine-thymine base pair, are essential for replication or transcription of DNA.[68] The self-replicating properties of nucleobase-containing compounds are the basis of the hypothesis that interactions of nucleobases and amino acids led to the origination of life.[69] Nucleobases and their derivatives have been extensively used and studied in medical science. For example, they have been used to design and generate anticancer and antiviral agents.[70–74] Nucleobase analogues (synthetic non-canonical nucleobases) have been utilized as fluorescent probes for DNA detection or as a basis for determining the sequence of biomacromolecules such as DNA and RNA.[75]

These and many other efforts to exploit the properties of nucleobases have inspired material scientists to explore nucleobases as biocompatible ligands, water dispersible supramolecular agents, and morphology regulators in a variety of applications.[76] For

example, to take advantage of their hydrogen bonding capability, nucleobases have been added to the structure of phospholipids. These molecules can self-assemble to form bilayer structures in aqueous solution, which enables them to transport drugs, enter tumor cells, and release the loaded drug in a controlled fashion in response to the acidic intracellular environment.[77]

The π–π interaction between nucleobases, which stems from their conjugated structure, promotes stacking of the bases and adds stability to the helical structure of the DNA.[78] Researchers have shown that the strong π–π stacking of adenine and guanine can trigger the formation of a helical structures and chirality transfer.[79] Also, the π–π interaction between nucleobases and enzymes may accelerate enzymatic reactions and promote, for example, phosphate ester hydrolysis.[80]

Nucleobases are also known for their strong and effective metal-binding character. There are several sites on nucleobases that can participate in metal binding. Particular sites include the amine at C6, N1 and N3 of pyrimidine rings, and N7 and N9 of the imidazole ring of the purines. (See Figure 1.4 for numbering of purine and pyrimidine rings.) Researchers have exploited this behavior in different ways. For example, Nishiyabu *et al.* showed that combinations of nucleotides and lanthanide ions result in coordinated polymer nanoparticles, and changing the metal ion to Ag^+ resulted in the formation of a hydrogel.[81, 82] In solvothermal synthesis of CdS nanoparticles, adenine has been used as a caping agent to control CdS nanoparticle size and stabilize these quantum dots. This is reported to occur due to a binding interaction between Cd^{2+} and N9 of the adenine ring.[83]

These small molecule behaviors have been extended to polymeric materials by the creation of polymers with nucleobases as pendant or end groups, typically in vinyl polymers.[84–86] One of the first examples was work by Long and coworkers, who incorporated thymine and adenine into the side chain of a poly(acrylate). Their thymine- and adenine-functionalized polymers demonstrated strong adhesive properties through H-bonding, which created supramolecular materials.[87] Nucleobase-containing polymers, which are inspired by nature, have also been used in the fabrication of self-healing materials because H-bonding can be disrupted as high temperature. For example, Ye and coworkers created an efficient self-healing polymeric system based on the triple hydrogen bonding between

cytosine and guanosine in a nucleobase-functionalized hyaluronic acid hydrogel.[88] Cha and coworkers studied a nucleobase-containing triblock terpolymer (poly(ethylene glycol)-*block*-nucleic acids-*block*-poly(lactic-co-glycolic acid), which is able to encapsulate and deliver DNA. They view these materials as having the potential to be utilized as a chemotherapy agent and gene silencer.[89]

These studies demonstrate that the incorporation of nucleobases in the structure of non-conjugated polymers expands their functionality and improves their performance. This also suggests that properties of CPs or their suitability in different applications are also likely to be improved when nucleobases are added to the structure of CPs. These types of materials could, for example, combine the charge transport and signaling properties of CPs with recognition properties of nucleobases. The presence of nucleobases in the side chain of conjugated polymers also might be expected to promote main chain packing through π-stacking or hydrogen bonding interactions, or help to immobilize the conjugated polymer on different surfaces. However, examples of incorporation of nucleobases into side chain of CPs are very limited due to synthetic challenges and processability issues caused by the presence of the nucleobases. The tendency of nucleobases to chelate metal species has been suggested to interfere with metal-catalyzed polymerization, which would makes the polymerization of nucleobase-containing monomers challenging.[90–92] As a result, to-date nucleobase-functionalized CPs have been obtained either by non-controlled oxidative chemical or electrochemical polymerizations, which result in low molecular weight polymers ($\approx 2.8\,\mathrm{kg/mol}$).[93] In addition, the strong hydrogen bonding and π–π stacking of nucleobases pose limitations on solution processability due to the loss of solubility.[92]

In my dissertation research, I focused on rational monomer design and polymerization optimization, which included addressing the processability issues in order to obtain a series of nucleobase-functionalized CPs. Then, I examined structure-property relationships and explored novel applications, such as oil-water separations, for those side chain functionalized CPs. I chose to study adenine-functionalized copolymers (Chapters 2, 3, 4), and thymine-functionalized copolymers (Chapter 2) as representatives of purine- and pyrimidine-type nucleobases, respectively. In the next section, I will discuss in general how the design of the nucleobase-functionalized monomer is connected to the selected polymerization method.

1.4 Monomer Design: Polymerization of Nucleobase Functionalized Monomer *vs* Post-Polymerization Functionalization

As indicated in the previous section, there are compelling reasons to produce a functional and processable nucleobase-containing polymers. Two main approaches are generally used to prepare functionalized polymers. These are polymerization of the functionalized monomer and post-polymerization functionalization. Each method has its advantages and requires different synthetic methodologies. In thinking about the synthesis of nucleobase-functionalized CPs, polymerization of a nucleobase-functionalized monomer will result in a higher functionalization density, but the polymerization might be more complicated due to undesired interactions of the nucleobase with catalyst or decreased solubility of the growing chain. The post-polymerization functionalization route requires a monomer with a synthetically addressable site that is inactive during polymerization. This approach usually results in incomplete functionalization, although the polymerization might be easier to conduct. A specific issue with nucleobases that may occure in post-polymrization functionalization is that nucleobases have multiple sites that are reactive. As a result, they may be connected to the conjugated main chain from different sites, leading to a mixture of structural isomers. This is less of a problem if the monomer is functionalized before polymerization because the isomers can be separated and purified. However in the case of post-polymerization functionalization, isomeric connections are inherently imbedded throughout the polymer chain. This is evident, for example, in the alkylation of adenine, shown in Figure 1.5. The alkylation of adenine can occur at N7 or N9 positions and two alkylated isomers will be obtained, with the N9 isomer being the major product.[94] (See Figure 1.5a.) These monomeric isomers having adenine functionality can be isolated and purified using column chromatography, which is suggested in Figure 1.5b. This is not possible if post-polymerization modification is used, as shown in Figure 1.5c. Based on this background, I chose to polymerize nucleobase-functionalized monomers in order to have structural control of side chain functionality on the repeating units, which avoids

complications due to isomerization. However, as will be described in various chapters of this dissertation, specific care is required to circumvent unwanted interactions between nucleobases and the catalyst.

1.4.1 Monomer Design: Nucleobase-Catalyst Interactions

Nucleobase-catalyst interactions should be considered with care for a successful polymerization because nucleobases can easily interact with metal species, potentially deactivating the catalyst used in the polymerization. For example, nucleobases are known to interfere with metal-mediated radical polymerizations. Specifically, polymerization of a cytosine-containing methacrylate monomer by atom transfer radical polymerization (ATRP) using 2,2'-bipyridine (bpy) as the ligand and ethyl 2-bromoisobutyrate (EBiB) as the initiator was not successful, and the authors attributed this to complex formation involving cytosine and the copper catalyst.[95] My results show evidence that nucleobases in side chain interfere with the catalyst in direct arylation polymerization (DArP), but they appear to not prevent chain growth by Stille polymerization. (These polymerization methods are elaborated in the following section.) Specifically, strong chelation of palladium appears to deactivate the catalyst used in DArP. I will discuss how I tested this hypothesis of deactivation of the DArP catalyst due to interactions with adenine in Chapter 3. We will also discuss how the use of a bulky protecting group enables a successful DArP. Although this requires post-polymerization removal of protecting groups in order to revive the chelating and hydrogen binding properties of the attached nucleobase, I successfully streamlined the polymerization by developing a one-pot polymerization-deprotection. This is discussed in Chapter 4. To provide a basis for research described later in this dissertation, in the next section I will briefly outline the history of CP synthesis and then discuss in detail the specific polymerization methods that were used in this dissertation research.
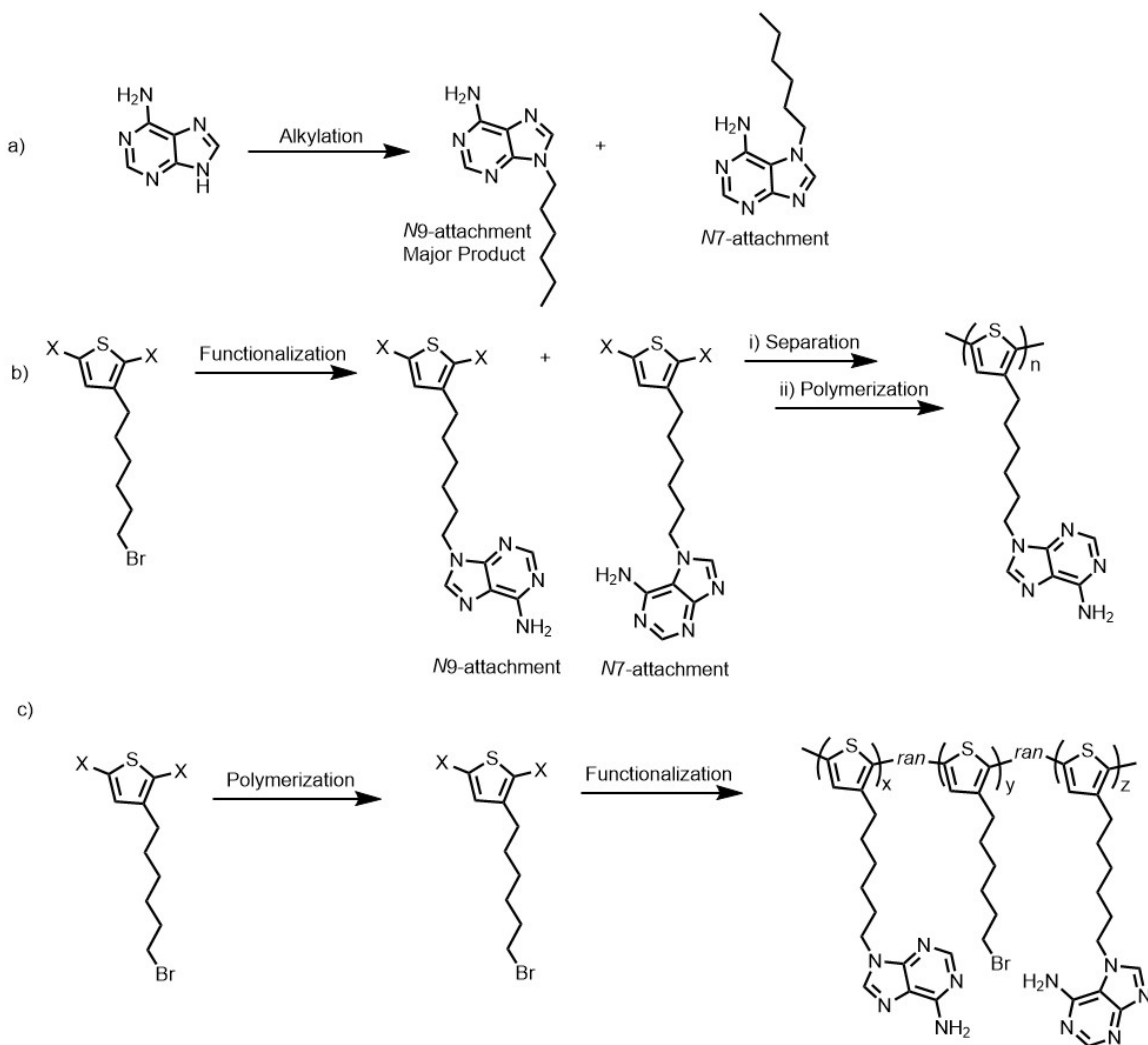
Figure 1.5: a) Structural isomers resulting from alkylation of adenine and comparison of b) polymerization of purified monomers where structural isomers were first separated and c) post-polymerization functionalization showing structural isomers due to N7 and N9 reactivity.

1.5 Key Polymerization Methods for Synthesis of Nucleobase-Functionalized CPs

Since the accidental synthesis of polyacetylene in the 1970s, which led to the discovery of CPs, researchers have tried to improve the synthesis of conjugated polymers.[1, 14] For example, oxidative chemical polymerization was introduced in 1984 by Sugimoto. This method, which uses ferric chloride ($FeCl_3$) as an oxidation agent, was widely used to prepare conjugated polymers of thiophene and pyrrole, for example.[96] Despite the simplicity, this method does not offer control over regioregularity, which is the ratio of head-to-tail (HT) couplings to all possible couplings, including head-to-head (HH) and tail-to-tail (TT) couplings, or molecular wight of the resulting polymer.[97] Also, an excess amount of $FeCl_3$ (> 1 equiv.) is necessary for the polymerization, which results in considerable amount of metal ions being left in the product, even after several purifications.[98] As a result, oxidative polymerization is not commonly used, as other synthetic methods that are mainly inspired by small molecule coupling reactions, have gained importance. These typically enable control over structural features and allow high molecular weight to be reached reproducibly. For instance, polycondensation based on Stille cross-coupling has been used to obtain various CPs, and this method is compatible with a wide variety of monomers. Stille polycondensations, which gained popularity in the mid 90's, are less air-sensitive than other CP synthesis methods, such as Grignard metathesis polymerization. Thus, these step-growth polymerizations are easier to handle for larger scale productions.[99, 100] Figure 1.6 shows the various types of polycondensations based on the general structure of monomers needed for each type of polymerization. In my research, I used Stille cross-coupling polymerization, and direct arylation and each will be discussed in greater detail.

Stille polymerization creates a new C-C bond through reaction of an aromatic bromide bond, $C(sp^2)$-Br, with an aryl stannane, $C(sp^2)$-SnR_3, through a palladium (Pd) catalyzed reaction cycle. Stille cross-coupling polymerization has become a widely used polymerization method for synthesizing CPs that are used in organic photovoltaics (OPVs), organic light emitting diodes (OLEDs), and organic field effect transistors (OFETs).[101–105] Organostannanes and aromatic halide electrophiles are complementary functional groups,
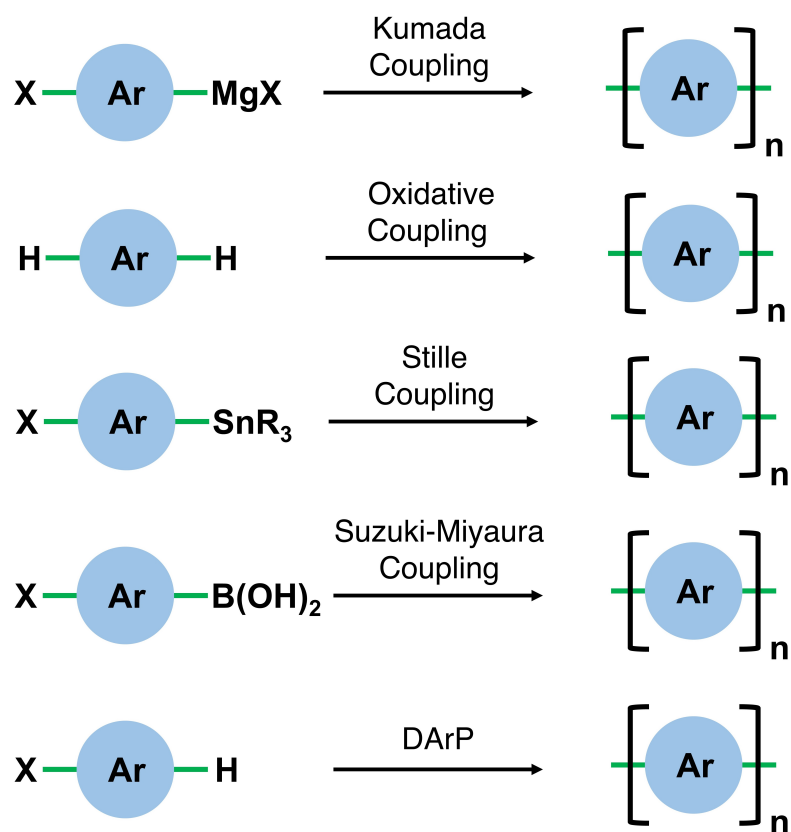
Figure 1.6: Overview of monomer designs used in AB-type polycondensation to create CPs. X represents halide functionality.

and these can be used in AB or AA+BB polycondensations, forming a new C-C bond through Stille coupling. The active catalyst is believed to be $PdL_2(0)$ (L: ligand) where the palladium is either directly added as a Pd(0) compound or generated from a Pd(II) precursor that is reduced to Pd(0) by reaction with the solvent or phosphine ligands before entering the catalytic cycle.[106–111] The catalytic cycle of an aromatic Stille coupling starts with the oxidative addition of the active catalyst to the aromatic halide, Ar1–X, to form $Ar1PdL_2X$. Then, a transmetalation with the organostannane agent, $Ar2SnR_3$, will produce $Ar1PdL_2Ar2$. At the end, a reductive elimination step results in the coupled product Ar1-Ar2 and regenerates PdL_2 active species. The accepted catalyst cycle for Stille cross-coupling is depicted in Scheme 1.1.

Despite the excellent functional group tolerance and oxygen and moisture stability of organostannanes compared to other organometallics (such as Grignard reagents), there are some challenges that have motivated researchers to find an alternative synthetic method. One of the biggest challenges for Stille condensation is the toxicity of the organotin reagents, which are used for preparation of the monomers and produced in stoichiometric proportion as a side product during the polymerization. The organotin impurities remaining in the resulting polymer can prevent it from being used in bio-related applications. These safety and environmental concerns over heavy metal species has motivated efforts to study the possibility of directly coupling aromatic hydrogens, $C(sp^2)$-H, instead of activating those bonds by replacing the aromatic carbon-hydrogen bond, $C(sp^2)$-H, with a carbon-metal bond, $C(sp^2)$-M. Activation of C-H bonds through metalation has been an integral part of many of coupling reactions, such as Stille, Kumada, Suzuki, and Negishi couplings. Small molecule studies suggest that the (hetero)aromatic hydrogens, $C(sp^2)$-H, can directly be activated through metal catalyzed reactions. These C-H activations are called direct arylation since the intermediate metalation step is skipped. The direct arylation concept has been applied to the synthesis of conjugated polymers, and the synthetic method is referred to as direct arylation polymerization or "DArP".

Direct arylation polymerization is considered as an environmentally friendly, atom efficient, scalable, and cost-effective alternative synthetic method. Even though direct aryl-aryl coupling in small molecules has been known for a long time,[112, 113] the first report of
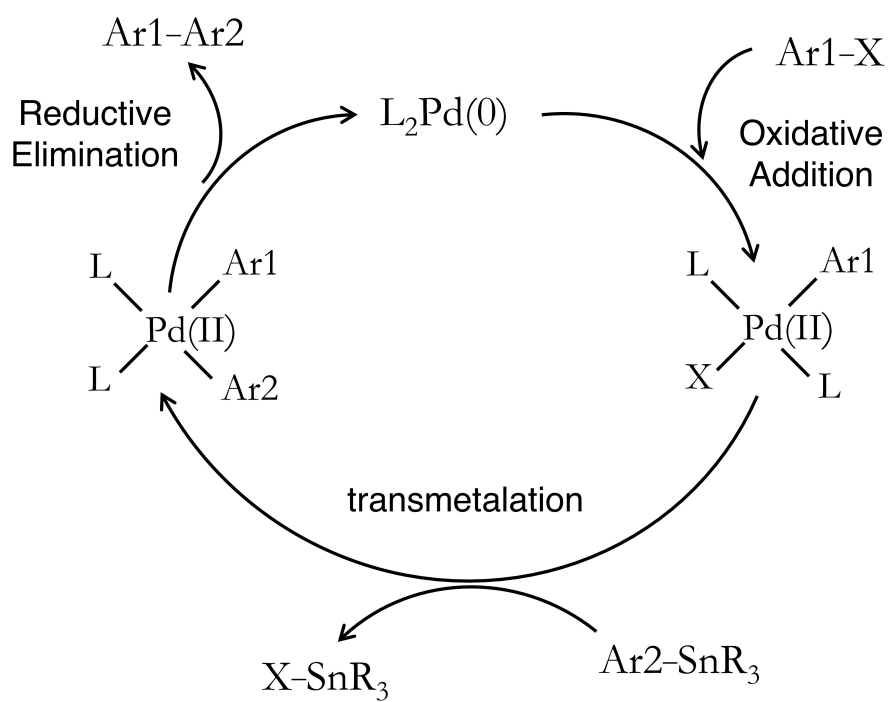
Scheme 1.1: The catalytic cycle for Stille cross-coupling reactions.

direct arylation polymerization was published by Lemaire and coworkers in 1999.[114] Almost a decade after that, Ozawa identified optimal conditions for a highly efficient and regioregular DArP synthesis of poly(alkylthiophene)s, which has sparked and attracted much attention from researchers.[115] Concerted metalation–deprotonation (CMD) is believed to accurately describe aspects of DArP mechanism. The catalyst cycle starts with oxidative addition of the aromatic halide bond to the Pd(0) catalyst, similar to most palladium-catalyzed couplings. Then, a carboxylate anion replaces the halide ligand. Through a six-membered transition state in the CMD step, the carboxylate group deprotonates the incoming aryl C-H while the Pd-carbon bond is simultaneously formed. The final coupled product is formed by the reductive elimination step.[116–119] Scheme 1.2 depicts the proposed catalyst cycle. Many efforts have focused on optimizing reaction conditions, including monomer concentration, solvent, temperature, ligand, and the carboxylic acid additive, which has expanded the scope of monomers suitable for DArP.[120, 121]

Both the Stille cross-couplings and direct arylation polymerizations are considered to be step-growth polymerizations in which a bifunctional (AB) monomer or a complementary set of difunctional monomers (AA+BB) can be used to create chains. The number-average degree of polymerization, or the average number of repeating units in a polymer molecule, $\overline{X}_n$, is related to the monomer conversion, p, through Carothers' equation, which describes step-growth polymerizations. For step-growth polymerizations performed using perfect stoichiometric balance ($r = [A]/[B] = 1$), the Carothers' equation is shown in Equation 1.2:

$$\overline{X}_n = \frac{1}{1-p} \tag{1.1}$$

In most cases, higher molecular weight polymers are preferred so that the polymers are above their effective conjugation length and mechanical robustness is obtained. Based on the nature of the step-growth polymerization and evident by Equation 1.2, a high conversion (usually above 97%) is required to obtain a high molecular weight polymer. Stoichiometric balance and purity of monomers are also important to obtain high molecular weight polymers
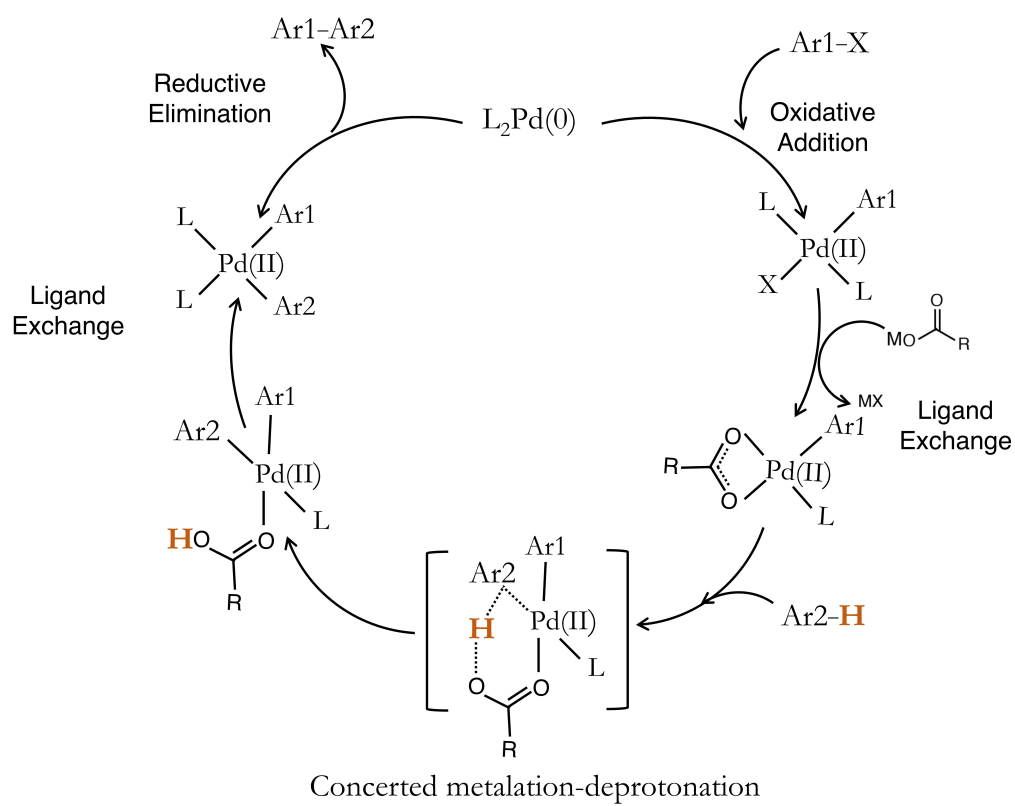
Scheme 1.2: The catalytic cycle proposed for direct arylation coupling reactions.

in step-growth polymerization. Stoichiometric excess or imbalance will reduce the ultimate number-average degree of polymerization, shown in the revised Carothers' equation:

$$\overline{X}_n = \frac{1+r}{1+r-2rp} \tag{1.2}$$

In this equation, r is the stoichiometric ratio of reactants, and it is defined in a way so that the excess reactant is in the denominator so $r \leqslant 1$. High molecular weight polymers are difficult to obtain when there is stoichiometric imbalance or impurities, as shown in Figure 1.7.

1.6 Characterizations of Nucleobase-Functionalized CPs

In the following sections, I will describe characterization methods we chose to confirm small molecule and polymer synthesis. Then, methods for structural, thermal, and photophysical analyses of the synthesized polymers are discussed. The structure of monomers and intermediate molecules synthesized in this work are characterized using several common methods. Nuclear magnetic resonance (NMR) spectroscopy (^{1}H and ^{13}C) and direct analysis in real time mass spectrometry (DART-MS) are used to confirm successful synthesis of the small molecules. Molecular weight and dispersity of the polymers ($Đ = M_w/M_n$) are analyzed using a triple-detection gel permeation chromatography (GPC) system. Molecular weights are reported based on universal calibration. Polystyrene standards of narrow molecular weight were used to create a universal calibration curve. Thermal properties, such as thermal stability and thermal transition phenomena, such as the glass transition temperature (T_g) and melting/crystallization temperatures (T_m), are determined by thermal gravimetric analysis (TGA) and differential scanning calorimetry (DSC), respectively.

The optical absorbance profile measured by UV-Vis spectroscopy is used to establish the wavelength of maximum absorbance and onset wavelength, which are indicative of conjugation length and energy difference between the ground state and the excited state. Measurement of the absorbance as a function of concentration (of the CP or other material) are used to determine the molar absorptivity. Molar absorptivity is an optical property
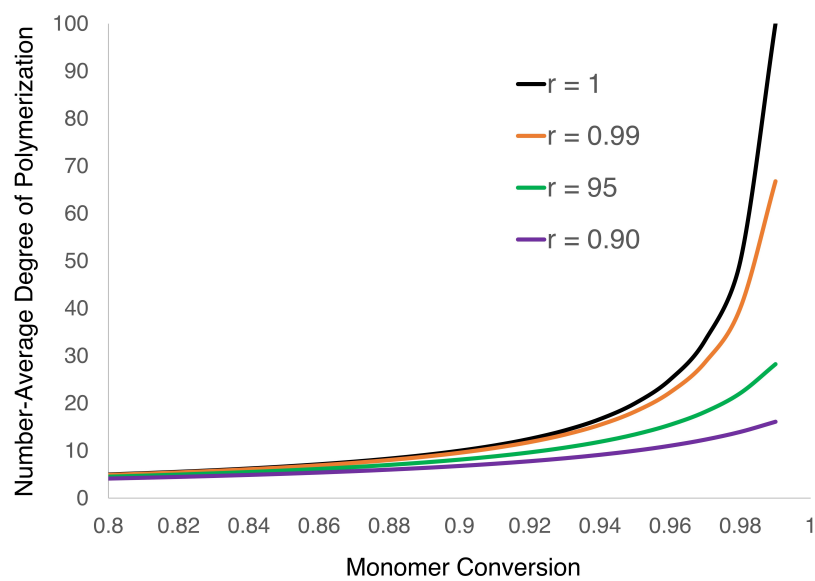
Figure 1.7: Visualized Carothers' equation highlighting the growth of polymer chains in a step-growth polymerization as a function of monomer conversion and stoichiometric imbalance.

of semiconducting materials, and some studies suggest that there is an empirical relation between molar absorptivity and exciton binding energies for CPs.[122] Beer's Law (Equation 1.3) is used to determine the molar absorptivity, ε, by measuring absorbance intensity, A, at various concentrations, c, using cells of fixed path length, l. The molar absorptivity is found by linear regression.

$$A = \varepsilon \cdot l \cdot c \tag{1.3}$$

Electrons promoted to the excited state may relax by radiative or non-radiative decay, as shown in the Jablonski diagram (Figure 1.8). A radiative relaxation process is commonly referred to as static fluorescence emission, which plays an important role in applications such as OLEDs and optical sensors.[21, 37] The difference between maximum absorbance wavelength and maximum emission wavelength indicates the energy difference between the absorbed photon and the emitted photon. Usually, due to vibrational relaxation or solvent reorganization, the emitted photon has less energy than the absorbed photon. This difference is called Stokes shift, and a lower Stokes shift is usually interpreted as smaller energy loss as a result of less structural reorganization. While a low Stokes shift is desired in some applications, such as OPVs, a larger Stokes shift is more appropriate for CPs used in optical sensors. I determined the Stokes shift of the polymers by comparing absorbance and emission profiles.

Another relevant property of electronic materials is the quantum yield, which is defined as the ratio of the emitted photons to absorbed photons. I used the comparative method to experimentally determine the quantum yield of the polymers I synthesized. To do this, a plot of the integrated fluorescence intensity versus absorbance intensity for a standard with a known quantum yield is constructed by measuring a set of solutions of different concentrations. This series of measurements is repeated for the sample (the CPs). Figure 1.9 shows the results schematically.

The slope determined from the best-fit lines for the sample and the reference, m_S and m_R, respectively, are used to find the quantum yield, ϕ_S:
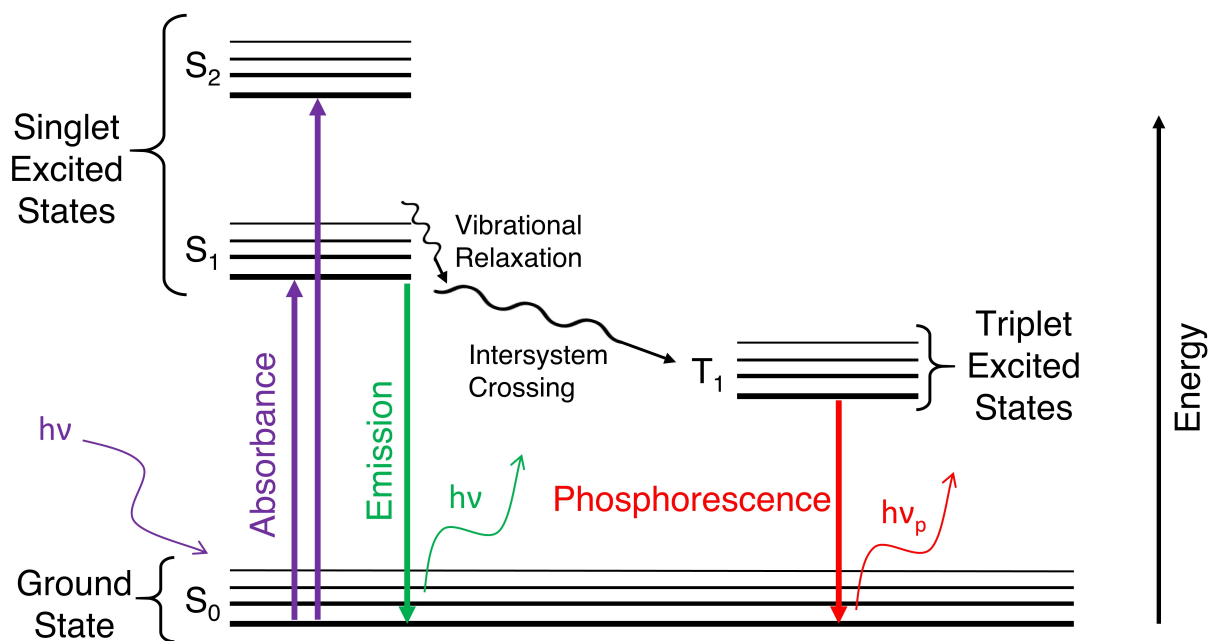
Figure 1.8: Jablonski diagram which illustrates the electronic states and the radiative or non-radiative transitions between them.
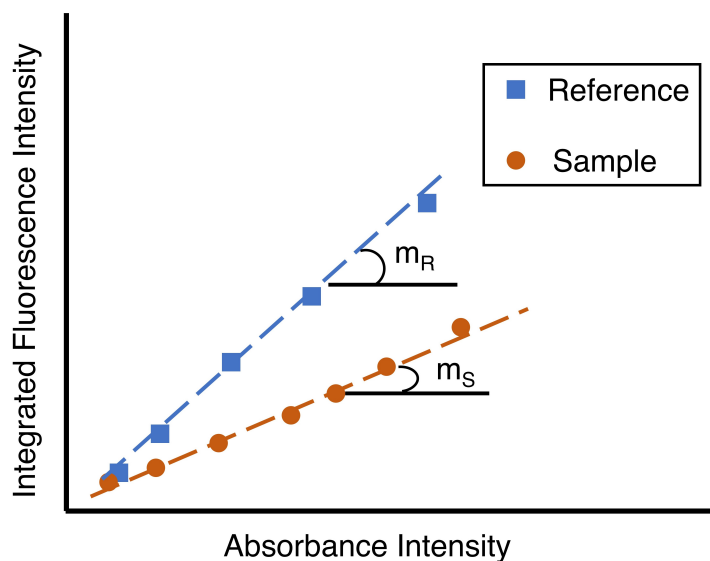
Figure 1.9: Plot of the integrated fluorescence intensity (representative of emitted photons) versus absorbance intensity (representative of absorbed photons) for a known reference material and sample. The slopes, m_R and m_S, are used to find quantum yield.

$$\phi_S = \phi_R(\frac{m_S}{m_R})(\frac{n_R^2}{n_S^2}) \tag{1.4}$$

In this equation, ϕ_R is the known quantum yield of the reference standard, and n_S and n_R are the refractive indices of solvents used for measurements of the sample and the reference. To ensure that emitted photons from a given CP is not reabsorbed by another CP molecule, measurements are made using very dilute solutions: I made sure that absorbance intensities of the samples were below 0.1.

The fluorescence of CPs and small molecule chromophores can be quenched in presence of an external stimuli, which is the basis for many optical sensors.[37, 123] The reduction in the emission intensity is frequently reported as the Q_{eff}, which is defined as:

$$Q_{eff} = \frac{I_0 - I(c)}{I_0} \tag{1.5}$$

In this equation, I_0 is the fluorescence intensity of the probe molecule in solution in the absence of a quenching reagent and $I(c)$ is the measured fluorescence intensity in presence of the quencher at concentration c. The correlation between emission intensity and concentration can be used for quantitative determination of the quencher-probe interaction. The binding strength of the quencher and emitter is related to the slope of the line created by plotting the fluorescence intensity ratio ($I_0/I(c)$) versus the concentration of the quencher ($[c]$). The slope is known as the Stern–Volmer constant (K_{SV}),[124] and the Stern–Volmer relationship is expressed in Equation 1.6. The Stern–Volmer constant, K_{SV}, describes the binding strength of the quencher to the emitter, which in my case was the CP.

$$\frac{I_0}{I(c)} = 1 + K_{SV}[c] \tag{1.6}$$

I also studied the strength of inter- and intra-base hydrogen bonding interactions to explain observed behaviors and related them to the structure of the nucleobase-functionalized copolymers. For instance, the intra-base hydrogen bonding or self-dimerization can be described by an equilibrium between the isolated and dimerized nucleobase. This is shown in Figure 1.10 for adenine. ^{1}H NMR can be used to assess either inter- or intra-base hydrogen

bonding, because the participating protons shift downfield compared to isolated protons of the same molecule. However, the observed chemical shifts are the weighted average of those isolated and hydrogen bonding protons. If we express the hydrogen bonding interaction between the isolated molecules and the dimerized nucleobase in terms of an equilibrium between them (see Figure 1.10.), the self-association constant (K_d) of this equilibrium is expressed as shown in equation 1.7. In this expression, $[A_d]$ is the concentration of the dimerized nucleobase, $[A]_0$ is total concentration of the nucleobase (initially added), and $[A]$ is concentration of the isolated molecule.

$$K_d = \frac{[A_d]}{[A]^2} = \frac{[A]_0 - [A]}{2[A]^2} \tag{1.7}$$

Protons in the isolated and dimerized form have different chemical shifts, but due to fast equilibration, one average peak is observable for the protons that are studied. Thus, we need to define three chemical shifts: i) chemical shift of protons in the isolated molecule (δ_f), ii) chemical shift of protons in the dimer (δ_d), and iii) the observed chemical shift (δ_{obs}), which is the weighted average of δ_f and δ_d. Equation 1.8 is written based on this relation.

$$\delta_{obs} = \frac{[A]}{[A]_0}\delta_f + \frac{[A]_0 - [A]}{[A]_0}\delta_d \tag{1.8}$$

If we combine Equation 1.7, and Equation 1.8, with some simplification we obtain the following equation:

$$\delta_{obs} = \delta_f + (\delta_d - \delta_f)\frac{\sqrt{(1 + 8K_d[A]_0)} - 1}{\sqrt{(1 + 8K_d[A]_0)} + 1} \tag{1.9}$$

Although the only two knowns are δ_{obs}, and $[A]_0$, there are three unknowns: δ_f, δ_d, and K_d. Thus, ^{1}H NMR spectroscopy at multiple concentrations or ^{1}H NMR titration experiments are used to find δ_f, δ_d, and K_d from an iterative non-linear least-squares regression. I did these calculations as part of the research described in Chapter 2 to find self-isomerization constant for thymine and adenine (small molecule dimerization) to assess intra-base hydrogen bonding effects of nucleobase-functionalized polymers. In Chapter 4, similar calculations are
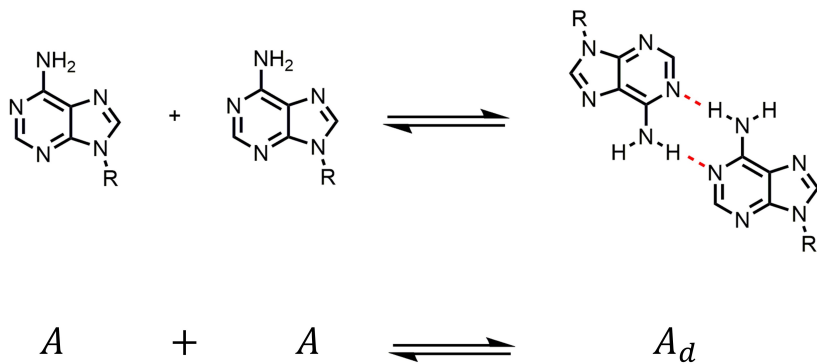
Figure 1.10: Self-association of alkylated adenine (R=alkyl chain).

performed to assess hydrogen bonding of nucleobase-functionalized CPs with complementary nucleobases present as small molecules in solution.

1.7   Research Objectives

The overarching goal of my dissertation is to develop structure-property relationships for conjugated polymers bearing nucleobase functionality. To achieve this, I have designed, synthesized, and characterized sets of nucleobase-functionalized conjugated polymers using Stille polycondensation and DArP. The specific copolymer designs and polymerization methods are aimed at addressing key limitations and complexities, including nucleobase-containing materials. In pursuit of these research activities, the specific goals of my research include the following:

1. Investigate how the incorporation of adenine and thymine into side chains of a series of low bandgap conjugated polymers affects the processing, surface immobilization, and transport properties;

2. Examine the polymerizability of nucleobase-functionalized thiophene-based monomers by direct arylation polymerization and test their fluorescence detection properties;

3. Study the hydrogen bonding ability of nucleobase (adenine) functionality in side chains for surface modification and potential applications involving these thin films, and expand the scope of direct arylation polymerization for polymerizing nucleobase-containing monomers.

In Chapter 2, I prepare alternating copolymers consisting of thiophene- and benzodithiophene-based monomers where the thiophene repeating units bear adenine or thymine at the end of the alkyl side chain and the benzodithiophene repeat units have linear alkyl or branched alkoxy side chains to aid solubility. We utilize Stille cross-coupling polymerization because it is tolerant of nucleobase groups. ^{1}H NMR titration is performed to assess the self-association of alkylated nucleobases (N1-hexyl-thymine and N9-hexyl-adenine). Because hydrogen bonding substantially reduces the solubility of these polymers,

I developed a specific solvent exchange method to purify the copolymers and enable film formation. Solvent resistivity of films cast on glass was evaluated, and basic thermal properties of the copolymers were evaluated. Photophysical measurements of thin films were used to assess transport properties to gain insight into the impact of the nucleobases. Chapter 3 explains how I synthesized an adenine-modified polythiophene using an atom-efficient and green polymerization method, direct arylation polymerization. I designed and used a flexible and bulky comonomer that incorporated four hexyl side chains to improve the solubility of the copolymer. Screening studies that examined various DArP conditions in the presence and absence of nucleobases as additives identified probable causes of catalyst cycle poisoning. Protection of amine functionality of adenine with tert-butyloxycarbonyl (Boc) groups circumvented this undesired interaction. Removal of the Boc groups after polymerization and purification revived the ability to bind metal ions, enabling applications such as "turn-off" fluorescence detection. The work described in Chapter 4 builds on those findings, as I show that careful thermal regulation of DArP conditions simplifies the synthesis, enabling polymerization and post-polymerization deprotection in a one-pot method. The findings and methodology of the newly developed one-pot DArP and Boc deprotection have applicability in wider contexts, such as synthesis of small molecule pharmaceuticals. In addition to studying the hydrogen bonding ability of the adenine-functionalized copolymer in solution, I show how the hydrogen bonding ability can be exploited to modify H-bond active surfaces. Specifically, I demonstrate how the surface properties of cellulosic materials change drastically upon surface modification, switching from being hydrophilic to superhydrophobic. The modified filter papers were then tested in a proof-of-concept experiments to showcase their potential in oil-water separations. Chapter 5 briefly summarizes the importance this research and main findings in developing nucleobase-containing CPs. Opportunities for future work are also discussed. Finally, following the listing of references, various appendices elaborating synthesis procedures and characterization of intermediate molecules are included for completeness.

Chapter 2

Synthesis and optoelectronic properties of benzodithiophene-based conjugated polymers with hydrogen bonding nucleobase side chain functionality

This chapter describes the work published in Polymer Chemistry, 11, (2020), 5735-5749. I designed and synthesized all monomers and polymers described in this work and performed all of the thermal and structural (^{1}H NMR and FTIR) characterizations. I designed the "solvent transfer method" for purification and solution processing of these polymers. I also performed the solvent resistivity test and the hydrogen bonding studies. Coauthors include Tyler J. Adams, Margaret Kocherga, and Prof. Michael G. Walter, who fabricated, and tested devices and performed photophysical and cyclic voltametric characterizations, and Prof. S. Michael Kilbey II, who advised this work.

2.1 Abstract

Fundamental properties of conjugated copolymers are sensitively linked to their constitution and features of their repeat unit design that govern assembly and organization across multiple length scales, ultimately impacting device performance. Herein we report the efficient synthesis and characterization, and optical, electrochemical and transport properties of nucleobase-functionalized, fully conjugated copolymers based on benzo[1,2-b:4,5-b']-dithiophene (BDT) and 3-hexylthiophene (3hT), which is a quintessential low bandgap polymer. Stille cross-coupling polymerizations enable access to high molecular weight, alternating copolymers of modest dispersity containing pendant adenine or thymine groups in each repeating unit, which provide the capacity to direct molecular assembly. Variations in nucleobase type and design of alkyl side chains on BDT units give rise to a strongly red-shifted absorbance onset for the copolymers containing thymine and adenine functionality in comparison to solution and dried films. Higher hole mobilities were also observed and attributed to the tendency of the nucleobase inclusion to heighten organization. The influence of the nucleobases on the organization is further revealed when thermal pre-treatment is used during film formation: Modest heating before casting the non-functionalized BDT-3hT copolymers leads to increases in the mobility, optical absorbance and fluorescence, while copolymers with adenine or thymine pendant groups do not show analogous improvements, suggesting that the nucleobases have promoted nanoscale organization, which is consistent with assessments of hydrogen bonding interactions. Given the structure-directing ability

of nucleobases through hydrogen bonding, π-stacking, and complementary base pairing, these novel materials offer myriad opportunities to examine how specific molecular-level interactions that promote self-assembly affect optoelectronic properties and device-level performance.

2.2   Introduction

Conjugated polymers have been used in numerous types of organic electronic devices, such as light-emitting diodes, field-effect transistors, photodetectors, and solar cells, as well as in applications like electrochromic windows and sensors, batteries and supercapacitors.[125–130] A rich variety of modifications to either the main chain or side chains have been utilized to enhance key performance attributes of conjugated polymers.[131, 132] For instance, the incorporation of fused ring monomeric units such as carbazole, fluorene, and benzo[1,2-b:4,5-b']-dithiophene (BDT) are shown to extend the conjugation length, narrow the band gap, and thus increase the light absorbance limits.[131, 133–135] Diketopyrrolopyrrole (DPP)-based polymers show promising charge transport properties and application in organic electronics that emerges from enhanced interconnectivity of polymer chains due to DPP polar backbone.[136, 137] Similarly, BDT-based polymers have received considerable attention, where modulating the constituents of the polymer backbone and adding electron withdrawing halogenated thienyl units to BDT have recently been shown to deepen HOMO levels of the donor-acceptor type polymers, which along with enhancements in planarity of the chain, lead to dramatic improvements in photovoltaic performance.[138–140]

Side chain engineering also is widely used to tailor the properties of conjugated polymers, oligomers, and small molecules with changes in functionality or design affecting the photophysical properties, solubility, phase separation, and intermolecular packing.[51, 136, 141–146] Beyond varying the size or branch location in alkyl side chains,[64, 147, 148] as discussed by Bao *et al.*, integrating ionic, polar, or other types of functionality within side chains provides a means to enhance optoelectronic properties and expand the applicability of conjugated polymers.[51] Within this pursuit, a handful of works have focused on functionalities that participate in hydrogen bonding. For example, Yao *et al.* showed

that when urea groups were present in side chains of DPP-based copolymers, higher hole mobilities were observed. This improvement was attributed to hydrogen bonding that enhanced ordering and increased domain sizes upon self-aggregation.[143] Ocheje *et al.* similarly showed that hydrogen bonding interactions provided by amide groups present in alkyl side chains of DPP-based conjugated polymers improved charge carrier mobility and nanoscale organization.[146] Hydrogen bonding interactions can also be used to organize small conjugated molecules, as shown by Lam *et al.*[149] Specifically, hydrogen bonding between carboxylic acid end groups on small molecules generated conjugated pseudo-polymer structures. With these self-organized pseudo-polymers, optimal device performance was achieved with as-cast films rather than thermally annealed samples.[149] In addition to reducing the reliance on thermal or solvent annealing and promoting molecular organization to enhance device performance, hydrogen bonding motifs also provide a viable strategy for surface immobilization and improving resistance to removal by solvent.[150–152] In total, these studies illustrate the close connections between improving optoelectronic properties of conjugated materials and structural features, as the ability to control structure across length scales ranging from molecular-level to mesoscopic not only affects chain conformation, packing, crystallization and domain sizes, but also impacts fundamental material properties and performance of organic electronic devices.[138, 139, 153, 154]

Among the variety of structure-directing functionalities, nucleobases represent an intriguing type of functionality that may be used as an order-inducing motif.[86, 155] Inspired by the potential for biomimicry, a well-known capacity for complementary, multi-dentate hydrogen bonding (as well as self-complementary hydrogen bonding), π-stacking, and the ability to bind cations, polymeric[90, 141, 156] or oligomeric[157, 158] materials containing nucleobase functionalities have been widely explored. For instance, nucleobases have been examined in applications such as adhesives, self-healing materials, sensors, and templated arrays of nanoparticles, and they represent an emerging concept in organic electronic devices.[91, 141, 159–164] Bäuerle and coworkers studied self-organization and functionality of π-conjugated oligomers appended with nucleosides and other biomolecules.[165–167] Guanine-functionalized oligothiophenes exhibited liquid crystalline and ion responsive behaviors due to the ability of guanine motifs to participate in self-complementary hydrogen

bonding and form complexes with ions.[168] In the realm of polymeric materials, uracil, which is one of the four nucleobases of RNA, has been used as a pendant group in poly(alkyl thiophene) side chains. Cheng *et al.* used oxidative polymerizations or post-polymerization "click" reactions to create uracil-containing polythiophenes with different degrees of regioregularity and evaluated their impact as hole injection layers in OLED devices. Improvements in device characteristics were observed, with uracil-functionalized polythiophenes of low regioregularity displaying a significantly higher external quantum efficiency, brightness, and luminance efficiency compared either to devices without the hole injection layer or to devices made using a hole injection layer comprising high regioregular, uracil-tagged polythiophene (made by post-polymerization functionalization by an azide-alkyne click reaction). They attributed this improvement to physical connectivity between polythiophene chains brought on by self-complementary hydrogen bonding.[91] In a later study, Cheng *et al.* used Suzuki cross-coupling polymerizations to produce the first complementary pair of thymine- and adenine-functionalized polycarbazoles, and evaluated their impact as hole injection layers in OLEDs. While these copolymers were of modest molecular weight ($\approx$ 5 kg/mol), similar to the behavior exemplified in studies of uracil-functionalized poly(thiophene)s, physical cross-linking attributed to complementary adenine-thymine hydrogen bonding enhanced the performance of organic light-emitting diodes (OLEDs) relative to the performance of OLEDs constructed using poly(3,4-ethylenedioxythiophene):poly(styrene sulfonate) as the hole injection layer.[169] Recently, Yang *et al.* harnessed the ability of nucleobases to bind metal ions, creating organic field effect transistors (OFETs) based on DPP/bithiophene alternating copolymers in which 5 mol% of DPP repeat units contained thymine-terminated, alkyl side chains. OFETs based on the resulting terpolymer, when first exposed to either Pd^{2+} or Hg^{2+} ions, demonstrated remarkable selectively toward CO or H_2S gases, respectively. In addition, the terpolymers containing thymine at the terminus of the side chain displayed higher mobilities due to enhanced crystallinity, which was attributed to the directional H-bonding interactions between thymine groups.[141]

The combination of these themes of research—altering conjugated polymer type, changing side chain design, and adding structure-directing motifs—exemplify the premise

of molecular engineering, which relies on deliberately manipulating molecular constituents and connectivity, and precisely encoding molecular-level interactions that operate at the nanoscale to generate new and useful material systems having enhanced properties and improved macroscopic performance. This represents a compelling challenge in the field of conjugated polymers, as organic semiconductors are marked by a strong interdependence between electronic and geometric structure,[170, 171] and fundamental properties such as charge carrier mobility and excited state lifetimes, which are crucial to device performance, depend on efficient intermolecular contact, either in ordered structures or interconnected aggregates.[125, 136, 172, 173] Moreover, interfacial properties,[64, 174], domain sizes,[175, 176] composition,[52, 135] and connectivity[142] also play crucial roles. Motivated by the premise of harnessing non-bonded physical interactions to influence inter-chain interactions in semiconducting conjugated polymers, in this study we describe the synthesis of well-defined alternating copolymers based on BDT and 3-hexylthiophene (3hT) in which the hexyl side chains are terminated with either thymine (Thy) or adenine (Ad) nucleobases as pendant functionality. Throughout the chapter, the nucleobase functionality on the side chains on 3hT are identified by subscripting Thy or Ad. The BDT repeating units have either linear alkyl (dodecyl) or branched alkoxy (ethyl hexyloxy) side chains, which are identified using subscript d or eho, respectively. In addition to the four nucleobase-modified copolymers, the analogous copolymers without nucleobases in the side chain are synthesized and studied in order to begin to elucidate the impact of nucleobase functionality on optical, electrochemical and photophysical properties in solution and thin films.

2.3   Synthesis and Characterization

2.3.1   Materials and Methods

All chemicals and solvents were purchased from Sigma-Aldrich or Fisher Scientific and used as received unless otherwise stated. Tetrakistriphenylphosphine palladium(0) $(Pd(PPh_3)_4)$ was purchased from Strem Chemicals and used without additional purification. (4,8-Didodecylbenzo[1,2-b:4,5-b']dithiophene-2,6-diyl)bis(trimethylstannane) (BDT_d) and

((4,8-bis((2-ethylhexyl)oxy) benzo[1,2-b:4,5-b']dithiophene-2,6-diyl)bis(trimethylstannane) (BDT$_\text{eho}$) were purchased from Solarmer Energy Inc. Toluene, THF and *N,N*-dimethylformamide (DMF) were purified using an Innovative Technologies MD-5 Solvent Purification System and degassed prior to use. *N*-bromosuccinimide was recrystallized from hot (distilled) water prior to use. All synthesized materials were purified via column chromatography using 60 Å silica gel (40-63 µm, Sorbent Technologies).

^{13}C and ^{1}H NMR spectra of synthesized molecules and polymers were acquired using a Varian Mercury Vx 300 MHz NMR at room temperature from 15-20 mg/mL solutions in CDCl$_3$. Chemical shifts are reported in units of δ (ppm) and referenced to the residual solvent peak. A JEOL AccuTOF DART mass spectrometer was used to analyze samples that were constituted at $\approx$ 1 mg/mL using toluene as the solvent. The average molecular weight and dispersity of synthesized polymers were determined by size exclusion chromatography using an Agilent 1260 Infinity II GPC system. Macromolecular characteristics reported are based on universal calibration using polystyrene standards. The system contained two Agilent PLgel Mixed-D columns (7.5 × 300 mm) in sequence, and detectors include an Optilab® T-rEX™ RI detector, a Wyatt Dawn® Helios® Multi-Angle Light Scattering Detector, and a ViscoStar® III viscometer. Samples were dissolved in THF ($\approx$ 5 mg/mL) and passed through a 0.2 μm PTFE filter prior to analysis. The flow rate of the THF mobile phase was set at 1 mL/min.

A Nicolet iS50 FT-IR Spectrometer equipped with a deuterated triglycine sulfate (DTGS) detector was used to measure the absorption spectrum of dry powder samples in the mid-IR region (4000-400 cm^{-1}) in attenuated total reflection (ATR) mode. Thermal stability of the polymers was determined using a TA Instruments Q50 Thermogravimetric Analyzer (TGA) in an inert atmosphere of N$_2$ by ramping from room temperature to 800 °C at a heating rate of 20 °C min^{-1}. For TGA measurements, the analytes were loaded in a platinum pan. Thermal properties were examined by differential scanning calorimetry (DSC) using a TA instruments Q-2000 DSC and a protocol consisting of a heat–cool–heat cycle from 50 °C to 270 °C with a heating rate of 10 °C min^{-1} and a cooling rate of 10 °C min^{-1} under an inert N$_2$ atmosphere. Samples ($\approx$ 5 mg) were sealed in standard aluminum pans.

Absorbance and fluorescence measurements were performed by making micromolar solutions of the polymers in tetrahydrofuran (THF). Molar absorptivity of BDT_d-$3hT_{Ad}$ was measured in 1:1 DMSO:1,2-dichlorobenzene. This also includes fluorescence quantum yield and molar absorptivity measurements. Thin films for UV-Vis measurements were prepared by drop-casting from THF solutions. These measurements were performed using a Varian Cary Bio 300 UV-Vis spectrophotometer and a Shimadzu RF-5301PC spectrofluorophotometer. The oxidation of all 6 copolymers were determined by drop-casting each polymer onto a glassy carbon working electrode. Toluene was used to make films of BDT_{eho}-$3hT$ and BDT_{eho}-$3hT_{Thy}$, chloroform was used for BDT_{eho}-$3hT_{Ad}$, chlorobenzene was used for BDT_d-$3hT$ and BDT_d-$3hT_{Thy}$, and THF was used for BDT_d-$3hT_{Ad}$. A platinum flag counter electrode was used with a saturated calomel reference electrode in a 0.1 M tetrabutylammonium hexafluorophosphate in acetonitrile solution. The copolymers are not soluble in acetonitrile, so all of the copolymers remained on the working electrode. After purging the solution with argon for 5 min, each copolymer thin film was scanned 0 to 2 V at a scan rate of 100 mV/s. Three cycles were performed each time to prove that all the deposited polymer was oxidized after one cycle. When the second and third cycles were performed, the oxidation peak(s) disappeared. When scanned -2 to 2 V, the polymers were irreversibly oxidized.

Patterned ITO glass (6 pixel) substrates from Ossila were cleaned by sonicating in DI water for 15 min, acetone for 15 min, then isopropyl alcohol for 15 minutes. Substrates were dried with nitrogen and treated in a UV/ozone ProCleaner for 10 min before PEDOT:PSS (Heraeus Clevios™ AI 4083) was applied by spin coating. Solution preparation and spin coating were performed under ambient conditions. The PEDOT:PSS (10 nm) was spin coated at 5000 RPM for 50 seconds with 90 μL using a Chemat Technology KW-4A spin coater. The ITO edge contacts were wiped off before annealing at 125 °C for 15 minutes. The BDT_R-$3hT_X$ copolymers were spin coated on top of the PEDOT:PSS. BDT_{eho}-$3hT$ was spin coated at 2000 RPM for 20 seconds with 45 μL from a 15 mg/mL 1,2-dichlorobenzene solution that was heated to 60 °C. BDT_d-$3hT$ was dissolved in 1,2-dichlorobenzene at 10 mg/mL and spin coated with 90 μL at 5000 RPM for 50 seconds, after being heated to 60 °C. The BDT_{eho}-$3hT_{Ad}$ and BDT_d-$3hT_{Ad}$ polymers were spin coated at 2000 RPM for 50 seconds using

45 μL of 5 mg/mL solutions with 1,2-dichlorobenzene/DMSO (1/1 by volume). BDT_{eho}-$3hT_{Thy}$ and BDT_d-$3hT_{Thy}$ were spin coated from 10 mg/mL 1,2-dichlorobenzene/THF (1/1 by volume) at 5000 RPM for 50 seconds with 90 μL after being heated at 60 °C. When testing heating protocols, all devices were spin cast at 2000 RPM for 50 seconds using 45 μL of solution, with heating of the solution and substrates to either 60 °C or 120 °C. BDT_{eho}-$3hT$ and BDT_d-$3hT$ were dissolved in 1,2-dichlorobenzene at 10 mg/mL. The BDT_{eho}-$3hT_{Ad}$ and BDT_d-$3hT_{Ad}$ were spin coated using 5 mg/mL solutions with a mixed solvent of 1,2-dichlorobenzene/DMSO (1/1 by volume). BDT_{eho}-$3hT_{Thy}$ and BDT_d-$3hT_{Thy}$ were dissolved in 1,2-dichlorobenzene/THF (1/1 by volume) at 10 mg/mL. The multilayer devices (ITO glass/PEDOT:PSS/BDT_R–$3hT_X$ copolymer) were then capped with a gold contact through thermal evaporation using a MB-EVAP system inside an MBRAUN glovebox. The gold films were deposited under high vacuum (10-6 mbar) and the thickness was controlled with a SQC-310C Deposition Controller. The gold was evaporated from a tungsten boat at a rate of approximately 1 Å s $^{-1}$. During deposition, the samples were rotated at 15 RPM and the source-to-film distance was 28 cm. A push-fit test board for pixelated anode substrates from Ossila was used with a Keithley 2602 A System SourceMeter$^{®}$ to measure J – V curves.

2.3.2 Synthesis of 3-(6-Bromohexyl)thiophene

An oven-dried 3-neck flask sealed with rubber septa was cooled under vacuum to room temperature and refilled with Ar gas. 50 mL of dry, degassed hexane was transferred to the 3-neck flask via cannula and cooled to -78 °C using a dry ice/isopropanol bath, after which time 4.0 mL of n-butyllithium solution (2.5 M in hexane, 10 mmol) was added dropwise to the reaction flask over 30 minutes. Then, 5 mL of dry and degassed THF was added and the mixture stirred at -78 °C for 30 minutes before dropwise addition of 1.0 mL of 3-bromothiophene (10.65 mmol). This mixture was stirred for 1 h, and after that time, an excess of 1,6-dibromohexane (16 mL, 106.5 mmol) was added as shown in Figure 2.1. While stirring, the mixture was allowed to warm to the room temperature by removing the isopropanol bath.

After allowing the reaction to proceed overnight, the reaction was quenched by adding 100 mL water. The product was extracted using 100 mL of diethyl ether, and the aqueous phase

separated using an extraction funnel. The organic phase was dried over $MgSO_4$ and then filtered and concentrated via rotary evaporation. Excess 1,6-dibromohexane was removed by vacuum distillation at 65 °C (30 mtorr) and the product was purified by silica gel column chromatography using hexanes as the mobile phase. The product was recovered as a colorless oil (70% yield based on isolated product). ^{1}H NMR (300 MHz, $CDCl_3$), δ (ppm): 7.24 (dd, 1H, J = 4.9, 3.0 Hz), 6.94 – 6.90 (m, 2H), 3.41 (t, 2H, J = 6.7 Hz), 2.64 (t, 2H, J = 7.5 Hz), 1.90 – 1.83 (m, 2H) 1.68 – 1.61 (m, 2H), 1.51 – 1.44 (m, 2H) 1.40 – 1.33 (m, 2H). ^{13}C NMR (300 MHz, $CDCl_3$) δ (ppm): 142.9, 128.2 ,125.2, 119.9, 33.9, 32.7, 30.3, 30.1, 28.4, 28.0. AccuTOF DART: calc'd $[M+H^+]$: 247.0156, found: 247.0155.

2.3.3   Synthesis of 2,5-Dibromo-3-(6-bromohexyl)thiophene

An oven-dried 3-neck round bottom flask was cooled to room temperature under vacuum. To ensure an inert environment, the flask was evacuated and then refilled with Ar 3 times. 25 mL of dry and degassed THF and 25 mL of glacial acetic acid were added via syringe. 3-(6-bromohexyl) thiophene (0.985 g, 4 mmol, 1 equiv.) was added to the THF/acetic acid mixture and stirred for 30 min at room temperature. Under positive argon pressure, 1.495 g of freshly recrystalized NBS (8.4 mmol, 2.1 equiv.) was added in one portion to the mixture and the flask covered from light (See Figure 2.2.). The resulting mixture was stirred for 3 h at room temperature.

After this time, the reaction was quenched by adding a saturated solution of sodium bicarbonate. The product was extracted to the organic phase with 100 mL of diethyl ether and the aqueous phase was discarded. The organic phase was washed with brine, isolated, then dried over $MgSO_4$. The $MgSO_4$ was removed by filtration and the product was concentrated via rotary evaporation. Silica gel column chromatography using hexanes as the mobile phase was used to purify the product, which was collected as a colorless oil. (75% yield based on the isolated product.) ^{1}H NMR (300 MHz, $CDCl_3$), δ (ppm): 6.77 (s, 1H), 3.40 (t, 2H, J = 6.8 Hz), 2.52 (t, 2H, J = 7.6 Hz), 1.91 – 1.81 (m, 2H) 1.62 – 1.52 (m, 2H), 1.50 – 1.40 (m, 2H) 1.40 – 1.30 (m, 2H). ^{13}C NMR (300 MHz, $CDCl_3$) δ (ppm): 142.6, 130.9, 110.5, 108.1, 33.8, 32.6, 29.34, 29.29, 28.2, 27.9. AccuTOF DART: calc'd $[M+H^+]$: 404.8346 Found: 404.8312.
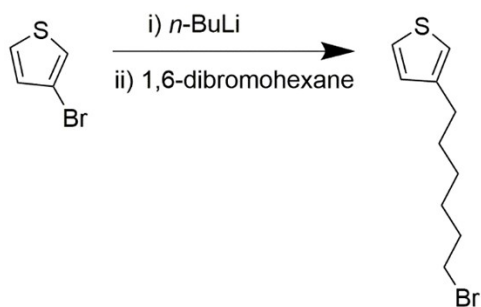
Figure 2.1: Synthesis of 3-(6-bromohexyl)thiophene through halogen-metal exchange followed by nucleophilic substitution.
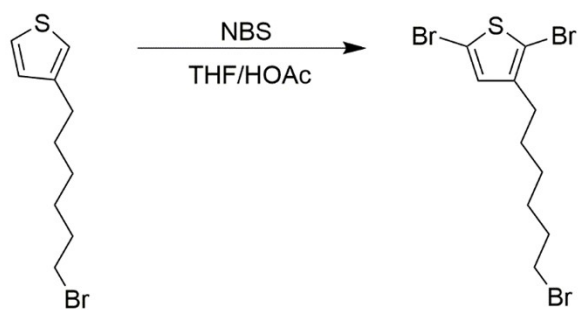
Figure 2.2: Aromatic bromination to synthesize the 2,5-dibromo-3-(6-bromohexyl)thiophene.

2.3.4 Synthesis of Adenine-Containing Dibromo Thiophene Monomer, 3hT$_{Ad}$

50 mL of dry and degassed DMF was added to a dry 100 mL round bottom flask under positive Ar pressure. Then, 821 mg (2.03 mmol) of 2,5-dibromo-3-(6-bromohexyl)thiophene, 547 mg of adenine (4.05 mmol, 2 equiv.), and 839 mg (6.08 mmol, 3 equiv.) of potassium carbonate were added to the mixture, as depicted in Figure 2.3. The mixture was stirred at room temperature for 24 h. After this time, the solvent was removed under high vacuum at 50 C. Then, the product was extracted using 100 mL of dichloromethane (DCM) and washed using water and brine solutions. Silica gel column chromatography was used to recover the product, using 5% MeOH in DCM as the mobile phase. The product of N9 alkylation was collected as the major product with 55% yield (based on isolated product) as a white solid. ^{1}H NMR (300 MHz, CDCl$_3$), δ (ppm): 8.35 (s, 1H), 7.77 (s, 1H), 6.72 (s, 1H), 6.13 (s, 2H) 4.17 (t, 2H, J = 7.2 Hz), 2.46 (t, 2H, J = 7.5 Hz), 1.96 − 1.81 (m, 2H) 1.58 − 1.44 (m, 2H), 1.40 − 1.28 (m, 4H). ^{13}C NMR (300 MHz, CDCl$_3$) δ (ppm): 155.6, 152.9, 150.1, 142.5, 140.3, 130.8, 119.7, 110.5, 108.1, 43.9, 30.0, 29.3, 29.2, 28.4, 26.4. AccuTOF DART: calc'd [M+H$^+$]: 459.9629 Found: 459.9484.

2.3.5 Synthesis of Thymine-Containing Dibromo Thiophene Monomer, 3hT$_{Thy}$

50 mL of dry and degassed DMF was added to a dry 100 mL round bottom flask under positive Ar pressure. Then, 619 mg (1.53 mmol, 1 equiv.) of 2,5-dibromo-3-(6-bromohexyl)-thiophene, 385 mg of thymine (3.06 mmol, 2 equiv.), and 633 mg (4.59 mmol, 3 equiv.) of potassium carbonate were added to the mixture as shown in Figure 2.4. The mixture was stirred at room temperature for 24 h. After this time, the solvent was removed under high vacuum at 50 °C. Then, the product was extracted using 100 mL of DCM and washed with water and brine solutions. Silica gel column chromatography was used to recover the product, using 3% MeOH in DCM as the mobile phase. The product of N1 alkylation was collected as a white solid with a 62% yield based on isolated product. ^{1}H NMR (300 MHz, CDCl$_3$), δ (ppm): 9.69 (s, 1H) 6.95 (s, 1H), 6.74 (s, 1H), 3.66 (t, 2H, J = 7.2 Hz), 2.48

(t, 2H, J = 7.5 Hz), 1.90 (s, 3H) 1.68 − 1.62 (m, 2H), 1.56 − 1.49 (m, 2H) 1.35 − 1.31 (m, 4H). ^{13}C NMR (300 MHz, CDCl$_3$) δ (ppm): 164.6, 151.1, 142.6, 140.4, 130.9, 110.6, 110.5, 108.1, 48.4, 29.3, 29.0, 28.5, 26.2, 12.3. AccuTOF DART: calc'd [M+H$^+$]: 450.9513 Found: 450.9527.

2.3.6 General Synthesis Procedure of the Copolymers

Dibromo thiophene monomer (3hT$_{Ad}$, 3hT$_{Thy}$, or 3hT; 1 equiv., 1 mmol), bistannylben-zodithiophene (BDT$_d$, or BDT$_{eho}$; 1 equiv., 1mmol), and Pd catalyst (Pd(PPh$_3$)$_4$, 0.1 mmol, 10 mol%) were added to a dry 50 mL round bottom flask while it was under positive Ar pressure and sealed with rubber septa. Dry DMF (10 mL) was then transferred via cannula to the reaction flask and the reaction mixture was heated at 100 °C for 24 h as shown in Figure 2.5. After the prescribed time, the reaction mixture was cooled to room temperature and the polymer was precipitated into methanol. The precipitate was washed with methanol and acetone in a Soxhlet thimble. The product was then extracted with chloroform and concentrated ($\approx$ 10 mL solution) in rotary evaporator. Then, 1,4-dioxane ($\approx$ 5 mL) was added and chloroform was selectively removed under reduced pressure yielding a polymer solution in dioxane. (This step is called "wet solvent exchange", which I will discuss it in greater detail in Section 2.4) The solid was recovered after freeze-drying from dioxane solution. Molecular weight data (relative to polystyrene standards) for these polymers are presented in Table 2.1.

BDT$_d$-3hT$_{Ad}$: Dark red solid, 55% yield, ^{1}H NMR (300 MHz, CDCl$_3$), δ (ppm): 8.35, 7.76, 7.52, 7.48, 7.21, 4.17, 3.14, 2.92, 1.89 − 1.60, 1.51 − 1.35, 0.89 − 0.76.

BDT$_d$-3hT$_{Thy}$: Red solid, 88% yield, ^{1}H NMR (300 MHz, CDCl$_3$), δ (ppm): 7.46, 7.22, 6.92, 3.67, 3.16, 2.94, 1.94 − 1.58, 1.56 − 1.15, 0.91 − 0.80.

BDT$_{eho}$-3hT$_{Ad}$: Dark red solid, 64% yield, ^{1}H NMR (300 MHz, CDCl$_3$), δ (ppm): 8.26, 8.17, 7.82, 7.50, 7.16, 4.21, 3.36, 2.90, 1.90 − 1.53, 1.51 − 1.27, 1.12 − 0.81.

BDT$_{eho}$-3hT$_{Thy}$: Dark red solid, 85% yield, ^{1}H NMR (300 MHz, CDCl$_3$), δ (ppm): 7.51, 7.18, 6.91, 4.22, 3.64, 2.93, 1.90 − 1.54, 1.48 − 1.18, 1.11 − 0.74.

BDT$_d$-3hT: Red solid, 53% yield, ^{1}H NMR (300 MHz, CDCl$_3$), δ (ppm): 7.44, 7.23, 3.12, 2.91, 1.97 − 1.66, 1.53 − 1.21, 1.01 − 0.74.
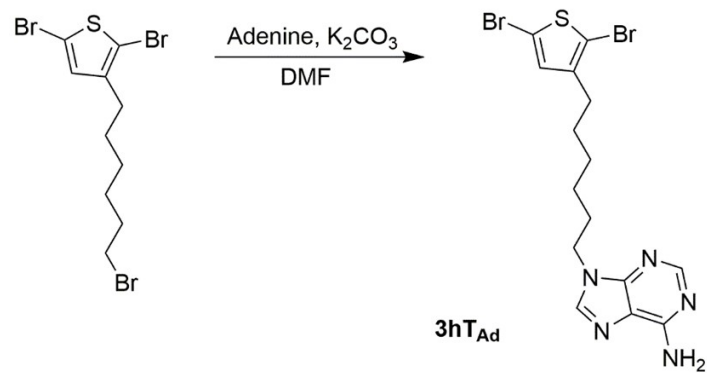
Figure 2.3: Alkylation of adenine at the N9 position under basic conditions to synthesize 3hT$_{Ad}$.
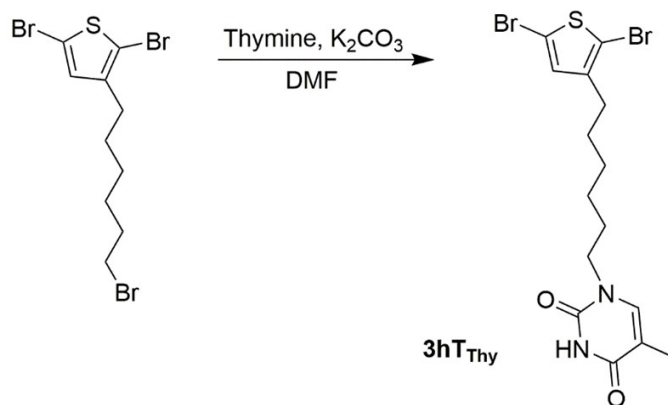
Figure 2.4: Alkylation of thymine at the N1 position under basic conditions to synthesize monomer 3hT$_{Thy}$.
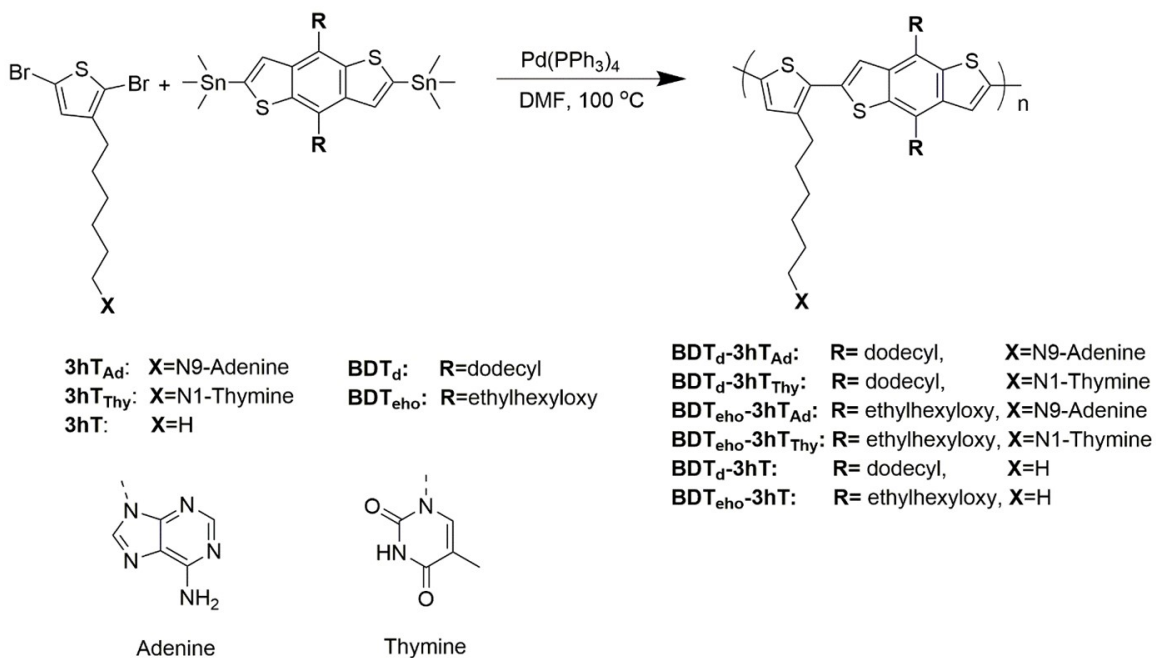
Figure 2.5: Synthesis scheme of BDT-3hT alternating, regiorandom copolymers prepared by Stille cross-coupling polymerization. These are generally referred to as BDT_R-$3hT_X$ copolymers, with the identity of R and X defined herein.

BDT$_{eho}$-3hT: Light red solid, 79% yield, ^{1}H NMR (300 MHz, CDCl$_3$), δ (ppm): 7.52, 7.20, 6.90, 4.19, 2.90, 1.86 – 1.61, 1.59 – 1.37, 1.18 – 0.86.

2.4 Results and Discussion

A series of high molecular weight alternating copolymers based on benzodithiophene (BDT) and 3-alkyl thiophene were synthesized by Stille cross-coupling, as shown in Figure 2.5. Within this series, the side chains on BDT were either dodecyl (BDT$_d$) or branched ethyl hexyloxy (BDT$_{eho}$) and hexyl side chains on thienyl repeating units were terminally functionalized with either adenine (3hT$_{Ad}$) or thymine (3hT$_{Thy}$) pendant groups. These variations give rise to four distinct alternating, fully conjugated polymers that are identified by their alternating repeating units: BDT$_d$-3hT$_{Ad}$, BDT$_d$-3hT$_{Thy}$, BDT$_{eho}$-3hT$_{Ad}$, and BDT$_{eho}$-3hT$_{Thy}$. In addition and for comparison purposes, two alternating copolymers of BDT and 3-hexylthiophene were also synthesized, and these are referred to as simply BDT$_d$-3hT and BDT$_{eho}$-3hT. Macromolecular size and dispersity of these six fully conjugated, alternating copolymers are presented in Table 2.1. Although we maintained synthesis conditions, including monomer concentration and catalyst loading, consistent across all samples, the alternating copolymers containing nucleobase functionalities were of lower molecular weight, likely due to limited solubility of the nucleobase- functionalized polymer[93] as well as potential undesired catalyst-nucleobase interactions, which we described in chapter 3 and have published recently.[156]

Although solubility issues are not uncommon with fully conjugated polymers, the presence of the nucleobases heightened these challenges: For example, Stille cross-coupling polymerization of 2,5-bis-(trimethylstannyl)thiophene with 2,5-dibromo-3-(6-adenine)hexylthiophene (3hT$_{Ad}$) produced a polymer that was soluble only in hot DMF, rendering it impossible to characterize. Similarly, in the case of a semi-random terpolymer produced by Stille cross-coupling polymerization of 2,5-bis-(trimethylstannyl)thiophene, 2,5-dibromo-3,4-dihexylthiophene, and 3hT$_{Ad}$, only the material recovered after Soxhlet extraction with acetone could be redissolved and characterized by GPC (2,900 g mol^{-1}, Đ = 1.2). As a result, BDT$_d$ and BDT$_{eho}$ were used as comonomers to help mitigate these

Table 2.1: Characteristics of BDT_R-$3hT_X$ Alternating Copolymers.

Copolymer	M_n (g mol^{-1})^a	Đ	Yield(%)	Nucleoabse attachment
BDT_d-$3ht_{Ad}$	17,300	2.36	55	N9
BDT_d-$3hT_{Thy}$	16,000	2.40	88	N1
BDT_{eho}-$3hT_{Ad}$	11,300	1.50	64	N9
BDT_{eho}-$3hT_{Thy}$	19,900	1.55	85	N1
BDT_d-$3hT$	45,000	1.43	53	-
BDT_{eho}-$3hT$	36,900	1.58	79	-

^{a} measured by GPC; relative to PS standards

solubility issues. While the data in Table 2.1. clearly suggests that Stille polymerizations are effective for the synthesis of nucleobase-functionalized and fully conjugated copolymers, we found that if those copolymers were dried as part of a purification process, their redissolution was challenged. This phenomenon is also observed in self-aggregating colloidal dispersions, where slow solvent removal step promotes irreversible aggregations and thus results in a non-processable solid.[177–179] Inspired by efforts to mitigate aggregation driven by π-stacking in graphene-polymer nanocomposites[180] and hydrogen bonding in pharmaceuticals[181] we developed a solution-based processing step to exchange the solvent from chloroform – the extraction solvent used in post-polymerization purification – to the desired, higher boiling-point solvent, such as dioxane. The solvent transfer method, which is discussed in the next section, proved to be effective for casting homogeneous and smooth thin films because it avoids aggregation.

2.4.1 Solvent Transfer Method

Nucleobase-functionalized copolymers isolated from chloroform solution following Soxhlet extraction could not be redissolved in common organic solvents, even at elevated temperatures, if they were rotovapped to complete dryness. This proved to be true for chloroform, THF, DCM, DMF, DMAc, acetonitrile, benzene, chlorobenzene, and dioxane, both at room temperature and elevated temperatures (up to the reflux temperature). These outcomes, along with the acknowledged importance of solution processability, led us to develop a novel solvent transfer method for these strongly aggregating, marginally-soluble conjugated polymers. Complete and slow removal of solvent results in irreversible aggregation and insolubility. However, the sequential addition of a solvent with boiling point that is higher than chloroform and selective removal of chloroform enables processable solutions in that desired solvent to be created. Fast freezing of the solution followed by solvent removal via freeze-drying circumvents irreversible aggregation, ostensibly resulting in powders with high void volume rather than a highly packed solid obtained by rotovaping.

An overview of the solvent transfer process used in this work is shown in Figure 2.8. We chose dioxane as the exchange solvent because it has a relatively high boiling point of 101.1 °C and because its freezing point of 11.8 °C makes it an excellent candidate for

freeze drying. Solvent exchange of the copolymers was achieved by sequential additions of dioxane as chloroform was removed by rotary evaporation. Once the solvents were exchanged, purified polymer was isolated by freeze drying under vacuum. The freeze-dried powder can be dissolved in most (organic) solvents, whereas if the nucleobase functionalized samples were dried after Soxhlet extraction using chlorogrom, they would not dissolve in dioxane, rendering it impossible to freeze dry the material. Additionally, it should be noted that solutions can be made directly using this solvent transfer method (without freeze-drying) if the desired solvent has a boiling point higher than the extraction solvent (chloroform).

To prepare samples for GPC or ^{1}H NMR analysis, after completing the solvent-transfer to dioxane, the samples were subjected to freeze-drying. Freeze-drying has been used to overcome irreversible aggregations in palygorskite, which is a type of clay shown that organizes by strong hydrogen bonding interactions in the solid state.[182] After freeze-drying, samples for analysis by GPC or ^{1}H NMR spectroscopy were dissolved in THF or CDCl$_3$, respectively. We expect that our method of solvent transfer, which is shown in Figure 2.8, also will be applicable to other marginally-soluble or self-aggregating conjugated (or non-conjugated) polymeric materials.[183]

2.4.2 Thermal Properties

All polymers exhibit high thermal stability, with BDT$_d$-based copolymers showing higher stability compared to BDT$_{eho}$-based copolymers. Unfunctionalized copolymers were more thermally stable than Ad-functionalized copolymers, which were more stable than Thy-functionalized copolymers. An extra feature in the degradation profile, ostensibly corresponding to loss of ethyl hexyloxy side chains, was observed in thermogravimetry studies of BDT$_{eho}$-based copolymers. (See Figure 2.6 where this process occurred in the range of $\approx$ 400 °C – 500 °C, representing $\approx$ 10% weight loss.) Although DSC measurements shown in Figure 2.7 did not show evidence of a distinct glass transition, it is noted that similar behavior (no T$_g$ by DSC) has been reported for a variety of BDT-based conjugated polymers.[147, 184–187] Also, no crystallization peaks were observed in thermograms recorded by DSC for any of the 6 copolymers. This lack of crystallinity is attributed to regiorandom incorporation of 3hT repeating units.
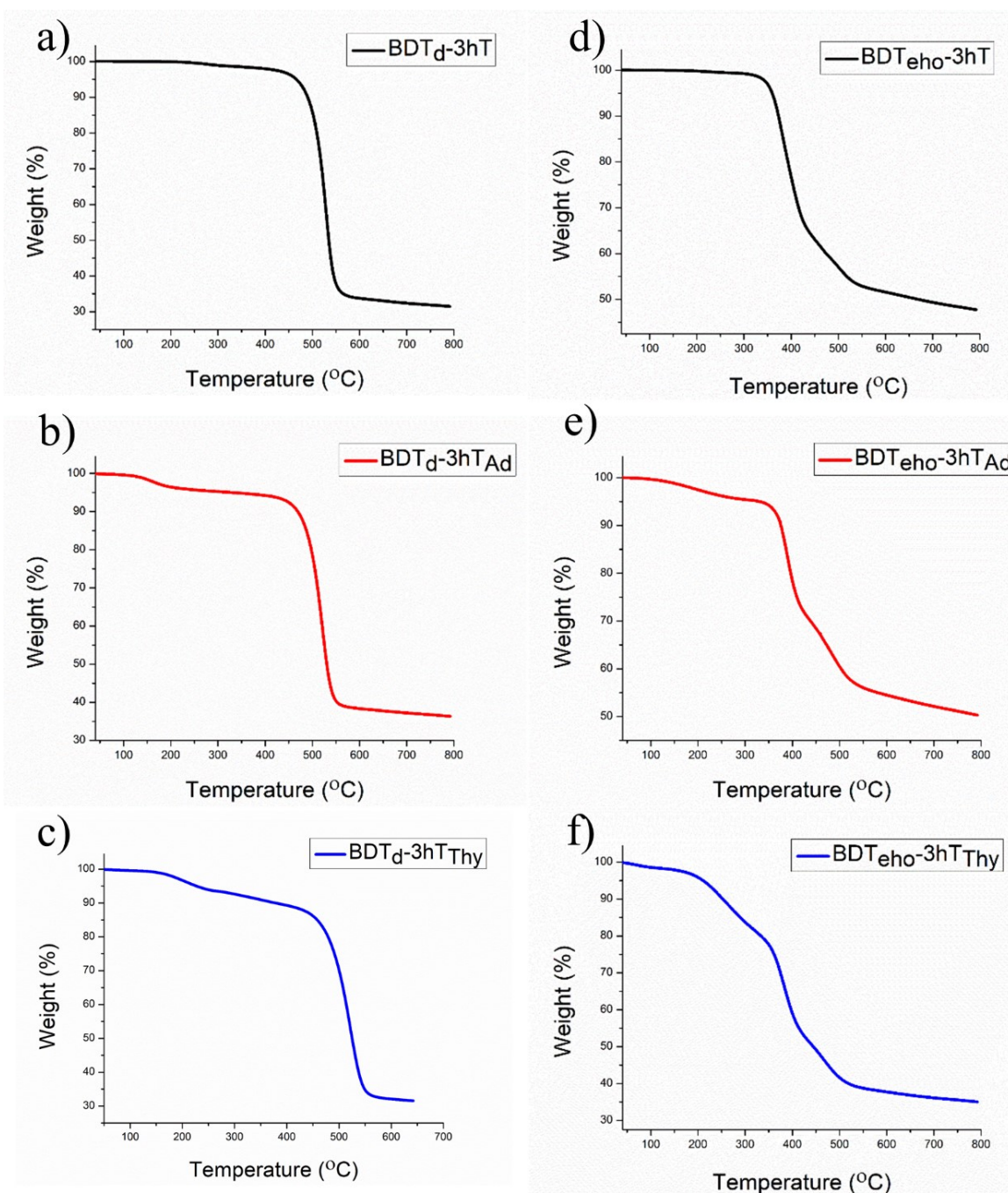
Figure 2.6: Thermogravimetric analysis of a) BDT_d-3hT (T_d = 465 °C), b) BDT_d-3hT$_{Ad}$ (T_d = 317 °C), c) BDT_d-3hT$_{Thy}$ (T_d = 230 °C), d) BDT_{eho}-3hT (T_d = 360 °C), e) BDT_{eho}-3hT$_{Ad}$ (T_d = 333 °C), f) BDT_{eho}-3hT$_{Thy}$ (T_d = 209 °C) ramping 40 °C to 800 °C at a rate of 20 °C/min. T_d values are based on temperature at 5% weight loss. The minor weight loss observed in f) at ≈ 150 °C is most likely due to residual solvent such as DMF (used in polymerization) or dioxane (used for freeze-drying).

47
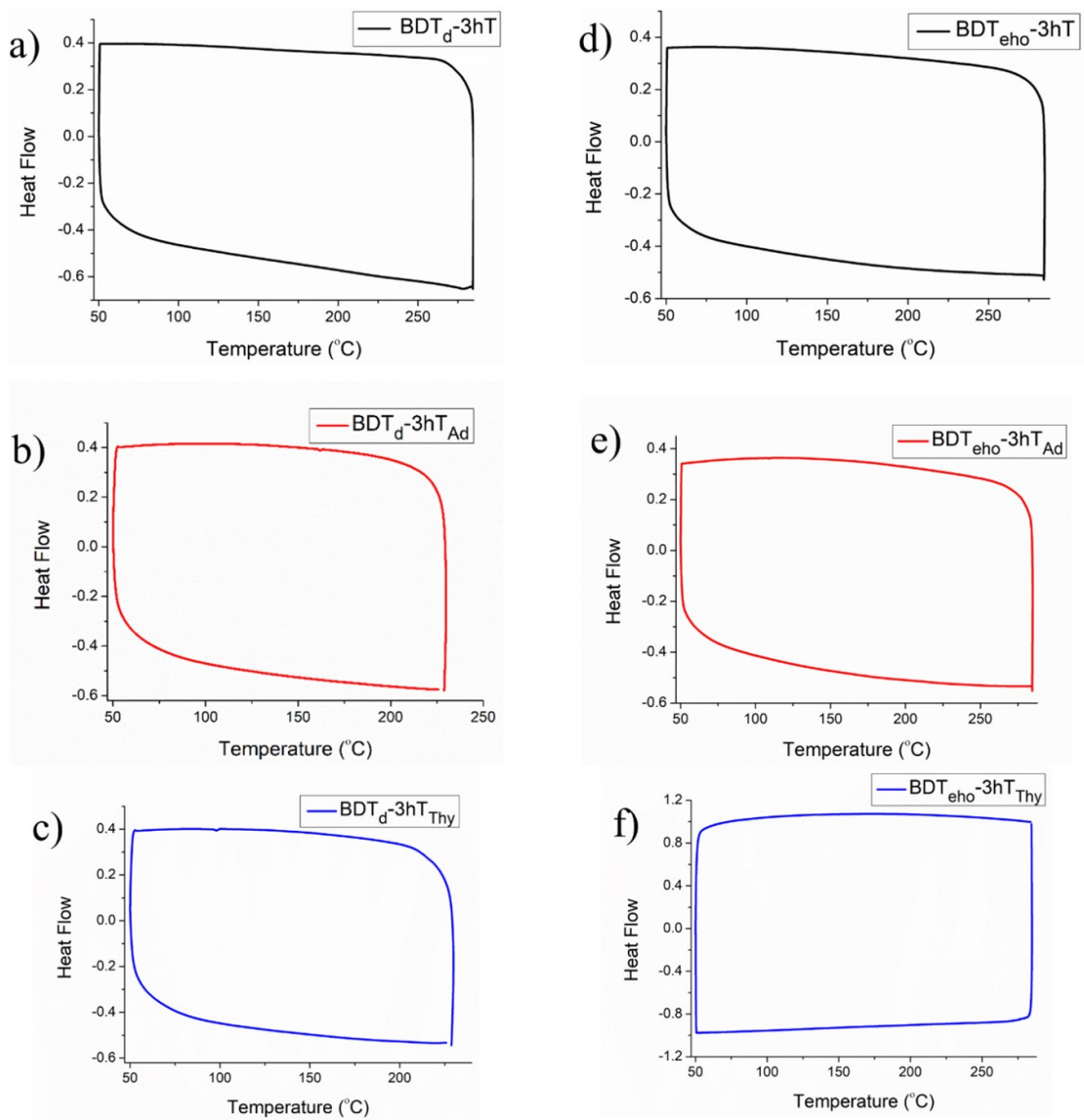
Figure 2.7: DSC curves (second heating ramp and cooling at the rate of 10 °C/min) of a) BDT_d-3hT, b) BDT_d-3hT$_{Ad}$, c) BDT_d-3hT$_{Thy}$, d) BDT_{eho}-3hT, e) BDT_{eho}-3hT$_{Ad}$, f) BDT_{eho}-3hT$_{Thy}$. No evidence of crystallinity is observed, nor are features due to a glass transition
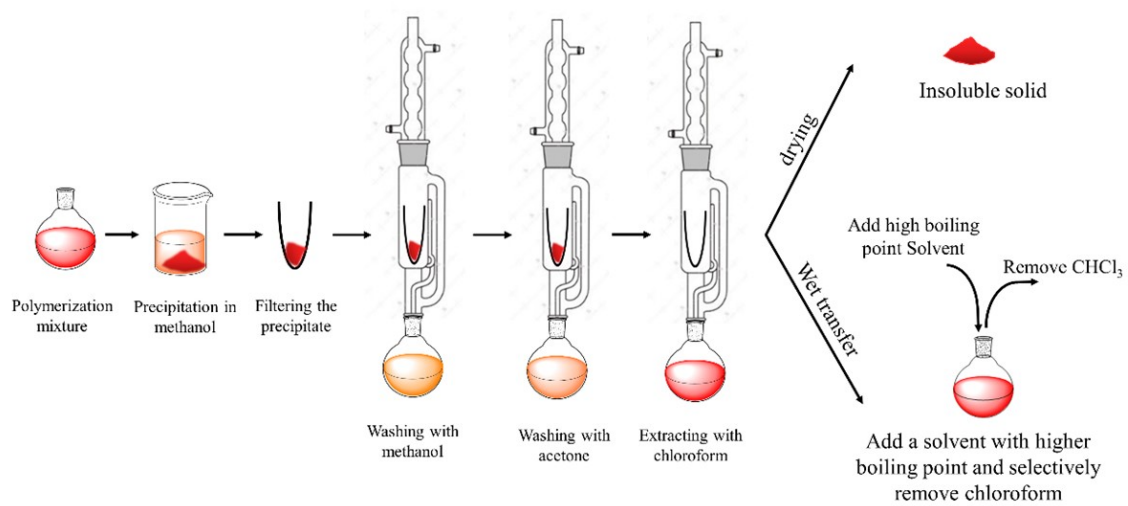
Figure 2.8: Schematic showing the solvent transfer method used to isolate the purified polymers and make solutions that could be used for film casting.

Nonlinear regression analysis yielded a dimerization constant of $K_{dimer, Thy\text{-}Thy} = 19$ M^{-1} for thymine-N1-hexyl (structure inset in Figure 2.9d).

These values are in good agreement with reported values for nucleobase-containing molecules[193] and consistent with the idea that self-complementary Thy$\cdots$Thy and Ad$\cdots$Ad hydrogen bonds are weaker than Thy$\cdots$Ad host-guest interactions. To assess this quantitatively, we performed titration experiment in which adenine-N9-hexyl was systematically added to thymine-N1-hexyl (concentration = 8 mM). As shown in Figure 2.10, the measured chemical shift of the N3-H proton of thymine-N1-hexyl as a function of adenine-N9-hexyl was analyzed using the Benesi–Hildebrand model,[194] which yielded a host-guest association constant, $K_{HG} = 29$ M^{-1} in chloroform. The dimerization association constants resulting from these studies support the contention that side chain functionalities present in the conjugated copolymer lead to interbase hydrogen bonds.

2.4.4 Hydrogen Bonding Ability of Nucleobase Functionalities in Solid State

Insights about hydrogen bonding in the solid state were obtained by FTIR spectroscopy and by testing resistance of thin films to removal by solvent (solvent resistivity). It is reported that hydrogen bonding in alternating copolymers in the solid state can improve surface immobilization and solvent resistivity.[150–152] Thin films of BDT$_R$-3hT$_X$ copolymers were fabricated on glass slides from dilute (1 mg/mL) chloroform solutions (3 samples for each copolymer). One sample was used as the control sample, one thin film was rinsed in chloroform twice for 20 s each time, and the third sample was sonicated in methanol for 20 minutes. (Methanol was used because it is a non-solvent that can participate in hydrogen bonding.) Images of the samples are shown in Table 2.2 with quantitative analysis presented in Figure 2.11.

In adition to images, we derived the relative solvent resistivity by normalizing the optical absorbance intensity of solvent-exposed films by the absorbance intensity of the as-cast film. The results (Figure 2.11 show that the control copolymers, BDT$_d$-3hT, and BDT$_{eho}$-3hT, have the lowest chloroform resistivity, with the former having only a 34% absorbance

Table 2.2: Images of thin films of alternating copolymers created by film casting and tested for solvent resistivity.

Sample	As-cast	Rinsed (2X) in chloroform	Sonicated in methanol
BDT_d-3ht			
BDT_d-$3hT_{Ad}$			
BDT_d-$3hT_{Thy}$			
BDT_{eho}-3hT			
BDT_{eho}-$3hT_{Ad}$			
BDT_{eho}-$3hT_{Thy}$			
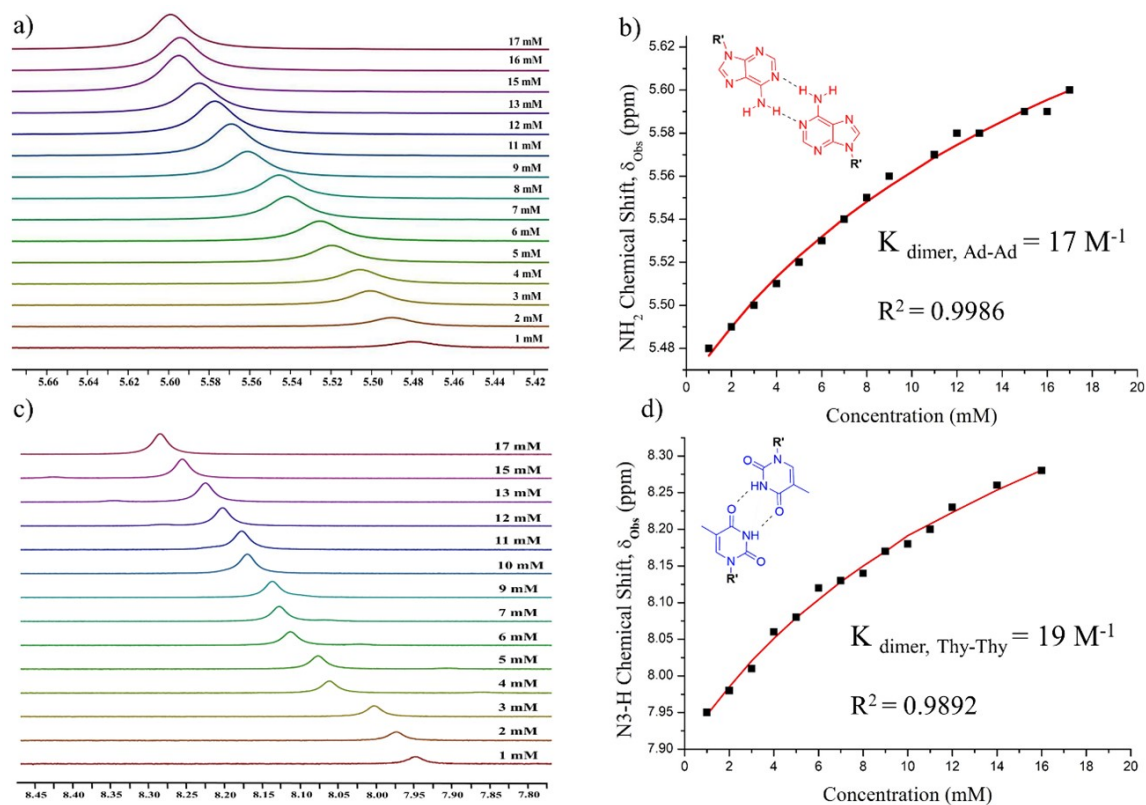
Figure 2.9: Small molecule analogs are used to assess self-dimerization of pendant nucleobase functionalities. Changes in the chemical shift of a) NH_2 (in adenine) and c) N3-H (in thymine) protons upon hydrogen bond dimerization as a function of concentration. Structures (R' = hexyl) and self-association constants determined by nonlinear regression analysis are shown for b) adenine-N9-hexyl and d) thymine-N1-hexyl.

The figure shows a plot with the equation:

$$1/\Delta\delta = 1/(\Delta\delta_{max} \cdot K_{HG}) \cdot 1/[G] + 1/\Delta\delta_{max}$$

$$y = 3.83\,x + 0.110$$

$$R^2 = 0.999$$

$$K_{HG} = 29\ M^{-1}$$

Y-axis: $1/\Delta\delta$ N3–H

X-axis: $1/[\text{Adenine-N9-hexyl}]$ mM^{-1}
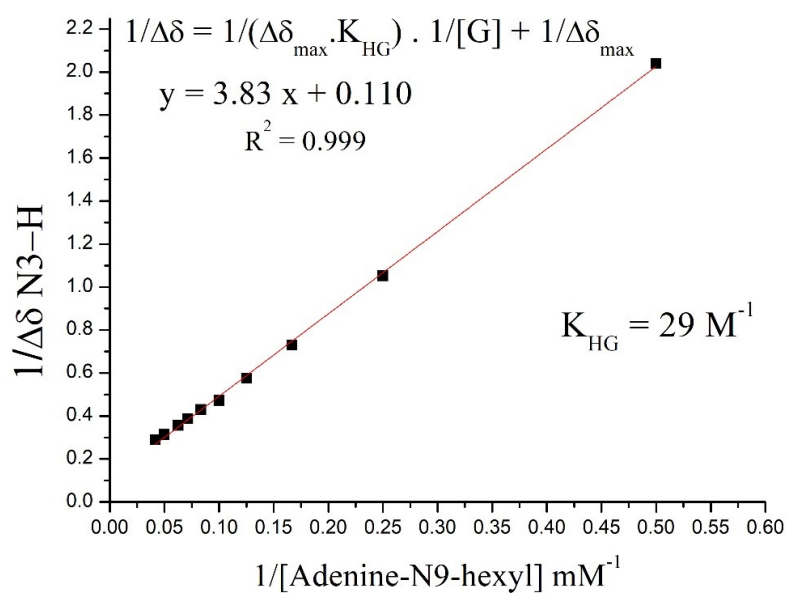
Figure 2.10: Dependence of chemical shift of N3-H proton of thymine-N1-hexyl (host) as a function of concentration of adenine-N9-hexyl as the guest molecule. Data are plotted according to the Benesi–Hildebrand model,[194] which is used to find host-guest association constant, K_{HG}.

retention and the latter having only 15% absorbance retention after two chloroform rinses. Methanol resistivity did not show a specific pattern; however, it is notable that the nucleobase containing polymers showed moderate to high adhesion to glass slide where we tried to weaken hydrogen bonds using methanol. The adenine-functionalized copolymers showed highest solvent resistivity, with relative retention of absorbance intensities of 96% and 81% for BDT_d-3hT$_{Ad}$ and BDT_{eho}-3hT$_{Ad}$, respectively, followed by the thymine-containing copolymers, BDT_d-3hT$_{Thy}$ and BDT_{eho}-3hT$_{Thy}$, which retained 60% and 53% absorbance, respectively. Although it is better to avoid from direct quantitative comparisons because the Ad- and Thy-functionalized copolymers have different solubility toward chloroform (and presumably methanol), the essential point is that the ability of the nucleobase functionalized copolymers to interact through self-dimerization between groups is reflected in their relative solvent resistivity as compared to the non-functionalized copolymers.

In addition to somewhat qualitative assessments of solvent resistivity, additional information can be extracted by examining the intensity and shift in vibrational energies, as they are influenced by the hydrogen bonding environment.[195] FTIR spectra acquired from the BDT_{eho} and BDT_d series of copolymers dry powder samples are shown in Figure 2.12. Signatures due to CH bond stretching of the side chains at 2855 cm^{-1} and 2920 cm^{-1} are more prominent for the BDT_d-3hT$_X$ series than for the BDT_{eho}-3hT$_X$ copolymers, as expected.[196] The presence of adenine in BDT_R-3hT$_{Ad}$ copolymers is evident from the band at 1130 cm^{-1}, which is due to C–N bond stretching of the pyrimidine ring, and the mode at 1610 cm^{-1} correlates to both C=C and C=N stretches of the six-membered ring of adenine. In addition, the broad peak above 3000 cm^{-1} is attributed to stretching of N–H bonds (of the NH$_2$ group) and the mode at 1640 cm^{-1} derives from a scissoring mode of the NH$_2$ of adenine.[197–199] The spectra for the BDT_R-3hT$_{Thy}$ copolymers show characteristic bands due to the presence of thymine pendent groups. Specifically, broad bands due to vibrational modes of C(2)=O, C(4)=O, and C(5)=C(6) are seen $\approx$ 1680 cm^{-1}, a band arising from C(5)–CH3 bending is present at 1380 cm^{-1}, and the endocyclic C–N stretching mode is seen at 1260 cm^{-1}.[198, 200]

Previous studies report that the peak positions of out-of-plane N–H bending in thymine and NH$_2$ wagging in adenine are most sensitive to the hydrogen bonding environment.[197,
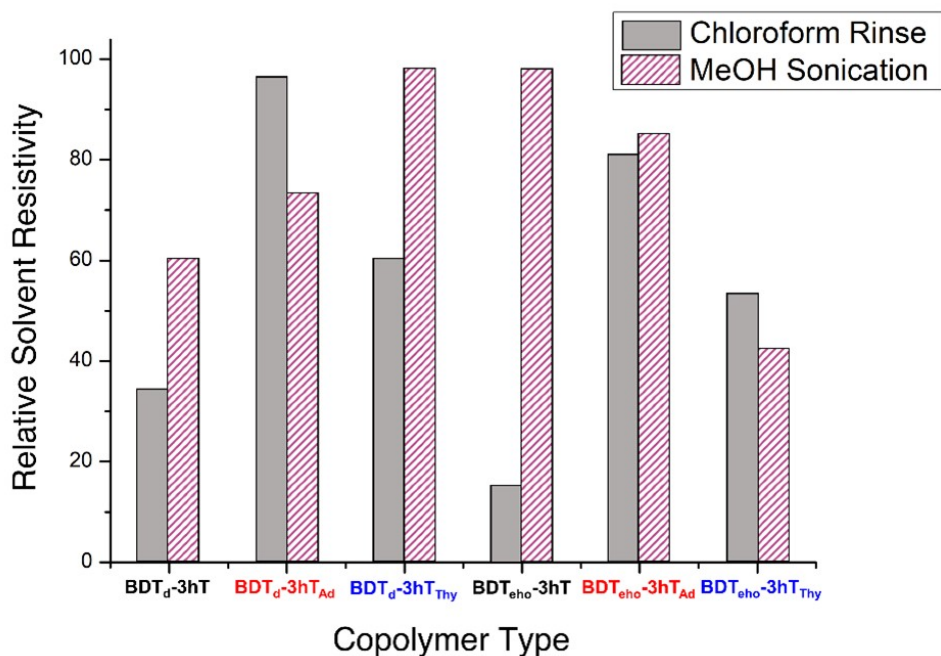
Figure 2.11: Relative solvent resistivity of BDT_R-$3hT_X$ copolymers, which results from normalizing the optical absorbance intensity of solvent-exposed films by the absorbance intensity of the as-cast thin film samples.
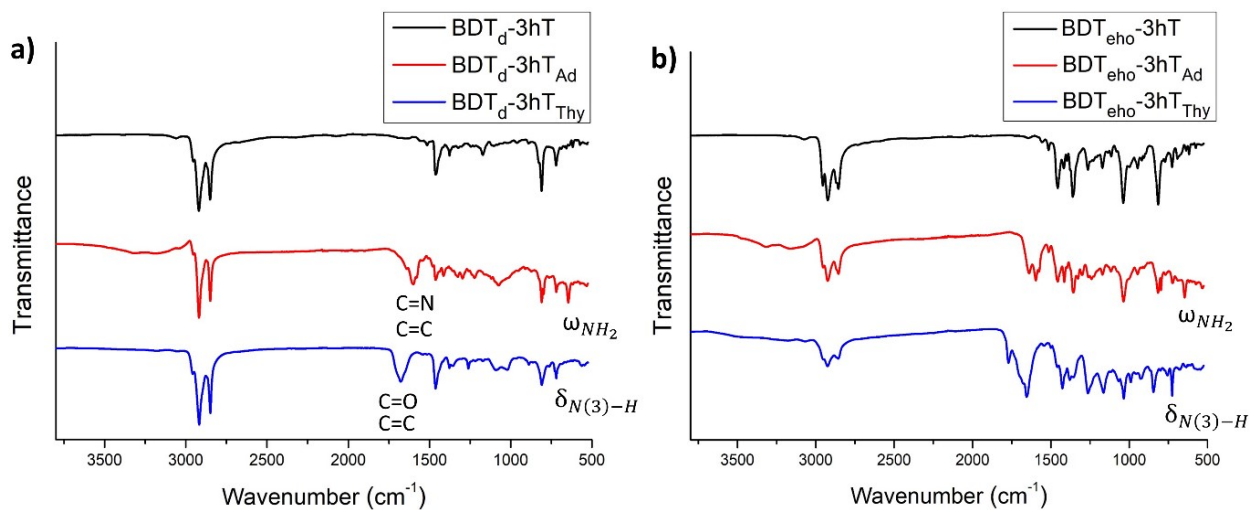
Figure 2.12: FTIR spectra of a) BDT_d-$3hT_X$ and b) BDT_{eho}-$3hT_X$ copolymers. Characteristic vibrational peaks for adenine and thymine groups in the region of 1600-1800 cm^{-1} are labeled. Bands that are correlated to NH_2 wagging (ω_{NH_2}) and N(3)H out of plane bending ($\delta_{N(3)-H}$) are specified.

198] In the BDT_{eho}-$3hT_{Thy}$, and BDT_d-$3hT_{Thy}$ copolymers, the out-of-plane N–H bending peaks are observed at 845 cm^{-1} and 810 cm^{-1}, respectively, which is similar to that of N1-methylthymine in the solid state (845 cm^{-1}). It is worth noting that the out of plane N–H bending of single-crystalline thymine-N1-methyl is reported at 882 cm^{-1},[198, 200] while the peak for isolated N(3)–H out-of-plane bending is estimated to be at 664 cm^{-1}.[197] Thus, the relative position of these modes suggest slightly stronger Thy$\cdots$Thy hydrogen bonding in BDT_{eho}-$3hT_{Thy}$ compared with BDT_d-$3hT_{Thy}$. For the BDT_d-$3hT_{Ad}$ and BDT_{eho}-$3hT_{Ad}$ copolymers, the NH_2 wagging band is observed at 646 cm^{-1}. NH_2 wagging band of adenine-N9-methyl in the solid state[199] and in single-crystalline[198] and matrix-isolated[197] forms are reported at 636 cm^{-1}, 690 cm^{-1}, and 530 cm^{-1}, respectively. The presence of this band at 646 cm^{-1} confirms that there is relatively strong hydrogen bonding in the adenine containing alternating copolymers, despite differences in their molecular weight. Small but noticeable differences between ethyl hexyloxy- and dodecyl-solublized polymers were observed in their FTIR spectra. Slightly sharper peaks in the region of 1600-1800 cm^{-1} and an extra shoulder peak are observed for the ethyl hexyloxy-substituted copolymers. These may be due to the ether groups of the side chains participating in hydrogen bonding, which has been reported for other alkoxyl groups.[201, 202] It is hard to conclusively compare O$\cdots$nucleobase hydrogen bonding and nucleobase$\cdots$nucleobase hydrogen bonding due to presence of multiple absorbance bands in that region from 1600-1800 cm^{-1}; however, it is expected that the ether-nucleobase hydrogen bonding interactions are weaker than hydrogen bonding between nucleobases.

2.4.5   Optical and Electronic Characterizations

As these alternating copolymers are novel, we used a variety of methods to assess the impact of the nucleobase functionality on the optical and electronic properties of the polymers. Results of UV-Vis and fluorescence spectroscopy for each of the copolymers in solution are shown in Figure 2.13. The unfunctionalized BDT_d-3hT copolymer shows an onset absorbance that is red-shifted by 50 nm from the BDT_{eho}-3hT copolymer, and this translates to a lower optical band gap energy as seen in Table 2.3. Both unfunctionalized copolymers exhibited very distinct absorbances with the BDT_d-3hT exhibiting three intense singlet transitions (S_0

– S_N, π-π^*) from $475 - 600$ nm, whereas the BDT_{eho}-3hT exhibited a strong absorbance peak at 500 nm and a shoulder at 550 nm. The absorption characteristics of the four functionalized copolymers show similar absorbance maxima ($\lambda_{max} = 450 - 500$ nm) with absorbance onsets ranging from $550 - 600$ nm, and are all blue-shifted from the unfunctionalized copolymers (BDT_{eho}-3hT and BDT_d-3hT). As evident from Figure 2.13, the fluorescence spectrum of each of the alternating copolymers in dilute solution show nearly identical emission profiles. Fluorescent quantum yields were $\phi = 0.16$ and $\phi = 0.19$ for the unfunctionalized copolymers and ranged from $\phi = 0.11 - 0.26$ for the BDT_d-3hT$_{Ad}$, BDT_d-3hT$_{Thy}$, DT_{eho}-3hT$_{Ad}$ and BDT_{eho}-3hT$_{Thy}$. Although no clear trend in fluorescence yield was observed in solution, polymer conformation at low concentrations can impact the fluorescence intensity.[203] The addition of adenine pendant groups to the BDT_{eho}-3hT copolymer lowered the fluorescence yield to $\phi = 0.11$ whereas the addition of a thymine group (BDT_{eho}-3hT$_{Thy}$) increased the emission intensity to $\phi = 0.23$. For the BDT_d-3hT copolymers, the quantum yields increased for the addition of both adenine and thymine pendant groups. Overall, the radiative rates of emission, k_s presented in Table 2.3 (or fluorescence lifetime, τ) are similar for all of the copolymers. Slightly varied quantum yields and radiative rates may be related to emission quenching or polymer conformations in solution induced by the nucleobase groups.[204]

In the solid state, solution cast thin films exhibited a red-shifted absorbance spectrum, which is common with close packing and π-π interactions in conjugated molecular materials.[205] The red-shifted peak absorbance (compared to solution) for the unfunctionalized BDT_{eho}-3hT was small ($\Delta\lambda = 4$ nm), whereas the analogous copolymer having the thymine or adenine pendant groups resulted in a red-shifted absorbance spectrum of $\Delta\lambda = 28$ nm (BDT_{eho}-3hT$_{Thy}$) and $\Delta\lambda = 36$ nm (BDT_{eho}-3hT$_{Ad}$) (Figure 2.14). The variation between thin film and solution absorbance is even greater with the BDT_d-3hT functionalized polymers, with a peak absorbance red-shift of $\Delta\lambda = 47$ nm for BDT_d-3hT$_{Thy}$ and $\Delta\lambda = 41$ nm for BDT_d-3hT$_{Ad}$. (See data in Table 2.3) The optical band gaps and slight absorbance shift for the unfunctionalized BDT_d-3hT and BDT_{eho}-3hT are consistent with behaviors reported by Yang *et al.* for a donor-acceptor alternating copolymer consisting BDT (with didodecyl oxide side chains) and thiophene.[206] For both types of nucleobase functionalized copolymers (BDT_d-3hT$_{Thy}$ and BDT_{eho}-3hT$_{Thy}$) there is a large spectroscopic
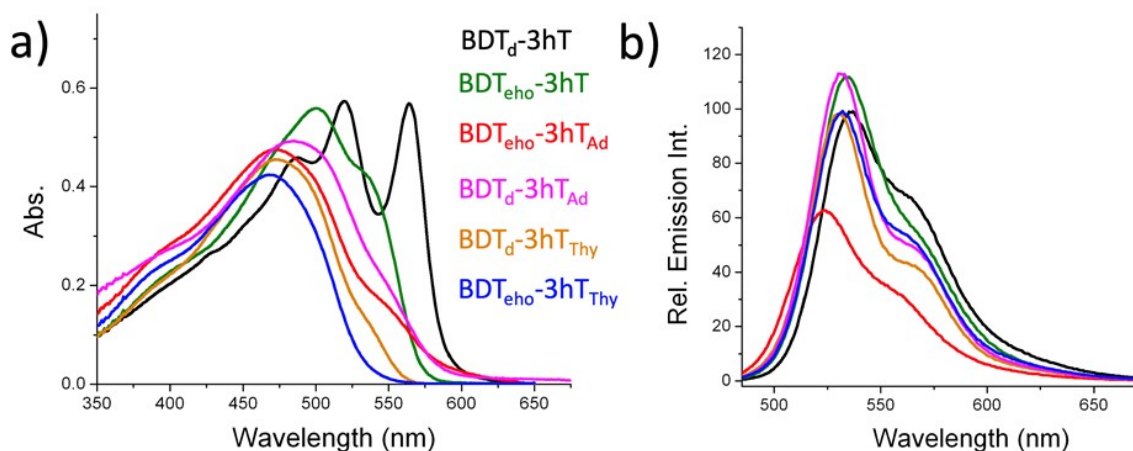
Figure 2.13: UV-Vis a) and fluorescence b) spectra of alternating copolymers in solution. Concentrations vary from 0.2-1.0 mM with emission spectra collected at 476 nm excitation. (Spectra were acquired using THF as the solvent, with the exception of BDT_d-$3hT_{Ad}$, which required a 1:1 mixture of DMSO and dichlorobenzene.) Line colors representing each copolymer are preserved between the two plots.
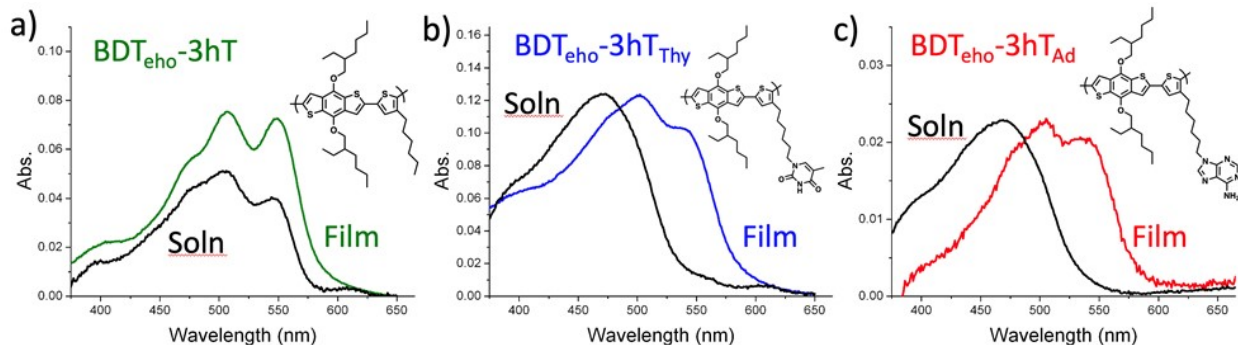
Figure 2.14: UV-Vis absorbance spectra of alternating copolymers in solution (THF) and thin films drop-cast from THF for a) BDT_{eho}-3hT, b) BDT_{eho}-$3hT_{Thy}$, and c) BDT_{eho}-$3hT_{Ad}$.

impact, presumably as a result of its impact on thin film structure and polymer chain packing.[141] Interestingly, the optical band gaps measured using the absorbance onset of the thin films are nearly identical for all of the functionalized and unfunctionalized copolymers (Table 2.3). This is encouraging and potentially useful for the development of polymer electronics, as it indicates that nucleobase pendant groups can be added to conjugated polymers for modulating their organization without strongly affecting their optical properties.

The electrochemical oxidative properties of all the copolymers were evaluated as dried films on glassy carbon electrodes. As seen in Figure 2.15, electrochemical characterization shows the onset of oxidation at 1.0 V vs. SCE for the BDT_d-3hT and BDT_{eho}-3hT unfunctionalized copolymers (Table 2.3). The addition of adenine and thymine pendant groups to the BDT_{eho}-3hT copolymer, shifts the onset of oxidation to more negative potentials, with a prominent strong oxidation peak indicating the presence of the nucleobases. The parent, non-nucleobase copolymer with (BDT_{eho}-3hT) had an oxidation onset of 0.99 V vs. SCE, which decreased with the addition of the adenine pendant group (BDT_{eho}-$3hT_{Ad}$) to 0.88 V vs. SCE and 0.85 V vs. SCE for thymine containing copolymers (BDT_{eho}-$3hT_{Thy}$). In the case of dodecyl side chain copolymers, the parent copolymer (BDT_d-3hT) had an oxidation onset of 1.00 V vs. SCE, which decreased to 0.97 V vs. SCE for BDT_d-$3hT_{Thy}$ and 0.79 V vs. SCE for BDT_d-$3hT_{Ad}$. This observation agrees with previous reports of electrochemical oxidation of adenine and thymine.[207] The BDT_d-$3hT_{Ad}$ and BDT_d-$3hT_{Thy}$ copolymers also show a more negative oxidation onset than the non-nucleobase parent copolymer; however, the adenine and thymine oxidation waves are hidden by the strong oxidation of BDT and thiophene heterocycles present in the backbone.

The charge transport properties of the copolymers were examined by solution processing thin films in hole-only devices for measuring the space charge limited current (SCLC) regime.[170] Devices consisted of spin coating the dissolved alternating copolymers onto PEDOT:PSS coated patterned ITO electrodes followed by thermal evaporation of a gold top contact. Due to variations in solubility, each copolymer required a particular solvent (or blend of solvents) to obtain uniform thin films. Film thicknesses measured by AFM were

Table 2.3: Photophysical Properties and Molecular Energy Levels of BDT_R-$3hT_X$ Alternating Copolymers.

Copolymer	$\lambda_\text{max-soln}$ $\lambda_\text{max-film}$ (nm)	$\Delta E_\text{gap-opt}$ (eV)[a]	ϕ[b]	τ (ps) k_s ($\times 10^8$ s^{-1})	E_ox (V)[c]	HOMO (eV)[d]	LUMO (eV)[d]
BDT_eho-3hT	503 (507)	2.12	0.16	855 (1.87)	0.99	-5.39	-3.27
BDT_eho-3hT$_\text{Ad}$	472 (505)	2.13	0.11	979 (1.12)	0.88	-5.28	-3.15
BDT_eho-3hT$_\text{Thy}$	469 (502)	2.11	0.23	855 (2.69)	0.85	-5.25	-3.14
BDT_d-3hT	519 (516)	2.10	0.19	897 (1.91)	1.00	-5.40	-3.30
BDT_d-3hT$_\text{Ad}$	477 (518)	2.07	0.26	886 (2.94)	0.79	-5.19	-3.12
BDT_d-3hT$_\text{Thy}$	473 (520)	2.09	0.22	828 (2.66)	0.97	-5.37	-3.28

[a] Estimated from the UV-Vis onset absorbance of the thin films
[b] Measured by comparison method using fluorescein standard
[c] Thin film electrochemical onset potentials are reported vs. SCE
[d] E_HOMO (eV) = -($E_\text{Ox-onset}$ + 4.4) eV, E_LUMO calculated using $E_\text{gap-opt}$
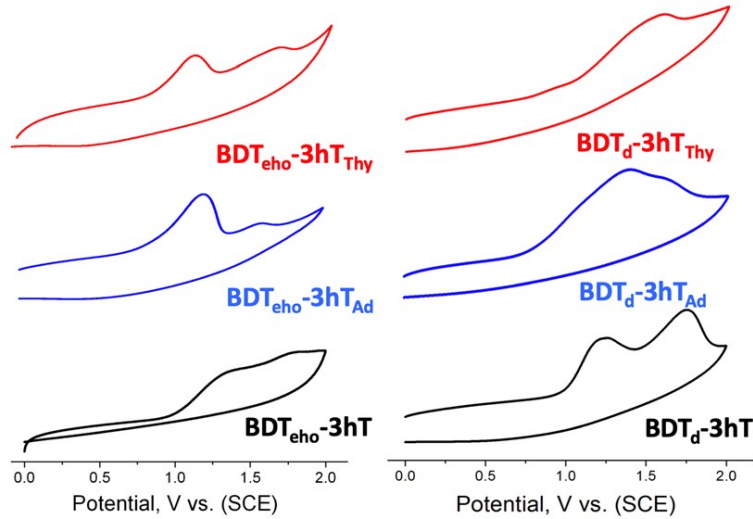
Figure 2.15: Cyclic voltammograms (electrochemical oxidative characterization) of alternating copolymers as dry films. The experiments were run in acetonitrile with 0.1 M TBAP and a scan rate of 100 mV s^{-1}.
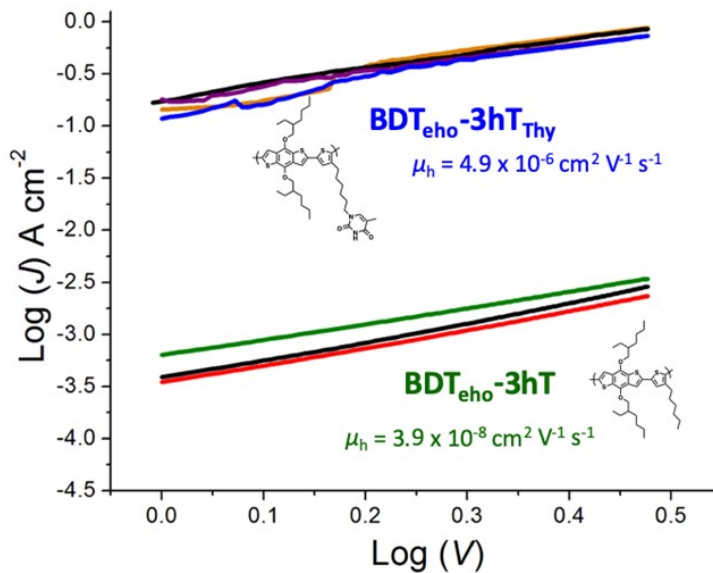
Figure 2.16: Hole mobility (Log J – Log V) for BDT$_{eho}$-3hT and BDT$_{eho}$-3hT$_{Thy}$ copolymer devices (ITO/PEDOT:PSS/BDT$_R$-3hT$_X$/Au) with structures and average mobilities inset in the plot. The individual lines correspond to tests of replicate devices. (Film thicknesses were 38 nm for BDT$_{eho}$-3hT and 30 nm for BDT$_{eho}$-3hT$_{Thy}$.)

8-38 nm, and these thicknesses agreed with model films produced on silicon wafers that were measured by spectroscopic ellipsometry.

Charge mobility, μ_h, for the BDT copolymers were determined from the slope of the current density (J) versus applied potential (V_a) and fit to the simplified Mott-Gurney equation:

$$J = \frac{9}{8}\epsilon\epsilon_0\mu_h\frac{V_a{}^2}{L^3} \tag{2.1}$$

In this expression, L is the measured polymer film thickness, μ_h is the hole mobility, ϵ_0 is the absolute permittivity and relative permittivity taken as $\epsilon = 3$. A representative plot, expressed as log J versus log V, is presented as Figure 2.16, which compares the behavior of BDT$_\text{eho}$-3hT and BDT$_\text{eho}$-3hT$_\text{Thy}$. The devices show slopes ranging from 1.4 to 2.3, which are in close agreement with SCLC charge mobility model.[208] For each copolymer, an average hole mobility derived from measurements of three to six device mobilities is reported in Table 2.4. Unfunctionalized BDT$_\text{eho}$-3hT showed the lowest hole mobility with little device-to-device variation and an average hole mobility of 3.9×10^{-8} cm^2 V^{-1} s^{-1}. Higher mobilities were observed for the unfunctionalized dodecyl-functionalized BDT copolymer, BDT$_\text{d}$-3hT, which displayed an average hole mobility of 7.1×10^{-6} cm^2 V^{-1} s^{-1}. Although molecular weight can have a significant impact on mobility, polymer chain packing is also a strong contributing factor for conjugated polymeric materials.[209] The hole mobility for BDT$_\text{d}$-3hT is similar to values previously reported for BDT-based polymers.[210] A significant enhancement of hole mobility was shown with the addition of nucleobases for the BDT$_\text{eho}$-3hT copolymers. The parent, non-nucleobase BDT$_\text{eho}$-3hT yielded a hole mobility of $\mu_h = 3.9 \times 10^{-8}$ cm^2 V^{-1} s^{-1}, but adenine pendant group copolymer (BDT$_\text{eho}$-3hT$_\text{Ad}$) increased the hole mobility to $\mu_h = 1.8 \times 10^{-7}$ cm^2 V^{-1} s^{-1}, while thymine pendant group copolymer (BDT$_\text{eho}$-3hT$_\text{Thy}$) yielded even higher hole mobility of $\mu_h = 4.9 \times 10^{-6}$ cm^2 V^{-1} s^{-1}. The dodecyl-functionalized BDT copolymers had similar hole mobilities of $\mu_h = 7.1 \times 10^{-6}$ cm^2 V^{-1} s^{-1} for BDT$_\text{d}$-3hT, $\mu_h = 6.1 \times 10^{-6}$ cm^2 V^{-1} s^{-1} for BDT$_\text{d}$-3hT$_\text{Ad}$ and $\mu_h = 1.5 \times 10^{-6}$ cm^2 V^{-1} s^{-1} for BDT$_\text{d}$-3hT$_\text{Thy}$. Although the nucleobase functionalized copolymers have slightly lower hole mobilities than the parent BDT$_\text{d}$-3hT, they are also one-third the

molecular weight, as seen in Table 2.1. This molecular weight difference may offset the impact of the nucleobase-induced organization.

The mobility enhancements observed with BDT_{eho}-$3hT_{Thy}$ and BDT_{eho}-$3hT_{Ad}$ correlate with close and well-organized packing, which has been shown to greatly improve charge mobility in thymine-containing conjugated polymers.[141] The dodecyl side chain of the BDT_d-$3hT_{Thy}$ may influence the copolymer stacking such that the probability of H- bonding interactions between nucleobases on adjacent copolymer chains is reduced, and therefore lowers organization and free-charge carrier conduction. Taken in aggregate, these results demonstrate a slightly more intricate overall picture of nucleobase inclusion on organization and interactions of conjugated polymers, which along with the robust and generally facile syntheses, provides opportunities to further tune their optoelectronic properties using subtle structural variations through side chain engineering.

Finally, to examine whether enhancing the solubility and breaking interbase hydrogen bonding affected mobility, we increased the temperature to heat the solutions before casting from 60 °C to 120 °C. As seen in Table 2.4, the hole mobility for BDT_{eho}-3hT increased by two orders of magnitude while the hole mobilities of the BDT_{eho}-$3hT_{Ad}$ and BDT_{eho}-$3hT_{Thy}$ copolymers were minimally affected. Considering that heating was necessary for the BDT_{eho}-3hT to achieve mobilities consistent with devices made using BDT_{eho}-$3hT_{Thy}$, one striking conclusion that can be inferred from these behaviors is that thymine groups in the side chains can improve the morphology or nanoscale organization in a manner similar to thermal annealing. In the case of dodecyl-functionalized copolymers, the hole mobility measured for the non-nucleobase containing BDT_d-3hT copolymer decreased when the 120 °C spin coating protocol was implemented, while the mobilities measured for films made from the BDT_d-$3hT_{Ad}$ and BDT_d-$3hT_{Thy}$ were minimally affected, suggesting better organization stability due to interbase interactions.

2.5   Conclusions

Stille cross-coupling polymerizations provide access to complementary pairs of donor-acceptor conjugated copolymers based on BDT and 3-alkyl thiophenes in which side

chains contain adenine or thymine functionalities. The facility of the synthetic approach engenders opportunities to examine links between copolymer design, self-complementary and complementary H-bonding interactions, and π-stacking interactions on fundamental material properties and performance. Evidence from a variety of studies on small molecules and conjugated polymers demonstrate that nucleobase functionalities can have significant effects on polymer stacking and solid-state electronic properties, with vibrational spectroscopy and solvent resistivity studies demonstrating inter-nucleobase hydrogen bonding in the solid state. The observation of enhancements in free charge carrier mobility has been reported previously, and we have also observed this phenomenon with adenine and thymine pendant groups attached to a novel BDT-containing conjugated copolymer having ethylhexoxy solubilizing side chains. The dodecyl-functionalized BDT copolymers also suggest this phenomenon, since the adenine and thymine nucleobase containing copolymers have hole mobilities similar to the parent non-nucleobase containing copolymer, even though they are one-third the molecular weight. Both results align with the degree of red-shifted absorbance onset observed when comparing solution and dried films, ultimately, providing early clues of copolymer organization that is influenced by inter-base hydrogen bonding in the adenine- and thymine-functionalized copolymers. Hole mobility of the polymers with nucleobase pendant groups are less dependent on the processing and thermal treatments, a behavior that also is attributed to inter-base hydrogen bonding in the solid state. These studies also suggest that there is a sensitive interplay between the strength, type, and number of non-bonded intermolecular interactions present in these copolymers. Additionally, this study provides spectroscopic clues of fluorescence quenching by an adenine pendant group, and the onset of electrochemical oxidation of the nucleobase pendant groups at lower potentials than the copolymer primary chain. Taken together, these materials show a range of exciting properties most notably, moderate hole mobilities and strong light absorbing and emission properties, which are useful for organic photovoltaic and light-emitting diode molecular electronic applications. Moreover, they offer the potential to tease apart connections between molecular design, organization, and properties.

Table 2.4: Charge (Hole) Mobility Measurements of BDT_R-$3hT_X$ Alternating Copolymers.

Copolymer	μ_h (T = 60 °C)^a cm^2 V^{-1} s^{-1}	μ_h (T = 120 °C)^b cm^2 V^{-1} s^{-1}	Nucleobase attachment
BDT_{eho}-$3hT$	3.9×10^{-8} $\pm 1.9 \times 10^{-8}$	3.8×10^{-6} $\pm 1.9 \times 10^{-6}$	-
BDT_{eho}-$3hT_{Ad}$	1.8×10^{-7} $\pm 3.1 \times 10^{-8}$	1.0×10^{-7} $\pm 2.6 \times 10^{-9}$	N9
BDT_{eho}-$3hT_{Thy}$	4.9×10^{-6} $\pm 6.5 \times 10^{-6}$	1.2×10^{-6} $\pm 7.3 \times 10^{-7}$	N1
BDT_d-$3hT$	7.1×10^{-6} $\pm 4.1 \times 10^{-7}$	7.7×10^{-7} $\pm 2.3 \times 10^{-7}$	-
BDT_d-$3hT_{Ad}$	6.1×10^{-6} $\pm 6.6 \times 10^{-7}$	5.2×10^{-6} $\pm 5.6 \times 10^{-6}$	N9
BDT_d-$3hT_{Thy}$	1.5×10^{-6} $\pm 4.7 \times 10^{-7}$	2.5×10^{-6} $\pm 9.6 \times 10^{-7}$	N1

^{a} Average mobility of three to six devices (device configuration ITO/PEDOT:PSS/BDT_R-$3hT_X$/Au) when textsubscriptR-$3hT_X$ was spin cast at 60 °C.
^{b} Average mobility of three to six devices (device configuration ITO/PEDOT:PSS/BDT_R-$3hT_X$/Au) when textsubscriptR-$3hT_X$ was spin cast at 120 °C.

Chapter 3

Synthesis of a Soluble Adenine-Functionalized Polythiophene through Direct Arylation Polymerization and its Fluorescence Responsive Behavior

This chapter describes the work published in Polymer Chemistry, 11, (2020), 820-829. I designed and tested the direct arylation polymerization method and optimized its conditions for the specific adenine-containing monomer that I synthesized. I also performed the structural, thermal, and optical characterizations, as well as the tests involving metal ion binding. Coauthors include Graham S. Collier and M. Nance Ericson who helped in narrating the photophysical properties, and Prof. S. Michael Kilbey II, who advised this work.

3.1 Abstract

Side chain engineering has been used widely to expand the functionality and enhance the solubility of conjugated polymers, promoting their utility in various applications. Herein, we report the synthesis of an adenine-functionalized, thiophene-based alternating copolymer via direct arylation polymerization. This nucleobase-modified, alkyl thiophene-based alternating copolymer was accessed by copolymerization of a Boc-protected, adenine functionalized thiophene monomer 9-(6-(2,5-dibromothiophen-3-yl)hexyl)-9H-purine-6-amine) (T_{Ad}), with 3,3',3'',4'-tetrahexyl-2,2':5',2''-terthiophene, (tT_{4h}). Quantitative post-polymerization deprotection of Boc groups results in the adenine bearing alternating copolymer (T_{Ad}-tT_{4h}), which is soluble in common organic solvents due to steric hindrance-induced flexibility of the tT_{4h} comonomer, which allows structure-property relationships to be established. In comparison to the unfunctionalized analogue, interchain hydrogen bonding through the adenine functionality increases the rigidity of the copolymer, resulting in a $\approx$ 70 °C increase in the glass transition temperature. Furthermore, the improved solubility of the copolymer and capacity for strong metal ion binding by the nucleobase leads to dramatic fluorescence quenching ($> 90\%$) upon the addition of Cu^{2+} ions, which is also reflected in a high Stern-Volmer constant of 1.28×10^4 M^{-1}. The fluorescence emission is recovered almost completely after washing the copolymer solution with EDTA-disodium salt aqueous solution. These findings demonstrate the viability of synthesizing soluble bio-inspired, fully conjugated copolymers via direct arylation polymerization as well as the influence of the hydrogen bonding nucleobase on thermal, optical, and metal-ion sensing properties.

3.2 Introduction

Side chain engineering is used extensively to manipulate optoelectronic or physical properties of conjugated polymers.[51, 136, 211–215] Solubilizing side chains minimize the tendency of conjugated polymers to aggregate or crystallize, which are behaviors driven by π-π stacking interactions and backbone rigidity.[216] In addition, side chain functionality also can be used to manipulate optoelectronic properties. Electron donating or electron withdrawing groups that are in close proximity to the backbone typically will change the HOMO and LUMO of the conjugated polymer.[51, 57, 217] Functional groups at the terminus of the side chain tend to influence electronic properties of the conjugated polymer indirectly by influencing the morphology, backbone planarity, or interchain interactions.[218–220] One useful strategy for controlling morphology while enhancing thermal stability and solvent resistivity of bulk heterojunction (BHJ) organic photovoltaics (OPVs) or organic field effect transistors (OFETs) is to integrate functional motifs into side chains that interact through hydrogen bonding interactions.[91, 221–223] For example, Stupp and coworkers compared the OPV performance of two diketopyrrolopyrrole-based, donor-type small molecules, where the only difference in design was the presence of either amide or ester functionalities at the same location in the side chains.[222] Although both molecules showed similar optoelectronic properties, OPVs based on the amide-functionalized molecule exhibited power conversion efficiencies (PCEs) that were 50% higher than OPVs made with the ester-functionalized molecule. They attributed the increase in PCE to the self-complementary hydrogen bonding between amide groups in the side chains. These non-bonded, pair-wise intermolecular interactions compete with π-π stacking, resulting in a morphology with a smaller domain size.[222] Additionally, Yao *et al.* showed interchain packing order of a diketopyrrolopyrrole copolymer is improved upon introduction of urea functionality in the side chain. The hydrogen bonding ability of urea groups promoted lamellar stacking that enhanced hole mobility.[143] The benefits of hydrogen bonding (H-bonding) motifs in the side chains of conjugated polymers extend beyond improving the performance of OPVs or OFETs. A variety of studies have shown that H-bonding groups in conjugated polymers engenders their use in applications such as optical DNA sensors or ion detectors.[224–231] In total,

these studies highlight the utility of hydrogen bonding groups, in side chains as means to expand or improve the performance of conjugated polymers.

Nucleobases, which are used by nature and offer complementary hydrogen bonding motifs, have been explored extensively as side chain functionality in polymeric materials, especially in non-conjugated polymers.[85, 87, 90, 232, 233] Nucleobase-functionalized polymers have shown promise in numerous applications, including polymer adhesives, self-healing materials, donor and acceptor compatibilization, and sensors.[91, 234, 235] In the realm of conjugated polymers, a promising improvement in hole transport properties was observed by Cheng *et al.*, who synthesized a uracil-functionalized polythiophene via oxidative polymerization and used this material as a hole transport layer.[91] Similarly, Yang *et al.* fabricated an organic field-effect transistor (OFET) device based on thymine-functionalized diketopyrrolopyrrole copolymer. They observed that hydrogen bonding between thymine groups located at the terminus of the side chains created interchain connectivity, which increased the charge mobility of the conjugated polymer. In the same study, the ability of metal ions, such as Pd^{2+} or Hg^{2+}, to coordinate with thymine was used as a basis to tailor the selectivity of an OFET-based gas sensor toward gases such as CO and H_2S.[141] This ability of metal ions to form strong coordinate bonds with nucleobases is also the basis of solution detection of metal ions.[236] In the realm of conjugated polymers, Tang *et al.* observed that the binding of Hg^{2+} with a thymine-functionalized analog of poly(3-hexylthiophene) resulted in fluorescence quenching.[231] Similarly, Xing *et al.* demonstrated that the fluorescence of a thymidine-functionalized polythiophene was quenched upon addition of Cu^{2+}.[224]

Although nucleobase functionalities provide a way to enhance the properties and improve the performance of conjugated polymers, there remains significant challenges related to synthetic methodology and solubility of nucleobase-functionalized conjugated polymers. For example, adenine-, thymine-, and uracil-functionalized polythiophenes have been synthesized via oxidative polymerization of 3-(ω-[nucleobase]hexyl)thiophene, which requires stoichiometric amounts of iron (III) chloride for polymerization and generally results in a polymer with limited solubility.[91, 93, 224, 231] Iron (III) chloride is a harmful and highly corrosive and even intense post-polymerization purification leaves behind substantial amount of iron compounds ($\approx$ 1000 ppm).[98, 237] The presence of these metal impurities

may limit use of the resulting nucleobase-functionalized conjugated polymers in biological applications.[238] Additionally, nucleobases are known to have limited solubility in organic solvents due to their strong hydrogen bonding and π-stacking. The adenine-functionalized poly(3-alkylthiophene) reported by Cheng *et al.* was found to be insoluble in most organic solvents, even at molecular weights as low as $M_n = 2.8$ kg/mol.[92, 93] These limitations motivate efforts to explore more benign synthetic methodologies as well as to develop useful routes to maintain functionality while offering improved solubility.

Recently, direct arylation polymerization, which is commonly referred to as "DArP", has become a robust methodology for synthesizing conjugated polymers using diverse comonomer building blocks.[116, 239] DArP is considered a green, less toxic polymerization method for two reasons. First, the need for organometallic comonomers is eliminated in DArP due to direct activation of (hetero)aromatic hydrogens, which simplifies monomer synthesis and reduces the number of synthetic steps.[116, 239–243] Second, because DArP does not require organometallic comonomers, toxic byproducts, such as organotin species that are produced in stoichiometric amounts in Stille cross-coupling polymerizations, for example, are no longer generated. Reynolds and coworkers found the polymer synthesized through DArP contain 100 times less catalyst impurities compared to the one synthesized by oxidative polymerization.[244] While DArP has been used to synthesize various conjugated polymers, especially polythiophenes, its functional group tolerance and more specifically its potential with nucleobase-functionalized materials remains unexamined.

Herein, we report the synthesis of a soluble adenine-functionalized, alternating polythiophene copolymers via DArP. Within this effort, the effect of the electron-rich and chelating adenine functionality on the polymerization is studied in detail. We describe the impact of adenine-functionality as a hydrogen bonding active and highly chelating group on photophysical properties, and thermal transitions. Additionally, chelation-induced fluorescent quenching upon binding copper ions with adenine and its reversibility are examined. This work expands the synthetic toolbox for nucleobase-functionalized conjugated polymers, while also providing insight into functional group tolerance of DArP, exemplifying the importance of monomer design and side chain engineering on the synthesis, solubility, and properties of these nucleobase-functionalized conjugated polythiophenes.

3.3 Synthesis and Characterization

3.3.1 Methods and Materials

All chemicals and solvents were purchased from Sigma-Aldrich or Fisher Scientific and used as received, unless stated otherwise. Tetrakis triphenylphosphine palladium(0) $(Pd(PPh_3)_4)$ was purchased from Strem Chemicals and used without extra purification. Toluene, tetrahydrofuran (THF), and N,N-dimethylformamide (DMF) were purified using an Innovative Technologies MD-5 Solvent Purification System and degassed prior to use. N-Bromosuccinimide (NBS) was recrystallized from hot water prior to use. All synthesized materials were purified via column chromatography using 60 Å silica gel (40-63 µm, Sorbent Technologies).

^{13}C and ^{1}H gradient-enhanced heteronuclear multiple bond correlation (gHMBC) and gradient-enhanced heteronuclear single quantum coherence (gHSQC) NMR spectra of synthesized molecules or polymers were acquired using a Varian VNMRS 500 MHz NMR or a Varian Mercury Vx 300 MHz NMR at room temperature using 15–20 mg mL^1 solutions in deuterated chloroform (CDCl$_3$). Chemical shifts are reported in units of δ (ppm) and referenced to the residual solvent peak. Mass spectrometry measurements used a JEOL AccuTOF DART mass spectrometer with toluene solutions at $\approx$ 1 mg mL^{-1}. The average molecular weight and dispersity of synthesized polymers were determined by gel permeation chromatography (GPC) using universal calibration analysis based on polystyrene (PS) standards (Agilent, EasiVial PS-M, MW 162, 370, 945, 1,230, 3,090, 6,320, 13,000, 27,800, 45,100, 107,000, 217,000, 364,000 g/mol). For this, an Agilent 1260 Infinity II isocratic pump equipped with two Agilent (7.5 × 300 mm) mixed-D type columns in sequence was used. Samples were dissolved in THF at nominal concentrations of 5 mg/mL and passed through a 0.2 µm PTFE filter prior to analysis. The flow rate of the THF mobile phase was set at 1 mL/min. Thermal stability of the polymers in a nitrogen (N$_2$) atmosphere was determined using a TA Instruments Q50 Thermogravimetric Analyzer (TGA). The protocol used consisted of ramping from room temperature to 800 °C using a heating rate of 10 °C/min with the analytes in a platinum pan. Thermal transitions were measured by differential scanning calorimetry (DSC) using a TA Instruments Q-2000 DSC. Samples of nominally $\approx$

5 mg were sealed standard aluminum pans and subjected to a heat–cool–heat cycle from 40 °C to 270 °C at a heating rate of 10 °C/min and a cooling rate of 10 °C/min under an N_2 atmosphere. Optical absorbance spectra were acquired using a Thermo Scientific Evolution 600 UV-Vis spectrophotometer by scanning from 225-650 nm. The polymer solution concentration was fixed at 0.01 mg/mL. Fluorescence emission spectra were acquired from polymer solutions (at 0.01 mg/mL in $CHCl_3$ and either 0.01 mg/mL or 0.02 mg/mL in THF) using a Cary Eclipse fluorescence spectrophotometer. An excitation wavelength of 360 nm was used, and emission measured by scanning from 370-700 nm.

3.3.2 Synthesis of Boc-Protected Adenine-Functionalized Monomer, M2

Synthesis of intermediate molecules required to synthesis of M2 including: 3-(6-bromohexyl)thiophene, 2,5-dibromo-3-(6-bromohexyl)thiophene, and adenine-containing dibromo thiophene monomer (labeled as M1 in this chapter) are described in Chapter 2.

50 mL of dry and degassed THF was added to a dry 100 mL round bottom flask under positive argon pressure. 485.3 mg (1.06 mmol, 1 equiv.) of (9-(6-(2,5-dibromothiophen-3-yl)hexyl)-9H-purine-6-amine) was added to the flask. Then, 38 mg (0.311 mmol, 0.3 equiv.) of 4-dimethylaminopyridine (DMAP) was added to the solution followed by 694 mg of di-*tert*-butyl dicarbonate (Boc$_2$O, 3.18 mmol, 3 equiv.). (All were added under positive Ar pressure.) The reaction flask was equipped with a mineral oil bubbler to allow carbon dioxide (CO_2) that is produced to be released, and the mixture was stirred for 24 h. After this time, the solvent was removed by rotary evaporation. Silica gel column chromatography was used to recover the desired product, using 3 vol% MeOH in DCM as the mobile phase. The bis-N-Boc protected product was collected as a pale brownish oil in 95% yield. ^{1}H NMR (300 MHz, CDCl$_3$), δ (ppm): 8.77 (s, 1H, adenine-C2-H), 8.00 (s, 1H, adenine-C8-H), 6.66 (s, 1H, thiophene-C4-H), 4.19 (t, 2H, J = 7.2 Hz, adenine-N9-CH$_2$), 2.39 (t, 2H, J = 7.5 Hz, thiophene-C3-CH$_2$), 1.92 – 1.79 (m, 2H) 1.50 – 1.40 (m, 2H), 1.36 (s, 18H, CH$_3$), 1.31 – 1.22 (m, 4H). ^{13}C NMR (300 MHz, CDCl$_3$) δ (ppm): 153.4 (adenine-C4), 151.8 (adenine-C2), 150.4 (Boc-carbonyl), 150.1 (adenine-C6), 144.7 (adenine-C8), 142.4 (thiophene-C3), 130.8

(thiophene-C4), 128.7 (adenine-C5), 110.4 (thiophene-C5), 108.0 (thiophene-C2), 83.5 (Boc-tertiary carbon), 44.1 (adenine-N9-CH2), 29.7, 29.2, 29.1, 28.3, 27.7 (Boc-methyls), 26.3. AccuTOF DART: calc'd [M+H$^+$]: 660.0678, found: 660.05927.

3.3.3 Synthesis of Terthiophene Comonomer, 3,3',3",4'-Tetrahexyl-2,2':5',2"-Terthiophene, tT$_{4h}$

30 mL of dry and degassed toluene was added to a dry 100 mL round bottom flask under positive argon pressure. 615.4 mg (483 μL, 1.5 mmol, 1 equiv.) of 2,5-dibromo-3,4-dihexylthiophene was added to the flask. Then, 1103 mg (1.291 mL, 3.75 mmol, 2.5 equiv.) of 3-hexylthiophene-2-boronic acid pinacol ester was added to the solution. While the flask was under positive argon pressure, 86.6 mg (0.075 mmol, 0.05 equiv.) of tetrakis(triphenylphosphine) palladium (0) (Pd(PPh$_3$)$_4$) and then 30 mL of a 2M aqueous K$_2$CO$_3$ solution (20 equiv.) were added to the reaction mixture. After adding the K$_2$CO$_3$, a reflux condenser was attached to the flask and the mixture was stirred for 24 h in an oil bath set to 100 °C. After this time, the reaction was quenched by adding 50 mL of water. The reaction mixture was extracted with 100 mL of toluene and the extract was washed with water and a brine solution. Toluene was removed under reduced pressure and the product was purified via column chromatography using hexanes as the mobile phase. The product was collected as a colorless oil in 80% yield. ^{1}H NMR (300 MHz, CDCl$_3$), δ (ppm): 7.28 (d, 2H, J = 5.3 Hz, thiophene-C5), 6.96 (d, 2H, J = 5.3 Hz, thiophene-C4), 2.58-2.44 (m, 8H, thiophene-CH$_2$), 1.62-1.50 (m, 4H, thiophene-alkyl) 1.49-1.37 (m, 4H, thiophene-alkyl), 1.30-1.19 (m, 24H, thiophene-alkyl) 0.91-0.82 (m, 12H, thiophene-alkyl-CH$_3$) ^{13}C NMR (300 MHz, CDCl$_3$) δ (ppm): 142.20 (thiophene-C2), 141.82 (thiophene-C2'), 129.37 (thiophene-C3'), 129.11 (thiophene-C3), 128.51 (thiophene-C4), 125.02 (thiophene-C5), 31.64, 31.49, 30.74, 30.66, 29.42, 29.13, 28.89, 28.00, 22.58, 22.53, 14.07, 14.04. AccuTOF DART: calc'd [M+H$^+$]: 585.3622, found: 585.3527.
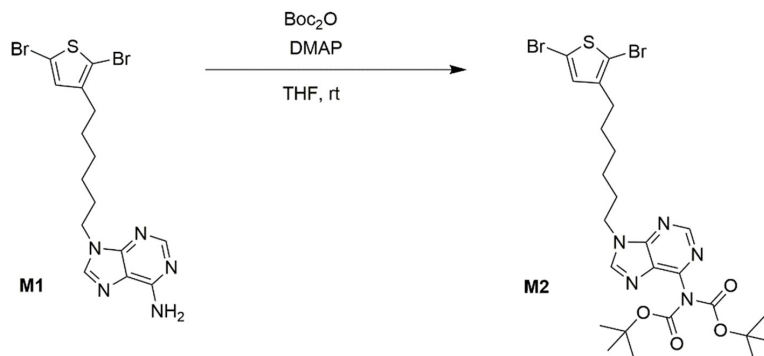
Figure 3.1: Protection of the amine group in adenine-containing monomer using bulky Boc groups.
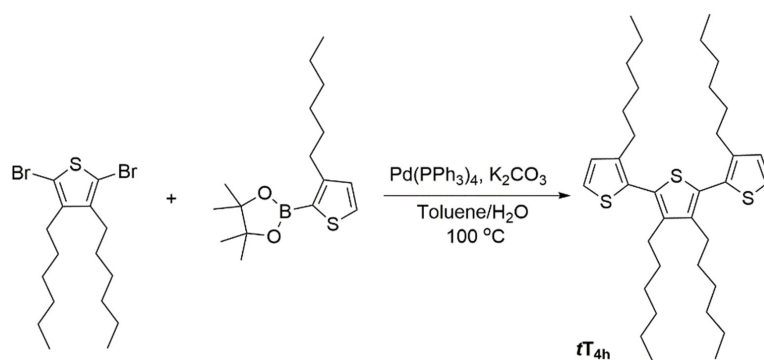
Figure 3.2: Suzuki cross-coupling to synthesize tetrathiophene, $t\text{T}_{4h}$, comonomer.

3.3.4 Synthesis of Other Small Molecules

Synthesis of Adenine-N9-Hexyl

Adenine (540 mg, 4 mmol, 1 equiv.) was dissolved in 50 mL of dry DMF in a 150 mL round bottom flask under an Ar atmosphere. Then, 1-bromohexane (556 μL, 660 mg, 6 mmol, 1.5 equiv.) and K_2CO_3 (1.104 g, 8 mmol, 2 equiv.) were added to the flask under a positive Ar atmosphere. The mixture was stirred for 24 h and then the solvent was removed under vacuum. The remaining solid was washed with water, dissolved in chloroform, and was subsequently purified via column chromatography with chloroform and MeOH (5 vol%) as the mobile phase. The product was collected and the solvent removed via rotary evaporation, resulting in a white powder (55% yield based on isolated product). ^{1}H NMR (500 MHz, CDCl$_3$), δ (ppm): 8.30 (s, 1H), 7.74 (s, 1H), 6.65 (s, 2H), 4.12 (t, 2H, J = 7.2 Hz), 1.85 − 1.79 (m, 2H) 1.26 − 1.21 (m, 6H), 0.81 − 0.78 (m, 3H). ^{13}C-NMR (500 MHz, CDCl$_3$) δ (ppm): 155.9, 152.8, 149.9, 140.2, 119.5, 43.9, 31.1, 30.0, 26.2, 22.4, 13.9. AccuTOF DART: calc'd [M+H$^+$]: 220.2998, found: 220.3104.

Synthesis of Adenine-N9-Methyl

50 mL of dry DMF was added to a 150 mL round bottom flask that contained adenine (75.1 mg, 0.56 mmol, 1 equiv.). Then, iodomethane (52.3 μL, 119.2 mg, 0.84 mmol, 1.5 equiv.) and K_2CO_3 (138 mg, 1 mmol, 2 equiv.) were added to the flask under a positive Ar atmosphere. The mixture was stirred for 24 h and then the solvent was removed under vacuum. The remaining solid was washed with water and then purified using silica gel column chromatography with chloroform and added MeOH (5 vol%) as mobile phase to recover the desired product. The product was collected and the solvent removed via rotary evaporation, resulting in a white powder (67% yield based on isolated product). ^{1}H NMR (300 MHz, (CD$_3$)$_2$SO), δ (ppm): 8.11 (s, 1H), 8.05 (s, 1H), 7.13 (S, 2H), 3.69 (s, 3H). AccuTOF DART: calc'd [M+H$^+$]: 149.0701, found: 149.0853.
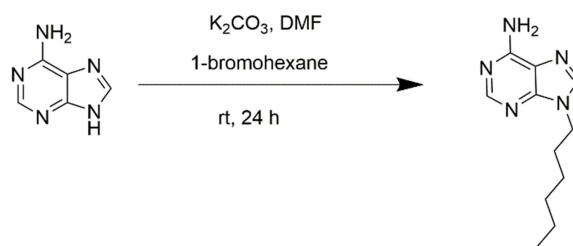
Figure 3.3: Alkylation of adenine to synthesize adenine-N9-hexyl.
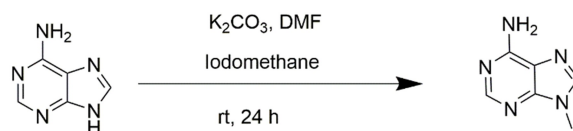
Figure 3.4: Alkylation of adenine to synthesize adenine-N9-methyl.
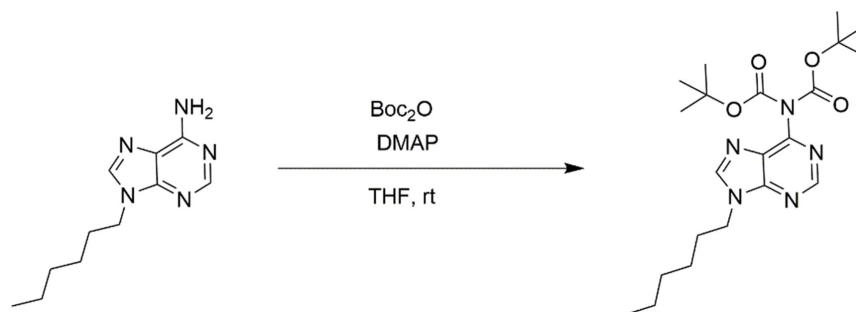
Figure 3.5: Addition of Boc groups to protect amine functionality of adenine.

Synthesis of Boc-Protected Adenine-N9-Hexyl

25 mL of dry and degassed THF was added to a dry 50 mL round bottom flask under positive argon pressure. Adenine-N9-hexyl (438.5 mg, 2 mmol, 1 equiv.) was added to the flask and then 76 mg (0.62 mmol, 0.3 equiv.) of DMAP (4-Dimethylaminopyridine) was added to the solution. 1.091 g of di-*tert*-butyl dicarbonate (Boc$_2$O, 5 mmol, 2.5 equiv.) was added to the mixture under positive argon pressure. Then, the mixture was stirred for 24 h while equipped with bubbler to allow CO$_2$ gas evolved during the reaction to escape. After this time, the solvent was removed by rotary evaporation. Silica gel column chromatography was used to recover the product, and DCM with 5 vol% MeOH was used as the mobile phase. The bis-N-Boc protected product, a pale brownish oil, was collected as the major product in 85% yield. ^{1}H NMR (300 MHz, CDCl$_3$), δ (ppm): 8.84 (s, 1H), 8.04 (s, 1H), 4.26 (t, 2H, J = 7.2), 1.92 – 1.87 (m, 2H), 1.42 (s, 18H), 1.33 – 1.26 (m, 6H), 0.86 – 0.81 (m, 3H). ^{13}C NMR (300 MHz, CDCl$_3$) δ (ppm): 153.4, 151.9, 150.5, 150.2, 144.7, 128.8, 83.6, 44.2, 31.1, 29.8, 27.8, 26.3, 22.4, 13.9. AccuTOF DART: calc'd [M+H$^+$]: 420.5338, found: 420.5374.

3.4 Optimization of DArP Conditions

3.4.1 Regular AA+BB DArP (Test) Reaction

Typical test conditions for direct arylation polymerization (DArP) of P3HT following procedures suggested by Thompson *et al.*[121] are shown in Figure 3.6. 15 mL of dry and degassed N,N-dimethylacetamide (DMAc) was transferred via cannula into a dry 50 mL round bottom flask. Then, 2,5-dibromo-3-hexylthiophene (326 mg, 1 mmol) and 3-hexylthiophene (168 mg, 1 mmol) were added to the flask via syringe. Neodecanoic acid (57 μL, 51 mg, 0.3 mmol), K$_2$CO$_3$ (276 mg, 2 mmol) and palladium catalyst (Pd(OAc)$_2$, 13.4 mg, 0.06 mmol) were added to the mixture under positive argon pressure. Then, the mixture was heated in an oil bath set to 100 °C and stirred for 24 h. At the end of this time, the reaction mixture was precipitated into cold methanol. The precipitate was transferred to a cellulose Soxhlet thimble and subsequently washed with methanol and acetone. The poly(3-hexylthiophene) was extracted from the thimble using chloroform and then the solution was

Figure 3.6: Optimized DArP conditions used to synthesize poly(3-hexylthiophene) as a test reaction.
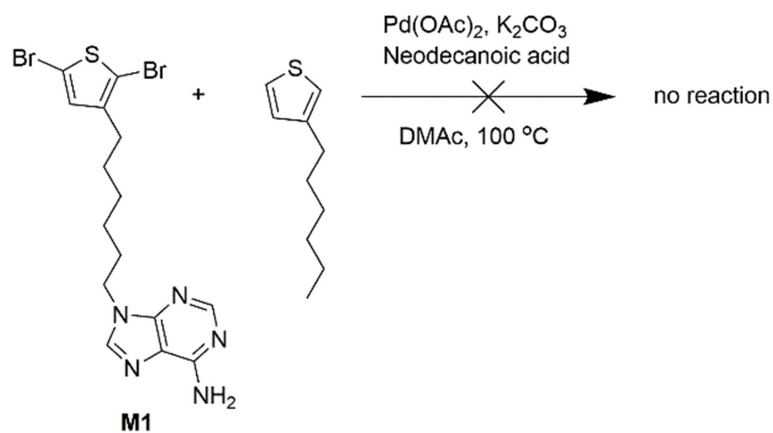
Figure 3.7: Attempts to use direct arylation polymerization to copolymerize dibromo adenine-containing monomer, M1, and 3-hexylthiophene were unsuccessful.

concentrated via rotary evaporation to obtain the product. This resulting polymer had a number-average molecular weight, M_n, = 35.0 kg/mol and dispersity, Đ = 2.10 at 68% yield.

3.4.2 DArP in the Presence of Adenine Functionality

Direct arylation polymerizations of the adenine containing dibromo monomer (M1) and 3-hexylthiophene using the optimized reaction conditions were unsuccessful (Figure 3.7). The reaction was performed in DMAc at 100 °C with 6 mol% palladium (II) acetate ($Pd(OAc)_2$) as the catalyst, 3 equiv. of potassium carbonate (K_2CO_3) as the base, and 0.3 equiv. of neodecanoic acid as the proton shuttle.

To test whether adenine interferes with the catalyst, a catalytic amount of N-alkylated adenine (0.04 equiv. of adenine-N9-hexyl) was added to a DArP of 2,5-dibromo-3-hexylthiophene and 3-hexylthiophene, as shown in Figure 3.8. Unlike the test reaction performed using optimized conditions described earlier, no P3HT was produced in the presence of the added adenine. This confirms that adenine interacts with and deactivates the palladium catalyst. In the following subsection, we describe a variety of attempts to conduct DArP in the presence of adenine functionality, changing the catalyst, addition of ligand, and auxiliary catalyst as a way to alter the interaction of adenine and Pd catalyst and enable DArP.

3.4.3 Screening DArP Conditions (With Adenine-N9-Hexyl as an Additive)

DArP of 2-bromo-3-hexylthiophene in the presence of N-alkylated adenine ("adenine functionality") under a variety of conditions was tested. (See Figure 3.9 and Table 3.1.) Many of the conditions tested as part of the screening study were based on adaptations of polymerization conditions reported in the literature. Daugulis et al. suggested that the addition of bulky, electron-rich phosphine ligands, such as di(1-adamantyl)-n-butylphosphine, can stabilize the catalyst for direct arylation of nitrogen containing heteroaromatics.[245] Heterogeneous palladium catalysts like Pd/C and $Pd(OH)_2$/C also may add functional tolerance to direct arylation, as reported by Alami et al.[246] Another
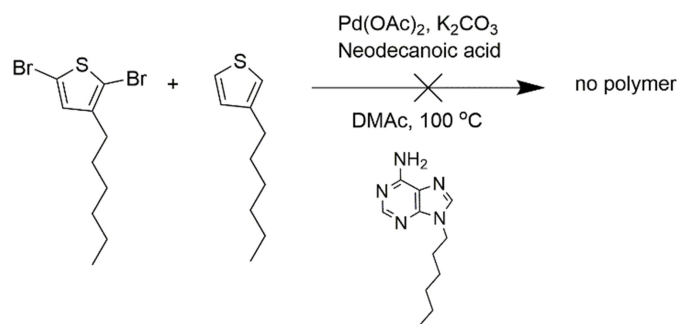
Figure 3.8: Attempted DArP reaction for synthesis of P3HT in the presence of adenine-N9-hexyl.
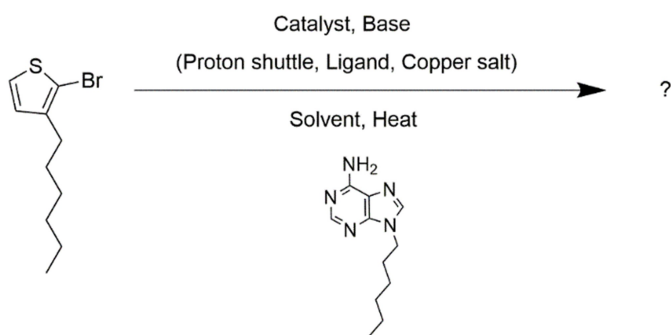
Figure 3.9: General conditions for DArP in presence of adenine-N9-hexyl.

possible method for maintaining the activity of Pd catalyst is to add an excess of a different metal ion that will sacrificially bond with adenine. This method has been used to temper the reactivity of hydrogens on imidazole, thereby enabling direct arylation. Specifically, the addition of CuI resulted in selective arylation of imidazole at C-2, rather than at C-5.[247, 248] These reports informed out comprehensive screening study that was used to find suitable conditions for DArP of 2-bromo-3-hexylthiophene in presence of adenine functionality, and Table 3.1 summarizes the results.

Among these possibilities, only the addition of CuI and a bulky phosphine ligand (together) allowed P3HT to be produced when adenine-N9-hexyl was present. Applying the same reaction conditions – added CuI and bulky phosphine ligand – to DArP of monomer M1 did not afford any polymer. This may be due to limited solubility of the polymer in the reaction solvent DMAc. In total, the results of these screening studies suggest that binding of adenine to the Pd catalyst plays significant role in deactivation of the catalyst or interference in the catalytic cycle.

3.4.4   Interaction of Pd Catalyst with Adenine

Metal ions, including platinum ions, can bind to nucleobases, and these interactions have been studied to explain the activity of platinum compounds as drugs or the effects of metal ions on the activity of metalloenzymes.[249–253] Adenine can bind with cations through its primary amine as well as through nitrogen atoms in the fused ring heterocycle, forming various bidentate or multidentate complexes. N-7 has greatest propensity for chelating Pt and Pd ions.[251, 252] To gain insight into complex formation of adenine with Pd catalysts, adenine-N9-methyl was synthesized and used. An equimolar mixture of $Pd(OAc)_2$ (30.1 mg, 0.134 mmol) and adenine-N9-methyl (20.3 mg, 0.134 mmol) was prepared in DMSO. Changes in chemical shifts of C-2 and C-8 are interpreted as indicating formation of Pd^{2+}/adenine complexes. At least five different complexes can be observed from coordination of Pd^{2+} with adenine. This finding is in general agreement with previous reports[251, 252] and highlights the strong interaction between adenine and Pd catalyst.

Table 3.1: Screening study used to identify appropriate conditions for synthesis of P3HT in presence of adenine-N9-hexyl by DArP.

Entry	Catalyst	Ligand	Solvent, Temperature	Base/Acid[a]	Other Additives[b]	Results And M_n
1	Pd(OAc)$_2$	-	DMAc, 100 °C	K$_2$CO$_3$ Neodecanoic acid	-	No Polymer
2	Pd(OAc)$_2$	-	DMAc, 100 °C	K$_2$CO$_3$ PivOH	-	No Polymer
3	Pd(OAc)$_2$	dppe, 12 mole%	DMAc, 100 °C	K$_2$CO$_3$ PivOH	-	No Polymer
4	Pd(OAc)$_2$	-	DMF, 100 °C	K$_2$CO$_3$ Neodecanoic acid	-	No Polymer
5	Pd(OAc)$_2$	PAd$_2$Bu, 6 mole%	DMAc, 100 °C	K$_2$CO$_3$ Neodecanoic acid	-	No Polymer
6	Pd(OAc)$_2$	dppe, 6 mole%	DMAc, 100 °C	K$_2$CO$_3$ PivOH	-	No Polymer
7	Pd(OAc)$_2$	XantPhos	DMAc, 100 °C	K$_2$CO$_3$ PivOH	-	No Polymer
8	Herrmann's 2 mole%	P(o-anisyl)$_3$ 4 mole%	THF, 100 °C	Cs$_2$CO$_3$	-	No Polymer
9	Herrmann's 2 mole%	P(o-anisyl)$_3$ 4 mole%	Toluene, 100 °C	Cs$_2$CO$_3$	-	No Polymer
10	Herrmann's 2 mole%	dppe	DMAc, 100 °C	K$_2$CO$_3$ Neodecanoic acid	-	No Polymer
11	Pd$_2$(dba)$_3$ 2 mole%	P(o-anisyl)$_3$ 6 mole%	Toluene, 100 °C	Cs$_2$CO$_3$ PivOH	-	No Polymer
12	Pd$_2$(dba)$_3$ 2 mole%	(tBu)$_3$PHBF$_4$ 6 mole%	Toluene, 100 °C	Cs$_2$CO$_3$ PivOH	-	No Polymer
13	Pd(PPh$_3$)$_4$ 2 mole%	P(o-anisyl)$_3$ 4 mole%	Toluene, 100 °C	Cs$_2$CO$_3$ PivOH	-	No Polymer
14	Pd(OH)$_2$/C 4 mole%	-	DMAc, 100 °C	K$_2$CO$_3$ PivOH	-	No Polymer
15	Pd(OAc)$_2$	-	DMAc, 100 °C	Cs$_2$CO$_3$ PivOH	CuI	No Polymer
16	Pd(OAc)$_2$	PAd$_2$Bu, 6 mole%	DMAc, 100 °C	Cs$_2$CO$_3$ PivOH	CuI	Polymer 15% yield, $M_n \approx 2$ kg/mol

[a] PivOH = pivalic acid
[b] molar ratio of CuI:adenine-N9-hexyl = 3:1
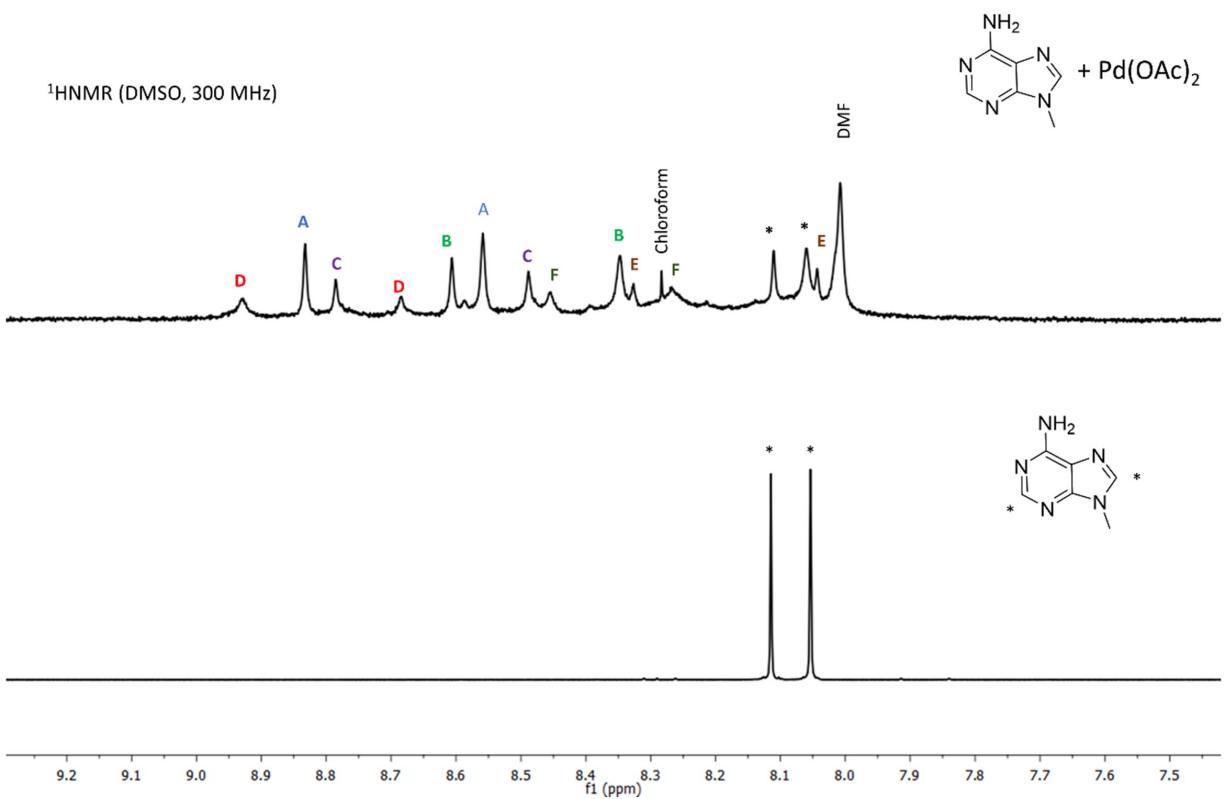
Figure 3.10: Aromatic region of (bottom) adenine-N9-methyl and (top) an equimolar mixture of adenine-N9-methyl and Pd^{2+} in DMSO-d_6. A, B, C, D, E, and F refer to different Pd^{2+}/adenine complexes.

3.4.5 Synthesis of Amine-Protected Adenine

Protecting the primary amine functionality of the adenine may weaken its interaction with palladium catalyst, thereby enabling DArP in the presence of the protected adenine. To test this, *tert*-butyloxycarbonyl (Boc) protecting groups were utilized. DArP of 2-bromo-3-hexylthiophene in presence of bis-Boc protected adenine-N9-hexyl (0.04 equiv.) was conducted using the same optimized conditions proven for DArP of 2-bromo-3-hexylthiophene. Under these conditions (see Figure 3.11), the direct arylation polymerization was successful, resulting in a 45% yield of P3HT having M_n = 5.90 kg/mol and Đ = 1.68. Thus, we conclude that amine protection is necessary to prevent interference due to complex formation between the adenine and the Pd catalyst. Based on this result, a Boc-protected, adenine containing monomer (M2) was synthesized.

3.4.6 DArP Synthesis of $T_{Ad\text{-}Boc}$-T and $T_{Ad\text{-}Boc}$-tT$_{4h}$

Two alternating copolymers, $T_{Ad\text{-}Boc}$-T and $T_{Ad\text{-}Boc}$-tT$_{4h}$, were synthesized in similar DArP conditions, as shown in Figure 3.12.

8 mL of dry and degassed DMAc was transferred via cannula to a dry 50 mL round bottom flask. Then, amine-protected dibromo monomer, M2, (329 mg, 0.5 mmol, 1 equiv.) was added to the flask. The other comonomer, either 3-hexylthiophene, T, (84 mg, 0.5 mmol, 1 equiv.) or 3,3',3'',4'-tetrahexyl-2,2':5',2''-terthiophene, tT$_{4h}$ (292.5 mg, 0.5 mmol), was added to the solution, which would yield either $T_{Ad\text{-}Boc}$-T or $T_{Ad\text{-}Boc}$-tT$_{4h}$, respectively. Then, neodecanoic acid (29 μL, 26 mg, 0.15 mmol, 0.3 equiv.) and K$_2$CO$_3$ (138 mg, 1 mmol, 2 equiv.) were added to the mixture while it was maintained under a positive argon atmosphere. After the additions, the flask was sealed with a septum and the mixture was heated to 100 °C and stirred for 24 h. At the end of this time, the reaction mixture was precipitated into cold methanol. The precipitate was washed with methanol and transferred to a cellulose thimble. The final product was extracted from the Soxhlet thimble by dissolving the soluble components in chloroform. $T_{Ad\text{-}Boc}$-T and $T_{Ad\text{-}Boc}$-tT$_{4h}$ were isolated in 56% and 72% yield, respectively.
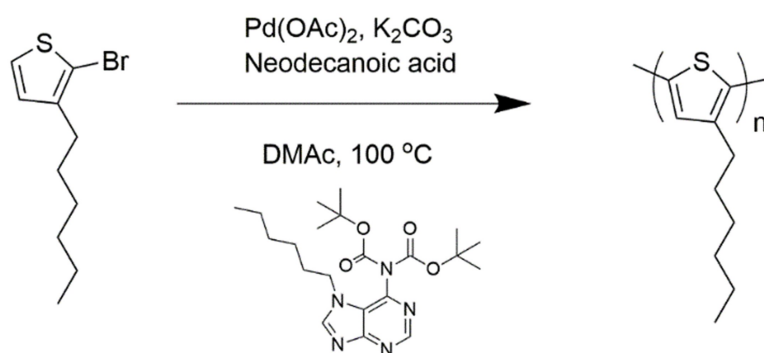
Figure 3.11: DArP conditions for successful polymerization in presence of Boc-protected adenine-N9-hexyl.
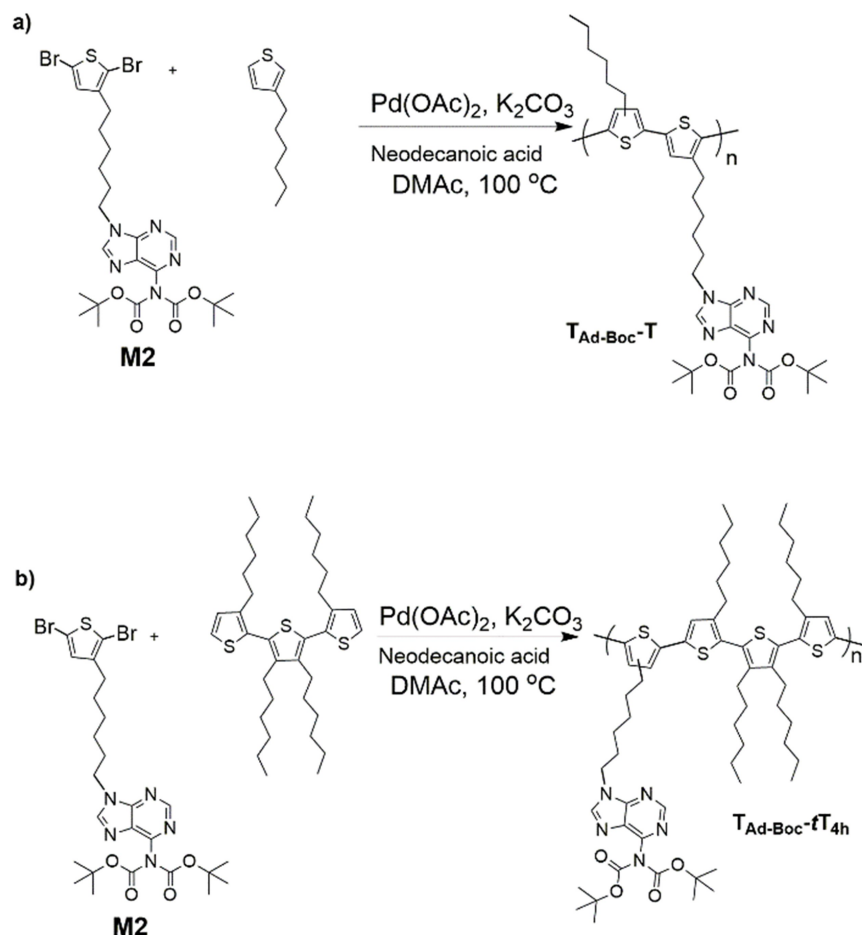
Figure 3.12: Scheme for polymerization of Boc-protected monomers via DArP to produce a) $T_{Ad\text{-}Boc}$-T and b) $T_{Ad\text{-}Boc}$-tT_{4h}.

3.4.7 General Procedure for Acid Catalyzed Deprotection of $T_{Ad\text{-}Boc}$-T and $T_{Ad\text{-}Boc}$-tT_{4h}

Boc groups were removed by acid catalysis, as shown in Figure 3.13. The Boc-protected polymer (either $T_{Ad\text{-}Boc}$-T or $T_{Ad\text{-}Boc}$-tT_{4h}) was added to a 100 mL dry round bottom flask. Then, 50 mL of a solution compared of trifluoroacetic acid (TFA) and dichloromethane (DCM) at a 1:1 volumetric ratio was added to the flask. The flask was connected to a bubbler to allow the gas produced (CO_2) to escape. The mixture was stirred for 24 h at room temperature. At the end of this time, the volatiles were removed under reduced pressure and then the rest of the mixture was precipitated into cold methanol. The precipitate was washed with methanol and acetone via subsequent Soxhlet washes and then extracted from the cellulose Soxhlet thimble using chloroform. The deprotected product of $T_{Ad\text{-}Boc}$-T was insoluble in various organic solvents and further characterization was impossible due to this solubility issue. On the other hand, $T_{Ad\text{-}Boc}$-tT_{4h} showed quantitative and complete deprotection and the resulting polymer, $T_{Ad\text{-}Boc}$-tT_{4h}, was soluble in most organic solvents, including chloroform, THF, and DCM.

3.4.8 Synthesis of T-tT_{4h} (Homologue of T_{Ad}-tT_{4h} Without Adenine)

A homologue without adenine was synthesized using the same DArP conditions. Specifically, 25 mL of dry and degassed DMAc was cannula transferred to a dry 50 mL round bottom flask. Then, 2,5-dibromo-3-hexylthiophene (163 mg, 0.5 mmol, 1 equiv.) and 3,3',3'',4'-tetrahexyl-2,2':5',2''-terthiophene (tT_{4h}) (292.5 mg, 0.5 mmol, 1 equiv.) were added to the flask. Neodecanoic acid (29 μL, 26 mg, 0.15 mmol, 0.3 equiv.) and K_2CO_3 (138 mg, 1 mmol, 2 equiv.) were added to the mixture while it was purging under argon. The mixture was heated to 100 °C and stirred for 24 h. Then, the reaction mixture was precipitated into cold methanol. The precipitate was washed with methanol and acetone. The precipitate was transferred to a cellulose thimble and then collected from the soluble material after Soxhlet extraction using chloroform. These reaction conditions resulted in a copolymer having a M_n = 8.5 kg/mol and Đ = 1.64 at 71% yield.
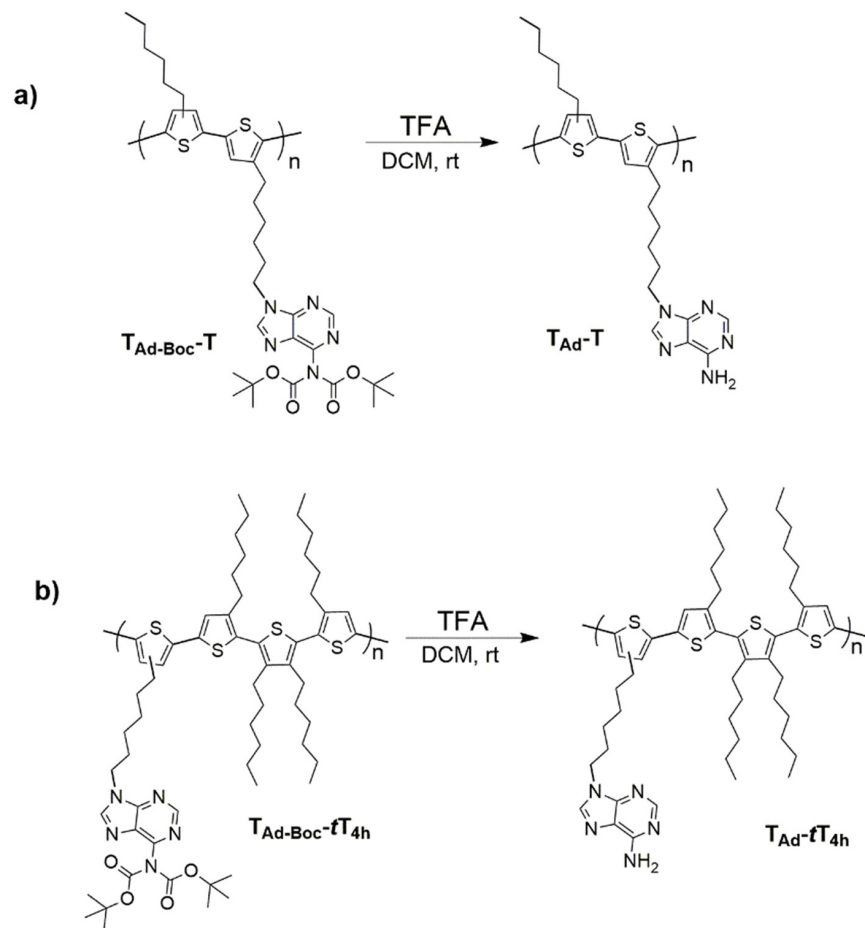
Figure 3.13: Acid catalyzed deprotection of a) $T_{Ad\text{-}Boc}$-T and b) $T_{Ad\text{-}Boc}$-tT$_{4h}$.
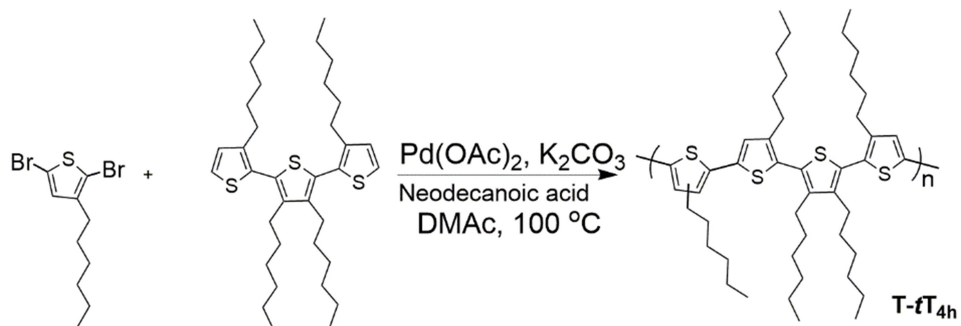
Figure 3.14: Synthesis of non-adenine containing homologue polymer, T-tT$_{4h}$ via DArP.

3.5 Results and Discussion

3.5.1 Monomer and Polymer Syntheses

As summarized in Figure 3.15, lithium-halogen exchange was used to produce 3-(6-bromohexyl)thiophene from 3-bromothiophene in 70% yield.[254, 255] After purification, the resulting 3-(6-bromohexyl)thiophene was brominated using N-bromosuccinimide (NBS) to generate 2,5-dibromo(3-(6-bromohexyl)thiophene in 75% yield.[255] Bromination preceded addition of adenine to avoid bromination of adenine at the C-8 position.[256] Finally, adenine-functionality was introduced at the terminus of the side chain functionality under alkylation conditions, as described by our group[164, 257] and others.[256, 258, 259] While this results in a mixture of N-7 and N-9 attachment,[260] the N-9 isomer, 9-(6-(2,5-dibromothiophen-3-yl)hexyl)-9H-purine-6-amine) (M1), was isolated by column chromatography, resulting in an overall yield of 55%. The adenine-functionalized monomer featuring N-9 attachment was chosen for polymerization due to its similarity to adenosine as well as its ability to participate in multi-dentate hydrogen bonding with other nucleobases, such as thymine.[260] The structure of the adenine-functionalized thiophene (M1) was confirmed by 2D multiple bond correlation gHMBC NMR spectroscopy, and relevant correlations are presented in the Appendix (Figure A.20).

Initial efforts to copolymerize M1 with 3-hexylthiophene by applying conditions reported extensively in the literature for the DArP of thiophenes[116, 121, 239, 243, 261] were unsuccessful, as mentioned in the Section 3.4. We hypothesized that adenine may interfere with polymerization in two possible ways: i) The C-H bond at the C-8 position of the purine scaffold may be activated,[262] creating a stoichiometric imbalance that inhibits the step-growth polymerization, or ii) the nucleobase may ligate the palladium catalyst,[236] thereby inhibiting the catalyst from participating in the catalytic cycle. A set of test polymerizations were performed to differentiate between these two effects. First, a catalytic amount of adenine-N9-hexyl (0.04 equiv.) was added to a copolymerization properly constituted with 2,5-dibromo-3-hexylthiophene and 3-hexylthiophene. If the issue were stoichiometric imbalance due to activation of the C-H bond at C-8, this test polymerization would result in low molecular weight polymer; however, if the second cause –disruption of catalytic activity–
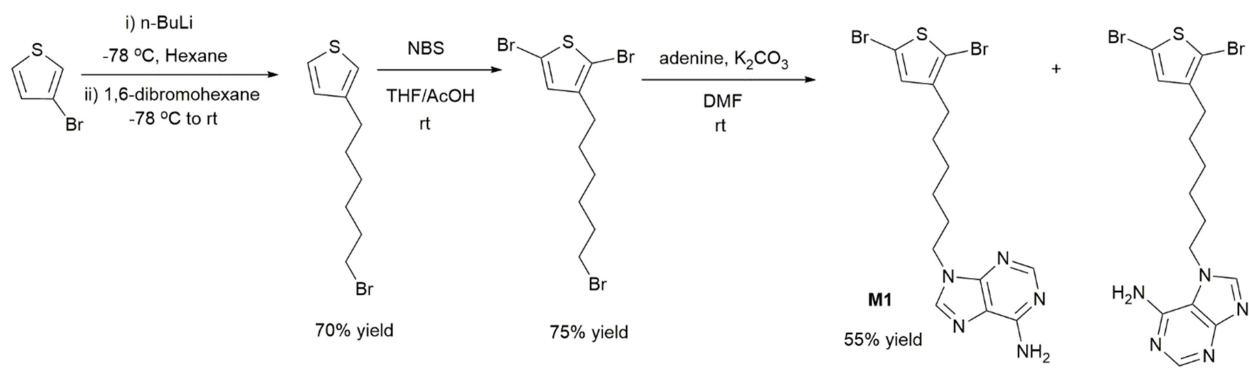
Figure 3.15: Synthetic pathway used to synthesize the adenine-containing dibromo monomer M1.

was operative, the polymerization would not proceed. Regardless of catalyst, solvent, temperature, and auxiliary ligand, no polymer was observed when a catalytic amount of adenine-N9-hexyl was present. Specific reaction conditions and outcomes are documented as entries 1-14 in Table 3.1. This screening study suggests that adenine is strongly binding with the palladium metal center, thereby deactivating the catalyst. This conclusion is consistent with the ability of nucleobases to bind with various metal ions, which has been reported widely.[249, 263–265]

Other conditions were tested to circumvent the irreversible binding of the adenine to the catalyst, such as i) addition of excess sacrificial complex forming metal ions (CuI), ii) addition of electron rich and bulky ligand that offers favorable but reversible ligation to catalyst center, and iii) usage of a catalyst absorbed on a heterogeneous support to reduce the chance of adenine-catalyst binding. However, even mixture of bulky phosphine ligand and CuI, as reflected by entries 15 and 16 in Table 3.1, resulted in only oligomers in low yield. Therefore, a second series of test polymerization were run, this time using a *tert*-butyloxycarbonyl (Boc) protected adenine-N9-hexyl (0.04 equiv.) as an additive in the reaction mixture. In this situation, the DArP of 2-bromo-3-hexylthiophene produced P3HT at 45% yield with a number-average molecular weight $M_n = $ of 5.9 kg/mol and dispersity of Đ = 1.68. These studies indicate that it is necessary to protect the amine functional group of adenine to enable a successful polymerization via DArP.

These test polymerization results prompted the synthesis of the amine-protected dibromo monomer, M2, which as shown in Figure 3.16, has two Boc protecting groups. The structure of the amine-protected dibromo monomer is confirmed by ^{1}H, ^{13}C, and 2D gHMBC NMR spectroscopy, which are presented in the Appendix (Figure A.16, A.17, and A.21). In addition and as shown in Figure 3.17, successful protection of the amine is evident from the change of chemical shifts corresponding to the C-2 and C-8 protons of adenine. Specifically, when M1 is transformed to M2, the C-2 proton shifts from 8.35 ppm to 8.77 ppm, and the C-8 proton shifts from 7.77 ppm to 8.00 ppm due to the addition of electron withdrawing Boc groups.

By using conditions described by Thompson and coworkers[121, 261] as optimized conditions for DArP of thiophene-based monomers, P3HT was synthesized with 68% yield
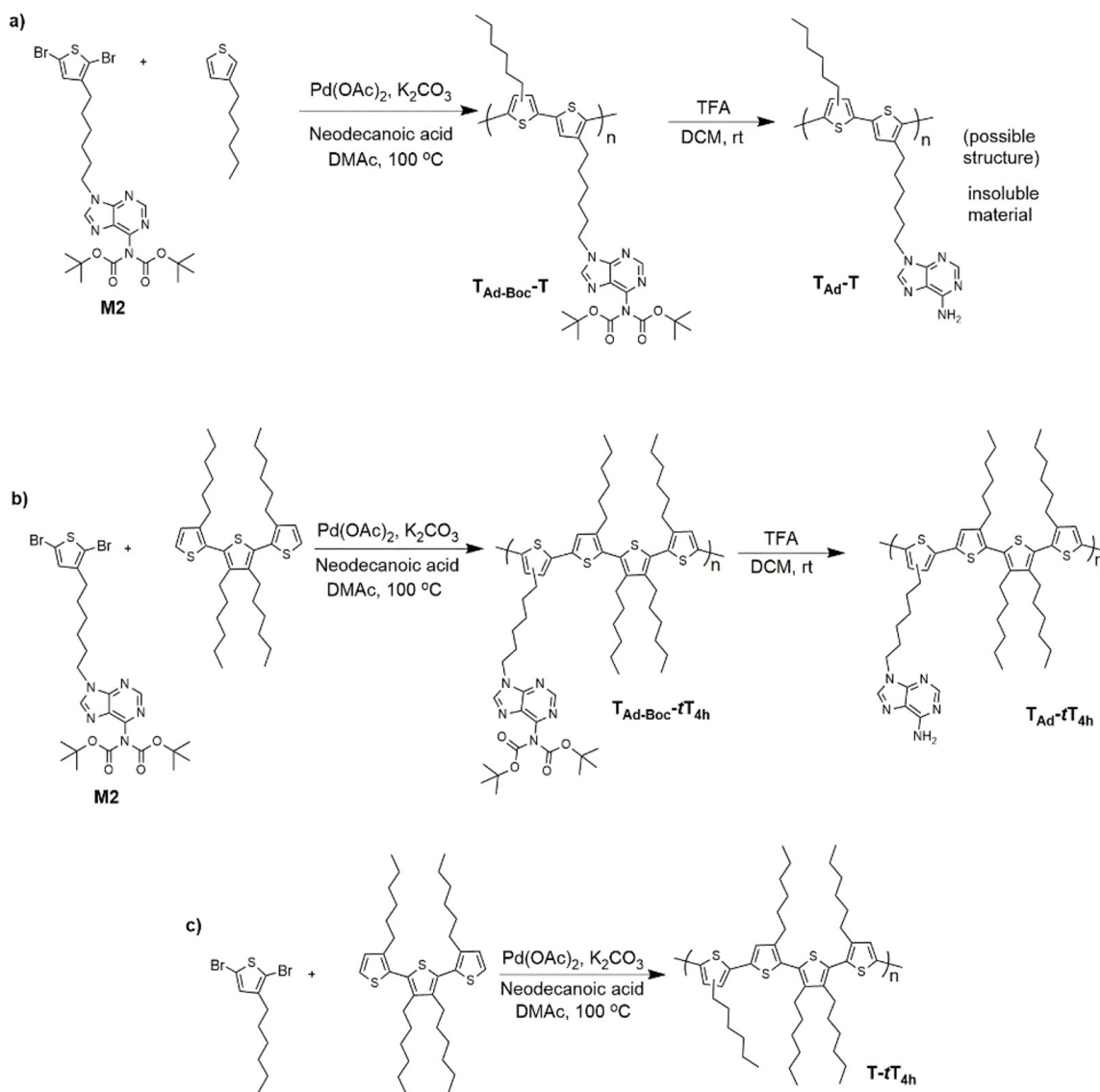
Figure 3.16: Synthesis of Boc-protected copolymers a) $T_{Ad\text{-}Boc}$-T, b) $T_{Ad\text{-}Boc}$-tT_{4h}, and c) the non-functionalized homologue, T-tT_{4h} via direct arylation polymerization as well as Boc deprotection conditions for $T_{Ad\text{-}Boc}$-T and $T_{Ad\text{-}Boc}$-tT_{4h}.
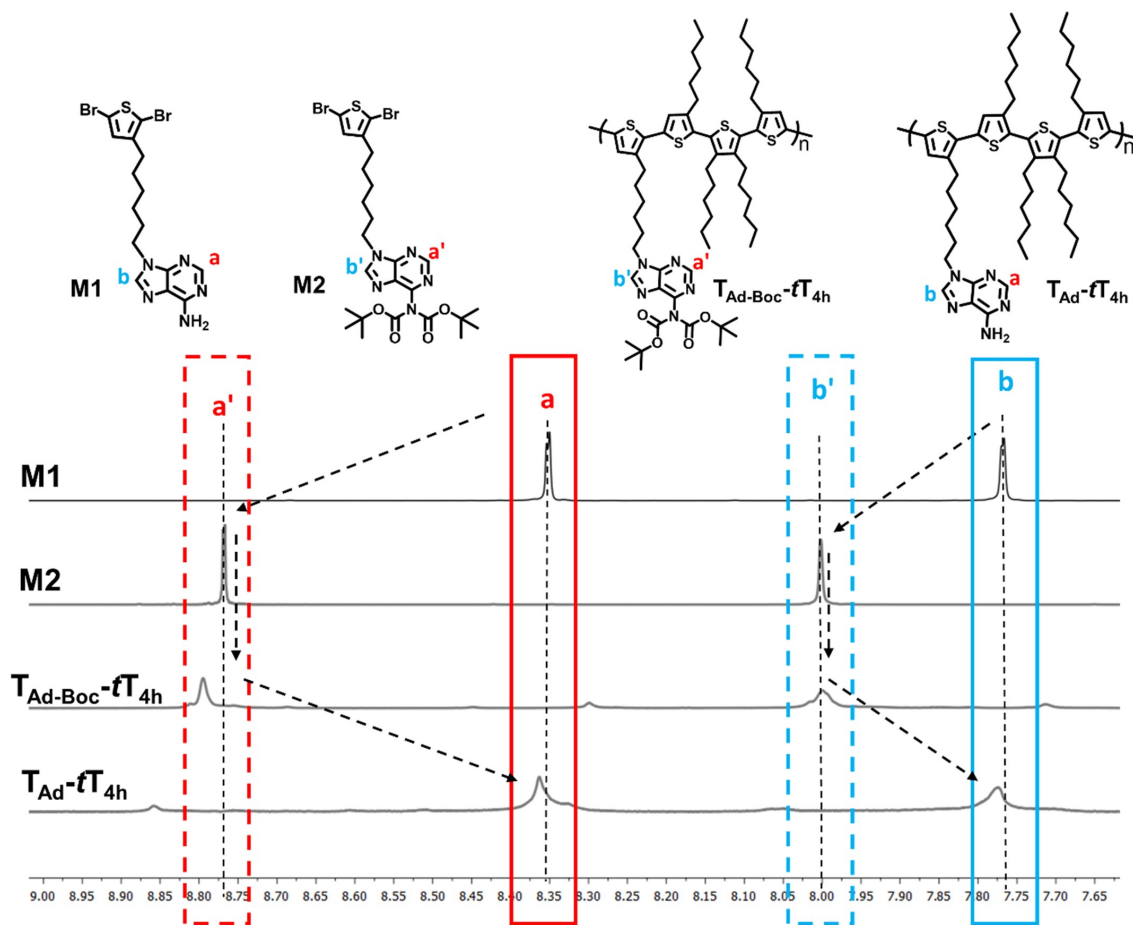
Figure 3.17: Overlay of the aromatic regions of ^{1}H NMR spectra acquired for M1, M2, $T_{Ad\text{-}Boc}$-tT$_{4h}$, and T_{Ad}-tT$_{4h}$. Comparison of the spectra shows that the C2 and C8 protons shift downfield (upfield) when adenine is Boc-protected (deprotected), and peak widths broaden and shift slightly upon the polymerization.

with a number-average molecular weight M_n = 35.0 kg/mol and dispersity Đ = 2.10. Therefore, these conditions were applied to the DArP of M2 with other comonomers. As shown in Figure 3.16a, direct arylation polymerization of M2 with 3-hexylthiophene as the complementary comonomer was successful. The resulting alternating regiorandom copolymer comprised of Boc-protected thiophene and 3-hexylthiophene repeating units, which are abbreviated as T_{Ad-Boc}-T, with subscripts designating the nature of the side chain, was purified and isolated as a green solid in 56% yield with M_n = 6.9 kg/mol and Đ = 1.37. Deprotection of the Boc functionality resulted in an insoluble dark-yellow solid. This drastic change in solubility after cleaving the protecting groups is attributed to strong interchain hydrogen bonding interactions between adenine groups, with the insolubility exacerbated by the lack of solubilizing alkyl side chains, which was also reported by Cheng and coworkers.[92, 93]

In an effort to improve the solubility of adenine-containing conjugated polymers, the comonomer 3,3',3",4'-tetrahexyl-2,2':5',2"-terthiophene (tT_{4h}) was synthesized. Here the key design element is additional solubilizing side chains within a bulkier complementary comonomer. In comparison to 3-hexylthiophene, this monomer contains more hexyl side chains per thiophenyl ring, which is expected to reduce main chain rigidity[266–268] and effectively dilute[269] the number of network-forming adenine groups throughout the copolymer, thereby improving copolymer solubility. As described in the previous section, tT_{4h} was synthesized in 80% yield using Suzuki cross-coupling between 2,5-dibromo-3,4-dihexyl-thiophene and 3-hexylthiophene-2-boronic acid pinacol ester in toluene and water biphasic system at 95 °C. Direct arylation polymerization of M2 with tT_{4h} (Figure 3.16b) using optimized DArP conditions[121, 261] resulted in T_{Ad-Boc}-tT_{4h} with M_n = 7.0 kg/mol, Đ = 2.01 (72% yield). Regiorandomness of this alternating copolymer, similar to T_{Ad-Boc}-T, comes from nature of AA and BB step-growth polymerization. However, intrinsic symmetry of tT_{4h} makes the tT_{4h}-based copolymers to have equal amount of head-tail and tail-tail connectivities, regardless of polymerization conditions. Acid catalyzed deprotection of Boc groups using trifluoroacetic acid (TFA) produced the alternating copolymer designated as T_{Ad}-tT_{4h} (M_n = 7.0 kg/mol, Đ = 1.82), which was soluble in common organic solvents such as THF and chloroform. GPC traces of T_{Ad-Boc}-tT_{4h} and T_{Ad}-tT_{4h} are unimodal (Figure 3.18)

and full ^{1}H NMR spectra of the Boc-protected and deprotected copolymers are presented in the Appendix (Figure A.31, and A.32). As a result of the improved solubility, extensive structural characterization of the adenine-functionalized copolymer T_{Ad}-tT_{4h} is possible. As shown in Figure 3.17, ^{1}H NMR spectroscopy suggests that amine groups remained protected during polymerization and the Boc deprotection is quantitative. Specifically, chemical shifts corresponding to protons at the C-2 and C-8 positions of adenine show retention of Boc functionality during polymerization for both T_{Ad}-tT_{4h} and $T_{Ad\text{-}Boc}$-tT_{4h}. Following deprotection of $T_{Ad\text{-}Boc}$-tT_{4h} with TFA, upfield shifts are observed for protons at the C-2 and C-8 positions of the adenine, which confirms complete deprotection.

To examine the effect of adenine side chain functionality on thermal and optical properties, a non-functionalized homologue, identified as T-tT_{4h}, was synthesized from tT_{4h} and 2,5-dibromo-3-hexylthiophene using optimized DArP conditions (Figure 3.16c and Section 3.4.8). This copolymer was produced as a viscous paste in 71% yield with a $M_n = $ 8.5 kg/mol and Đ = 1.64.

3.5.2   Thermal Characterizations of Copolymers

Thermogravimetric analysis (TGA) was used to assess the thermal stability of T_{Ad}-tT_{4h} and T-tT_{4h}. As shown in Figure 3.19a, T-tT_{4h} has a decomposition temperature (T_d), which is defined as the temperature at which a 5% weight loss is registered, of 397 °C. This T_d and ultimate weight of $\approx$ 46 wt% agree with values reported for poly(alkylthiophenes).[270] Alternatively, T_{Ad}-tT_{4h} exhibits a multi-step degradation, as observed in Figure 3.19b. T_{Ad}-tT_{4h} has a T_d of 171 °C, which is the first degradation event, and a second decomposition occurs at $\approx$ 410 °C (where the mass loss is 18%). The first degradation event is attributed to the decomposition of the purine structure in the side chain, which agrees with our previous studies of purine-based copolymers and donor-acceptor chromophores.[164, 257] The second decomposition is consistent with degradation of the poly(alkylthiophene)s. Other possible thermal transitions such as crystallization and glass transition were investigated using differential scanning calorimetry (DSC). T_{Ad}-tT_{4h} and T-tT_{4h} do not show a thermal transition corresponding to crystallization due to their highly flexible and twisted backbones. (See DSC curves presented in Figure 3.20.) However, comparison of the DSC traces clearly
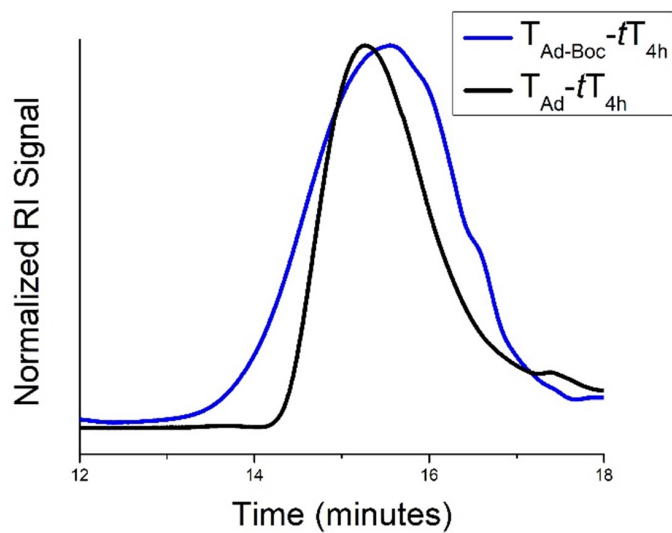
Figure 3.18: Overlay of GPC traces of $T_{Ad\text{-}Boc}\text{-}tT_{4h}$ ($M_n = 7.0$ and Đ $= 2.01$, blue trace) and $T_{Ad}\text{-}tT_{4h}$ ($M_n = 7.0$ kg/mol and Đ $= 1.82$, black trace). (These are the Boc-protected and deprotected copolymers, respectively.)
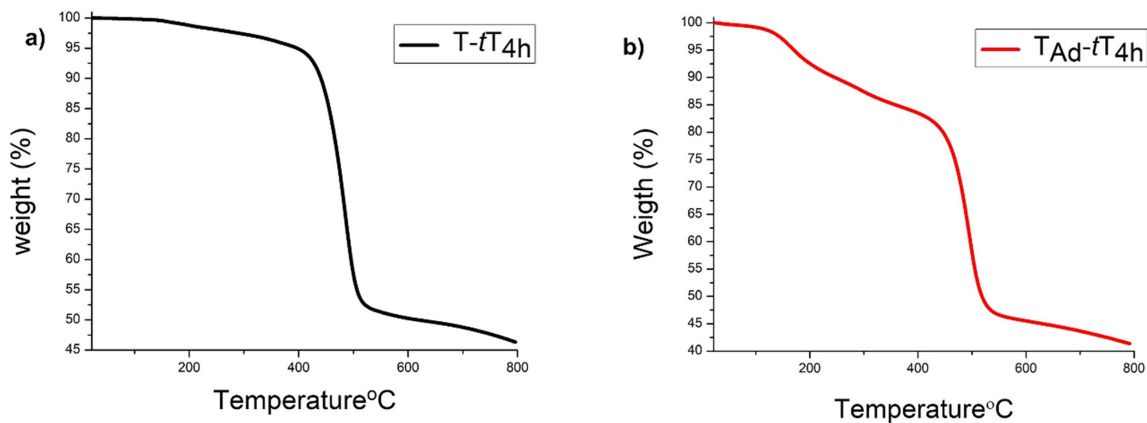
Figure 3.19: Mass loss measured by thermogravimetric analysis of a) T-tT$_{4h}$ and b) T$_{Ad}$-tT$_{4h}$. Data were acquired by ramping from 20 °C to 800 °C at a rate of 10 °C/min.
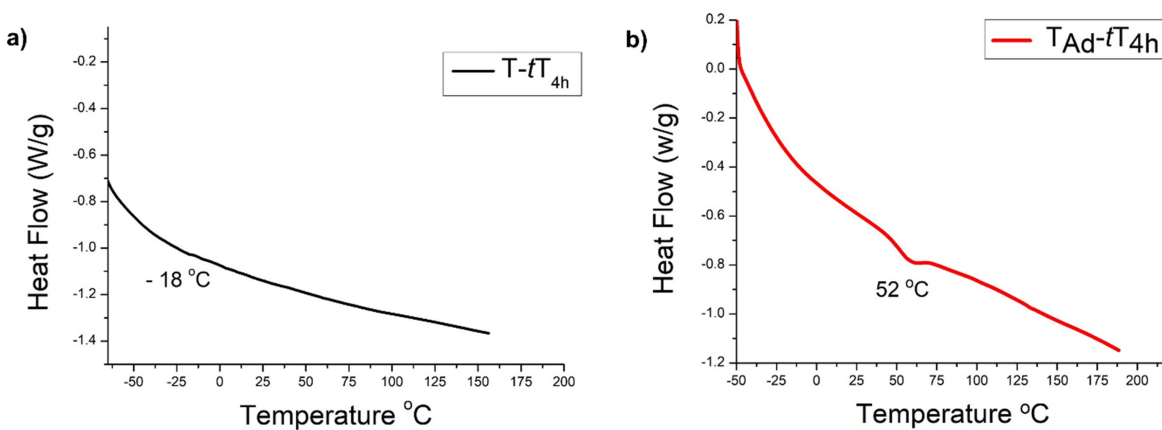
Figure 3.20: Results of differential scanning calorimetry measurements of a) T-tT$_{4h}$ (T$_g$ ≈ 18 °C) and b) T$_{Ad}$-tT$_{4h}$ (T$_g$ ≈ 52 °C). Experiments were performed using heating and cooling rates of 10 °C/min, with T$_g$'s determined from the second heating ramp.

96

shows that adenine and its ability to impart interchain hydrogen bonding significantly affects main-chain flexibility: The glass transition temperature (T_g) of the non-functionalized homologue T-tT$_{4h}$ is much lower (T_g = 18 °C) than that of the adenine functionalized T$_{Ad}$-tT$_{4h}$, which displays a T_g = 52 °C. An increase in T_g due to interchain hydrogen bonding has also been observed in conjugated[91, 204] and non-conjugated[87, 271] nucleobase-functionalized polymers and copolymers.

3.5.3 Optical Properties of Copolymers

Motivated by the possibility of conjugated polymers having site-specific intermolecular recognition via hydrogen-bonding abilities finding applicability in a variety of sensing, optoelectronic, and biological applications, the optical properties of the adenine-functionalized polythiophenes were investigated using absorbance and fluorescence spectroscopies. As illustrated in Figure 3.21a, UV-Vis absorption spectra of T$_{Ad}$-tT$_{4h}$ and T-tT$_{4h}$ in chloroform show an absorbance maximum (λ_{max}^{abs}) at 392 nm and 394 nm, which corresponds to the π-π* transition of a conjugated polythiophene with bulky side chains.[272] The adenine-containing polymer, T$_{Ad}$-tT$_{4h}$, shows an extra absorbance transition at 262 nm, which corresponds to the π–π* transition of adenine.[273] The same optical transition was observed for adenine-N9-hexyl in chloroform (blue trace in Figure 3.21a). Figures 3.22 and 3.22 show that absorbance is linearly dependent on concentration across a concentration range of 0.003-0.05 mg/mL in chloroform, resulting in extinction coefficients of ϵ = 27.8 (mg/mL)$^{-1}$ cm^{-1} for T-tT$_{4h}$, and ϵ = 21.1 (mg/mL)$^{-1}$ cm^{-1} for T$_{Ad}$-tT$_{4h}$ (based on absorbance modes at λ_{max}^{abs}). This indicates good solubility for both polymers. Both copolymers are soluble at higher concentrations, but the absorbance intensity exceeds the detection limit of the spectrophotometer at concentrations > 0.05 mg/ml. Additionally, the absence of extra absorbance shoulders attributed to vibronic fine structure is likely originates from regiorandomness in the structure of the polymer or excellent solubility.[274]

As shown in Figure 3.21b, fluorescence spectroscopy measurements show that both T$_{Ad}$-tT$_{4h}$ and T-tT$_{4h}$ have broad and featureless emission profiles, centered around an emission maximum of λ_{max}^{em} = 528 nm and λ_{max}^{em} = 536 nm for T$_{Ad}$-tT$_{4h}$ and T-tT$_{4h}$, respectively. The similarity of the emission profiles ofT$_{Ad}$-tT$_{4h}$ and T-tT$_{4h}$ suggests that the radiative
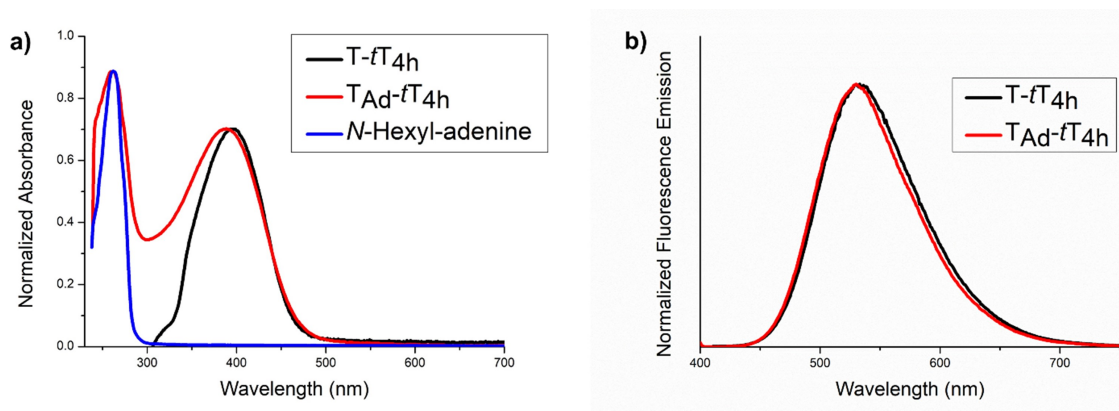
Figure 3.21: a) Normalized UV-Vis absorbance spectra of T-tT$_{4h}$ (black, 0.01 mg/mL), T$_{Ad}$-tT$_{4h}$ (red, 0.01 mg/mL), and adenine-N9-hexyl (blue, 50 μM) in chloroform. b) Normalized fluorescence spectra of T$_{Ad}$-tT$_{4h}$ (red) and T-tT$_{4h}$(black) in chloroform (0.01 mg/mL).
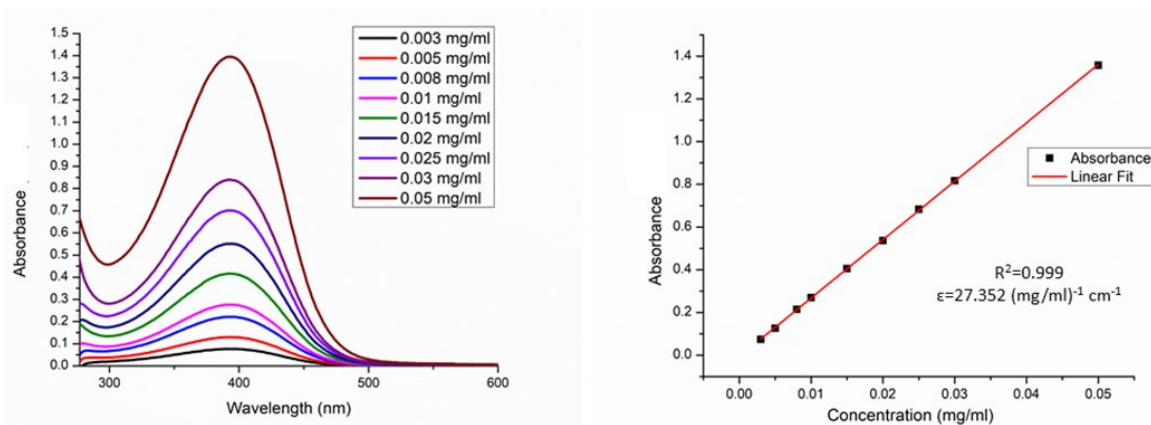
Figure 3.22: UV-Vis spectra of the non-adenine containing copolymer, T-tT$_{4h}$, at various concentrations in chloroform (left) and the Beer-Lambert plot (right).
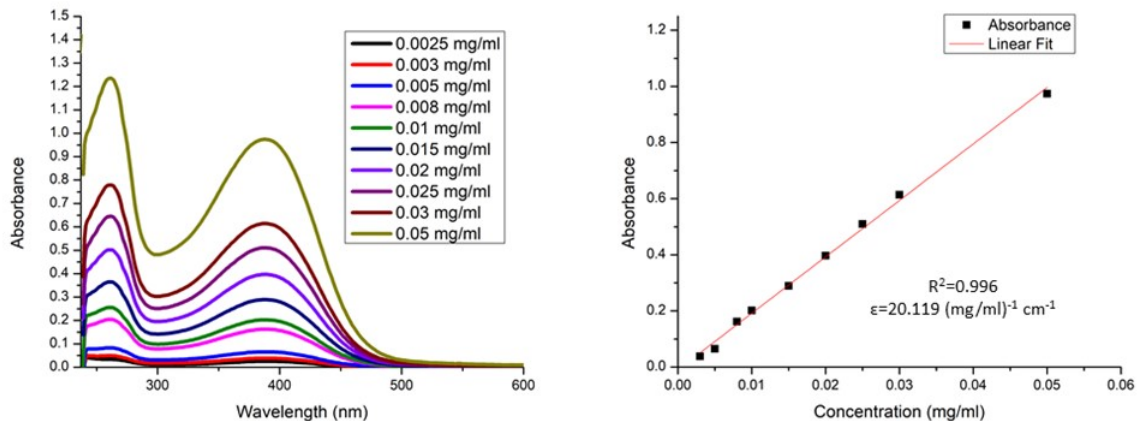
Figure 3.23: UV-Vis spectra of the adenine-containing copolymer, T_{Ad}-tT_{4h}, at various concentrations in chloroform (left) and the Beer-Lambert plot based on the absorbance mode attributed to the polythiophene backbone (right).
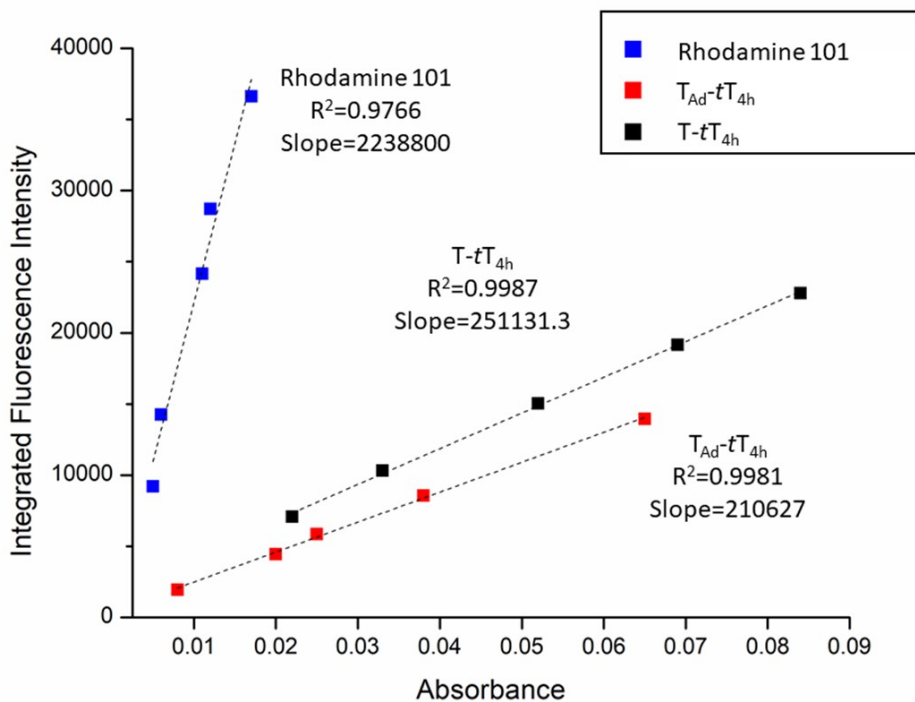
Figure 3.24: Integrated fluorescence intensity as a function of absorbance intensity maximum (of the polythiophene backbone) used for measurements of quantum yield by the comparative method (relative to Rhodamine 101).

decay pathways for both polymers mainly originate from the conjugated polythiophene backbone.[21, 275, 276] In order to gain more insight of optical properties, fluorescence quantum yields were determined by the comparative method,[164, 277] using Rhodamine 101 in ethanol (+0.01% HCl) as the fluorescence standard (quantum yield, $\phi = 1.00$).[278] The T_{Ad}-$t$$T_{4h}$ and T-$t$$T_{4h}$ copolymers have similar fluorescence quantum yields of ≈ 0.1, which is comparable to quantum yields reported for poly(alkylthiophenes).[279, 280] (See Figure 3.24.) Table 3.2 summarizes the measured optical properties of T_{Ad}-$t$$T_{4h}$ and T-$t$$T_{4h}$. In addition to similar emission profiles, the nearly identical quantum yield values indicate an absence of alternative decay pathways of the excited state, which suggests that the pendant nucleobase functionality does not interfere with the optical properties of the parent copolymer.

Both the adenine-functionalized copolymer and the corresponding unfunctionalized copolymer have a large Stokes shift of 136 nm for T_{Ad}-$t$$T_{4h}$ and 140 nm for T-$t$$T_{4h}$. These Stokes shift values are slightly larger than values reported for regioregular P3HT, which has a Stokes shift of ≈ 130 nm in chloroform[6] but smaller than values of ≈ 150 nm reported by Xu and Holdcroft for regiorandom P3HT in chloroform.[281] In addition, a large Stokes shift, which manifests by minimal overlap of absorbance and emission profiles, minimizes self-quenching and is beneficial for applications including molecular imaging, molecular recognition, and optical sensing.[282–284] Therefore, the large Stokes shift of the T_{Ad}-$t$$T_{4h}$ copolymer, its inherent solubility, and potential for molecular recognition through hydrogen bonding motivated fluorescent responsiveness studies.

3.5.4   Fluorescence Quenching Studies

Given the ability of adenine to bind with transition metals and motivated by previous examples where thymine-functionalized polymers interacted with metal ions,[231] we investigated fluorescence responsiveness of T_{Ad}-$t$$T_{4h}$ in the presence of a metal ion. T_{Ad}-$t$$T_{4h}$ quickly responded to the addition of a copper bromide salt (Cu^{2+}) solution, whereas T-$t$$T_{4h}$ showed no changes in its fluorescence profile when Cu^{2+} ions were present in solution at 20 μM. (See Figure 3.25 and 3.26.) In order to evaluate Cu^{2+} detection via fluorescence quenching, the emission profiles of a 0.01 mg/mL solution of T_{Ad}-$t$$T_{4h}$ in THF were monitored

Table 3.2: Summary of optical properties of T_{Ad}-$t$$T_{4h}$ and T-$t$$T_{4h}$.

Copolymer	λ_{max}^{abs} (nm)	λ_{max}^{em} (nm)	Stokes Shift (nm)^a	λ^b
T_{Ad}-$t$$T_{4h}$	262, 392	528	136	0.11
T-$t$$T_{4h}$	394	536	142	0.14

^{a} Stokes shifts are calculated as the difference between absorbance and emission maximums.
^{b} Quantum yields are calculated using the comparative method.

as a function of [Cu^{2+}]. Noticeable fluorescence quenching occurred in the solution of T$_{Ad}$-tT$_{4h}$ at 2×10^{-5} M Cu^{2+} without any shift in λ_{max}^{em}. As shown in Figure 3.25a, fluorescence intensity of the T$_{Ad}$-tT$_{4h}$ decreased with increasing [Cu^{2+}], culminating with a quenching efficiency as high as 91% at [Cu^{2+}] $= 5 \times 10^{-4}$ M. Here, the fluorescence quenching efficiency (Q_{eff}) at λ_{max}^{em} was calculated using the following expression:

$$Q_{eff} = \frac{I_0 - I(c)}{I_0} \tag{3.1}$$

In Equation 3.1, I_0 is the fluorescence intensity of the solution in the absence of a quenching reagent and $I(c)$ is the measured fluorescence intensity of the solution in the presence of the quencher (Cu^{2+} for these experiments) at concentration c. As shown in Figure 3.25b, a linear response is observed for [Cu^{2+}] ranging from 2.0×10^{-5} M to 9.0×10^{-5} M. This is indicative of chelation-induced quenching, which is analyzed by fitting the linear-response region with the Stern-Volmer equation, which is shown in Equation 3.2.[282, 285, 286] Here, K_{SV} is the Stern-Volmer quenching constant. K_{SV} is related to the propensity of complex formation, here between Cu^{2+} and adenine groups, and it reflects the strength of the association.[287]

$$\frac{I_0}{I(c)} = 1 + K_{SV}[Cu^{2+}] \tag{3.2}$$

While fluorescence quenching may occur through formation of non-radiative complexes (static) or chelation-elevated collision between complexes formed (dynamic), the nature of this behavior can only be determined through fluorescence lifetime studies or temperature dependent fluorescence measurements, though linearity suggests only one quenching mechanism is governing.[288] While Figure 3.27 shows that [Cu^{2+}] up to 500 μM were examined, the Stern-Volmer plot for T$_{Ad}$-tT$_{4h}$ only shows linear behavior up to $c = 9 \times 10^{-5}$ M Cu^{2+}. This is reflected in Figure 3.25b, where fitting yields $K_{SV(T_{Ad}-tT_{4h})} = 1.28 \times 10^{4}$ M^{-1}, which is similar to values reported for Cu^{2+} and amine-containing fluorescence probes, such as triphenylamine.[286] At [Cu^{2+}] $> 9 \times 10^{-5}$ M, both static and dynamic quenching contribute in chelation-induced quenching, where the Cu^{2+}-chelated adenine complexes are able to enhance formerly forbidden intersystem crossing or non-radiative decay of the singlet
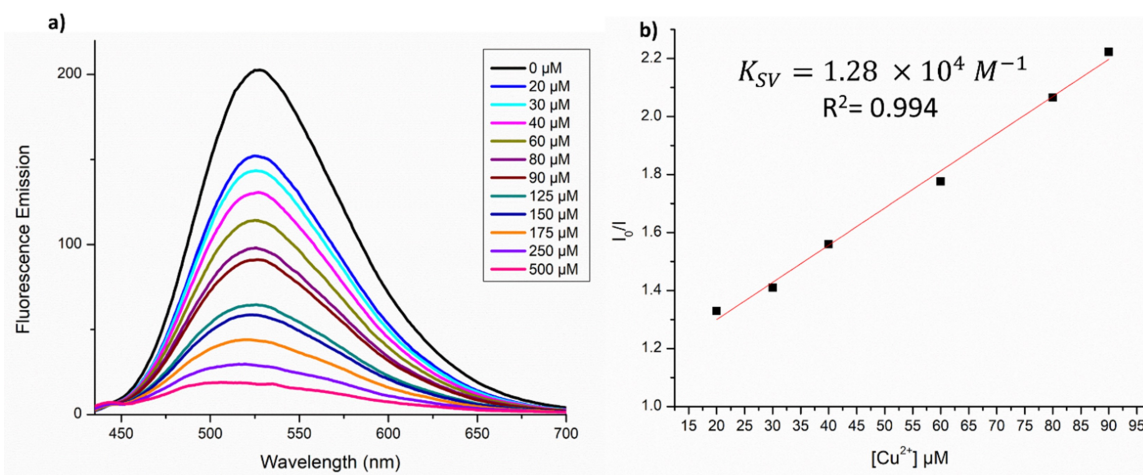
Figure 3.25: a) Fluorescence emission of T_{Ad}-$t T_{4h}$ in THF (at a copolymer concentration of 0.01 mg/mL) as a function of the concentration of Cu^{2+}. Although the fluorescence responsiveness persists to much higher concentrations, b) a linear fluorescence quenching response is observed for T_{Ad}-$t T_{4h}$ at $[Cu^{2+}]$ 90 μM.
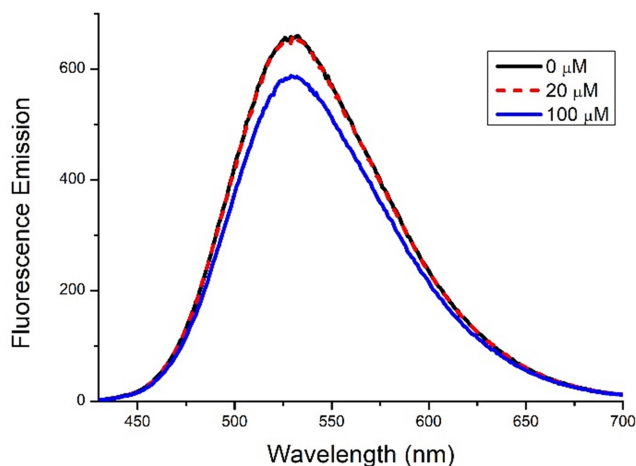
Figure 3.26: Fluorescence quenching response of T-$t T_{4h}$ (at 0.01 mg/mL) upon addition of Cu^{2+}. No detectable change in fluorescence emission is observed for at 20 μM Cu^{2+}. A 10% quenching efficiency is observed for T-$t T_{4h}$ at 100 μM Cu^{2+}, while T_{Ad}-$t T_{4h}$ shows a 54% quenching efficiency at the same Cu^{2+} concentration.

excited state.[224, 285, 287] Other metal ions Cu^+, Fe^{2+}, Fe^{3+}, K^+, and Na^+ were tested to grasp more information about nature and selectivity of fluorescence quenching behaviour. Cu^{2+} and Fe^{3+} showed highest quenching efficiencies followed by lower quenching from Fe^{2+}. Other metal ions (Cu^+, K^+, and Na^+) did not affect fluorescence. This is in agreement with intersystem crossing facilitated by paramagnetic ions/atoms.[287] These results are shown in Figure 3.28.

Reversibility of fluorescence quenching is examined by subjecting the solution, which contains complexes formed by association of pendant adenine groups and Cu^{2+} ions, to a stronger binding ligand, EDTA disodium. As shown in Figure 3.29, the fluorescence of T_{Ad}-tT_{4h}, here at 0.02 mg/mL in chloroform, was recovered almost quantitatively upon washing the solution with excess aqueous solution containing 1 mM EDTA disodium salt. (99% recovery based on intensity measured at λ_{max}^{em}.) The strong multidentate binding offered by EDTA extracts copper ions from the organic phase, resulting in recovery of the fluorescence emission. This reversibility suggests that adenine-functionalized polythiophenes may be useful as fluorescent probes for biological imaging applications.

3.6 Conclusions

The efficient synthesis of highly-soluble conjugated polymers with functional groups for site-specific interactions that generate changes in optical properties or control morphological evolution is conceptually important for myriad applications. Here, we used direct arylation polymerization (DArP) to synthesize alternating, thiophene-based copolymers containing adenine functionality in sidechains, which are represented as T_{Ad}-T and T_{Ad}-tT_{4h}. The use of Boc protection circumvented irreversible binding of the Pd catalyst to the amine group of the adenine pendant along the copolymer backbone, which otherwise prevented polymerization, and the tendency for decreased solubility due to pendant nucleobase functionality was overcome by introducing a terthiophene comonomer with additional solubilizing alkyl side chains. By comparison to an unfunctionalized homolog having the same regioregularity, interchain hydrogen bonding interactions are shown to create interlock between polymer chains manifesting in an increase in glass transition temperature. Adenine pendent groups

chelate copper ions, leading to fast fluorescence quenching that is triggered by energy transfer from the conjugated polymer main chain to the adenine-copper complex formed upon metal ion binding. The reversible binding enables fluorescence recovery, opening possibilities for metal ion sensing, as well as extensions to bio-related applications. Successful utilization of nucleobase-functionalized, conjugated copolymers in various applications will be contingent on balancing functionality with solubility. Therefore, the use of DArP to synthesize adenine-containing copolymers represents a foundational example that motivates future efforts to create functional, conjugated copolymers that offer site-specific interactions afforded by nucleobases, thereby opening new possibilities in sensing and diagnostics, coordination-driven self-assembly, and self-healing materials.
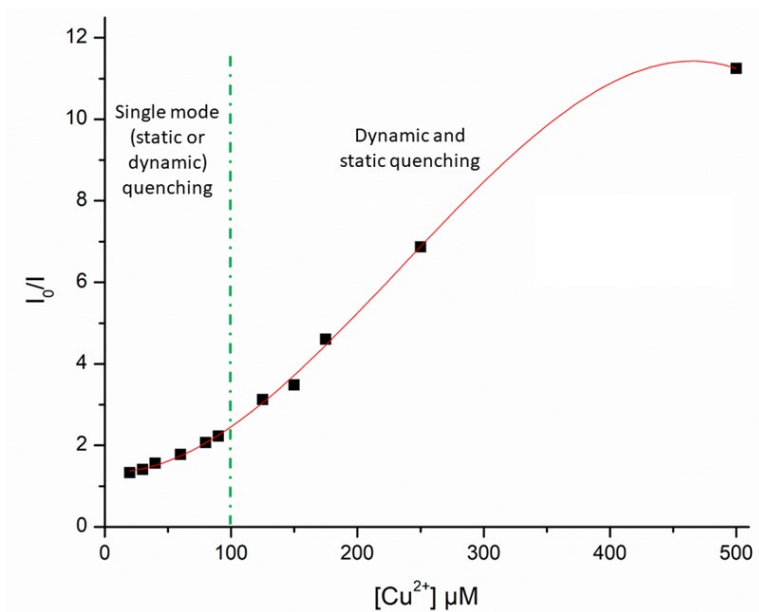
Figure 3.27: Fluorescence quenching response of T_{Ad}-tT_{4h} in the static and dynamic quenching regions, which are nominally demarcated by the dashed green line. The red line corresponds to a polynomial fit ($R^2 = 0.9986$).
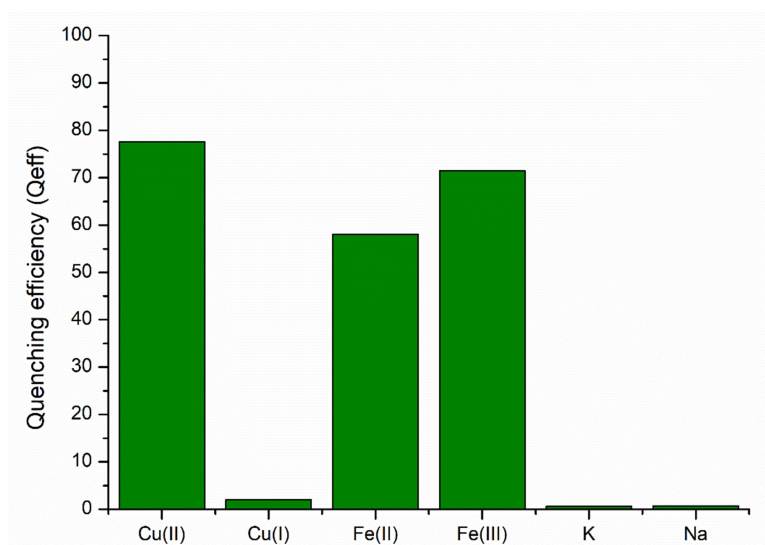
Figure 3.28: Fluorescence quenching response of T_{Ad}-tT_{4h} in presence of different ions.
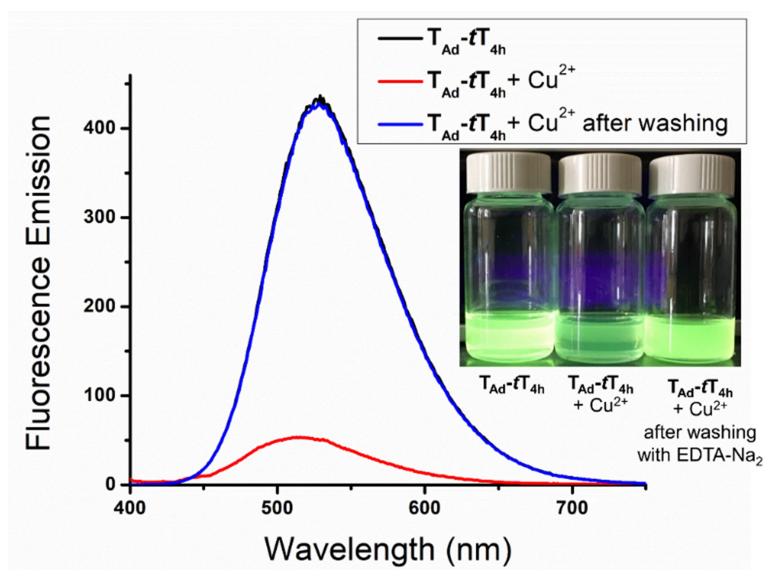
Figure 3.29: A sequence of measurements demonstrates that fluorescence emission of T_{Ad}-tT_{4h}, is quenched upon addition of Cu^{2+} and subsequently recovered after washing with an aqueous EDTA solution.

Chapter 4

Nucleobase Functionalized Poly(alkylthiophene)s by One-Pot Sequential Direct Arylation Polymerization and Deprotection: Thermally-regulated Synthesis and Hydrogen Bonding-Driven Surface Modification for Oil-Water Separations

This chapter describes the work published in ACS Applied Polymer Materials, 3, (2021), 1012–1021. I designed the one-pot direct arylation polymerization method and Boc group removal and confirmed its efficiency. I showed the host-guest hydrogen bonding between the synthesized copolymer and small molecule. I used the final product, adenine(unprotected)-functionalized polythiophene, to change hydrophilicity of a cellulosic surface and performed the tests to show their ability as a separatory filter. Coauthors include Ben LaRiviere, and M. Nance Ericson, who helped in characterizations, and Prof. S. Michael Kilbey II, who advised this work.

4.1 Abstract

Direct arylation polymerization (DArP) has emerged as an environmentally friendly, atom efficient method of synthesizing a variety of conjugated polymers. Here we report a one-pot approach consisting of DArP followed by Boc deprotection to synthesize a functional, surface-active adenine-containing poly(alkylthiophene). Careful control over the polymerization temperature enables the one-pot polymerization and deprotection strategy for synthesis, with quantitative ($> 99\%$) Boc deprotection achieved in 24 h. This temperature-controlled synthesis method reduces extra purification and isolation steps, which makes the total synthesis more efficient and practical, and allows higher molecular weight polymer to be made. We quantify the hydrogen bonding ability of the resulting adenine containing polythiophene, T_{Ad}-tT_{4h}, by ^{1}H NMR host-guest titration studies and analyze the results with Benesie-Hildebrand model, yielding an association constant of 18.7 M^{-1} between alkylated thymine and T_{Ad}-tT_{4h}. We demonstrate that T_{Ad}-tT_{4h} robustly modifies the surface of cellulosic filter paper, and the modified cellulosic filter paper, CFP-T_{Ad}-tT_{4h}, is an effective oil-water separatory filter with superhydrophobic properties (water contact angle $\approx 151°$). The utility of hydrogen bonding interactions between adenine and cellulose highlights the importance of side chain engineering for creating functional materials.

4.2   Introduction

Low-cost, rapid, effective and scalable oil-water separation is practically important due to increasing concerns over environmental and health consequences of oil leakage, oil spills, and organic contaminants, especially because processes for removal of organic pollutants are generally time-consuming, energy inefficient, and materially expensive.[289–291] Because superhydrophobic surfaces have shown success in oil-water separation via selective filtration,[292] hydrophobic conjugated polymers such as polythiophenes and poly(p-phenylenes) have been examined as model surface-modifying agents to create superhydrophobic surfaces capable of selective filtration.[293–295] For example, Advincula $et\ al.$ electropolymerized a terthiophene monomer around a stainless steel mesh to fabricate a superhydrophobic coating capable of oil-water separation.[295] In another study, Xu $et\ al.$ used physical absorption promoted by a non-solvent treatment to modify the surface of a commercially-available filter paper with oxidatively synthesized poly(p-phenylene), thereby achieving a superhydrophobic microstructure with the ability to separate oil from water.[294] Zhou and coworkers described the deposition of polyaniline to cover cotton fibers, imbuing them with oil-water separation behaviors.[296] An $et\ al.$ created superhydrophobic materials by treating different substrates such as cellulosic papers, steel mesh, and cotton threads with a solution of aminopyridine-containing microporous conjugated polymer networks that were synthesized via Sonogashira–Hagihara cross-coupling, and demonstrated efficient diesel oil/water separation.[293] Although in each case the polymer deposition is non-specific, these studies highlight the potential of conjugated polymers for creating functional surfaces.

Nature uses a variety of specific, non-bonded interactions to assemble and organize soft matter, thereby achieving elegant and superior functionality. As described in a recent review by O'Reily $et\ al.$, the central role of nucleobases in the machinery of life, protein biosynthesis, and the creation of sequence-specific macromolecules has motivated efforts to harness the specific and directional hydrogen bonding interactions inherent in nucleobases to expand the functionality of synthetic polymers.[86] In most of these contexts, ring opening polymerization or free radical polymerization methods are used. As an early example, Long $et\ al.$ used free radical polymerization to create supramolecular polymer adhesives

that containing adenine and thymine nucleobases as side chain functionality.[297] They also demonstrated that Watson–Crick base pairing could be used to immobilize thymine end-functionalized polymers through complementary pairing with adenine-decorated silica.[298]

The synthesis of nucleobase functionalized polymers by metal-mediated cross coupling or by controlled radical polymerizations requiring metal/ligand complexes is challenging due to interference of nucleobases with the metal species present in the organometallic catalysts used in those polymerizations.[95, 156, 299] For example, atom transfer radical polymerization (ATRP) of cytosine-containing methacrylate monomers using conventional conditions with copper/2,2'-bipyridine (bpy) as the metal/ligand catalyst complex and ethyl 2-bromoisobutyrate (EBiB) as an initiator did not result in polymerization due to the complex formation between cytosine groups and the copper catalyst.[95] The same issues of metal ligation arise when strategies involving C–H activation are used: In our recent report of the first example of direct arylation polymerization (DArP) to synthesize an adenine-containing, thiophene-based conjugated polymer, we showed that it was necessary to protect the amine group of adenine to avoid nucleobasecatalyst interactions that prohibit DArP.[156]

The development of DArP, which involves metal-promoted direct activation of (het-ero)aromatic hydrogens through a concerted metalation-deprotonation (CMD) pathway,[300] has been decisive for synthesis of conjugated polymers because it bypasses a number of synthetic steps, exhibits greater tolerance toward functional groups, and reduces the amount of synthetic byproducts produced in most metal-mediated cross-couplings.[116] Despite its tolerance toward many functional groups, our previous work demonstrated that DArP conditions require protection of the amine in adenine-containing monomers, which necessitates extra synthetic steps that complicates and intensifies the overall synthesis.[156] Noting that Boc protection/deprotection is arguably one of the most common steps in preparation of natural products and pharmaceuticals, developing efficient and environmentally-friendly approaches to cleave Boc protecting groups is of high interest.[301–303] Water-mediated,[304, 305] microwave assisted,[306] and thermal[307] methods are often reported, and in those approaches, no additional reagents are needed, which simplifies workups by eliminating salt removal, extraction, or isolation steps. Boc deprotection is usually conducted in acidic conditions, but deprotection in basic conditions

in polar organic solvents at elevated temperature is also reported.[308, 309] Along these lines, Kazzouli *et al.* described a simple method for Boc group cleavage using sodium carbonate (Na_2CO_3) in refluxing dimethoxyethane (DME).[303] Under conditions appropriate for palladium-catalyzed aromatic C–H activation used to synthesize an imidazoisoindol-3-one derivative, Williams and coworkers surprisingly observed Boc deprotection, rather than the desired cyclization product from C–H insertion reaction. As a result, they performed a separate Boc deprotection step in basic conditions prior to the C–H insertion.[306, 310] Yang and coworkers reported a microwave-assisted one-pot Suzuki-Miyaura cross-coupling and subsequent Boc deprotection.[299] This set of studies suggest that Boc deprotection may occur in conditions similar to those encountered in DArP, and they inspired us to carefully examine selective DArP and deprotection.

In this study, we refine DArP conditions, creating a one-pot approach to an adenine-containing, thiophene-based copolymer. The one-pot strategy streamlines the synthesis, making it more efficient by lessening the number of steps and concomitant demand for purification and isolation. In addition, we quantify the complementary hydrogen bonding ability of the adenine-functionalized alternating copolymer and use hydrogen bonding interactions of the nucleobase to create superhydrophobic cellulosic surfaces. These poly(alkylthiophene) coated filter papers perform exceptionally well in model assessments of gravimetric oil-water separation and underwater oil recovery.

4.3 Synthesis and Characterization

4.3.1 Methods and Materials

^{13}C and ^{1}H, gradient-enhanced heteronuclear multiple bond correlation (gHMBC) and gradient-enhanced heteronuclear single quantum coherence (gHSQC) NMR spectra of synthesized small molecules or polymers were acquired using a Varian VNMRS 500 MHz NMR spectrometer or a Varian Mercury Vx 300 MHz spectrometer at room temperature using 15–20 mg mL^{-1} solutions in deuterated chloroform (CDCl$_3$). Chemical shifts are reported in units of δ (ppm) and referenced to the residual solvent peak. Mass spectrometry

measurements were made using a JEOL AccuTOF DART mass spectrometer from toluene solutions at $\approx$ 1 mg mL^{-1}. The average molecular weight and dispersity of synthesized polymers were determined by gel permeation chromatography (GPC) using universal calibration analysis based on polystyrene (PS) standards. The standards are Agilent, EasiVial PS-M, which consist of molecular weights of MW, 370, 945, 1,230, 3,090, 6,320, 13,000, 27,800, 45,100, 107,000, 217,000, and 364,000 g mol^{-1}. The GPC system is based on an Agilent 1260 Infinity II isocratic pump equipped with two Agilent (7.5 $\times$ 300 mm) mixed-D type columns in sequence (and a guard column). Samples were dissolved in THF at nominal concentrations of 5 mg mL^{-1} and passed through a 0.2 μm PTFE filter prior to analysis. The flow rate of the THF mobile phase was set at 1 mL min^{-1}. Optical absorbance spectra were acquired using a Thermo Scientific Evolution 600 UV-Vis spectrophotometer by scanning from 225–650 nm. The polymer solution concentration was fixed at 0.01 mg mL-1 (in THF). Fluorescence emission spectra were acquired from polymer solutions (at 0.01 mg mL^{-1} in THF) using a Cary Eclipse fluorescence spectrophotometer. An excitation wavelength of 360 nm was used, and the emission spectrum was measured by scanning from 370-700 nm. For contact angle measurements, a polymer thin film was made by spin coating a 5 mg mL^{-1} solution (THF) on a glass slide that was previously cleaned by Piranha solution and rinsed with deionized water and isopropyl alcohol. Cellulosic filter paper modified with adenine-containing copolymer, referred as CFP-T$_{Ad}$-tT$_{4h}$, was prepared with simple immersion of Fisherbrand plain filter paper (grade p8, diameter 9 cm) in the 0.5 mg mL^{-1} solution of T$_{Ad}$-tT$_{4h}$ in chloroform for 10 minutes. The freshly prepare CFP-T$_{Ad}$-tT$_{4h}$ was rinsed with copious amounts of chloroform and then dried in a vacuum oven at room temperature for 5 h. After drying the CFP-T$_{Ad}$-tT$_{4h}$ was immersed in plain chloroform for 10 minutes and then dried again in a vacuum oven at room temperature. FTIR spectra were acquired in attenuated total reflectance (ATR) mode using a Nicolet iS50 FTIR Spectrometer equipped with mercury cadmium telluride (MCT) detector. Samples were dried in a vacuum oven for 3 h before acquiring the ATR FTIR spectra.

4.3.2 Synthesis of Small Molecules and Monomers

Intermediate small molecules and monomers, including 3-(6-bromohexyl)thiophene, 2,5-dibromo-3-(6-bromohexyl)thiophene, adenine-functionalized dibromothiophene monomer, 9-(6-(2,5-dibromothiophen-3-yl)hexyl)-9H-purine-6-amine (T_{Ad}), Boc-protected adenine-functionalized monomer (T_{Ad-Boc}), and 3,3',3",4'-tetrahexyl-2,2':5',2"-terthiophene (tT_{4h}), are synthesized as described in previous chapters.

4.3.3 Copolymer Synthesis –One-pot DArP and Deprotection

The one-pot strategy to produce adenine-functionalized polythiophene is shown in Scheme 4.1, where it is also compared to our previous approach. For the direct arylation polymerization, 8 mL of dry and degassed dimethylacetamide (DMAc) was transferred via cannula to a dry 50 mL round bottom flask. Then, 329 mg (0.5 mmol, 1 equiv.) of the dibromo monomer having the Boc protected adenine group, 9-(6-(2,5-dibromothiophen-3-yl)hexyl)-9H-purin-6-amine, referred to as T_{Ad-Boc} for simplicity, and 3,3',3",4'-tetrahexyl-2,2':5',2"-terthiophene, identified as tT_{4h}, were added (292.5 mg, 0.5 mmol). Then, neodecanoic acid (29 μL, 26 mg, 0.15 mmol, 0.3 equiv.), K_2CO_3 (138 mg, 1 mmol, 2 equiv.) and the catalyst, $Pd(OAc)_2$ (0.04 equiv.) were added to the comonomer solution while it was maintained under an argon atmosphere at positive pressure. After the additions, the flask was sealed with a septum and the mixture was heated to 90 °C and stirred for 18 h. After this time, the temperature was raised to 110 °C and stirred for additional 24 h. Aliquots were taken at the end of polymerization period (18 h), 1 h after changing the temperature (18 + 1 h), and at the end of synthesis (18 + 24 h), so that ^{1}H NMR spectroscopy could be used to monitor retention or removal of Boc groups during the one-pot synthesis. Finally, the reaction mixture was precipitated into cold methanol. The precipitate was washed with acetone and transferred to a cellulose thimble. The final product was extracted from the Soxhlet thimble by dissolving in chloroform.

4.4 Results and Discussion

4.4.1 Copolymer Synthesis and Characterization

The adenine-containing alternating copolymer, identified as T_{Ad}-tT_{4h}, was synthesized by DArP in an AA + BB fashion using Boc-protected 9-(6-(2,5-dibromothiophen-3-yl)hexyl)-9H-purin-6-amine and 3,3',3",4'-tetrahexyl-2,2':5',2"-terthiophene, which is referred as T_{Ad-Boc} and tT_{4h} respectively. (The subscripts describe the nature of the side chains.) Previously we showed that the unprotected amine functionality of the adenine pendant group prevents DArP by poisoning the palladium catalyst.[156] To overcome that issue and as depicted in Scheme 4.1, the synthesis of the soluble adenine-containing alternating copolymer involved consecutive steps involving monomer Boc-protection of the adenine-functionalized monomer, direct arylation polymerization, and finally acid-catalyzed post-polymerization deprotection.[156]

Conditions similar to those previously reported as optimized conditions for thiophene-based DArP were used,[120] but with a simple but crucial modification to create a two-step temperature profile. As shown in Scheme 4.1, direct arylation polymerization of T_{Ad-Boc} with tT_{4h} as the complementary comonomer was performed at 90 °C using $Pd(OAc)_2$ as the catalyst, dimethylacetamide (DMAc) as solvent, K_2CO_3 as the base, and neodecanoic acid as the proton shuttle. Neodecanoic acid as a bulky proton shuttle is used to ensure minimizing the branching defects due to the possible β-activation, coupling at C(4)-H, in the DArP reaction.[120] After 18 h, the temperature was raised to 110 °C without addition of any new reagents, and the solution was stirred at this temperature for 24 h in order to remove Boc protecting groups. The final product, T_{Ad}-tT_{4h}, was obtained at 70% yield and number-average molecular weight, M_n = 15.2 kg mol^{-1} with a dispersity, Đ = 1.55.

Aliquots taken at the end of DArP (18 h), 1 h after raising the temperature (18 + 1 h), and at the end of synthesis (18 + 24 h) were analyzed using ^{1}H NMR to monitor retention or removal of Boc groups during the synthesis. The chemical shifts of C-2 and C-8 protons of the purine scaffold provides insight into the state of amine protection/deprotection. These C-2 and C-8 protons shift downfield from 8.35 ppm and 7.77 ppm to 8.77 ppm and 8.00 ppm due to the addition of electron-withdrawing Boc groups. After thermally cleaving the
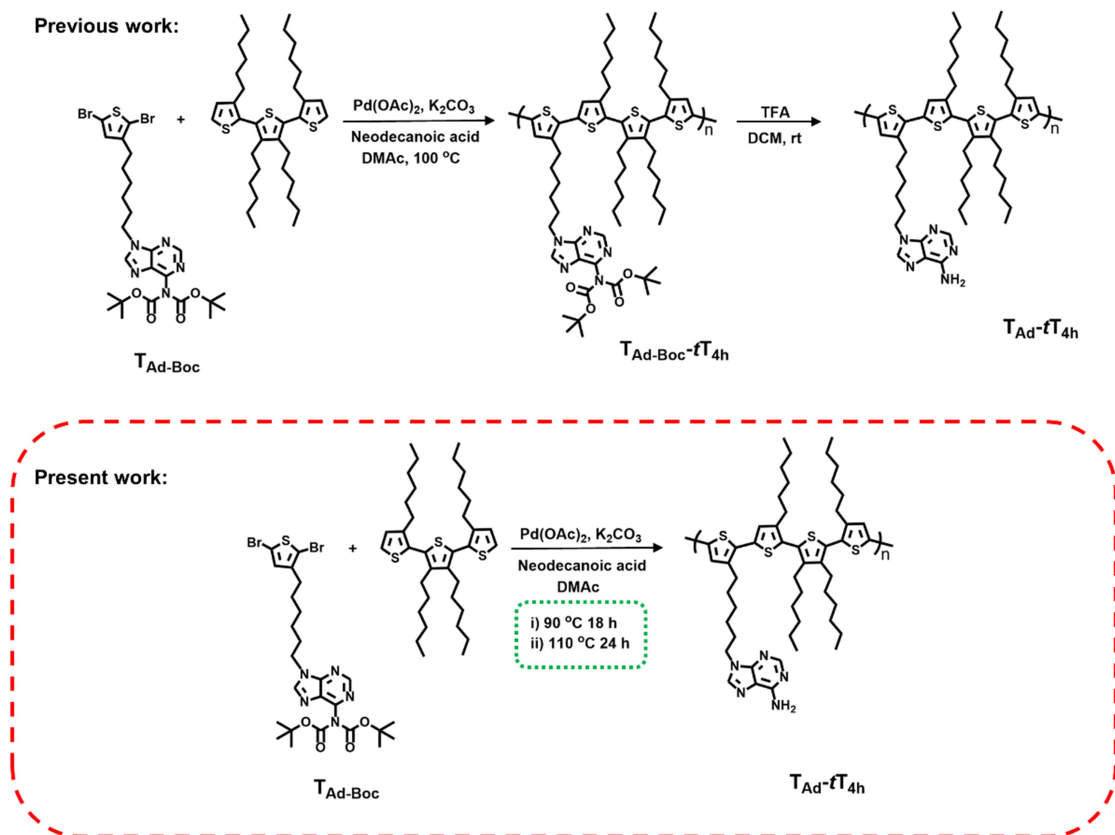
Scheme 4.1: Synthesis of T_{Ad}-tT_{4h} in a one-pot approach based on direct arylation polymerization of comonomers followed sequentially by acid-free Boc deprotection at elevated temperature and comparison to prior approach involving separate steps and acid-catalyzed deprotection.

Boc protecting groups, these signatures of the C-2 and C-8 protons return to their initial positions, which are consistent with protons of adenine. As observed from Figure 4.1, these changes are evident by comparing the spectrum for the Boc protected thiophene-based DArP monomer, T_{Ad-Boc}, with that of the adenine-containing thiophene molecule, T_{Ad}. (See spectra a and b in Figure 4.1.) After DArP for 18 h at 90 °C, the chemical shifts of C-2 and C-8 protons confirm the retention of protecting Boc groups (Figure 4.1, spectrum c). After increasing the temperature to 110 °C for 1 h, the ^{1}H NMR spectrum (Figure 4.1, spectrum d) indicates $\approx 5\%$ deprotection. As reflected in spectrum of Figure 4.1, the deprotection is nearly complete ($\approx 97\%$) after 24 h of continuous stirring at 110 °C. After this length of time, the reaction mixture was precipitated in the cold methanol, recovered by gravity filtration, and then unreacted monomers and small-molecule impurities were removed by washing with acetone in a Soxhlet apparatus. The final, purified product, T_{Ad}-tT_{4h}, was isolated by Soxhlet extraction using chloroform. As seen in Figure 4.1, spectrum f, no Boc residues are observed in the final, deprotected and purified product (after 18 + 24 h reaction time; washed with acetone and extracted with chloroform).

The ^{1}H NMR results support the conclusion of successful DArP of the adenine-containing thiophene monomer and confirm quantitative Boc removal by thermolysis in a one-pot approach. This outcome is important for green and economical production of functionalized polythiophenes that require Boc protection to ensure the retention of functional groups. Additionally, this general approach may be applied to reduce synthesis steps of complex small molecules or pharmaceutical products where C–H activation and Boc deprotection are used. For instance, Schnürch et al. synthesized a set of 1-aryl tetrahydroisoquinolines that have potential for their neuroprotective properties by iron-catalyzed direct arylation and Boc deprotection using two separate reactions in which each required purification.[311] Similarly, Oh *et al.* synthesized a therapeutic target using palladium-catalyzed regioselective direct arylation, purified the intermediate and then recovered the final product after a separate Boc deprotection.[312] As mentioned earlier, separate steps involving Boc deprotection followed by isolation and purification before direct C–H activation was required for preparation a polycyclic indole drug candidate.[306, 310] The one-pot method described
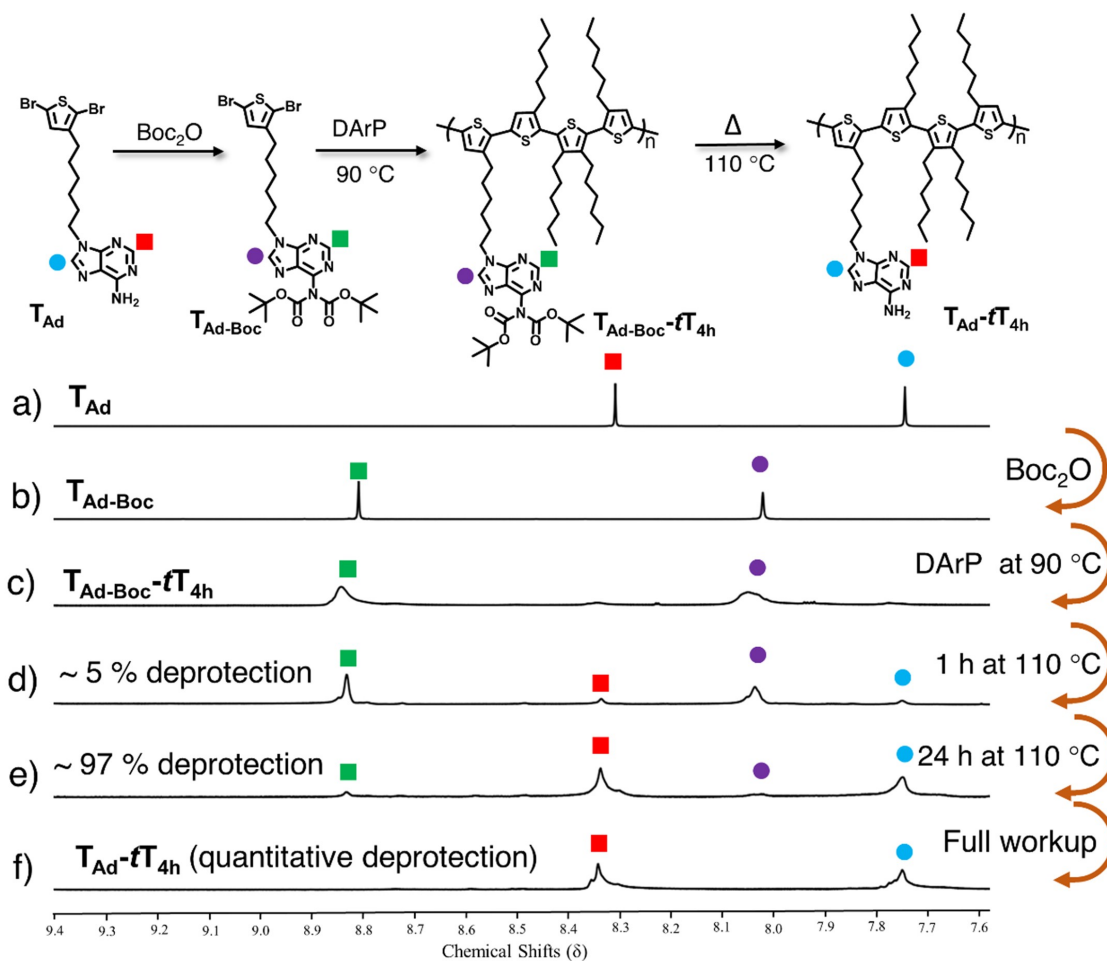
Figure 4.1: Chemical shifts of C-2 and C-8 protons associated with the purine in the side chain change upon addition of Boc protecting group (a ⟶ b). The Boc groups are retained after DArP at 90 °C for 18 h (c). Stirring at elevated temperature (110 °C) shows evidence of deprotection after 1 h (d) and nearly quantitative removal after 24 h in the crude product (e) and in the purified (f) product.

herein may eliminate intermediate isolation and purification steps, thereby reducing synthetic complexities in cases like these.

It is also noted that the T_{Ad}-tT_{4h} polymer obtained via the one-pot strategy had a higher molecular weight and lower dispersity (Mn = 15.2 kg mol^{-1}, Đ = 1.55) compared to the molecular weight of T_{Ad}-tT_{4h} (reported in Chapter 3) synthesized using the two-step process consisting of DArP at a slightly higher temperature (of 100 °C) followed by acid-catalyzed deprotection, which yielded a copolymer of Mn = 7.0 kg mol^{-1} and Đ = 1.82.[156] While higher temperature usually results in higher monomer conversion and, therefore, higher molecular weight, in this case, using a higher temperature may have resulted in removal of a few Boc groups. Because the adenine groups are present in significant excess to the metal catalyst, a few unprotected amines effectively inhibit the polymerization by coordinating with the palladium catalyst.[156] In light of this, it is hypothesized that performing DArP at the lower temperature of 90 °C, rather than at 100 °C, enables higher molecular weight to be attained. Besides, the typical side reactions of DArP, homocoupling and β-activation, can also become less important by running the polymerization at a lower temperature.[120]

4.4.2   Photophysical Properties

Photophysical properties of T_{Ad}-tT_{4h} were examined by measuring the absorption and fluorescence spectra in solution (tetrahydrofuran, THF) and in the solid state using spin-coated thin films on glass substrates. (See Figure 4.2.) The π-π* optical transition for the conjugated backbone exhibits a local maximum at λ_{max}^{abs} = 392 nm. The absorption spectrum of the solid polymer film (on a glass substrate) shows a $\lambda_{max,film}^{abs}$= 400 nm, which represents a slight red shift (bathochromic shift) compared to the absorbance of the copolymer in THF solution. This common behavior is a consequence of stronger intermolecular interactions, ostensibly due to π-stacking and hydrogen bonding, in the solid state.[313] Optical properties are similar to values reported previously for T_{Ad}-tT_{4h} copolymer of lower molecular weight (M_n = 7.0 kg mol^{-1}),[156] which suggests that both of the T_{Ad}-tT_{4h} alternating copolymers are above their effective conjugation length.[6, 314]
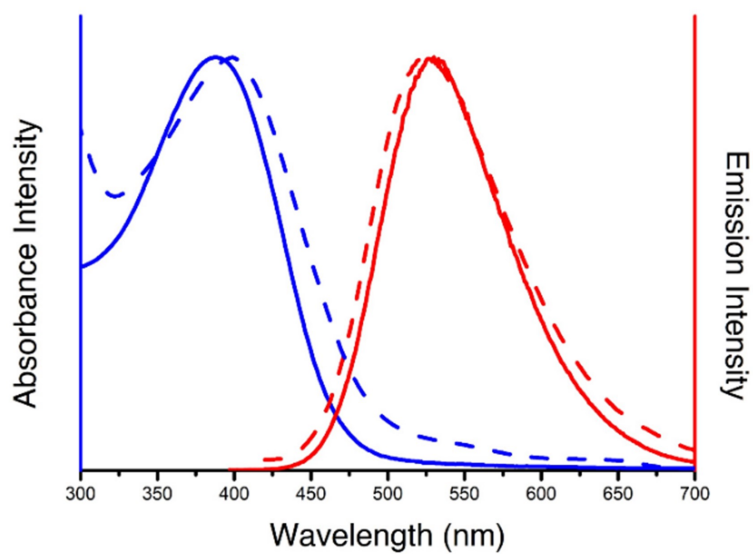
Figure 4.2: Normalized absorption and fluorescence spectra acquired from T_{Ad}-tT_{4h} in THF solution (blue solid line for absorbance and red solid line for emission) and from spin cast films on a glass substrate (blue dashed line for absorbance and red dashed line for emission.) Y-axes are colored according to the measured profile to facilitate readability (using blue and red for absorbance and fluorescence profiles, respectively).
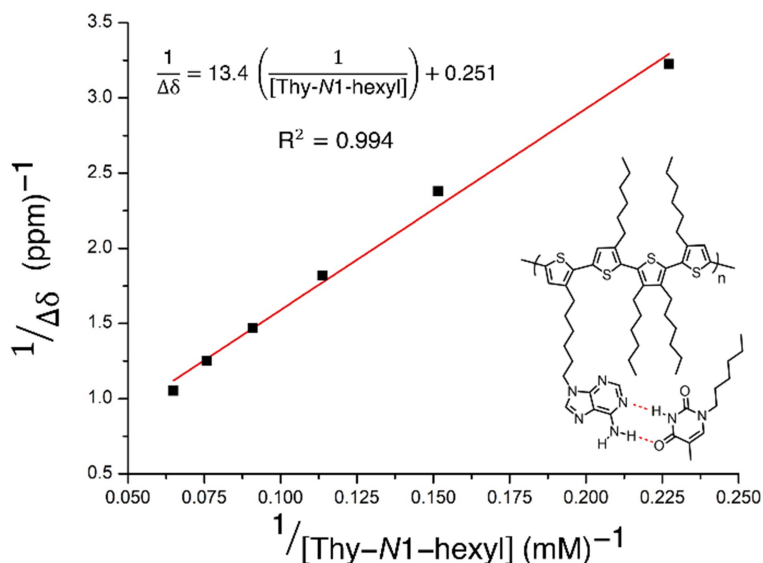
Figure 4.3: Complementary hydrogen bonding between the T_{Ad}-tT_{4h} (host) and thymine-N1-hexyl (guest) in CDCl$_3$ at 25 °C, expressed according to the Benesi-Hildebrand model. Linearity reflects a 1:1 association with an association constant, $K_a = 18.7$ M^{-1}.

4.4.3 Hydrogen Bonding of the Copolymer

The ability of the adenine side chain functionality in the T_{Ad}-tT_{4h} copolymer to participate in hydrogen bonding is investigated by ^{1}H NMR spectroscopy. Specifically, a titration study involving gradual addition of thymine-N1-hexyl as the guest molecule to a solution containing T_{Ad}-tT_{4h} (as the host molecule at fixed concentration) in deuterated chloroform was used, and complementary hydrogen bonding between nucleobases is reflected by downfield shifts of protons.[188] In this case, the position of the protons associated with the amine (NH_2) of adenine was recorded as thymine-N1-hexyl was added to the solution of T_{Ad}-tT_{4h}. The initial concentration of T_{Ad}-tT_{4h} was 7.7 mg mL^{-1}, which equates to 8.8 mM of adenine functionality. Resonance signals of NH_2 shifted downfield from 5.88 ppm to 6.51 ppm as the concentration of thymine-N1-hexyl was systematically increased from 0 to 15.4 mM. Changes in the chemical shift of the protons associated with NH_2 of adenine are plotted as a function of concentration of thymine-N1-hexyl, [Thy-N1-hexyl], in an inverse formalism as seen in Figure 4.3. This representation allows the Benesi-Hildebrand model, which is shown in equation 4.1, to be used to determine the association constant (K_a) for complex formation between a host at fixed concentration while the concentration of the guest is increased systematically during ^{1}H NMR titration experiments.[315, 316]

$$\frac{1}{\Delta\delta_{NH_2}} = \frac{1}{K_a \Delta\delta_{max(NH_2)}[Thy-N1-hexyl]} + \frac{1}{\Delta\delta_{max(NH_2)}} \qquad (4.1)$$

In this expression, $\Delta\delta_{(NH_2)}$ and $\Delta\delta_{max(NH_2)}$ are the concentration-dependent change and maximum change in the chemical shifts of NH_2 protons of the adenine in the bound complex, respectively.

The linear relationship reflected in Figure 4.3 confirms that the host-guest complex associates in a 1:1 stoichiometric ratio.[317–319] In addition, the association constant (K_a) calculated from the Benesi-Hildebrand model was determined to be 18.7 M^{-1} (in CDCl$_3$ at 25 °C), which is in good agreement with K_a values reported for complementary hydrogen bonding involving a polymer-attached nucleobase and nucleobase in a chloroform solution. For example, Long *et al.* reported K_a = 19 M^{-1} for a functionalized thymine guest interacting with a poly(ethylene glycol) host containing adenine functionality in

the side chain.[188] Similarly, in Chapter 2 we investigated complex formation between alkylated thymine (thymine-N1-hexyl) and alkylated adenine (adenine-N9-hexyl) in an adenine-functionalized low bandgap benzodithiophene-based copolymer, and found the host-guest association constant to be 29 M^{-1}.[320] Expectedly, small molecules show stronger complexation, however, the small difference and similarity between the association constants of polymer-small molecule and small molecule-small molecule complexes suggests that the hydrogen bonding ability of adenine is not significantly affected by being tethered to the chain through in the side chain. These studies highlight the accessibility of pendant adenine groups along the conjugated backbone and their ability to participate in hydrogen bonding, regardless of the nature of the backbone chain, which sets the basis for using this capacity of T_{Ad}-tT_{4h} in various applications.

4.4.4 Surface Modification and Separation Using T_{Ad}-tT_{4h}

Commercially available cellulosic filter paper has been used as a relatively low-cost substrate for making superhydrophobic surfaces.[321–324] Many of physical and chemical properties of cellulose are derived from and governed by its ability to participate in inter- and intramolecular hydrogen bonding, which arise from the abundance of hydroxyl groups. Researchers have taken advantage of this ability to modify cellulosic materials.[325–327] For example, Luo *et al.* used hydrogen bonding between glucose and cellulose fibrils to modify cellulosic filter paper and used it for oil-water separation.[328] Zhang and coworkers exploited the hydrogen bonding ability of hydroxyl groups in cellulosic substrates to assemble a siliconate-based waterproof reagent through a solution-immersion process,[329] and Musikavanhu and coworkers similarly tailored the wettability of cellulosic paper using amine-functionalized silica nanoparticles.[330]

Based on these works, we hypothesized that the multiplicity of hydrogen bonding between adenine groups along the T_{Ad}-tT_{4h} chain and abundantly-available hydroxyl groups of cellulose could be utilized to robustly modify cellulosic filter paper (CFP) by simple dip coating. Chloroform was used as the solvent because it does not prevent hydrogen bonding interactions, as evidenced from host-guest ^{1}H NMR studies and work of Long *et al.*[188]

Loosely attached polymers were removed from T_{Ad}-tT_{4h} modified cellulose filter paper (CFP-T_{Ad}-tT_{4h}) by rinsing with copious amounts of chloroform immediately after the dip coating step, and the modified filter paper was then dried under vacuum at room temperature for 5 h (room temperature is chosen to avoid any oxidation of the thiophene backbone). After drying, the CFP-T_{Ad}-tT_{4h} was immersed in chloroform for 10 minutes and then again dried under vacuum at room temperature. Figure 4.4 shows pictures of the modified filter paper, CFP-T_{Ad}-tT_{4h}, under visible light and UV irradiation: physisorbed T_{Ad}-tT_{4h} is evident by green emission under UV irradiation. Gravimetric measurements indicate that the mass increased by 0.5 ± 0.1 wt.% due to absorption of T_{Ad}-tT_{4h} on filter papers.

FTIR has commonly been used to analyze surface functionalization of cellulosic materials and, as a result, signatures associated with cellulose and modified derivatives are widely reported.[331–333] Characteristics of the natural cellulose structure of unmodified filter paper manifest in the absorbance bands at 899 cm^{-1}, 1014 cm^{-1}, 1050 cm^{-1}, 1151 cm^{-1}, 2883 cm^{-1}, which correspond to vibrational modes due to in-plane symmetric stretching of skeletal C–O–C bonding motifs, vibration of the C–OH bond of primary alcohols, vibration of the C–OH bond of secondary alcohols, C–C ring breathing modes, and vibrations associated with C–H stretching, respectively.[332] In addition, the absorbance in the 3000-3500 cm^{-1} region that is centered at $\approx$ 3300 cm^{-1} corresponds to stretching modes of hydroxyl groups (O–H) of the unmodified cellulose.[334] Close inspection of the absorbance in the hydroxyl region (3000-3500 cm^{-1}) is essential because it reveals information about the local environment of hydroxyl groups, which is affected by hydrogen bonding. In many cases and specifically for cellulosic hydroxyl groups, bands associated with hydrogen bonding shift to lower wavenumbers and are intensified, and those changes correlate with the strength of hydrogen bonding.[334–336]

The FTIR spectrum of unmodified cellulosic filter paper is shown in Figure 4.5 along with the spectrum of T_{Ad}-tT_{4h} in the solid state. In that spectrum, bands for the thiophene rings of the backbone and adenine fused ring heterocycles are seen: the band at 720 cm^{-1} corresponds to an in-phase breathing mode of the pyrimidine ring of adenine, the band at 1130 cm^{-1} is due to overlapping vibrations associated with C(2)–N(1)=C(6) bending of the pyrimidine ring and stretching of C(5)–N(7)=C(8) of the imidazole ring.[199] The band at 1608 cm^{-1} derives from C=C and C=N stretches of the six-member ring of adenine and
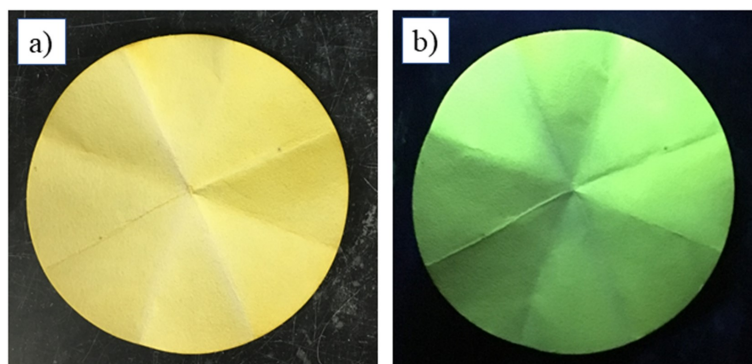
Figure 4.4: Images of CFP-T_{Ad}-tT_{4h} under a) visible light and b) UV irradiation.
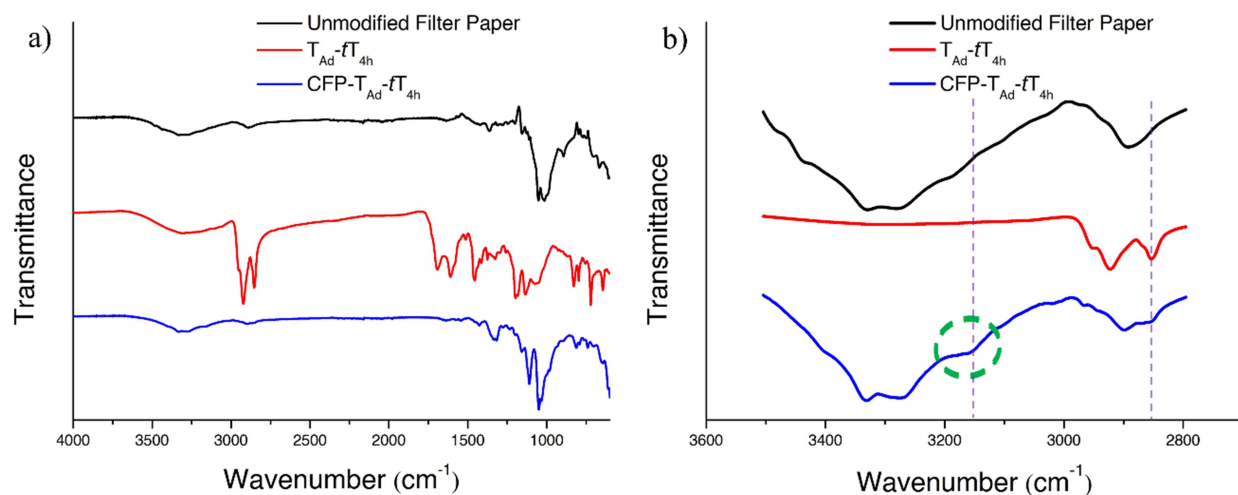
Figure 4.5: FTIR spectra of unmodified cellulose filter paper, T_{Ad}-tT_{4h}, and CFP-T_{Ad}-tT_{4h} in the range of a) 4000 cm^{-1} - 600 cm^{-1} and the b) spectral region between 3500 cm^{-1} and 2800 cm^{-1}. The green circle highlights the appearance of new band in CFP-T_{Ad}-tT_{4h} that is attributed to hydrogen bonding between adenine groups and cellulose. The dashed lines in b) at 2857 cm^{-1} and at 3158 cm^{-1} highlight presence of T_{Ad}-tT_{4h} in the CFP-T_{Ad}-tT_{4h} and the emergence of a new signal in the O–H region attributed to hydrogen bonding with adenine moiety, respectively.

124

the band at 1688 cm^{-1} is attributed to a scissoring mode of NH$_2$ of adenine. The broad peak from 3000 cm^{-1} – 3600 cm^{-1} is due to symmetric and asymmetric stretching of N–H bonds of the NH$_2$ group.[337–339] Modes attributed to thiophene rings are observed at 828 cm^{-1} and 1452 cm^{-1}, which represent the C–H$_\beta$ out-of-plane mode (where C is C(4) of 3-hexylthiophene) and C=C stretching in thiophene ring, respectively. Stretching modes attributed to CH$_2$ groups of the hexyl side chains appeared at 2855 cm^{-1} and 2920 cm^{-1}.[196, 340] In the zoomed-in spectrum (Figure 4.5b) for CFP, the local minimum seen at $\approx$ 3327 cm^{-1} in the hydroxyl region (3000-3500 cm^{-1}) is attributed to O(3)–H$\cdots$O(5) intramolecular hydrogen bonds within the cellulose I structure, and a second local minimum at 3284 cm^{-1} is attributed to inter-and intramolecular hydrogen bonds at O(6)–H in the natural cellulose I structure.[331]

The FTIR spectra of treated cellulosic paper, identified in Figure 4.5 as CFP-T$_{Ad}$-tT$_{4h}$, is dominated by bands related to cellulose structure but signatures associated with T$_{Ad}$-tT$_{4h}$ and hydrogen bonding can be resolved with close inspection. An extra shoulder appears at 2857 cm^{-1}; although this mode is difficult to resolve due to overlap with C–H stretching of cellulose, it is due to the stretching of alkyl side chains of absorbed T$_{Ad}$-tT$_{4h}$. In addition and more prominently, a shoulder at 3158 cm^{-1} for CFP-T$_{Ad}$-tT$_{4h}$ is observed (highlighted by the green circle in Figure 4.5b). This vibrational mode results from hydrogen bonding between hydroxyl and adenine groups, signifying successful modification of CFP. Both O–H$\cdots$N and N–H$\cdots$O hydrogen bonds are possible in the complementary hydrogen bonding interaction between adenine and cellulose I. In the first case, nitrogen atoms of the purine scaffold act as hydrogen bonding acceptors to cellulosic hydroxyl groups that function as the hydrogen bonding donor. In the second case, oxygen atoms from cellulose (from either hydroxyl groups or ether oxygens in the backbone) are the acceptor in hydrogen bonding with N–H from the NH$_2$ group of the adenine. Even though both interactions are possible, the former situation of O–H$\cdots$N is expected to be the stronger interaction based on bond length values reported as typical for H$\cdots$A (where A represents the acceptor in the hydrogen bonding interaction).[195, 341–343] Małecka *et al.* compared N–H$\cdots$O and O–H$\cdots$N internal hydrogen bonds in the two tautomers of a fused ring heterocycle containing a primary amine and concluded that the O–H$\cdots$N bond is stronger.[344] This type of hydrogen bonding (O–H$\cdots$N) has been

reported in the RNA structure between nucleobases like adenine and hydroxyl groups along the backbone.[345, 346] The spectrum of the CFP-T_{Ad}-tT_{4h} also shows an extra peak at 3158 cm^{-1}, which is most likely due to O–H vibrations that are shifted to lower frequency due to hydrogen bonding. This agrees with results reported for O–H bond stretching vibrations in O–H$\cdots$N type hydrogen bonds in the solid state, which appear in the range 3113 cm^{-1} – 3181 cm^{-1}.[341, 342] This phenomenon of vibrational bands shifting to lower frequencies also has been reported for N–H bonds in polyurethane, which shift from 3445 cm^{-1} to 3315 cm^{-1} upon hydrogen bonding,[336] and the N–H bond stretching mode of adenine moves from 3454 cm^{-1} to 3328 cm^{-1} upon hydrogen bonding with thymine.[347] In combination, this information and the analyses of FTIR results suggest that surface modification of cellulosic filter paper by T_{Ad}-tT_{4h} is efficient and promoted by intermolecular hydrogen bonds that are formed during the simple solution-immersion process.

The static water contact angle (CA$_W$) of CFP-T_{Ad}-tT_{4h} is compared to that of a film created by spin coating on a flat glass substrate in order to highlight the effect of the template structure on superhydrophobicity. As shown in Figure 4.6, the film made by spin coating a 5 mg mL^{-1} solution of T_{Ad}-tT_{4h} in THF exhibited a CA$_W$ = 100°± 1°. On the other hand, the modified cellulose filter paper, CFP-T_{Ad}-tT_{4h}, had a CA$_W$ = 150 °± 1°, which falls into the range of superhydrophobic surfaces.

The performance of superhydrophobic CFP-T_{Ad}-tT_{4h} in oil-water separations was tested and the results are captured in Figure 4.7. First, a mixture of 10 g of water and 10 g of diethyl ether (organic phase) was used to show the selectivity of the modified filter paper. In this case, the aqueous phase of the biphasic system contains rhodamine B, as can be inferred from Figure 4.7-a1. The oil-water mixture was poured on top of folded CFP-T_{Ad}-tT_{4h} in a funnel. As shown in Figures 4.7-a2 through 4.7-a4, the aqueous phase (dyed pink) is retained above the filter paper while the organic phase passes through the CFP-T_{Ad}-tT_{4h}. Diethyl ether is recovered in high efficiency ($\approx$ 97 wt%) without applying any external pressure. Selective filtration of the lighter diethyl ether phase ($\rho_{E_2O} < \rho_{H_2O}$, ρ being density) indicates that the separation is not based on gravimetric phase separation. Rather, the superhydrophobic nature of the modified filter paper is the dominating factor driving the separation. Superhydrophobic surfaces are able to trap air, and even when they
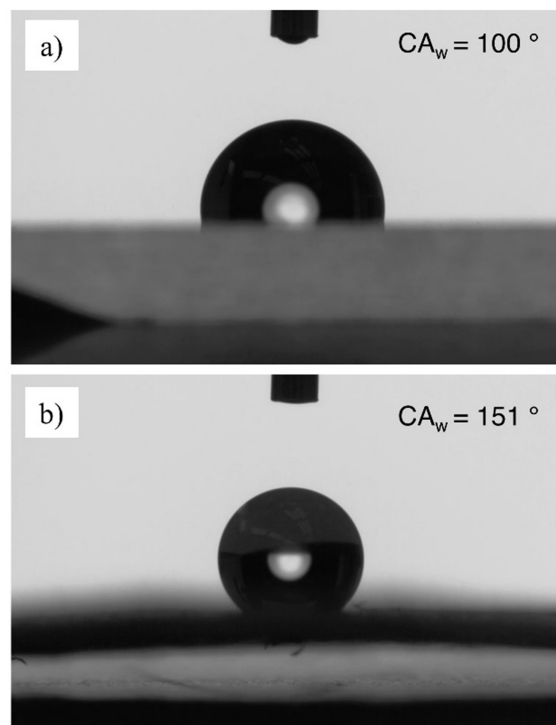
Figure 4.6: Water droplets and contact angles measured on a) T_{Ad}-$t$$T_{4h}$ film created by spin casting on a glass substrate and on b) CFP-T_{Ad}-$t$$T_{4h}$, which is made by dipping cellulosic filter paper in a chloroform solution of T_{Ad}-$t$$T_{4h}$.

are fully submerged in water they can retain underwater superhydrophobicity.[348] This superhydrophobicity of CFP-T_{Ad}-tT_{4h} was highlighted in another experiment that mimics an underwater oil recovery test. In this case and as shown in Figure 4.7-b1, chloroform (dyed blue) was used as the heavier phase. As the sequence of images show, the modified filter paper remains dry underwater (Figure 4.7-b2 and 4.7-b3) until it reaches the organic phase (Figure 4.7-b4), and then it quickly absorbs the chloroform (Figure 4.7-b5).

4.5 Conclusions

Expanding the functionality of materials is essential to improve their performance or expand their applicability. Here, an optimized one-pot synthesis involving only a two-step temperature profile is used to generate an adenine-functionalized polythiophene copolymer, which can efficiently modify cellulosic filter paper to create a superhydrophilic surface. The two-step temperature profile is essential, as it allows chain growth via direct arylation polymerization of the Boc-protetected, nucleobase-containing monomer to proceed, followed by efficient thermolytic cleaving of Boc protecting groups at higher temperatures without any added reagents. Pendant adenine groups in the T_{Ad}-tT_{4h} copolymer actively participate in hydrogen bonding interactions, and these are demonstrated to readily immobilize the conjugated polymer on cellulosic filter paper. The cellulosic filter paper modified with adenine containing conjugated copolymer, CFP-T_{Ad}-tT_{4h}, shows superhydrophobic properties and efficiently separates organic phases from aqueous phases in difficult situations, highlighting the multifunctional potential of nucleobase-containing conjugated polymers that take advantage of multipoint hydrogen bonding interactions, including the potential to utilize Watson-Crick base pairing to modify a wide variety of substrates. The retention of Boc protecting groups during polymerization predicated on C–H activation followed by thermolytic deprotection to generate the functional copolymer may widen the utility of DArP for more complex monomers, including functional bio-inspired monomers, and greatly simplify total synthesis in many contexts.
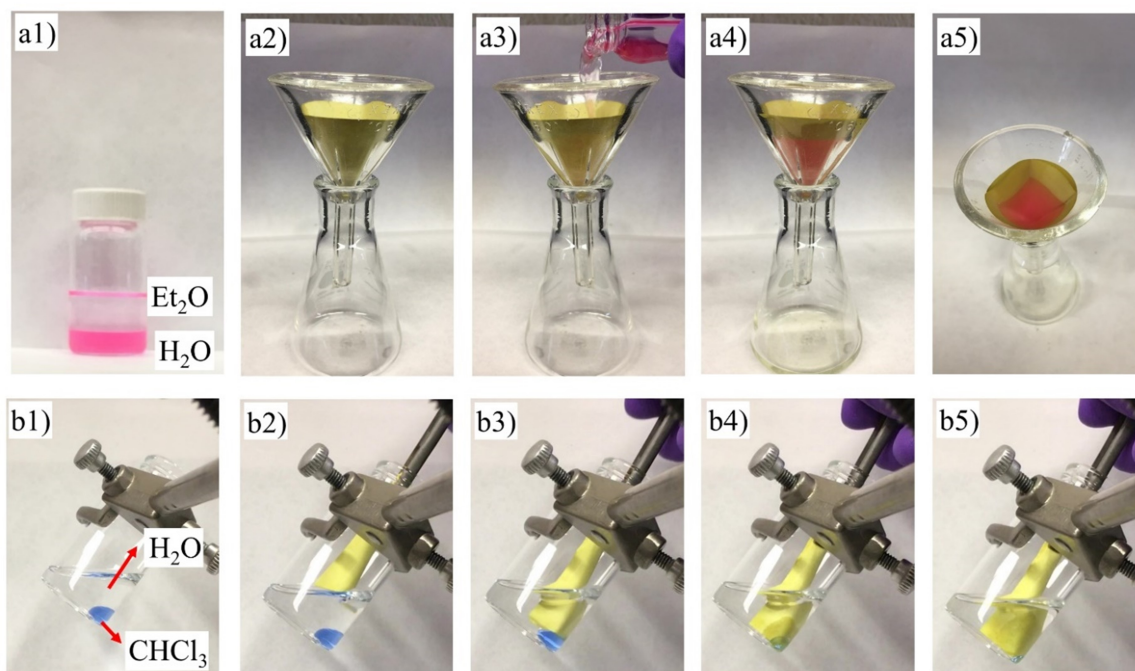
Figure 4.7: Sequences of images highlighting ability of CFP-T_{Ad}-tT$_{4h}$ to a1a5) separate a phase separated mixture of diethyl ether and rhodamine B-dyed water and to b1b5) recover chloroform, a mock oil, via underwater recovery.

Chapter 5

Summary, Key Conclusions, and Future Work

5.1 Summary and Key Conclusions

Effective contributions to material development require formulation of structure-property relationships that provide a fundamental understanding of design features and connect the chemical structure to performance in desired applications. The work I described in this dissertation follows such notions, beginning with careful design and synthesis and continuing through in-depth characterizations. This work examines how the incorporation of nucleobases, which are nature inspired molecules that bring specific and directional hydrogen bonding, into the structure of conjugated polymers affects their properties. The research efforts start with the synthesis of benzodithiophene-based conjugated polymers having adenine or thymine at the terminus of side chains. Hole transport properties are improved relative to the non-functionalized homologs when thymine functionality is added to the side chains. This behavior is attributed to to inter-base hydrogen bonding interactions that affect the packing of these materials, resulting in enhanced transport properties. More interestingly, the as-cast films made with nucleobase-functionalized copolymers had similar hole transport properties to thermally annealed films made from polymers without nucleobase side chain functionalities. This suggests that properties of non-functionalized homologues depend on the thermal history, but hydrogen bonding promotes effective organization without the need for annealing. This study demonstrates that nucleobases in the side chains are accessible to actively participate in complementary and self-complementary hydrogen bonding interactions. The hydrogen bonding ability is also harnessed in immobilizing these nucleobase-containing conjugated polymers on surfaces, which creates solvent-resistant thin films.

The second main part of my dissertation involves successfully redefining and optimizing synthesis of nucleobase-functionalized conjugated polymers by direct arylation polymerization. I found that the presence of adenine functionality during the direct arylation polymerization prohibits the polymerization due to complex formation or binding between the catalyst and nucleobase. This complexation between the catalyst and adenine is debilitated by the addition of a bulky Boc groups that protect the amine. Successful polymerization of the protected adenine-functionalized thiophene monomer is achieved, and

removal of the protecting groups recovers the ability of the adenine in each side chain to chelate metal ions. The complex formation involving adenines in the side chains is the basis of using these adenine-containing polythiophenes in fluorescence ion detection in solution. This work new insights into the functional group tolerance of direct arylation polymerization and widens the synthetic pathways to obtain nucleobase-functionalized conjugated polymers.

I refined the synthetic approach to streamline the synthesis of adenine-functionalized conjugated polymers. In this work, thermal regulation is implemented to combine the polymerization and deprotection steps, which shortens the synthesis procedure and reduces environmental impacts by avoiding the need to purify and isolate the protected nucleobase-functionalized copolymer before reformulating and carrying out the deprotection reaction. In this part of the study, the hydrogen bonding ability of adenine in the side chain effectively anchors the copolymer to cellulosic surfaces, which changes the surface energy of the cellulosic substrate drastically from being hydrophilic to superhydrophobic. I demonstrated the ability of these superhydrophobic surfaces to perform difficult separations. This work is impactful because the one-pot synthetic approach used is applicable in the synthesis of various small molecules and therapeutics that utilize C–H activation.

In total, these efforts demonstrate that relatively well-defined polymerization strategies based on Stille cross-coupling or DArP are useful in the synthesis of conjugated polymers with nucleobase functionality and the resulting polymers have improved performance and wider applicability compared to parent (unfunctionalized) conjugated copolymers. For example, the adenine-containing polythiophene is sensitive to the presence of metal ions while the non-functionalized homolog does not show a strong fluorescence-quenching behavior. As another example, thymine functionality in the benzodithiophene-based copolymers lead to an increase in the hole mobility by two-orders of magnitude. The common theme in these efforts is relating observed properties to structural aspects of polymers, which is made possible by careful synthesis and optimized polymerization conditions.

Altogether, my research contributes to establishing deeper understandings of the structure-property relationships of nucleobase-functionalized conjugated polymers and advances the synthesis of these multifunctional materials. The presented research exemplifies how hydrogen bonding can be used to improve the properties and widen the applicability

of conjugated polymers. This research sets the groundwork for developing side chain engineering approach to use nucleobases for various applications.

5.2 Future Work

Nucleobases contribute to material properties through various ways, such as hydrogen bonding, metal chelation, π-stacking, and acid/base properties. Synthesis and processing of nucleobase-functionalized materials are considered to be challenging due to the nucleobases having multiple reactive sites (that can lead to the possibility of undesired side reactions) and hydrogen binding interactions (that leads to aggregation or reduces solubility). This work successfully addresses these issues, allowing nucleobases to be incorporated into the structure of conjugated polymer, which sets the groundwork for further development of these materials. The fact that nucleobases are prevalent in nature also suggests that this group of polymers are potentially useful for bio-related applications. In addition, the polymerization method used, direct arylation polymerization, is considered to be a green and environmentally friendly polymerization method, that makes it more feasible for these materials to be used in bio-related applications. Water-miscibility would also be a factor in this venue, thus improving water solubility in conjunction with incorporating nucleobase functionalities seems to be a worthwhile pursuit.

In this regard, it seems reasonable to incorporate oligoether side chains into the structure of the thiophene comonomer to improve water solubility. The synthesis and purification details of a bithiophene monomer bearing oligoether side chains at the 3 and 3' positions are presented in Appendix B. This monomer is polymerizable through DArP with a dibromo complementary comonomer. This approach can make nucleobase-functionalized conjugated polymers a candidate for bio-related applications.

5.2.1 Traceable Drug Delivery

Fluorescence signaling by the conjugated backbone and the ability of nucleobases to bind with a variety of molecules (potentially therapeutic molecules) can lead to the development of traceable drug carriers. More importantly, nucleobases are known to have acid-base activity,

which could ultimately be used as a way to release drugs from the carrier based on the pH of the environment. Water solubility of the carrier is important for effective delivery, and this requirement would be met by the oligoether side chains. The direct arylation polymerization method we used for synthesis of nucleobase-functionalized monomers (Chapter 3 and 4), which uses a minimal amount of metal catalyst and does not produce byproducts in stoichiometric proportion is useful for polymers that are used in bioapplications. The release rate depends on interaction strength between the target molecule and carrier. Molecules that have H-bonding ability are well-suited for this study because their interactions with target drugs, and ultimately the release rate, depends on the pH and ionic strength of the medium. The study of different nucleobase-target molecule pairs could be used to establish structure-property relationships for a given class of nucleobase-functionalized copolymers.

5.2.2 Using Nucleobase-Containing Conjugated Polymers as Adhesion Layers

Using small molecules or surface-attached species in thin layers to modify surface energy (surface passivation) in the fabrication of devices such as field-effect transistors is common. As shown in Chapter 2 and 4, the hydrogen bonding ability of nucleobases can be exploited for surface immobilization. Currently, poly-L-lysine (non-covalent) and alkyl silane (covalently bonded) are common materials used to passivate silicon oxide. A thin layer of a nucleobase-functionalized conjugated polymer could be used to cover the oxide layer of silicon wafer and reduce the surface energy so that the active layer can wet the surface more effectively. We showed in Chapter 4 that the nucleobase-functionalized copolymers are able to attach to high energy surfaces (a cellulosic surface was used in Chapter 4) and reduce the surface energy significantly (a superhydrophobic surface was obtained). Various film forming methods are possible for making a thin layer, including, dip coating, Langmuir-Blodgett deposition, or spin coating. Film formation conditions and the copolymer concentration and solvent type would need to be optimized to control the thickness of the interlayer. Devices made using the nucleobase-modified copolymer as the passivator layer could be made and compared to devices that use poly-L-lysine as the passivation interlayer. This study will help to

understand the role of the passivation layer in multilayer structures of organic field-effect transistors.

5.2.3 Synthesis of Polymers with Multiple Nucleobase Side Chain Functionalities

As expected and tested in Chapter 2, complementary base pairing interactions are stronger than self-complementary interactions. In this realm, three studies focused on self-assembly behaviors seem interesting. It seems worthwhile to probe design-structure-property relationships using a I) combination of two copolymers made such that each has one type of nucleobase. For example, examine assembly of a thymine-containing polythiophene with an adenine-functionalized polythiophene. Along this line of complementary interactions, one could also II) synthesize and characterize copolymers that have two different nucleobases in the side chains (for example, thymine and adenine). Finally, ideas about integrating different nucleobases provide inspiration to the idea of III) synthesis and characterization of sequence regulated nucleobase-functionalized conjugated polymers.

The blending of two structurally similar conjugated polymers with different nucleobase-containing side chains might result in better packing and improve device properties. Although we did not see this effect when we combined BDT_R-T_{Thy} and BDT_R-T_{Ad} as a part of work described in Chapter 2, we did not devote much attention to this type of work, and we did not modify any of the polymer designs. We envision that examining this hypothesis will require more time and elaborate characterizations. The BDT-based polymers already have limited solubility, and thus their mixture might suffer from large scale aggregation. Therefore, these studies would benefit from a more soluble class of polymers, which would promote better mixing of two copolymers. A significant focus of these studies would examine changes in solid state macro-structure, which will help to understand the effect of base pairing on organization and photophysical properties.

In an extension of this proposed study, it sees reasonable to compare behaviors if two different nucleobases are incorporated in the same polymer. This study will provide insight

into the impact of the distribution of bases through the polymer chain on intra- and inter-molecular base pairing compared to binary mixtures of two copolymers. Ultimately, using a polymeric template with a specific sequence already built into the chain structure can result in sequence specific conjugated polymer. This method has been used to synthesize non-conjugated polymers. integrating a specific sequence of nucleobases in a side chain-functionalized conjugated polymer would enable sequence-specific binding of DNA, which has specific relevance in biotechnology.

Bibliography

1 Shirakawa, H., Louis, E. J., MacDiarmid, A. G., Chiang, C. K., & Heeger, A. J. (1977). Synthesis of electrically conducting organic polymers: Halogen derivatives of polyacetylene, $(CH)_x$. *Journal of the Chemical Society, Chemical Communications*, 578–580.

2 Shirakawa, H., Ito, T., & Ikeda, S. (1978). Electrical properties of polyacetylene with various cis-trans compositions. *Die Makromolekulare Chemie*, *179*(6), 1565–1573.

3 Shirakawa, H. (2001). The discovery of polyacetylene film: The dawning of an era of conducting polymers (nobel lecture). *Angewandte Chemie International Edition*, *40*(14), 2574–2580.

4 Rissler, J. (2004). Effective conjugation length of π-conjugated systems. *Chemical Physics Letters*, *395*(1), 92–96.

5 Ma, J., Li, S., & Jiang, Y. (2002). A time-dependent DFT study on band gaps and effective conjugation lengths of polyacetylene, polyphenylene, polypentafulvene, polycyclopentadiene, polypyrrole, polyfuran, polysilole, polyphosphole, and polythiophene. *Macromolecules*, *35*(3), 1109–1115.

6 Wells, N. P., Boudouris, B. W., Hillmyer, M. A., & Blank, D. A. (2007). Intramolecular exciton relaxation and migration dynamics in poly(3-hexylthiophene). *The Journal of Physical Chemistry C*, *111*(42), 15404–15414.

7 Roncali, J. (1992). Conjugated poly(thiophenes): Synthesis, functionalization, and applications. *Chemical Reviews*, *92*(4), 711–738.

8 Günes, S., Neugebauer, H., & Sariciftci, N. S. (2007). Conjugated polymer-based organic solar cells. *Chemical Reviews*, *107*(4), 1324–1338.

9 Reynolds, J. R., Thompson, B. C., & Skotheim, T. A. (2019). *Conjugated polymers: Properties, processing, and applications*. CRC press.

10 Elsenbaumer, R., Jen, K., & Oboodi, R. (1986). Processible and environmentally stable conducting polymers [Proceedings of the Workshop on Conductive Polymers]. *Synthetic Metals*, *15*(2), 169–174.

11 Heeger, A. J. (2010). Semiconducting polymers: The third generation. *Chemical Society Reviews*, *39*, 2354–2371.

12 van Mullekom, H., Vekemans, J., Havinga, E., & Meijer, E. (2001). Developments in the chemistry and band gap engineering of donor–acceptor substituted conjugated polymers. *Materials Science and Engineering: R: Reports*, *32*(1), 1–40.

13 Su, Y.-W., Lin, Y.-C., & Wei, K.-H. (2017). Evolving molecular architectures of donor–acceptor conjugated polymers for photovoltaic applications: From one-dimensional to branched to two-dimensional structures. *Journal of Materials Chemistry A*, *5*, 24051–24075.

14 Cheng, Y.-J., Yang, S.-H., & Hsu, C.-S. (2009). Synthesis of conjugated polymers for organic solar cell applications. *Chemical Reviews*, *109*(11), 5868–5923.

15 Li, G., Chang, W.-H., & Yang, Y. (2017). Low-bandgap conjugated polymers enabling solution-processable tandem solar cells. *Nature Reviews Materials*, *2*(8), 1–13.

16 Facchetti, A. (2011). π-conjugated polymers for organic electronics and photovoltaic cell applications. *Chemistry of Materials*, *23*(3), 733–758.

17 Kwon, Y. S., Lim, J., Yun, H.-J., Kim, Y.-H., & Park, T. (2014). A diketopyrrolopyrrole-containing hole transporting conjugated polymer for use in efficient stable organic–inorganic hybrid solar cells based on a perovskite. *Energy & Environmental Science*, *7*(4), 1454–1460.

18 Cai, F., Cai, J., Yang, L., Li, W., Gurney, R. S., Yi, H., Iraqi, A., Liu, D., & Wang, T. (2018). Molecular engineering of conjugated polymers for efficient hole transport and defect passivation in perovskite solar cells. *Nano Energy*, *45*, 28–36.

19 Tian, L., Hu, Z., Liu, X., Liu, Z., Guo, P., Xu, B., Xue, Q., Yip, H.-L., Huang, F., & Cao, Y. (2019). Fluoro-and amino-functionalized conjugated polymers as electron transport materials for perovskite solar cells with improved efficiency and stability. *ACS Applied Materials & Interfaces*, *11*(5), 5289–5297.

20 Burroughes, J. H., Bradley, D. D., Brown, A., Marks, R., Mackay, K., Friend, R. H., Burns, P., & Holmes, A. (1990). Light-emitting diodes based on conjugated polymers. *Nature*, *347*(6293), 539–541.

21 Grimsdale, A. C., Leok Chan, K., Martin, R. E., Jokisz, P. G., & Holmes, A. B. (2009). Synthesis of light-emitting conjugated polymers for applications in electroluminescent devices. *Chemical Reviews*, *109*(3), 897–1091.

22 AlSalhi, M. S., Alam, J., Dass, L. A., & Raja, M. (2011). Recent advances in conjugated polymers for light emitting devices. *International Journal of Molecular Sciences, 12*(3), 2036–2054.

23 Wang, C., Dong, H., Hu, W., Liu, Y., & Zhu, D. (2012). Semiconducting π-conjugated systems in field-effect transistors: A material odyssey of organic electronics. *Chemical Reviews, 112*(4), 2208–2267.

24 Sirringhaus, H. (2014). 25th anniversary article: Organic field-effect transistors: The path beyond amorphous silicon. *Advanced Materials, 26*(9), 1319–1335.

25 Fratini, S., Nikolka, M., Salleo, A., Schweicher, G., & Sirringhaus, H. (2020). Charge transport in high-mobility conjugated polymers and molecular semiconductors. *Nature Materials, 19*(5), 491–502.

26 DiCarmine, P. M., Schon, T. B., McCormick, T. M., Klein, P. P., & Seferos, D. S. (2014). Donor–acceptor polymers for electrochemical supercapacitors: Synthesis, testing, and theory. *The Journal of Physical Chemistry C, 118*(16), 8295–8307.

27 Li, X.-C., Zhang, Y., Wang, C.-Y., Wan, Y., Lai, W.-Y., Pang, H., & Huang, W. (2017). Redox-active triazatruxene-based conjugated microporous polymers for high-performance supercapacitors. *Chemical Science, 8*(4), 2959–2965.

28 Mohamadzadeh Moghadam, M. H., Sabury, S., Gudarzi, M. M., & Sharif, F. (2014). Graphene oxide-induced polymerization and crystallization to produce highly conductive polyaniline/graphene oxide composite. *Journal of Polymer Science Part A: Polymer Chemistry, 52*(11), 1545–1554.

29 Zhao, C., Chen, Z., Shi, R., Yang, X., & Zhang, T. (2020). Recent advances in conjugated polymers for visible-light-driven water splitting. *Advanced Materials, 32*(28), 1907296.

30 Zhang, G., Lan, Z.-A., & Wang, X. (2016). Conjugated polymers: Catalysts for photocatalytic hydrogen evolution. *Angewandte Chemie International Edition, 55*(51), 15712–15727.

31 Yao, C.-J., Zhang, H.-L., & Zhang, Q. (2019). Recent progress in thermoelectric materials based on conjugated polymers. *Polymers, 11*(1), 107.

32 Kang, K., Schott, S., Venkateshvaran, D., Broch, K., Schweicher, G., Harkin, D., Jellett, C., Nielsen, C. B., Mcculloch, I., & Sirringhaus, H. (2019). Investigation of the thermoelectric response in conducting polymers doped by solid-state diffusion. *Materials Today Physics*, *8*, 112–122.

33 Schwartz, G., Tee, B. C.-K., Mei, J., Appleton, A. L., Kim, D. H., Wang, H., & Bao, Z. (2013). Flexible polymer transistors with high pressure sensitivity for application in electronic skin and health monitoring. *Nature Communications*, *4*(1), 1–8.

34 Someya, T., Bao, Z., & Malliaras, G. G. (2016). The rise of plastic bioelectronics. *Nature*, *540*(7633), 379–385.

35 Sapp, S. A., Sotzing, G. A., & Reynolds, J. R. (1998). High contrast ratio and fast-switching dual polymer electrochromic devices. *Chemistry of Materials*, *10*(8), 2101–2108.

36 Beaujuge, P. M., & Reynolds, J. R. (2010). Color control in π-conjugated organic polymers for use in electrochromic devices. *Chemical Reviews*, *110*(1), 268–320.

37 Wu, W., Bazan, G. C., & Liu, B. (2017). Conjugated-polymer-amplified sensing, imaging, and therapy. *Chem*, *2*(6), 760–790.

38 Anantha-Iyengar, G., Shanmugasundaram, K., Nallal, M., Lee, K.-P., Whitcombe, M. J., Lakshmi, D., & Sai-Anand, G. (2019). Functionalized conjugated polymers for sensing and molecular imprinting applications. *Progress in Polymer Science*, *88*, 1–129.

39 Zhu, C., Liu, L., Yang, Q., Lv, F., & Wang, S. (2012). Water-soluble conjugated polymers for imaging, diagnosis, and therapy. *Chemical Reviews*, *112*(8), 4687–4735.

40 Pang, X., Tan, Y., Tan, C., Li, W., Du, N., Lu, Y., & Jiang, Y. (2019). One-step construction of fluorenone-based donor–acceptor-type conjugated polymers via direct arylation polymerization for cell-imaging applications. *ACS Applied Materials & Interfaces*, *11*(31), 28246–28253.

41 Baek, P., Voorhaar, L., Barker, D., & Travas-Sejdic, J. (2018). Molecular approach to conjugated polymers with biomimetic properties. *Accounts of Chemical Research*, *51*(7), 1581–1589.

42 Senthilkumar, T., Lv, F., Zhao, H., Liu, L., & Wang, S. (2019). Conjugated polymer nanogel binding anticancer drug through hydrogen bonds for sustainable drug delivery. *ACS Applied Bio Materials*, *2*(12), 6012–6020.

43 Chen, P., Ma, Y., Zheng, Z., Wu, C., Wang, Y., & Liang, G. (2019). Facile syntheses of conjugated polymers for photothermal tumour therapy. *Nature Communications*, *10*(1), 1–10.

44 Wang, Y., Meng, H.-M., Song, G., Li, Z., & Zhang, X.-B. (2020). Conjugated-polymer-based nanomaterials for photothermal therapy. *ACS Applied Polymer Materials*, *2*(10), 4258–4272.

45 Bendrea, A.-D., Cianga, L., & Cianga, I. (2011). Progress in the field of conducting polymers for tissue engineering applications. *Journal of Biomaterials Applications*, *26*(1), 3–84.

46 Zeglio, E., Rutz, A. L., Winkler, T. E., Malliaras, G. G., & Herland, A. (2019). Conjugated polymers for assessing and controlling biological functions. *Advanced Materials*, *31*(22), 1806712.

47 Ran, X., Duan, L., Chen, X., & Yang, X. (2018). Photocatalytic degradation of organic dyes by the conjugated polymer poly (1, 3, 4-oxadiazole) s and its photocatalytic mechanism. *Journal of Materials Science*, *53*(9), 7048–7059.

48 Lee, J. J., Noh, W., Huh, T.-H., Kwark, Y.-J., & Lee, T. S. (2020). Synthesis of conjugated microporous polymer and its embedding in porous nanofibers for visible-light-driven photocatalysis with reusability. *Polymer*, *211*, 123060.

49 Tiitu, M., Talo, A., Forsén, O., & Ikkala, O. (2005). Aminic epoxy resin hardeners as reactive solvents for conjugated polymers: Polyaniline base/epoxy composites for anticorrosion coatings. *Polymer*, *46*(18), 6855–6861.

50 Frau, A. F., Pernites, R. B., & Advincula, R. C. (2010). A conjugated polymer network approach to anticorrosion coatings: Poly (vinylcarbazole) electrodeposition. *Industrial & Engineering Chemistry Research*, *49*(20), 9789–9797.

51 Mei, J., & Bao, Z. (2014). Side chain engineering in solution-processable conjugated polymers. *Chemistry of Materials*, *26*(1), 604–615.

52   Lei, T., Dou, J.-H., & Pei, J. (2012). Influence of alkyl chain branching positions on the hole mobilities of polymer thin-film transistors. *Advanced Materials*, *24*(48), 6457–6461.

53   Savikhin, V., Babics, M., Neophytou, M., Liu, S., Oosterhout, S. D., Yan, H., Gu, X., Beaujuge, P. M., & Toney, M. F. (2018). Impact of polymer side chain modification on OPV morphology and performance. *Chemistry of Materials*, *30*(21), 7872–7884.

54   Causin, V., Marega, C., Marigo, A., Valentini, L., & Kenny, J. M. (2005). Crystallization and melting behavior of poly (3-butylthiophene), poly (3-octylthiophene), and poly (3-dodecylthiophene). *Macromolecules*, *38*(2), 409–415.

55   Li, M., Leenaers, P. J., Wienk, M. M., & Janssen, R. A. (2020). The effect of alkyl side chain length on the formation of two semi-crystalline phases in low band gap conjugated polymers. *Journal of Materials Chemistry C*, *8*(17), 5856–5867.

56   Ma, J., Zhao, Z., Guo, Y., Geng, H., Sun, Y., Tian, J., He, Q., Cai, Z., Zhang, X., Zhang, G. et al. (2019). Improving the electronic transporting property for flexible field-effect transistors with naphthalene diimide-based conjugated polymer through branching/linear side-chain engineering strategy. *ACS Applied Materials & Interfaces*, *11*(17), 15837–15844.

57   Cui, C., & Wong, W.-Y. (2016). Effects of alkylthio and alkoxy side chains in polymer donor materials for organic solar cells. *Macromolecular Rapid Communications*, *37*(4), 287–302.

58   Garcıa, G., Timón, V., Hernández-Laguna, A., Navarro, A., & Fernández-Gómez, M. (2011). Influence of the alkyl and alkoxy side chains on the electronic structure and charge-transport properties of polythiophene derivatives. *Physical Chemistry Chemical Physics*, *13*(21), 10091–10099.

59   Liu, Y., Wang, M., Zhao, J., Cui, C., & Liu, J. (2014). Effects of alkyl or alkoxy side chains on the electrochromic properties of four ambipolar donor–acceptor type polymers. *RSC Advances*, *4*(95), 52712–52726.

60   Liu, X., Zhang, C., Duan, C., Li, M., Hu, Z., Wang, J., Liu, F., Li, N., Brabec, C. J., Janssen, R. A. et al. (2018). Morphology optimization via side chain engineering enables all-polymer solar cells with excellent fill factor and stability. *Journal of the American Chemical Society*, *140*(28), 8934–8943.

61 Hu, Z., Wang, Z., Zhang, X., Tang, H., Liu, X., Huang, F., & Cao, Y. (2019). Conjugated polymers with oligoethylene glycol side chains for improved photocatalytic hydrogen evolution. *Iscience*, *13*, 33–42.

62 Meng, B., Song, H., Chen, X., Xie, Z., Liu, J., & Wang, L. (2015). Replacing alkyl with oligo (ethylene glycol) as side chains of conjugated polymers for close π–π stacking. *Macromolecules*, *48*(13), 4357–4363.

63 Kroon, R., Kiefer, D., Stegerer, D., Yu, L., Sommer, M., & Müller, C. (2017). Polar side chains enhance processability, electrical conductivity, and thermal stability of a molecularly p-doped polythiophene. *Advanced Materials*, *29*(24), 1700930.

64 Lobez, J. M., Andrew, T. L., Bulovic, V., & Swager, T. M. (2012). Improving the performance of P3HT–fullerene solar cells with side-chain-functionalized poly (thiophene) additives: A new paradigm for polymer design. *ACS Nano*, *6*(4), 3044–3056.

65 Gaylord, B. S., Heeger, A. J., & Bazan, G. C. (2002). DNA detection using water-soluble conjugated polymers and peptide nucleic acid probes. *Proceedings of the National Academy of Sciences*, *99*(17), 10954–10957.

66 Gaylord, B. S., Heeger, A. J., & Bazan, G. C. (2003). DNA hybridization detection with water-soluble conjugated polymers and chromophore-labeled single-stranded DNA. *Journal of the American Chemical Society*, *125*(4), 896–900.

67 Šponer, J., Leszczynski, J., & Hobza, P. (2001). Electronic properties, hydrogen bonding, stacking, and cation binding of DNA and RNA bases. *Biopolymers: Original Research on Biomolecules*, *61*(1), 3–31.

68 Thuong, N. T., & Hélène, C. (1993). Sequence-specific recognition and modification of double-helical DNA by oligonucleotides. *Angewandte Chemie International Edition in English*, *32*(5), 666–690.

69 Liu, B., Pappas, C. G., Ottelé, J., Schaeffer, G., Jurissek, C., Pieters, P. F., Altay, M., Marić, I., Stuart, M. C., & Otto, S. (2020). Spontaneous emergence of self-replicating molecules containing nucleobases and amino acids. *Journal of the American Chemical Society*, *142*(9), 4184–4192.

70 De Clercq, E., & Field, H. J. (2006). Antiviral prodrugs–the development of successful prodrug strategies for antiviral chemotherapy. *British Journal of Pharmacology*, *147*(1), 1–11.

71 Yssel, A., Vanderleyden, J., & Steenackers, H. (2017). Repurposing of nucleoside- and nucleobase-derivative drugs as antibiotics and biofilm inhibitors. *Journal of Antimicrobial Chemotherapy*, *72*(8), 2156–2170.

72 Thimm, D., Schiedel, A., Peti-Peterdi, J., Kishore, B., & Müller, C. (2015). The nucleobase adenine as a signalling molecule in the kidney. *Acta Physiologica*, *213*(4), 808–818.

73 Lu, X., Gong, S., Monks, A., Zaharevitz, D., & Moscow, J. A. (2002). Correlation of nucleoside and nucleobase transporter gene expression with antimetabolite drug cytotoxicity. *Journal of Experimental Therapeutics and Oncology*, *2*(4), 200–212.

74 Cai, T.-T., Lei, Q., Yang, B., Jia, H.-Z., Cheng, H., Liu, L.-H., Zeng, X., Feng, J., Zhuo, R.-X., & Zhang, X.-Z. (2014). Utilization of H-bond interaction of nucleobase uralic with antitumor methotrexate to design drug carrier with ultrahigh loading efficiency and PH-responsive drug release. *Regenerative Biomaterials*, *1*(1), 27–35.

75 Xu, W., Chan, K. M., & Kool, E. T. (2017). Fluorescent nucleobases as tools for studying DNA and RNA. *Nature Chemistry*, *9*(11), 1043.

76 Pu, F., Ren, J., & Qu, X. (2018). Nucleobases, nucleosides, and nucleotides: Versatile biomolecules for generating functional nanomaterials. *Chemical Society Reviews*, *47*(4), 1285–1306.

77 Wang, D., Tu, C., Su, Y., Zhang, C., Greiser, U., Zhu, X., Yan, D., & Wang, W. (2015). Supramolecularly engineered phospholipids constructed by nucleobase molecular recognition: Upgraded generation of phospholipids for drug delivery. *Chemical Science*, *6*(7), 3775–3787.

78 Karabıyık, H., Sevinçek, R., & Karabıyık, H. (2014). π-cooperativity effect on the base stacking interactions in DNA: Is there a novel stabilization factor coupled with base pairing H-bonds? *Physical Chemistry Chemical Physics*, *16*(29), 15527–15538.

79 Deng, M., Zhang, L., Jiang, Y., & Liu, M. (2016). Role of achiral nucleobases in multicomponent chiral self-assembly: Purine-triggered helix and chirality transfer. *Angewandte Chemie International Edition*, *55*(48), 15062–15066.

80 Pecsi, I., Leveles, I., Harmat, V., Vertessy, B. G., & Toth, J. (2010). Aromatic stacking between nucleobase and enzyme promotes phosphate ester hydrolysis in dutpase. *Nucleic Acids Research*, *38*(20), 7179–7186.

81 Nishiyabu, R., Hashimoto, N., Cho, T., Watanabe, K., Yasunaga, T., Endo, A., Kaneko, K., Niidome, T., Murata, M., Adachi, C. et al. (2009). Nanoparticles of adaptive supramolecular networks self-assembled from nucleotides and lanthanide ions. *Journal of the American Chemical Society*, *131*(6), 2151–2158.

82 Sharma, B., Mahata, A., Mandani, S., Sarma, T. K., & Pathak, B. (2016). Coordination polymer hydrogels through Ag (I)-mediated spontaneous self-assembly of unsubstituted nucleobases and their antimicrobial activity. *RSC Advances*, *6*(67), 62968–62973.

83 Kumar, A., & Mital, S. (2001). Electronic properties of Q-CdS clusters stabilized by adenine. *Journal of Colloid and Interface Science*, *240*(2), 459–466.

84 Li, J., Wang, Z., Hua, Z., & Tang, C. (2020). Supramolecular nucleobase-functionalized polymers: Synthesis and potential biological applications. *Journal of Materials Chemistry B*, *8*(8), 1576–1588.

85 Yang, H., & Xi, W. (2017). Nucleobase-containing polymers: Structure, synthesis, and applications. *Polymers*, *9*(12), 666.

86 McHale, R., & O'Reilly, R. K. (2012). Nucleobase containing synthetic polymers: Advancing biomimicry via controlled synthesis and self-assembly. *Macromolecules*, *45*(19), 7665–7675.

87 Cheng, S., Zhang, M., Dixit, N., Moore, R. B., & Long, T. E. (2012). Nucleobase self-assembly in supramolecular adhesives. *Macromolecules*, *45*(2), 805–812.

88 Ye, X., Li, X., Shen, Y., Chang, G., Yang, J., & Gu, Z. (2017). Self-healing PH-sensitive cytosine- and guanosine-modified hyaluronic acid hydrogels via hydrogen bonding. *Polymer*, *108*, 348–360.

89 Harguindey, A., Domaille, D. W., Fairbanks, B. D., Wagner, J., Bowman, C. N., & Cha, J. N. (n.d.). Synthesis and assembly of click-nucleic-acid-containing PEG-PLGA nanoparticles for DNA delivery. *Advanced Materials*, *29*(24), 1700743.

90 Bäuerle, P., & Emge, A. (1998). Specific recognition of nucleobase-functionalized polythiophenes. *Advanced Materials*, *10*(4), 324–330.

91 Cheng, C.-C., Chu, Y.-L., Huang, P.-H., Yen, Y.-C., Chu, C.-W., Yang, A. C.-M., Ko, F.-H., Chen, J.-K., & Chang, F.-C. (2012). Bioinspired hole-conducting polymers for application in organic light-emitting diodes. *Journal of Materials Chemistry*, *22*(35), 18127–18131.

92 Cheng, C.-C., Chen, J.-K., Shieh, Y.-T., & Lee, D.-J. (2016). Supramolecular core–shell nanoparticles for photoconductive device applications. *Nanotechnology*, *27*(32), 32LT01.

93 Cheng, C.-C., Chang, F.-C., Ko, F.-H., Yu, F.-C., Lin, Y.-T., Shieh, Y.-T., Chen, J.-K., & Lee, D.-J. (2015). Supramolecular polymeric micelles as high performance electrochemical materials. *Journal of Materials Chemistry C*, *3*(37), 9528–9533.

94 Martınez, D., Pérez, A., Cañellas, S., Silió, I., Lancho, A., Garcıa-Raso, A., Fiol, J. J., Terrón, A., Barceló-Oliver, M., Ortega-Castro, J. et al. (2020). Synthesis, reactivity, x-ray characterization and docking studies of N7/N9-(2-pyrimidyl)-adenine derivatives. *Journal of Inorganic Biochemistry*, *203*, 110879.

95 Spijker, H. J., van Delft, F. L., & van Hest, J. C. (2007). Atom transfer radical polymerization of adenine, thymine, cytosine, and guanine nucleobase monomers. *Macromolecules*, *40*(1), 12–18.

96 Yoshino, K., Hayashi, S., & Sugimoto, R.-i. (1984). Preparation and properties of conducting heterocyclic polymer films by chemical method. *Japanese Journal of Applied Physics*, *23*(12A), L899.

97 Amou, S., Haba, O., Shirato, K., Hayakawa, T., Ueda, M., Takeuchi, K., & Asai, M. (1999). Head-to-tail regioregularity of poly (3-hexylthiophene) in oxidative coupling polymerization with fecl3. *Journal of Polymer Science Part A: Polymer Chemistry*, *37*(13), 1943–1948.

98   Abdou, M. S., Lu, X., Xie, Z. W., Orfino, F., Deen, M. J., & Holdcroft, S. (1995). Nature of impurities in π-conjugated polymers prepared by ferric chloride and their effect on the electrical properties of metal-insulator-semiconductor structures. *Chemistry of Materials*, *7*(4), 631–641.

99   Bao, Z., Chan, W., & Yu, L. (1993). Synthesis of conjugated polymer by the stille coupling reaction. *Chemistry of Materials*, *5*(1), 2–3.

100   Bao, Z., Chan, W. K., & Yu, L. (1995). Exploration of the stille coupling reaction for the synthesis of functional polymers. *Journal of the American Chemical Society*, *117*(50), 12426–12435.

101   Carsten, B., He, F., Son, H. J., Xu, T., & Yu, L. (2011). Stille polycondensation for synthesis of functional materials. *Chemical Reviews*, *111*(3), 1493–1528.

102   Cordovilla, C., Bartolomé, C., Martınez-Ilarduya, J. M., & Espinet, P. (2015). The stille reaction, 38 years later. *Acs Catalysis*, *5*(5), 3040–3053.

103   Kim, J.-H., Park, J. B., Jung, I. H., Grimsdale, A. C., Yoon, S. C., Yang, H., & Hwang, D.-H. (2015). Well-controlled thieno [3, 4-c] pyrrole-4, 6-(5 H)-dione based conjugated polymers for high performance organic photovoltaic cells with the power conversion efficiency exceeding 9%. *Energy & Environmental Science*, *8*(8), 2352–2356.

104   Mishra, S. P., Palai, A. K., Kumar, A., Srivastava, R., Kamalasanan, M. N., & Patri, M. (2010). Highly air-stable thieno [3, 2-b] thiophene-thiophene-thiazolo [5, 4-d] thiazole-based polymers for light-emitting diodes. *Macromolecular Chemistry and Physics*, *211*(17), 1890–1899.

105   Liu, J., Zhang, R., Sauvé, G., Kowalewski, T., & McCullough, R. D. (2008). Highly disordered polymer field effect transistors: N-alkyl dithieno [3, 2-b: 2, 3-d] pyrrole-based copolymers with surprisingly high charge carrier mobilities. *Journal of the American Chemical Society*, *130*(39), 13167–13176.

106   Amatore, C., Jutand, A., & Thuilliez, A. (2001). Formation of palladium (0) complexes from Pd(OAc)$_2$ and a bidentate phosphine ligand (dppp) and their reactivity in oxidative addition. *Organometallics*, *20*(15), 3241–3249.

107   Johansson Seechurn, C. C., Sperger, T., Scrase, T. G., Schoenebeck, F., & Colacot, T. J. (2017). Understanding the unusual reduction mechanism of Pd (II) to pd (I):

Uncovering hidden species and implications in catalytic cross-coupling reactions. *Journal of the American Chemical Society*, *139*(14), 5194–5200.

108   Scott, N. W., Ford, M. J., Schotes, C., Parker, R. R., Whitwood, A. C., & Fairlamb, I. J. (2019). The ubiquitous cross-coupling catalyst system 'Pd(OAc)2'/2pph₃ forms a unique dinuclear Pd I complex: An important entry point into catalytically competent cyclic Pd 3 clusters. *Chemical Science*, *10*(34), 7898–7906.

109   Wei, C. S., Davies, G. H., Soltani, O., Albrecht, J., Gao, Q., Pathirana, C., Hsiao, Y., Tummala, S., & Eastgate, M. D. (2013). The impact of palladium (II) reduction pathways on the structure and activity of palladium (0) catalysts. *Angewandte Chemie*, *125*(22), 5934–5938.

110   Wagschal, S., Perego, L. A., Simon, A., Franco-Espejo, A., Tocqueville, C., Albaneze-Walker, J., Jutand, A., & Grimaud, L. (2019). Formation of xphos-ligated palladium (0) complexes and reactivity in oxidative additions. *Chemistry–A European Journal*, *25*(28), 6980–6987.

111   Shaughnessy, K. H. (2020). Development of palladium precatalysts that efficiently generate LPd (0) active species. *Israel Journal of Chemistry*, *60*(3-4), 180–194.

112   Kasahara, A., Izumi, T., Yodono, M., Saito, R.-i., Takeda, T., & Sugawara, T. (1973). Arylation and vinylation reactions of benzo [b] furan via organopalladium intermediates. *Bulletin of the Chemical Society of Japan*, *46*(4), 1220–1225.

113   Mizoroki, T., Mori, K., & Ozaki, A. (1971). Arylation of olefin with aryl iodide catalyzed by palladium. *Bulletin of the Chemical Society of Japan*, *44*(2), 581–581.

114   Se, M., Papillon, J., Schulz, E., Lemaire, M. et al. (1999). New synthetic method for the polymerization of alkylthiophenes. *Tetrahedron Letters*, *40*(32), 5873–5876.

115   Wang, Q., Takita, R., Kikuzaki, Y., & Ozawa, F. (2010). Palladium-catalyzed dehydrohalogenative polycondensation of 2-bromo-3-hexylthiophene: An efficient approach to head-to-tail poly (3-hexylthiophene). *Journal of the American Chemical Society*, *132*(33), 11420–11421.

116   Bura, T., Blaskovits, J. T., & Leclerc, M. (2016). Direct (hetero) arylation polymerization: Trends and perspectives. *Journal of the American Chemical Society*, *138*(32), 10056–10071.

117 Pouliot, J.-R., Grenier, F., Blaskovits, J. T., Beaupré, S., & Leclerc, M. (2016). Direct (hetero) arylation polymerization: Simplicity for conjugated polymer synthesis. *Chemical Reviews*, *116*(22), 14225–14274.

118 Ackermann, L. (2011). Carboxylate-assisted transition-metal-catalyzed C–H bond functionalizations: Mechanism and scope. *Chemical Reviews*, *111*(3), 1315–1345.

119 Bohra, H., & Wang, M. (2017). Direct C–H arylation: A "greener" approach towards facile synthesis of organic semiconducting molecules and polymers. *Journal of Materials Chemistry A*, *5*(23), 11550–11571.

120 Gobalasingham, N. S., & Thompson, B. C. (2018). Direct arylation polymerization: A guide to optimal conditions for effective conjugated polymers. *Progress in Polymer Science*, *83*, 135–201.

121 Rudenko, A. E., & Thompson, B. C. (2015). Optimization of direct arylation polymerization (DArP) through the identification and control of defects in polymer structure. *Journal of Polymer Science Part A: Polymer Chemistry*, *53*(2), 135–147.

122 Leenaers, P. J., Maufort, A. J., Wienk, M. M., & Janssen, R. A. (2020). Impact of π-conjugated linkers on the effective exciton binding energy of diketopyrrolopyrrole–dithienopyrrole copolymers. *The Journal of Physical Chemistry C*.

123 Thomas, S. W., Joly, G. D., & Swager, T. M. (2007). Chemical sensors based on amplifying fluorescent conjugated polymers. *Chemical Reviews*, *107*(4), 1339–1386.

124 Gehlen, M. H. (2020). The centenary of the stern-volmer equation of fluorescence quenching: From the single line plot to the SV quenching map. *Journal of Photochemistry and Photobiology C: Photochemistry Reviews*, *42*, 100338.

125 Holliday, S., Donaghey, J. E., & McCulloch, I. (2014). Advances in charge carrier mobilities of semiconducting polymers used in organic transistors. *Chemistry of Materials*, *26*(1), 647–663.

126 Xie, G., Luo, J., Huang, M., Chen, T., Wu, K., Gong, S., & Yang, C. (2017). Inheriting the characteristics of tadf small molecule by side-chain engineering strategy to enable bluish-green polymers with high plqys up to 74% and external quantum efficiency over 16% in light-emitting diodes. *Advanced Materials*, *29*(11), 1604223.

127 Wu, Z., Zhai, Y., Kim, H., Azoulay, J. D., & Ng, T. N. (2018). Emerging design and characterization guidelines for polymer-based infrared photodetectors. *Accounts of Chemical Research*, *51*(12), 3144–3153.

128 Xie, J., Gu, P., & Zhang, Q. (2017). Nanostructured conjugated polymers: Toward high-performance organic electrodes for rechargeable batteries. *ACS Energy Letters*, *2*(9), 1985–1996.

129 Liao, Y., Wang, H., Zhu, M., & Thomas, A. (2018). Efficient supercapacitor energy storage using conjugated microporous polymer networks synthesized from buchwald–hartwig coupling. *Advanced Materials*, *30*(12), 1705710.

130 Zhang, S., Ye, L., & Hou, J. (2016). Breaking the 10% efficiency barrier in organic photovoltaics: Morphology and device optimization of well-known PBDTTT polymers. *Advanced Energy Materials*, *6*(11), 1502529.

131 Zhou, H., Yang, L., & You, W. (2012). Rational design of high performance conjugated polymers for organic solar cells. *Macromolecules*, *45*(2), 607–632.

132 Colladet, K., Fourier, S., Cleij, T. J., Lutsen, L., Gelan, J., Vanderzande, D., Huong Nguyen, L., Neugebauer, H., Sariciftci, S., Aguirre, A. et al. (2007). Low band gap donor- acceptor conjugated polymers toward organic solar cells applications. *Macromolecules*, *40*(1), 65–72.

133 Morin, J.-F., & Leclerc, M. (2002). 2, 7-carbazole-based conjugated polymers for blue, green, and red light emission. *Macromolecules*, *35*(22), 8413–8417.

134 Donat-Bouillud, A., Levesque, I., Tao, Y., D'Iorio, M., Beaupré, S., Blondin, P., Ranger, M., Bouchard, J., & Leclerc, M. (2000). Light-emitting diodes from fluorene-based π-conjugated polymers. *Chemistry of Materials*, *12*(7), 1931–1936.

135 Liu, Y., Liu, Y., & Zhan, X. (2011). High-mobility conjugated polymers based on fused-thiophene building blocks. *Macromolecular Chemistry and Physics*, *212*(5), 428–443.

136 Kang, I., Yun, H.-J., Chung, D. S., Kwon, S.-K., & Kim, Y.-H. (2013). Record high hole mobility in polymer semiconductors via side-chain engineering. *Journal of the American Chemical Society*, *135*(40), 14896–14899.

137 Liu, Q., Bottle, S. E., & Sonar, P. (2020). Developments of diketopyrrolopyrrole-dye-based organic semiconductors for a wide range of applications in electronics. *Advanced Materials*, *32*(4), 1903882.

138 Li, S., Ye, L., Zhao, W., Yan, H., Yang, B., Liu, D., Li, W., Ade, H., & Hou, J. (2018). A wide band gap polymer with a deep highest occupied molecular orbital level enables 14.2% efficiency in polymer solar cells. *Journal of the American Chemical Society*, *140*(23), 7159–7167.

139 Liu, Z., Gao, Y., Dong, J., Yang, M., Liu, M., Zhang, Y., Wen, J., Ma, H., Gao, X., Chen, W. et al. (2018). Chlorinated wide-bandgap donor polymer enabling annealing free nonfullerene solar cells with the efficiency of 11.5%. *The Journal of Physical Chemistry Letters*, *9*(24), 6955–6962.

140 Yao, H., Ye, L., Zhang, H., Li, S., Zhang, S., & Hou, J. (2016). Molecular design of benzodithiophene-based organic photovoltaic materials. *Chemical Reviews*, *116*(12), 7397–7457.

141 Yang, Y., Liu, Z., Chen, L., Yao, J., Lin, G., Zhang, X., Zhang, G., & Zhang, D. (2019). Conjugated semiconducting polymer with thymine groups in the side chains: Charge mobility enhancement and application for selective field-effect transistor sensors toward CO and H$_2$S. *Chemistry of Materials*, *31*(5), 1800–1807.

142 Liu, Z., Zhang, G., & Zhang, D. (2018). Modification of side chains of conjugated molecules and polymers for charge mobility enhancement and sensing functionality. *Accounts of Chemical Research*, *51*(6), 1422–1432.

143 Yao, J., Yu, C., Liu, Z., Luo, H., Yang, Y., Zhang, G., & Zhang, D. (2016). Significant improvement of semiconducting performance of the diketopyrrolopyrrole–quaterthiophene conjugated polymer through side-chain engineering via hydrogen-bonding. *Journal of the American Chemical Society*, *138*(1), 173–185.

144 Ye, L., Li, W., Guo, X., Zhang, M., & Ade, H. (2019). Polymer side-chain variation induces microstructural disparity in nonfullerene solar cells. *Chemistry of Materials*, *31*(17), 6568–6577.

145 Wang, Z., Liu, Z., Ning, L., Xiao, M., Yi, Y., Cai, Z., Sadhanala, A., Zhang, G., Chen, W., Sirringhaus, H. et al. (2018). Charge mobility enhancement for conjugated

DPP-selenophene polymer by simply replacing one bulky branching alkyl chain with linear one at each DPP unit. *Chemistry of Materials*, *30*(9), 3090–3100.

146   Ma, J., Liu, Z., Yao, J., Wang, Z., Zhang, G., Zhang, X., & Zhang, D. (2018). Improving ambipolar semiconducting properties of thiazole-flanked diketopyrrolopyrrole-based terpolymers by incorporating urea groups in the side-chains. *Macromolecules*, *51*(15), 6003–6010.

147   Li, Z., Zhang, Y., Tsang, S.-W., Du, X., Zhou, J., Tao, Y., & Ding, J. (2011). Alkyl side chain impact on the charge transport and photovoltaic properties of benzodithiophene and diketopyrrolopyrrole-based copolymers. *The Journal of Physical Chemistry C*, *115*(36), 18002–18009.

148   Chen, M. S., Lee, O. P., Niskala, J. R., Yiu, A. T., Tassone, C. J., Schmidt, K., Beaujuge, P. M., Onishi, S. S., Toney, M. F., Zettl, A. et al. (2013). Enhanced solid-state order and field-effect hole mobility through control of nanoscale polymer aggregation. *Journal of the American Chemical Society*, *135*(51), 19229–19236.

149   Lam, K. H., Foong, T. R. B., Ooi, Z. E., Zhang, J., Grimsdale, A. C., & Lam, Y. M. (2013). Enhancing the performance of solution-processed bulk-heterojunction solar cells using hydrogen-bonding-induced self-organization of small molecules. *ACS Applied Materials & Interfaces*, *5*(24), 13265–13274.

150   Freudenberg, J., Jänsch, D., Hinkel, F., & Bunz, U. H. (2018). Immobilization strategies for organic semiconducting conjugated polymers. *Chemical Reviews*, *118*(11), 5598–5689.

151   Yang, K., He, T., Chen, X., Cheng, S. Z., & Zhu, Y. (2014). Patternable conjugated polymers with latent hydrogen-bonding on the main chain. *Macromolecules*, *47*(24), 8479–8486.

152   Guo, Z.-H., Ai, N., McBroom, C. R., Yuan, T., Lin, Y.-H., Roders, M., Zhu, C., Ayzner, A. L., Pei, J., & Fang, L. (2016). A side-chain engineering approach to solvent-resistant semiconducting polymer thin films. *Polymer Chemistry*, *7*(3), 648–655.

153 Huang, Y., Guo, X., Liu, F., Huo, L., Chen, Y., Russell, T. P., Han, C. C., Li, Y., & Hou, J. (2012). Improving the ordering and photovoltaic properties by extending π–conjugated area of electron-donating units in polymers with D-A structure. *Advanced Materials*, *24*(25), 3383–3389.

154 Zhang, F., Hu, Y., Schuettfort, T., Di, C.-a., Gao, X., McNeill, C. R., Thomsen, L., Mannsfeld, S. C., Yuan, W., Sirringhaus, H. et al. (2013). Critical role of alkyl chain branching of organic semiconductors in enabling solution-processed n-channel organic thin-film transistors with mobility of up to 3.50 cm^2 v^{-1} s^{-1}. *Journal of the American Chemical Society*, *135*(6), 2338–2349.

155 Zhao, Y., Sakai, F., Su, L., Liu, Y., Wei, K., Chen, G., & Jiang, M. (2013). Progressive macromolecular self-assembly: From biomimetic chemistry to bio-inspired materials. *Advanced Materials*, *25*(37), 5215–5256.

156 Sabury, S., Collier, G. S., Ericson, M. N., & Kilbey, S. M. (2020). Synthesis of a soluble adenine-functionalized polythiophene through direct arylation polymerization and its fluorescence responsive behavior. *Polymer Chemistry*, *11*(4), 820–829.

157 Spada, G. P., Lena, S., Masiero, S., Pieraccini, S., Surin, M., & Samorı, P. (2008). Guanosine-based hydrogen-bonded scaffolds: Controlling the assembly of oligothiophenes. *Advanced Materials*, *20*(12), 2433–2438.

158 Navacchia, M. L., Favaretto, L., Treossi, E., Palermo, V., & Barbarella, G. (2010). Self-complementary nucleoside-thiophene hybrid systems: Synthesis and supramolecular organization. *Macromolecular Rapid Communications*, *31*(4), 351–355.

159 Liu, X., Zhang, Q., Duan, L., & Gao, G. (2019). Bioinspired nucleobase-driven nonswellable adhesive and tough gel with excellent underwater adhesion. *ACS Applied Materials & Interfaces*, *11*(6), 6644–6651.

160 Kim, E., Mishra, A. K., Choi, C., Kim, M., Park, S., Park, S. Y., Ahn, S., & Kim, J. K. (2018). Phase behavior of adenine-containing block copolymer. *Macromolecules*, *51*(24), 10223–10229.

161 Cheng, C.-C., Chang, F.-C., Dai, S. A., Lin, Y.-L., & Lee, D.-J. (2015). Bio-complementary supramolecular polymers with effective self-healing functionality. *RSC Advances*, *5*(110), 90466–90472.

162 González-Rodríguez, D., & Schenning, A. P. (2011). Hydrogen-bonded supramolecular π-functional materials. *Chemistry of Materials*, *23*(3), 310–325.

163 Bou Zerdan, R., Cohn, P., Puodziukynaite, E., Baker, M. B., Voisin, M., Sarun, C., & Castellano, R. K. (2015). Synthesis, optical properties, and electronic structures of nucleobase-containing π-conjugated oligomers. *The Journal of Organic Chemistry*, *80*(3), 1828–1840.

164 Collier, G. S., Brown, L. A., Boone, E. S., Kaushal, M., Ericson, M. N., Walter, M. G., Long, B. K., & Kilbey, S. M. (2017). Linking design and properties of purine-based donor–acceptor chromophores as optoelectronic materials. *Journal of Materials Chemistry C*, *5*(27), 6891–6898.

165 Jatsch, A., Kopyshev, A., Mena-Osteritz, E., & Bäuerle, P. (2008). Self-organizing oligothiophene- nucleoside conjugates: Versatile synthesis via "click"-chemistry. *Organic Letters*, *10*(5), 961–964.

166 Mishra, A., Ma, C.-Q., & Bauerle, P. (2009). Functional oligothiophenes: Molecular design for multidimensional nanoarchitectures and their applications. *Chemical Reviews*, *109*(3), 1141–1276.

167 Jatsch, A., Schillinger, E.-K., Schmid, S., & Bäuerle, P. (2010). Biomolecule assisted self-assembly of π-conjugated oligomers. *Journal of Materials Chemistry*, *20*(18), 3563–3578.

168 Gan, K. P., Yoshio, M., Sugihara, Y., & Kato, T. (2018). Guanine–oligothiophene conjugates: Liquid-crystalline properties, photoconductivities and ion-responsive emission of their nanoscale assemblies. *Chemical Science*, *9*(3), 576–585.

169 Cheng, C.-C., Chu, C.-W., Huang, J.-J., & Liao, Z.-S. (2017). Complementary hydrogen bonding interaction-mediated hole injection in organic light-emitting devices. *Journal of Materials Chemistry C*, *5*(19), 4736–4741.

170 Coropceanu, V., Cornil, J., da Silva Filho, D. A., Olivier, Y., Silbey, R., & Brédas, J.-L. (2007). Charge transport in organic semiconductors. *Chemical Reviews*, *107*(4), 926–952.

171 Cornil, J., Beljonne, D., Calbert, J.-P., & Brédas, J.-L. (2001). Interchain interactions in organic π-conjugated materials: Impact on electronic structure, optical response, and charge transport. *Advanced Materials*, *13*(14), 1053–1067.

172 Zhang, X., Bronstein, H., Kronemeijer, A. J., Smith, J., Kim, Y., Kline, R. J., Richter, L. J., Anthopoulos, T. D., Sirringhaus, H., Song, K. et al. (2013). Molecular origin of high field-effect mobility in an indacenodithiophene–benzothiadiazole copolymer. *Nature Communications*, *4*(1), 1–9.

173 Lamport, Z. A., Haneef, H. F., Anand, S., Waldrip, M., & Jurchescu, O. D. (2018). Tutorial: Organic field-effect transistors: Materials, structure and operation. *Journal of Applied Physics*, *124*(7), 071101.

174 Jang, W., Cheon, H., Park, S., Cho, J. S., Yi, M., Kwon, S.-K., Kim, Y.-H., & Wang, D. H. (2017). Interface engineering on phenanthrocarbazole/thienopyrroledione-based conjugated polymer for efficient organic photovoltaic devices with ideal nano-morphology and improved charge carrier dynamics. *Dyes and Pigments*, *145*, 29–36.

175 Chasteen, S. V., Sholin, V., Carter, S. A., & Rumbles, G. (2008). Towards optimization of device performance in conjugated polymer photovoltaics: Charge generation, transfer and transport in poly (p-phenylene-vinylene) polymer heterojunctions. *Solar Energy Materials and Solar Cells*, *92*(6), 651–659.

176 Nguyen, T.-Q., Kwong, R. C., Thompson, M. E., & Schwartz, B. J. (2000). Improving the performance of conjugated polymer-based devices by control of interchain interactions and polymer film morphology. *Applied Physics Letters*, *76*(17), 2454–2456.

177 Wang, B., Zhang, W., Zhang, W., Mujumdar, A. S., & Huang, L. (2005). Progress in drying technology for nanomaterials. *Drying Technology*, *23*(1-2), 7–32.

178 Moghaddam, S. Z., Sabury, S., & Sharif, F. (2014). Dispersion of rGO in polymeric matrices by thermodynamically favorable self-assembly of GO at oil–water interfaces. *RSC Advances*, *4*(17), 8711–8719.

179 Sabury, S., Kazemi, S. H., & Sharif, F. (2015). Graphene–gold nanoparticle composite: Application as a good scaffold for construction of glucose oxidase biosensor. *Materials Science and Engineering: C*, *49*, 297–304.

180 Gudarzi, M. M., & Sharif, F. (2012). Enhancement of dispersion and bonding of graphene-polymer through wet transfer of functionalized graphene oxide. *Express Polymer Letters*, *6*(12).

181 D'Addio, S. M., Kafka, C., Akbulut, M., Beattie, P., Saad, W., Herrera, M., Kennedy, M. T., & Prud'homme, R. K. (2010). Novel method for concentrating and drying polymeric nanoparticles: Hydrogen bonding coacervate precipitation. *Molecular Pharmaceutics*, *7*(2), 557–564.

182 Wang, Q., Zhang, J., & Wang, A. (2014). Freeze-drying: A versatile method to overcome re-aggregation and improve dispersion stability of palygorskite for sustained release of ofloxacin. *Applied Clay Science*, *87*, 7–13.

183 Ledford, W. K., Sabury, S., & Kilbey, S. M. (2021). Enhancing nanomaterial dispersion and performance of parts printed via FFF by a solution casting method. *MRS Communications*, 1–7.

184 Chuang, H.-Y., Hsu, S. L.-C., Lee, P.-I., Lee, J.-F., Huang, S.-Y., Lin, S.-W., & Lin, P.-Y. (2014). Synthesis and properties of a new conjugated polymer containing benzodithiophene for polymer solar cells. *Polymer Bulletin*, *71*(5), 1117–1130.

185 Hou, J., Chen, H.-Y., Zhang, S., & Yang, Y. (2009). Synthesis and photovoltaic properties of two benzo [1, 2-b: 3, 4-b] dithiophene-based conjugated polymers. *The Journal of Physical Chemistry C*, *113*(50), 21202–21207.

186 Wang, X., Deng, W., Chen, Y., Wang, X., Ye, P., Wu, X., Yan, C., Zhan, X., Liu, F., & Huang, H. (2017). Fine-tuning solid state packing and significantly improving photovoltaic performance of conjugated polymers through side chain engineering via random polymerization. *Journal of Materials Chemistry A*, *5*(11), 5585–5593.

187 Lee, K.-H., Lee, H.-J., Morino, K., Sudo, A., & Endo, T. (2010). Synthesis and optical properties of π-conjugated polymers composed of benzo [1, 2-b: 4, 5-b] dithiophene and thiophenes bearing electron-deficient ethenyl groups in the side chains. *Macromolecular Chemistry and Physics*, *211*(23), 2490–2496.

188 Tamami, M., Hemp, S. T., Zhang, K., Zhang, M., Moore, R. B., & Long, T. E. (2013). Poly (ethylene glycol)-based ammonium ionenes containing nucleobases. *Polymer*, *54*(6), 1588–1595.

189 Thordarson, P. (2011). Determining association constants from titration experiments in supramolecular chemistry. *Chemical Society Reviews*, *40*(3), 1305–1323.

190 Chen, J. S., & Shirts, R. B. (1985). Iterative determination of the NMR monomer shift and dimerization constant in a self-associating system. *The Journal of Physical Chemistry*, *89*(9), 1643–1646.

191 Henry, K. (1994). Determination of the NMR monomer shift and dimerization constant in a self-associating system by direct application of the least-squares method. *Journal of the Chemical Society, Faraday Transactions*, *90*(23), 3521–3525.

192 Zhang, K., Aiba, M., Fahs, G. B., Hudson, A. G., Chiang, W. D., Moore, R. B., Ueda, M., & Long, T. E. (2015). Nucleobase-functionalized acrylic ABA triblock copolymers and supramolecular blends. *Polymer Chemistry*, *6*(13), 2434–2444.

193 Fagnani, D. E., Bou Zerdan, R., & Castellano, R. K. (2018). Synthesis, optoelectronic properties, self-association, and base pairing of nucleobase-functionalized oligothiophenes. *The Journal of Organic Chemistry*, *83*(20), 12711–12721.

194 Benesi, H. A., & Hildebrand, J. (1949). A spectrophotometric investigation of the interaction of iodine with aromatic hydrocarbons. *Journal of the American Chemical Society*, *71*(8), 2703–2707.

195 Steiner, T. (2002). The hydrogen bond in the solid state. *Angewandte Chemie International Edition*, *41*(1), 48–76.

196 Hirai, T., Nagae, Y., White, K., Kamitani, K., Kido, M., Uchiyama, T., Nishibori, M., Konishi, Y., Yokomachi, K., Sugimoto, R. et al. (2016). Solvent free oxidative coupling polymerization of 3-hexylthiophene (3HT) in the presence of $fecl_3$ particles. *RSC Advances*, *6*(113), 111993–111996.

197 Rozenberg, M., Shoham, G., Reva, I., & Fausto, R. (2005). Spontaneous self-association of adenine and uracil in polycrystals from low temperature FTIR spectra in the range below 1000 cm$-$1. *Spectrochimica Acta Part A: Molecular and Biomolecular Spectroscopy*, *62*(1-3), 233–238.

198 Kyogoku, Y., Higuchi, S., & Tsuboi, M. (1967). Intra-red absorption spectra of the single crystals of 1-methyl-thymine, 9-methyladenine and their 1: 1 complex. *Spectrochimica Acta Part A: Molecular Spectroscopy*, *23*(4), 969–983.

199 Mathlouthi, M., Seuvre, A.-M., & Koenig, J. L. (1984a). FT-IR and laser-raman spectra of adenine and adenosine. *Carbohydrate Research*, *131*(1), 1–15.

200 Mathlouthi, M., Seuvre, A.-M., & Koenig, J. L. (1984b). FT-IR and laser-raman spectra of thymine and thymidine. *Carbohydrate Research*, *134*(1), 23–38.

201 de Jesus, J. C., Pires, P. A., Scharf, M., & El Seoud, O. A. (2017). Solvation by aqueous solutions of imidazole-based ionic liquids: 2-A comparison between alkyl and alkoxy side-chains. *Fluid Phase Equilibria*, *451*, 48–56.

202 Ajayaghosh, A., & George, S. J. (2001). First phenylenevinylene based organogels: Self-assembled nanostructures via cooperative hydrogen bonding and π-stacking. *Journal of the American Chemical Society*, *123*(21), 5148–5149.

203 Hou, L., Adhikari, S., Tian, Y., Scheblykin, I. G., & Orrit, M. (2017). Absorption and quantum yield of single conjugated polymer poly [2-methoxy-5-(2-ethylhexyloxy)-1, 4-phenylenevinylene](MEH-PPV) molecules. *Nano Letters*, *17*(3), 1575–1581.

204 Cheng, C.-C., Chu, Y.-L., Chang, F.-C., Lee, D.-J., Yen, Y.-C., Chen, J.-K., Chu, C.-W., & Xin, Z. (2015). New bioinspired hole injection/transport materials for highly efficient solution-processed phosphorescent organic light-emitting diodes. *Nano Energy*, *13*, 1–8.

205 Kaushal, M., Ortiz, A. L., Kassel, J. A., Hall, N., Lee, T. D., Singh, G., & Walter, M. G. (2016). Enhancing exciton diffusion in porphyrin thin films using peripheral carboalkoxy groups to influence molecular assembly. *Journal of Materials Chemistry C*, *4*(24), 5602–5609.

206 Hou, J., Park, M.-H., Zhang, S., Yao, Y., Chen, L.-M., Li, J.-H., & Yang, Y. (2008). Bandgap and molecular energy level control of conjugated polymer photovoltaic materials based on benzo [1, 2-b: 4, 5-b] dithiophene. *Macromolecules*, *41*(16), 6012–6018.

207 Goncalves, L. M., Batchelor-McAuley, C., Barros, A. A., & Compton, R. G. (2010). Electrochemical oxidation of adenine: A mixed adsorption and diffusion response on an edge-plane pyrolytic graphite electrode. *The Journal of Physical Chemistry C*, *114*(33), 14213–14219.

208 Wang, Z., Helander, M. G., Greiner, M. T., Qiu, J., & Lu, Z.-H. (2010). Carrier mobility of organic semiconductors based on current-voltage characteristics. *Journal of Applied Physics*, *107*(3), 034506.

209 Dixon, A. G., Visvanathan, R., Clark, N. A., Stingelin, N., Kopidakis, N., & Shaheen, S. E. (2018). Molecular weight dependence of carrier mobility and recombination rate in neat P3HT films. *Journal of Polymer Science Part B: Polymer Physics*, *56*(1), 31–35.

210 Mohammad, L., Chen, Q., Mitul, A., Sun, J., Khatiwada, D., Vaagensmith, B., Zhang, C., Li, J., & Qiao, Q. (2015). Improved performance for inverted organic photovoltaics via spacer between benzodithiophene and benzothiazole in polymers. *The Journal of Physical Chemistry C*, *119*(33), 18992–19000.

211 Fall, S., Biniek, L., Odarchenko, Y., Anokhin, D. V., de Tournadre, G., Lévêque, P., Leclerc, N., Ivanov, D. A., Simonetti, O., Giraudet, L. et al. (2016). Tailoring the microstructure and charge transport in conjugated polymers by alkyl side-chain engineering. *Journal of Materials Chemistry C*, *4*(2), 286–294.

212 Wang, Y., Liu, Y., Chen, S., Peng, R., & Ge, Z. (2013). Significant enhancement of polymer solar cell performance via side-chain engineering and simple solvent treatment. *Chemistry of Materials*, *25*(15), 3196–3204.

213 Li, L., Feng, L., Yuan, J., Peng, H., Zou, Y., & Li, Y. (2018). Fine-tuning blend morphology via alkylthio side chain engineering towards high performance non-fullerene polymer solar cells. *Chemical Physics Letters*, *696*, 19–25.

214 Ocheje, M. U., Charron, B. P., Cheng, Y.-H., Chuang, C.-H., Soldera, A., Chiu, Y.-C., & Rondeau-Gagné, S. (2018). Amide-containing alkyl chains in conjugated polymers: Effect on self-assembly and electronic properties. *Macromolecules*, *51*(4), 1336–1344.

215 Kroon, R., Lundin, A., Lindqvist, C., Henriksson, P., Steckler, T. T., & Andersson, M. R. (2013). Effect of electron-withdrawing side chain modifications on the optical properties of thiophene–quinoxaline acceptor based polymers. *Polymer*, *54*(4), 1285–1288.

216 Prosa, T., Winokur, M., & McCullough, R. (1996). Evidence of a novel side chain structure in regioregular poly (3-alkylthiophenes). *Macromolecules*, *29*(10), 3654–3656.

217 Ye, L., Zhang, S., Zhao, W., Yao, H., & Hou, J. (2014). Highly efficient 2D-conjugated benzodithiophene-based photovoltaic polymer with linear alkylthio side chain. *Chemistry of Materials*, *26*(12), 3603–3605.

218 Feng, F., He, F., An, L., Wang, S., Li, Y., & Zhu, D. (2008). Fluorescent conjugated polyelectrolytes for biomacromolecule detection. *Advanced Materials*, *20*(15), 2959–2964.

219 Kim, H. J., Pei, M., Ko, J. S., Ma, M. H., Park, G. E., Baek, J., Yang, H., Cho, M. J., & Choi, D. H. (2018). Influence of branched alkyl ester-labeled side chains on specific chain arrangement and charge-transport properties of diketopyrrolopyrrole-based conjugated polymers. *ACS Applied Materials & Interfaces*, *10*(47), 40681–40691.

220 Dou, J.-H., Zheng, Y.-Q., Lei, T., Zhang, S.-D., Wang, Z., Zhang, W.-B., Wang, J.-Y., & Pei, J. (2014). Systematic investigation of side-chain branching position effect on electron carrier mobility in conjugated polymers. *Advanced Functional Materials*, *24*(40), 6270–6278.

221 Xiao, Z., Duan, T., Chen, H., Sun, K., & Lu, S. (2018). The role of hydrogen bonding in bulk-heterojunction (BHJ) solar cells: A review. *Solar Energy Materials and Solar Cells*, *182*, 1–13.

222 Aytun, T., Barreda, L., Ruiz-Carretero, A., Lehrman, J. A., & Stupp, S. I. (2015). Improving solar cell efficiency through hydrogen bonding: A method for tuning active layer morphology. *Chemistry of Materials*, *27*(4), 1201–1209.

223 Bilger, D. W., Figueroa, J. A., Redeker, N. D., Sarkar, A., Stefik, M., & Zhang, S. (2017). Hydrogen-bonding-directed ordered assembly of carboxylated poly (3-alkylthiophene) s. *ACS Omega*, *2*(11), 8526–8535.

224 Xing, C., Yuan, H., Xu, S., An, H., Niu, R., & Zhan, Y. (2014). Nucleobase-functionalized conjugated polymer for detection of copper (ii). *ACS Applied Materials & Interfaces*, *6*(12), 9601–9607.

225 Feng, X., Liu, L., Wang, S., & Zhu, D. (2010). Water-soluble fluorescent conjugated polymers and their interactions with biomacromolecules for sensitive biosensors. *Chemical Society Reviews*, *39*(7), 2411–2419.

226 Baker, E. S., Hong, J. W., Gaylord, B. S., Bazan, G. C., & Bowers, M. T. (2006). PNA/dsDNA complexes: Site specific binding and dsDNA biosensor applications. *Journal of the American Chemical Society*, *128*(26), 8484–8492.

227 Liu, X., Ouyang, L., Cai, X., Huang, Y., Feng, X., Fan, Q., & Huang, W. (2013). An ultrasensitive label-free biosensor for assaying of sequence-specific DNA-binding protein based on amplifying fluorescent conjugated polymer. *Biosensors and Bioelectronics*, *41*, 218–224.

228 Liu, X., Fan, Q., & Huang, W. (2011). DNA biosensors based on water-soluble conjugated polymers. *Biosensors and Bioelectronics*, *26*(5), 2154–2164.

229 Lu, Y., Li, X., Wang, G., & Tang, W. (2013). A highly sensitive and selective optical sensor for Pb2+ by using conjugated polymers and label-free oligonucleotides. *Biosensors and Bioelectronics*, *39*(1), 231–235.

230 Liu, B., & Bazan, G. C. (2004). Homogeneous fluorescence-based DNA detection with water-soluble conjugated polymers. *Chemistry of Materials*, *16*(23), 4467–4476.

231 Tang, Y., He, F., Yu, M., Feng, F., An, L., Sun, H., Wang, S., Li, Y., & Zhu, D. (2006). A reversible and highly selective fluorescent sensor for mercury (II) using poly (thiophene) s that contain thymine moieties. *Macromolecular Rapid Communications*, *27*(6), 389–392.

232 Sivakova, S., & Rowan, S. J. (2005). Nucleobases as supramolecular motifs. *Chemical Society Reviews*, *34*(1), 9–21.

233 Kleiner, R. E., Brudno, Y., Birnbaum, M. E., & Liu, D. R. (2008). DNA-templated polymerization of side-chain-functionalized peptide nucleic acid aldehydes. *Journal of the American Chemical Society*, *130*(14), 4646–4659.

234 Hua, Z., Wilks, T. R., Keogh, R., Herwig, G., Stavros, V. G., & O'Reilly, R. K. (2018). Entrapment and rigidification of adenine by a photo-cross-linked thymine network leads to fluorescent polymer nanoparticles. *Chemistry of Materials*, *30*(4), 1408–1416.

235 Li, F., Dawson, N. M., Jiang, Y.-B., Malloy, K. J., & Qin, Y. (2015). Conjugated polymer/fullerene nanostructures through cooperative non-covalent interactions for organic solar cells. *Polymer*, *76*, 220–229.

236 Lippert, B. (2000). Multiplicity of metal ion binding patterns to nucleobases. *Coordination Chemistry Reviews*, *200*, 487–516.

237 Vangeneugden, D., Vanderzande, D., Salbeck, J., Van Hal, P., Janssen, R., Hummelen, J., Brabec, C., Shaheen, S., & Sariciftci, N. (2001). Synthesis and characterization of a poly (1, 3-dithienylisothianaphthene) derivative for bulk heterojunction photovoltaic cells. *The Journal of Physical Chemistry B*, *105*(45), 11106–11113.

238 Fraga, C. G. (2005). Relevance, essentiality and toxicity of trace elements in human health. *Molecular Aspects of Medicine*, *26*(4-5), 235–244.

239 Pankow, R. M., Ye, L., Gobalasingham, N. S., Salami, N., Samal, S., & Thompson, B. C. (2018). Investigation of green and sustainable solvents for direct arylation polymerization (DArP). *Polymer Chemistry*, *9*(28), 3885–3892.

240 Wang, X., Wang, K., & Wang, M. (2015). Synthesis of conjugated polymers via an exclusive direct-arylation coupling reaction: A facile and straightforward way to synthesize thiophene-flanked benzothiadiazole derivatives and their copolymers. *Polymer Chemistry*, *6*(10), 1846–1855.

241 Hayashi, S., Kojima, Y., & Koizumi, T. (2015). Highly regioselective Pd/C-catalyzed direct arylation toward thiophene-based π-conjugated polymers. *Polymer Chemistry*, *6*(6), 881–885.

242 Gobalasingham, N. S., Ekiz, S., Pankow, R. M., Livi, F., Bundgaard, E., & Thompson, B. C. (2017). Carbazole-based copolymers via direct arylation polymerization (DArP) for suzuki-convergent polymer solar cell performance. *Polymer Chemistry*, *8*(30), 4393–4402.

243 Mercier, L. G., & Leclerc, M. (2013). Direct (hetero) arylation: A new tool for polymer chemists. *Accounts of Chemical Research*, *46*(7), 1597–1605.

244 Estrada, L. A., Deininger, J. J., Kamenov, G. D., & Reynolds, J. R. (2013). Direct (hetero) arylation polymerization: An effective route to 3, 4-propylenedioxythiophene-based polymers with low residual metal content. *ACS Macro Letters*, *2*(10), 869–873.

245 Chiong, H. A., & Daugulis, O. (2007). Palladium-catalyzed arylation of electron-rich heterocycles with aryl chlorides. *Organic Letters*, *9*(8), 1449–1451.

246   Sahnoun, S., Messaoudi, S., Peyrat, J.-F., Brion, J.-D., & Alami, M. (2008). Microwave-assisted Pd(OH)$_2$-catalyzed direct C-H arylation of free-(NH$_2$) adenines with aryl halides. *Tetrahedron Letters*, *49*(51), 7279–7283.

247   Storr, T. E., Baumann, C. G., Thatcher, R. J., De Ornellas, S., Whitwood, A. C., & Fairlamb, I. J. (2009). Pd(0)/Cu(I)-mediated direct arylation of 2-deoxyadenosines: Mechanistic role of Cu (I) and reactivity comparisons with related purine nucleosides. *The Journal of Organic Chemistry*, *74*(16), 5810–5821.

248   Gorelsky, S. I. (2013). Origins of regioselectivity of the palladium-catalyzed (aromatic) CH bond metalation–deprotonation. *Coordination Chemistry Reviews*, *257*(1), 153–164.

249   Štarha, P., Novotná, R., & Trávníček, Z. (2010). X-ray structure and properties of a dinuclear palladium (II) complex [Pd$_2$(μ-L)$_4$] with four adenine-based bridges in a paddle wheel-like arrangement. *Inorganic Chemistry Communications*, *13*(6), 800–803.

250   Štarha, P., Trávníček, Z., & Popa, I. (2009). Synthesis, characterization and in vitro cytotoxicity of the first palladium (II) oxalato complexes involving adenine-based ligands. *Journal of Inorganic Biochemistry*, *103*(7), 978–988.

251   Mihaly, T., Garijo Añorbe, M., Albertı, F. M., Sanz Miguel, P. J., & Lippert, B. (2012). Multiple metal binding to the 9-methyladenine model nucleobase involving N1, N6, and N7: Discrete di-and trinuclear species with different combinations of monofunctional pdii and ptii entities. *Inorganic Chemistry*, *51*(19), 10437–10446.

252   Ibáñez, S., Albertı, F. M., Sanz Miguel, P. J., & Lippert, B. (2011). Exploring the metal coordination properties of the pyrimidine part of purine nucleobases: Isomerization reactions in heteronuclear PtII/PdII of 9-methyladenine. *Inorganic Chemistry*, *50*(20), 10439–10447.

253   Silaghi-Dumitrescu, R., Mihály, B., Mihály, T., Attia, A. A., Miguel, P. J. S., & Lippert, B. (2017). The exocyclic amino group of adenine in Pt II and Pd II complexes: A critical comparison of the x-ray crystallographic structural data and gas phase calculations. *Journal of Biological Inorganic Chemistry*, *22*(4), 567–579.

254   Zhai, L., Pilston, R. L., Zaiger, K. L., Stokes, K. K., & McCullough, R. D. (2003). A simple method to generate side-chain derivatives of regioregular polythiophene via

the grim metathesis and post-polymerization functionalization. *Macromolecules*, *36*(1), 61–64.

255 Palermo, E. F., van der Laan, H. L., & McNeil, A. J. (2013). Impact of π-conjugated gradient sequence copolymers on polymer blend morphology. *Polymer Chemistry*, *4*(17), 4606–4611.

256 Lambertucci, C., Antonini, I., Buccioni, M., Dal Ben, D., Kachare, D. D., Volpini, R., Klotz, K.-N., & Cristalli, G. (2009). 8-bromo-9-alkyl adenine derivatives as tools for developing new adenosine A2A and A2B receptors ligands. *Bioorganic & Medicinal Chemistry*, *17*(7), 2812–2822.

257 Collier, G. S., Brown, L. A., Boone, E. S., Long, B. K., & Kilbey, S. M. (2016). Synthesis of main chain purine-based copolymers and effects of monomer design on thermal and optical properties. *ACS Macro Letters*, *5*(6), 682–687.

258 Mishra, A. K., Prajapati, R. K., & Verma, S. (2010). Probing structural consequences of N9-alkylation in silver-adenine frameworks. *Dalton Transactions*, *39*(42), 10034–10037.

259 Dal Ben, D., Buccioni, M., Lambertucci, C., Thomas, A., Klotz, K.-N., Federico, S., Cacciari, B., Spalluto, G., & Volpini, R. (2013). 8-(2-furyl) adenine derivatives as A2A adenosine receptor ligands. *European Journal of Medicinal Chemistry*, *70*, 525–535.

260 Fonseca Guerra, C., Bickelhaupt, F., Saha, S., & Wang, F. (2006). Adenine tautomers: Relative stabilities, ionization energies, and mismatch with cytosine. *The Journal of Physical Chemistry A*, *110*(11), 4012–4020.

261 Rudenko, A. E., Wiley, C. A., Tannaci, J. F., & Thompson, B. C. (2013). Optimization of direct arylation polymerization conditions for the synthesis of poly (3-hexylthiophene). *Journal of Polymer Science Part A: Polymer Chemistry*, *51*(12), 2660–2668.

262 Cerna, I., Pohl, R., Klepetarova, B., & Hocek, M. (2008). Synthesis of 6, 8, 9-tri- and 2, 6, 8, 9-tetrasubstituted purines by a combination of the suzuki cross-coupling, N-arylation, and direct C–H arylation reactions. *The Journal of Organic Chemistry*, *73*(22), 9048–9054.

263 Szabó, Z. (2008). Multinuclear NMR studies of the interaction of metal ions with adenine-nucleotides. *Coordination Chemistry Reviews*, *252*(21-22), 2362–2380.

264 Lippert, B. (1997). Effects of metal-ion binding on nucleobase pairing: Stabilization, prevention and mismatch formation. *Journal of the Chemical Society, Dalton Transactions*, (21), 3971–3976.

265 Šponer, J., Sabat, M., Gorb, L., Leszczynski, J., Lippert, B., & Hobza, P. (2000). The effect of metal binding to the N7 site of purine nucleotides on their structure, energy, and involvement in base pairing. *The Journal of Physical Chemistry B, 104*(31), 7535–7544.

266 Bhattacharya, A., & De, A. (1999). Conducting polymers in solution—progress toward processibility. *Journal of Macromolecular Science, Part C, 39*(1), 17–56.

267 Wu, P.-T., Ren, G., & Jenekhe, S. A. (2010). Crystalline random conjugated copolymers with multiple side chains: Tunable intermolecular interactions and enhanced charge transport and photovoltaic properties. *Macromolecules, 43*(7), 3306–3313.

268 Lee, Y., Aplan, M. P., Seibers, Z. D., Xie, R., Culp, T. E., Wang, C., Hexemer, A., Kilbey, S. M., Wang, Q., & Gomez, E. D. (2018). Random copolymers allow control of crystallization and microphase separation in fully conjugated block copolymers. *Macromolecules, 51*(21), 8844–8852.

269 Rehahn, M., Schlüter, A.-D., & Wegner, G. (1990). Soluble poly (para-phenylene) s, 3. variation of the length and the density of the solubilizing side chains. *Die Makromolekulare Chemie: Macromolecular Chemistry and Physics, 191*(9), 1991–2003.

270 Rodrigues, A., Castro, M. C. R., Farinha, A. S., Oliveira, M., Tomé, J. P., Machado, A. V., Raposo, M. M. M., Hilliou, L., & Bernardo, G. (2013). Thermal stability of P3HT and P3HT: PCBM blends in the molten state. *Polymer Testing, 32*(7), 1192–1201.

271 Kuo, S.-W., Xu, H., Huang, C.-F., & Chang, F.-C. (2002). Significant glass-transition-temperature increase through hydrogen-bonded copolymers. *Journal of Polymer Science Part B: Polymer Physics, 40*(19), 2313–2323.

272 Kraft, A., Grimsdale, A. C., & Holmes, A. B. (1998). Electroluminescent conjugated polymers—seeing polymers in a new light. *Angewandte Chemie International Edition, 37*(4), 402–428.

273 Hammud, H. H., Bouhadir, K. H., Masoud, M. S., Ghannoum, A. M., & Assi, S. A. (2008). Solvent effect on the absorption and fluorescence emission spectra of some

purine derivatives: Spectrofluorometric quantitative studies. *Journal of Solution Chemistry, 37*(7), 895–917.

274 Domınguez, S., Cangiotti, M., Fattori, A., Ääritalo, T., Damlin, P., Ottaviani, M., & Kvarnström, C. (2018). Effect of spacer length and solvent on the concentration-driven aggregation of cationic hydrogen-bonding donor polythiophenes. *Langmuir, 34*(25), 7364–7378.

275 Perepichka, I. F., Perepichka, D. F., Meng, H., & Wudl, F. (2005). Light-emitting polythiophenes. *Advanced Materials, 17*(19), 2281–2305.

276 Dimitriev, O. P., Blank, D. A., Ganser, C., & Teichert, C. (2018). Effect of the polymer chain arrangement on exciton and polaron dynamics in P3HT and P3HT: PCBM films. *The Journal of Physical Chemistry C, 122*(30), 17096–17109.

277 Lakowicz, J. R. (2013). *Principles of fluorescence spectroscopy.* Springer science & business media.

278 Karstens, T., & Kobs, K. (1980). Rhodamine b and rhodamine 101 as reference substances for fluorescence quantum yield measurements. *The Journal of Physical Chemistry, 84*(14), 1871–1872.

279 Cook, S., Furube, A., & Katoh, R. (2008). Analysis of the excited states of regioregular polythiophene P3HT. *Energy & Environmental Science, 1*(2), 294–299.

280 Piris, J., Dykstra, T. E., Bakulin, A. A., Loosdrecht, P. H. v., Knulst, W., Trinh, M. T., Schins, J. M., & Siebbeles, L. D. (2009). Photogeneration and ultrafast dynamics of excitons and charges in P3HT/PCBM blends. *The Journal of Physical Chemistry C, 113*(32), 14500–14506.

281 Xu, B., & Holdcroft, S. (1993). Molecular control of luminescence from poly (3-hexylthiophenes). *Macromolecules, 26*(17), 4457–4460.

282 Weldeab, A. O., Li, L., Cekli, S., Abboud, K. A., Schanze, K. S., & Castellano, R. K. (2018). Pyridine-terminated low gap π-conjugated oligomers: Design, synthesis, and photophysical response to protonation and metalation. *Organic Chemistry Frontiers, 5*(21), 3170–3177.

283 Casey, A., Ashraf, R. S., Fei, Z., & Heeney, M. (2014). Thioalkyl-substituted benzothiadiazole acceptors: Copolymerization with carbazole affords polymers with large stokes shifts and high solar cell voltages. *Macromolecules*, *47*(7), 2279–2288.

284 Dutta, T., Woody, K. B., Parkin, S. R., Watson, M. D., & Gierschner, J. (2009). Conjugated polymers with large effective stokes shift: Benzobisdioxole-based poly (phenylene ethynylene) s. *Journal of the American Chemical Society*, *131*(47), 17321–17327.

285 Fan, L.-J., Zhang, Y., Murphy, C. B., Angell, S. E., Parker, M. F., Flynn, B. R., & Jones Jr, W. E. (2009). Fluorescent conjugated polymer molecular wire chemosensors for transition metal ion recognition and signaling. *Coordination Chemistry Reviews*, *253*(3-4), 410–422.

286 Wenfeng, L., Hengchang, M., Yuan, M., Chunxuan, Q., Zhonwei, Z., Zengming, Y., Haiying, C. et al. (2015). A self-assembled triphenylamine-based fluorescent chemosensor for selective detection of Fe3+ and Cu2+ ions in aqueous solution. *RSC Advances*, *5*(9), 6869–6878.

287 Formica, M., Fusi, V., Giorgi, L., & Micheloni, M. (2012). New fluorescent chemosensors for metal ions in solution. *Coordination Chemistry Reviews*, *256*(1-2), 170–192.

288 Fraiji, L. K., Hayes, D. M., & Werner, T. (1992). Static and dynamic fluorescence quenching experiments for the physical chemistry laboratory. *Journal of Chemical Education*, *69*(5), 424.

289 Sadeghi, I., Govinna, N., Cebe, P., & Asatekin, A. (2019). Superoleophilic, mechanically strong electrospun membranes for fast and efficient gravity-driven oil/water separation. *ACS Applied Polymer Materials*, *1*(4), 765–776.

290 Wang, X., Yu, P., Zhang, K., Wu, M., Wu, Q., Liu, J., Yang, J., & Zhang, J. (2019). Superhydrophobic/superoleophilic cotton for efficient oil–water separation based on the combined octadecanoyl chain bonding and polymer grafting via surface-initiated atrp. *ACS Applied Polymer Materials*, *1*(11), 2875–2882.

291 Hayase, G., & Nomura, S.-i. M. (2019). Macroporous silicone sheets integrated with meshes for various applications. *ACS Applied Polymer Materials*, *1*(8), 2077–2082.

292 Latthe, S. S., Sutar, R. S., Bhosale, A., Sadasivuni, K. K., & Liu, S. (2019). Superhydrophobic surfaces for oil-water separation. *Superhydrophobic polymer coatings* (pp. 339–356). Elsevier.

293 Jiao, R., Bao, L., Zhang, W., Sun, H., Zhu, Z., Xiao, C., Chen, L., & An, L. (2018). Synthesis of aminopyridine-containing conjugated microporous polymers with excellent superhydrophobicity for oil/water separation. *New Journal of Chemistry*, *42*(18), 14863–14869.

294 Bai, W., Guan, M., Lai, N., Yao, R., Xu, Y., & Lin, J. (2018). Superhydrophobic paper from conjugated poly (p-phenylene) s: Self-assembly and separation of oil/water mixture. *Materials Chemistry and Physics*, *216*, 230–236.

295 de Leon, A. C., Imperial, R. E. S., Chen, Q., & Advincula, R. C. (2019). One-step fabrication of superhydrophobic/superoleophilic electrodeposited polythiophene for oil and water separation. *Macromolecular Materials and Engineering*, *304*(7), 1800722.

296 Zhou, X., Zhang, Z., Xu, X., Guo, F., Zhu, X., Men, X., & Ge, B. (2013). Robust and durable superhydrophobic cotton fabrics for oil/water separation. *ACS Applied Materials & Interfaces*, *5*(15), 7208–7214.

297 Mather, B. D., Baker, M. B., Beyer, F. L., Berg, M. A., Green, M. D., & Long, T. E. (2007). Supramolecular triblock copolymers containing complementary nucleobase molecular recognition. *Macromolecules*, *40*(19), 6834–6845.

298 Viswanathan, K., Ozhalici, H., Elkins, C. L., Heisey, C., Ward, T. C., & Long, T. E. (2006). Multiple hydrogen bonding for reversible polymer surface adhesion. *Langmuir*, *22*(3), 1099–1105.

299 Huang, Z.-Y., Yang, J.-F., Song, K., Chen, Q., Zhou, S.-L., Hao, G.-F., & Yang, G.-F. (2016). One-pot approach to n-quinolyl 3/4-biaryl carboxamides by microwave-assisted suzuki–miyaura coupling and n-boc deprotection. *The Journal of Organic Chemistry*, *81*(20), 9647–9657.

300 Gorelsky, S. I., Lapointe, D., & Fagnou, K. (2008). Analysis of the concerted metalation-deprotonation mechanism in palladium-catalyzed direct arylation across a broad range of aromatic substrates. *Journal of the American Chemical Society*, *130*(33), 10848–10849.

301 Chakrabarty, M., Kundu, T., & Harigaya, Y. (2006). Mild deprotection of tert-butyl carbamates of NH-heteroarenes under basic conditions. *Synthetic Communications*, *36*(14), 2069–2077.

302 Li, B., Li, R., Dorff, P., McWilliams, J. C., Guinn, R. M., Guinness, S. M., Han, L., Wang, K., & Yu, S. (2019). Deprotection of N-Boc groups under continuous-flow high-temperature conditions. *The Journal of Organic Chemistry*, *84*(8), 4846–4855.

303 El Kazzouli, S., Koubachi, J., Berteina-Raboin, S., Mouaddib, A., & Guillaumet, G. (2006). A mild and selective method for the N-Boc deprotection by sodium carbonate. *Tetrahedron Letters*, *47*(48), 8575–8577.

304 Wang, G., Li, C., Li, J., & Jia, X. (2009). Catalyst-free water-mediated N-Boc deprotection. *Tetrahedron Letters*, *50*(13), 1438–1440.

305 Zinelaabidine, C., Souad, O., Zoubir, J., Malika, B., & Nour-Eddine, A. (2012). A simple and efficient green method for the deprotection of N-Boc in various structurally diverse amines under water-mediated catalyst-free conditions. *International journal of Chemistry*, *4*(3), 73.

306 Dandepally, S. R., & Williams, A. L. (2009a). Microwave-assisted N-Boc deprotection under mild basic conditions using $K_3PO_4 \cdot H_2O$ in MeOH. *Tetrahedron Letters*, *50*(9), 1071–1074.

307 Bhawal, S. S., Patil, R. A., & Armstrong, D. W. (2015). Rapid, effective deprotection of tert-butoxycarbonyl (Boc) amino acids and peptides at high temperatures using a thermally stable ionic liquid. *RSC Advances*, *5*(116), 95854–95856.

308 Gibson, F. S., Bergmeier, S. C., & Rapoport, H. (1994). Selective removal of an N-Boc protecting group in the presence of a tert-butyl ester and other acid-sensitive groups. *The Journal of Organic Chemistry*, *59*(11), 3216–3218.

309 Li, B., Berliner, M., Buzon, R., Chiu, C. K.-F., Colgan, S. T., Kaneko, T., Keene, N., Kissel, W., Le, T., Leeman, K. R. et al. (2006). Aqueous phosphoric acid as a mild reagent for deprotection of tert-butyl carbamates, esters, and ethers. *The Journal of Organic Chemistry*, *71*(24), 9045–9050.

310 Dandepally, S. R., & Williams, A. L. (2009b). Synthesis of imidazoisoindol-3-ones by a palladium-catalyzed intramolecular C–H insertion reaction. *Tetrahedron Letters*, *50*(13), 1395–1398.

311 Ghobrial, M., Harhammer, K., Mihovilovic, M. D., & Schnürch, M. (2010). Facile, solvent and ligand free iron catalyzed direct functionalization of n-protected tetrahydroisoquinolines and isochroman. *Chemical Communications*, *46*(46), 8836–8838.

312 Cho, S. Y., Lee, B. H., Jung, H., Yun, C. S., Du Ha, J., Kim, H. R., Chae, C. H., Lee, J. H., Seo, H. W., & Oh, K.-S. (2013). Design and synthesis of novel 3-(benzo [d] oxazol-2-yl)-5-(1-(piperidin-4-yl)-1h-pyrazol-4-yl) pyridin-2-amine derivatives as selective g-protein-coupled receptor kinase-2 and-5 inhibitors. *Bioorganic & Medicinal Chemistry Letters*, *23*(24), 6711–6716.

313 Más-Montoya, M., & Janssen, R. A. (2017). The effect of h-and j-aggregation on the photophysical and photovoltaic properties of small thiophene–pyridine–DPP molecules for bulk-heterojunction solar cells. *Advanced Functional Materials*, *27*(16), 1605779.

314 Hayashi, S., Yamamoto, S.-i., & Koizumi, T. (2017). Effects of molecular weight on the optical and electrochemical properties of edot-based π-conjugated polymers. *Scientific Reports*, *7*(1), 1–8.

315 Aoyama, Y., Asakawa, M., Matsui, Y., & Ogoshi, H. (1991). Molecular recognition. 16. molecular recognition of quinones: Two-point hydrogen-bonding strategy for the construction of face-to-face porphyrin-quinone architectures. *Journal of the American Chemical Society*, *113*(16), 6233–6240.

316 Kuntz Jr, I., Gasparro, F., Johnston Jr, M., & Taylor, R. (1968). Molecular interactions and the Benesi-Hildebrand equation. *Journal of the American Chemical Society*, *90*(18), 4778–4781.

317 Karikari, A. S., Mather, B. D., & Long, T. E. (2007). Association of star-shaped poly (d, l-lactide) s containing nucleobase multiple hydrogen bonding. *Biomacromolecules*, *8*(1), 302–308.

318 Kim, H. M., Jung, C., Kim, B. R., Jung, S.-Y., Hong, J. H., Ko, Y.-G., Lee, K. J., & Cho, B. R. (2007). Environment-sensitive two-photon probe for intracellular free magnesium ions in live tissue. *Angewandte Chemie*, *119*(19), 3530–3533.

319 Wang, R., & Yu, Z. (2007). Validity and reliability of benesi-hildebrand method. *Acta Physico-Chimica Sinica*, *23*(9), 1353–1359.

320 Sabury, S., Adams, T. J., Kocherga, M., Kilbey, S. M., & Walter, M. G. (2020). Synthesis and optoelectronic properties of benzodithiophene-based conjugated polymers with hydrogen bonding nucleobase side chain functionality. *Polymer Chemistry*, *11*(36), 5735–5749.

321 Mianehrow, H., Sabury, S., Bazargan, A., Sharif, F., & Mazinani, S. (2017). A flexible electrode based on recycled paper pulp and reduced graphene oxide composite. *Journal of Materials Science: Materials in Electronics*, *28*(6), 4990–4996.

322 Rohrbach, K., Li, Y., Zhu, H., Liu, Z., Dai, J., Andreasen, J., & Hu, L. (2014). A cellulose based hydrophilic, oleophobic hydrated filter for water/oil separation. *Chemical Communications*, *50*(87), 13296–13299.

323 Tang, X., Shen, C., Zhu, W., Zhang, S., Xu, Y., Yang, Y., Gao, M., & Dong, F. (2017). A facile procedure to modify filter paper for oil–water separation. *RSC Advances*, *7*(48), 30495–30499.

324 Teisala, H., Tuominen, M., & Kuusipalo, J. (2014). Superhydrophobic coatings on cellulose-based materials: Fabrication, properties, and applications. *Advanced Materials Interfaces*, *1*(1), 1300026.

325 Babiker, D. M., Zhu, L., Yagoub, H., Xu, X., Zhang, X., Shibraen, M. H., & Yang, S. (2019). Hydrogen-bonded methylcellulose/poly (acrylic acid) complex membrane for oil-water separation. *Surface and Coatings Technology*, *367*, 49–57.

326 Huang, Y., Zhan, H., Li, D., Tian, H., & Chang, C. (2019). Tunicate cellulose nanocrystals modified commercial filter paper for efficient oil/water separation. *Journal of Membrane Science*, *591*, 117362.

327 Liu, Y., Liu, N., Jing, Y., Jiang, X., Yu, L., & Yan, X. (2019). Surface design of durable and recyclable superhydrophobic materials for oil/water separation. *Colloids and Surfaces A: Physicochemical and Engineering Aspects*, *567*, 128–138.

328 Luo, Z., Duan, C., Li, Y., Wang, Y., & Wang, B. (2018). A glucose modified filter paper for effective oil/water separation. *RSC Advances*, *8*(52), 29570–29577.

329 Li, S., Zhang, S., & Wang, X. (2008). Fabrication of superhydrophobic cellulose-based materials through a solution-immersion process. *Langmuir*, *24*(10), 5585–5590.

330 Musikavanhu, B., Hu, Z., Dzapata, R. L., Xu, Y., Christie, P., Guo, D., & Li, J. (2019). Facile method for the preparation of superhydrophobic cellulosic paper. *Applied Surface Science*, *496*, 143648.

331 Duchemin, B. (2015). Mercerisation of cellulose in aqueous naoh at low concentrations. *Green Chemistry*, *17*(7), 3941–3947.

332 Garside, P., & Wyeth, P. (2003). Identification of cellulosic fibres by FTIR spectroscopy-thread and single fibre analysis by attenuated total reflectance. *Studies in Conservation*, *48*(4), 269–275.

333 Nelson, M. L., & O'Connor, R. T. (1964). Relation of certain infrared bands to cellulose crystallinity and crystal lattice type. part ii. a new infrared ratio for estimation of crystallinity in celluloses I and II. *Journal of Applied Polymer Science*, *8*(3), 1325–1341.

334 Maréchal, Y., & Chanzy, H. (2000). The hydrogen bond network in Iβ cellulose as observed by infrared spectrometry. *Journal of Molecular Structure*, *523*(1-3), 183–196.

335 Lee, C. M., Kubicki, J. D., Fan, B., Zhong, L., Jarvis, M. C., & Kim, S. H. (2015). Hydrogen-bonding network and OH stretch vibration of cellulose: Comparison of computational modeling with polarized ir and sfg spectra. *The Journal of Physical Chemistry B*, *119*(49), 15138–15149.

336 Teo, L.-S., Chen, C.-Y., & Kuo, J.-F. (1997). Fourier transform infrared spectroscopy study on effects of temperature on hydrogen bonding in amine-containing polyurethanes and poly (urethane- urea) s. *Macromolecules*, *30*(6), 1793–1799.

337 Hirakawa, A. Y., Okada, H., Sasagawa, S., & Tsuboi, M. (1985). Infrared and raman spectra of adenine and its 15n and 13c substitution products. *Spectrochimica Acta Part A: Molecular Spectroscopy*, *41*(1-2), 209–216.

338 Lin, Y.-T., Singh, R., Kuo, S.-W., & Ko, F.-H. (2017). Supramolecular control over the morphology of bio-inspired poly (3-hexylthiophene) for organic thin film transistors. *Organic Electronics*, *41*, 221–228.

339 Mohamed, T. A., Shabaan, I. A., Zoghaib, W. M., Husband, J., Farag, R. S., & Alajhaz, A. E.-N. M. (2009). Tautomerism, normal coordinate analysis, vibrational assignments, calculated IR, raman and NMR spectra of adenine. *Journal of Molecular Structure*, *938*(1-3), 263–276.

340 Yuan, Y., Zhang, J., Sun, J., Hu, J., Zhang, T., & Duan, Y. (2011). Polymorphism and structural transition around 54 °C in regioregular poly (3-hexylthiophene) with high crystallinity as revealed by infrared spectroscopy. *Macromolecules*, *44*(23), 9341–9350.

341 Nakamoto, K., Margoshes, M., & Rundle, R. (1955). Stretching frequencies as a function of distances in hydrogen bonds. *Journal of the American Chemical Society*, *77*(24), 6480–6486.

342 Kim, H.-D., & Ishida, H. (2002). A study on hydrogen-bonded network structure of polybenzoxazines. *The Journal of Physical Chemistry A*, *106*(14), 3271–3280.

343 Grabowski, S. J., Sokalski, W. A., & Leszczynski, J. (2006). The possible covalent nature of N–H· · · hydrogen bonds in formamide dimer and related systems: An ab initio study. *The Journal of Physical Chemistry A*, *110*(14), 4772–4779.

344 Grabowski, S. J., & Małecka, M. (2006). Intramolecular H-bonds: DFT and QTAIM studies on 3-(aminomethylene) pyran-2, 4-dione and its derivatives. *The Journal of Physical Chemistry A*, *110*(42), 11847–11854.

345 Liu, J., & Lilley, D. M. (2007). The role of specific 2-hydroxyl groups in the stabilization of the folded conformation of kink-turn RNA. *RNA*, *13*(2), 200–210.

346 Ulyanov, N. B., & James, T. L. (2010). RNA structural motifs that entail hydrogen bonds involving sugar–phosphate backbone atoms of RNA. *New Journal of Chemistry*, *34*(5), 910–917.

347 Wu, Y.-S., Wu, Y.-C., & Kuo, S.-W. (2014). Thymine-and adenine-functionalized polystyrene form self-assembled structures through multiple complementary hydrogen bonds. *Polymers*, *6*(6), 1827–1845.

348 Marmur, A. (2006). Underwater superhydrophobicity: Theoretical feasibility. *Langmuir*, *22*(4), 1400–1402.

Appendices

A ^{1}H and ^{13}C NMR spectra of small molecules, monomers, and polymers

A.1   Nucleobase-Containing Small Molecules
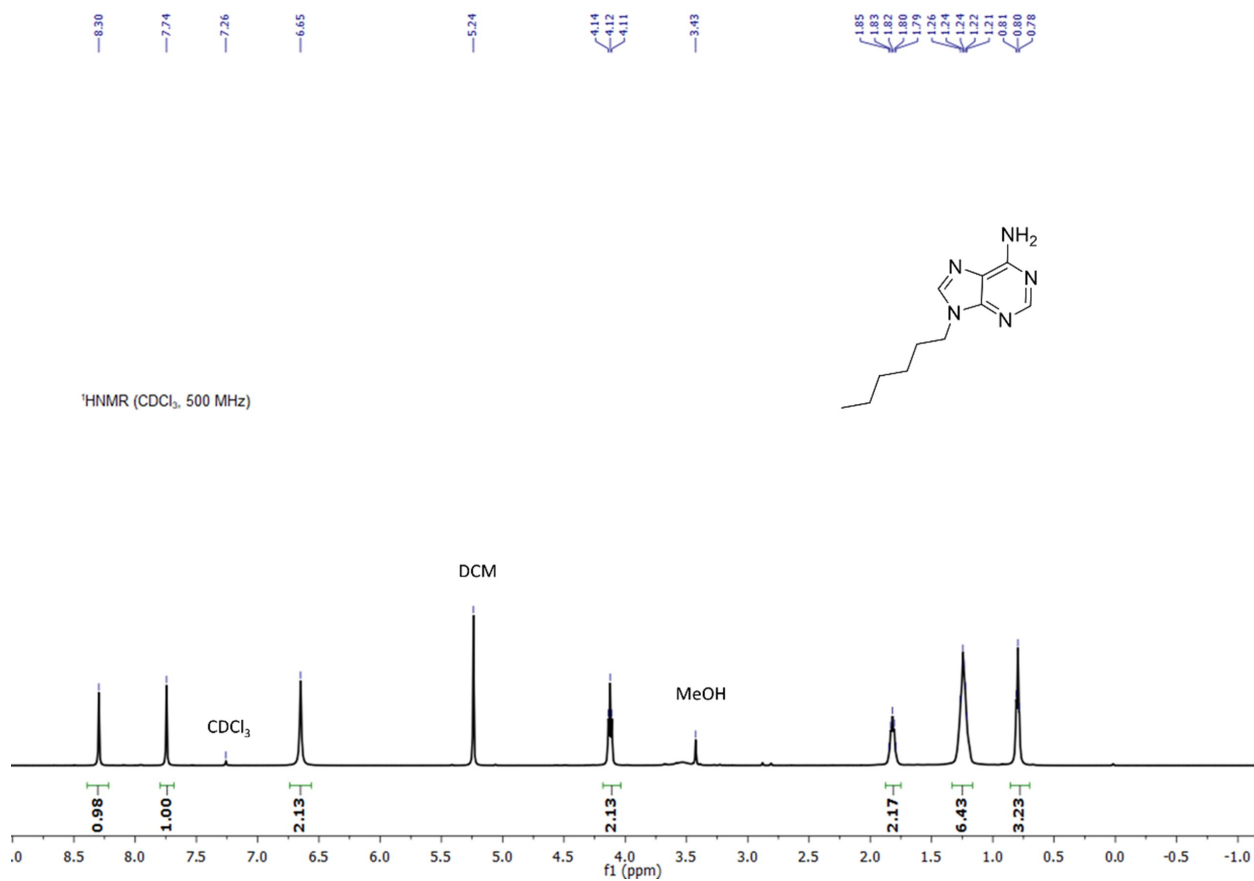
Figure A.1: ^{1}H NMR spectrum of adenine-N9-hexyl (CDCl$_3$, 25 °C).

13CNMR (CDCl₃, 500 MHz)
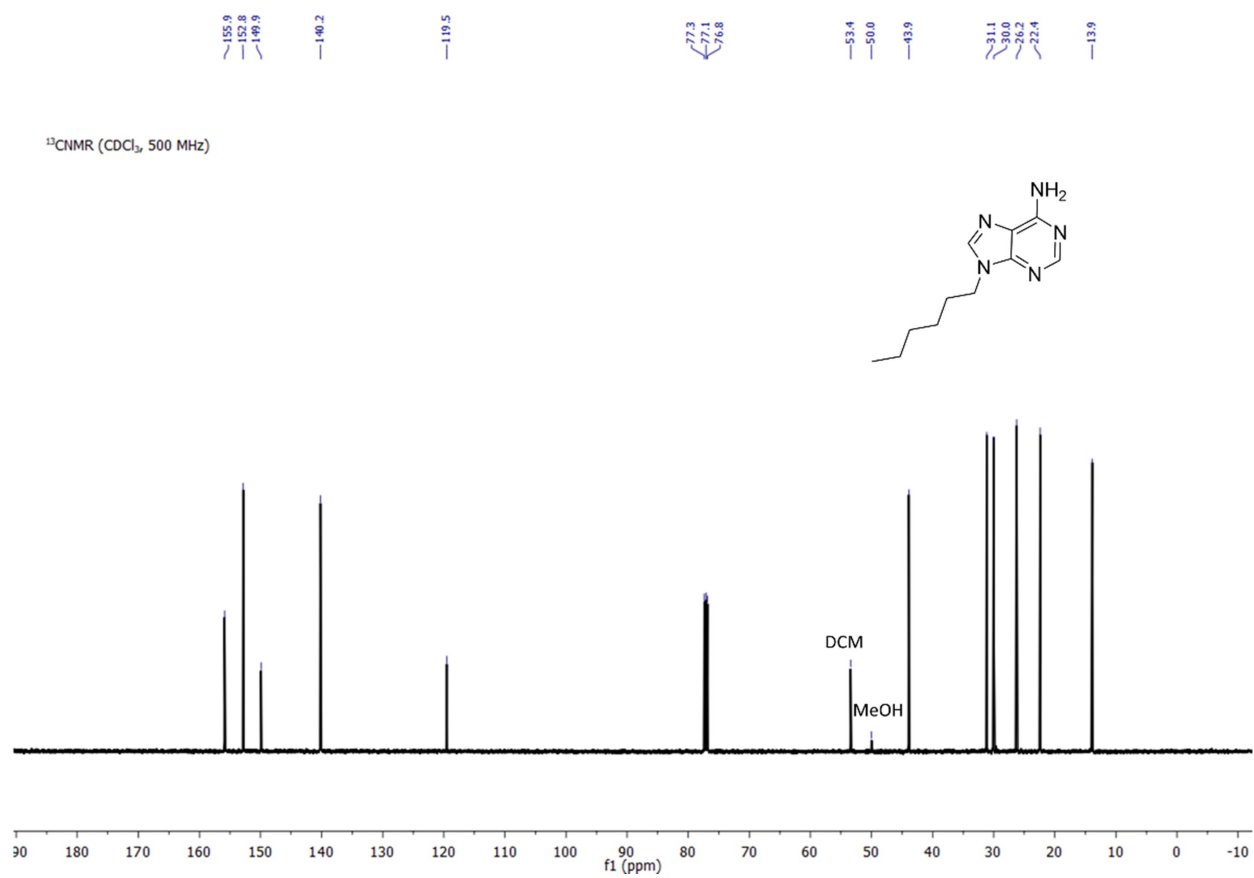
Figure A.2: ¹³C NMR spectrum of adenine-N9-hexyl (CDCl₃, 25 °C).
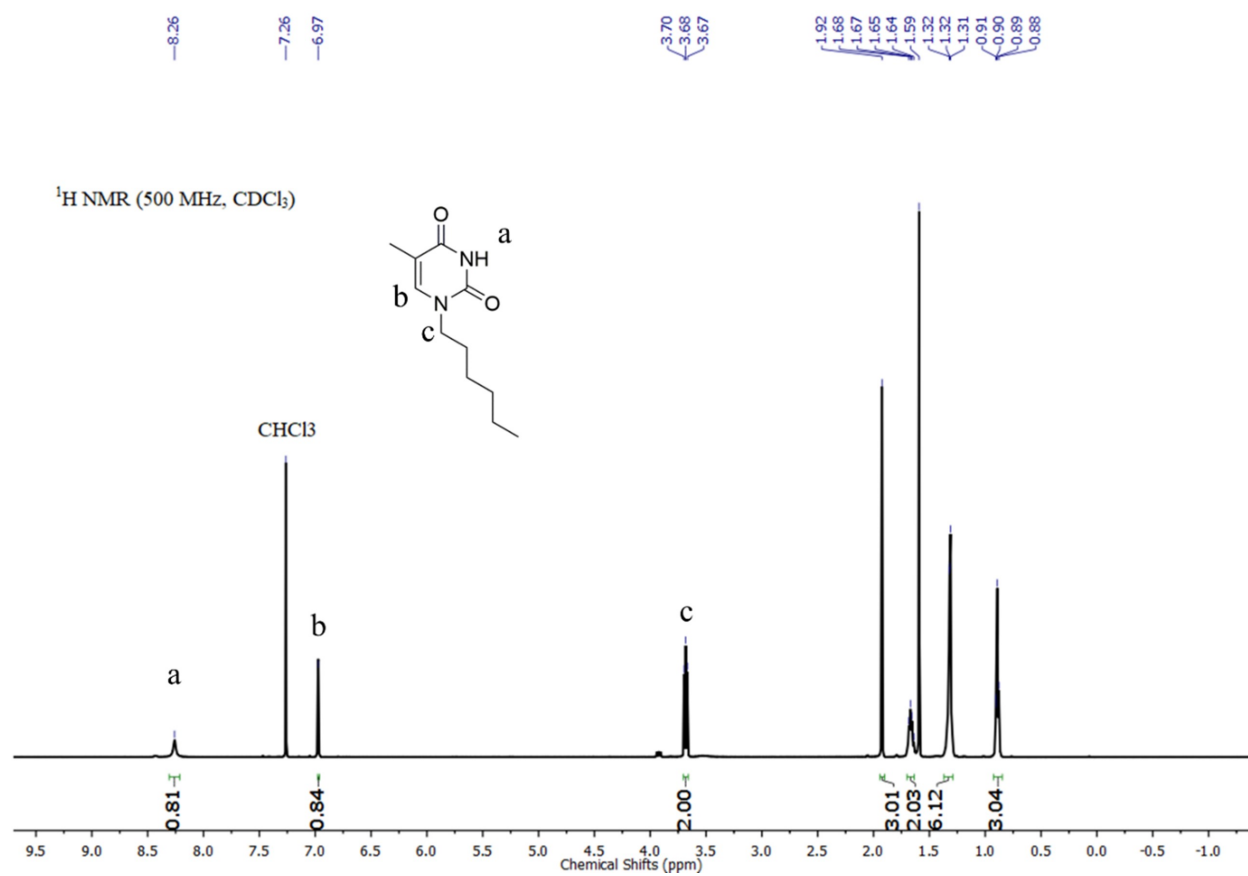
Figure A.3: ^{1}H NMR spectrum of thymine-N1-hexyl (CDCl$_3$, 25 °C).
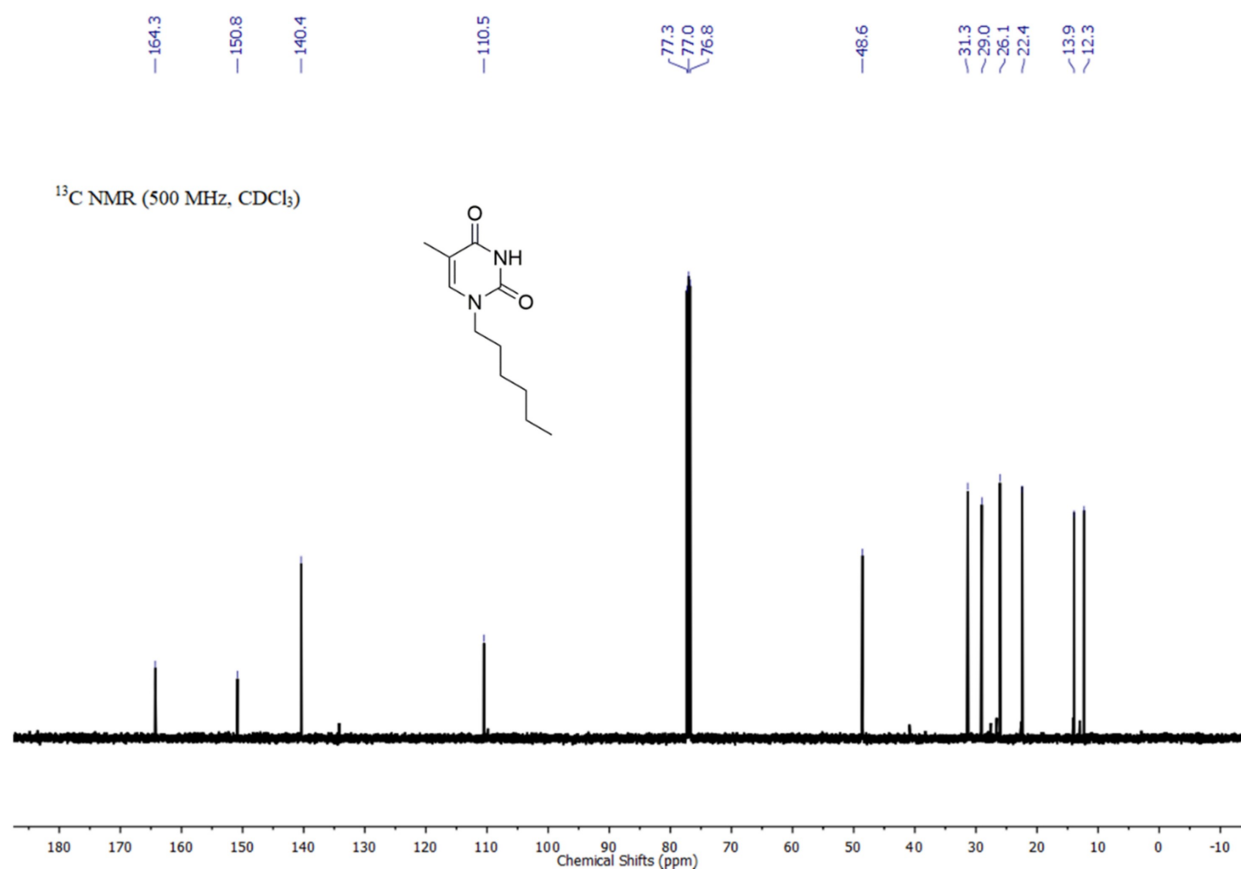
Figure A.4: ^{13}C NMR spectrum of thymine-N1-hexyl (CDCl$_3$, 25 °C).
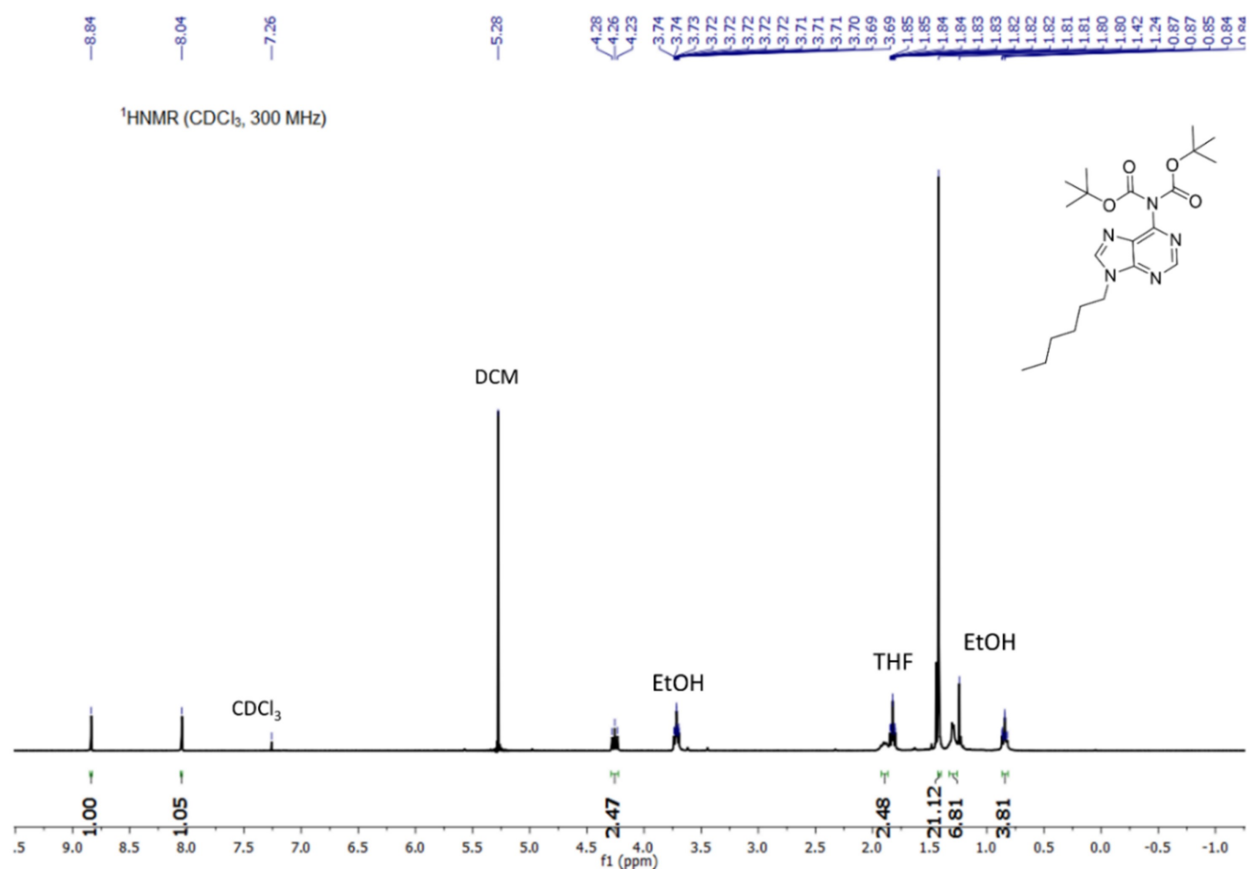
Figure A.5: ^{1}H NMR spectrum of Boc-protected adenine-N9-hexyl (CDCl$_3$, 25 °C).
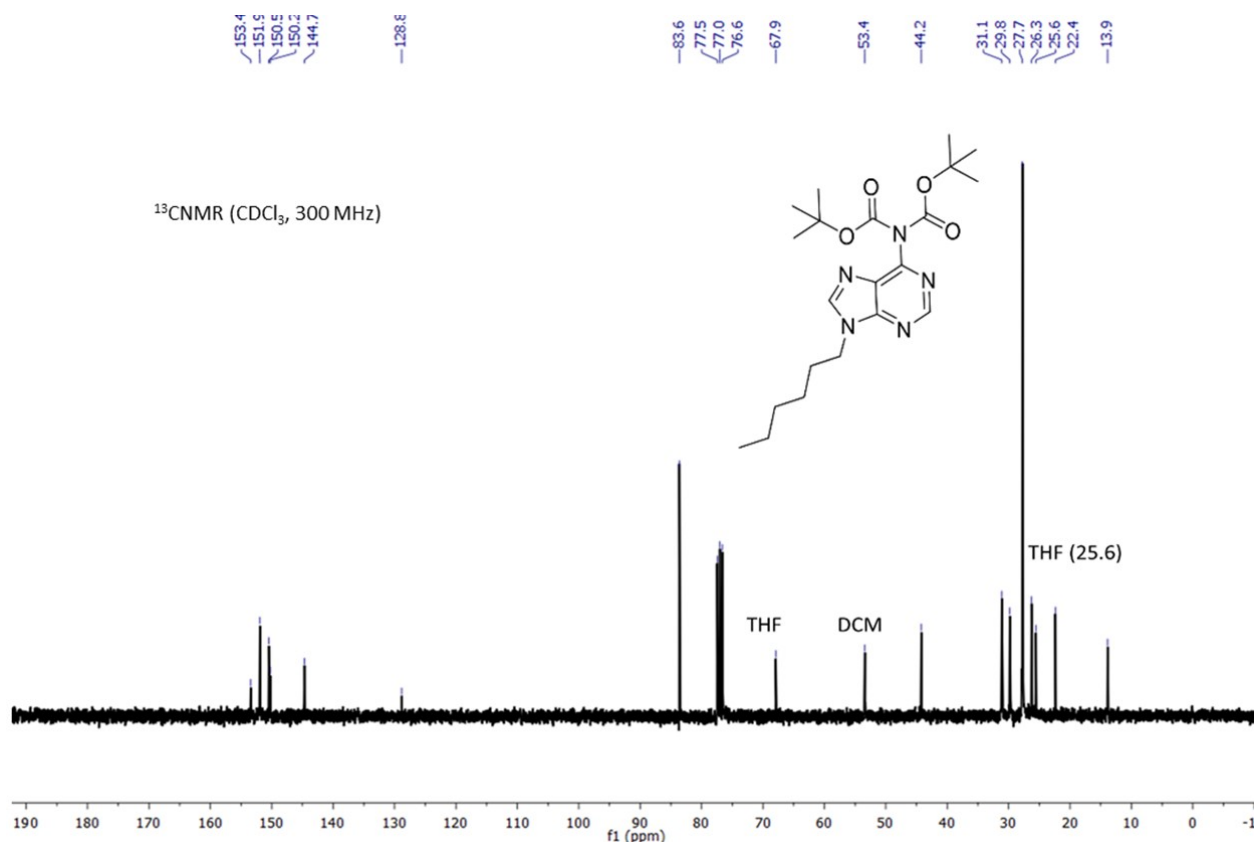
Figure A.6: ^{13}C NMR spectrum of Boc-protected adenine-N9-hexyl (CDCl$_3$, 25 °C).
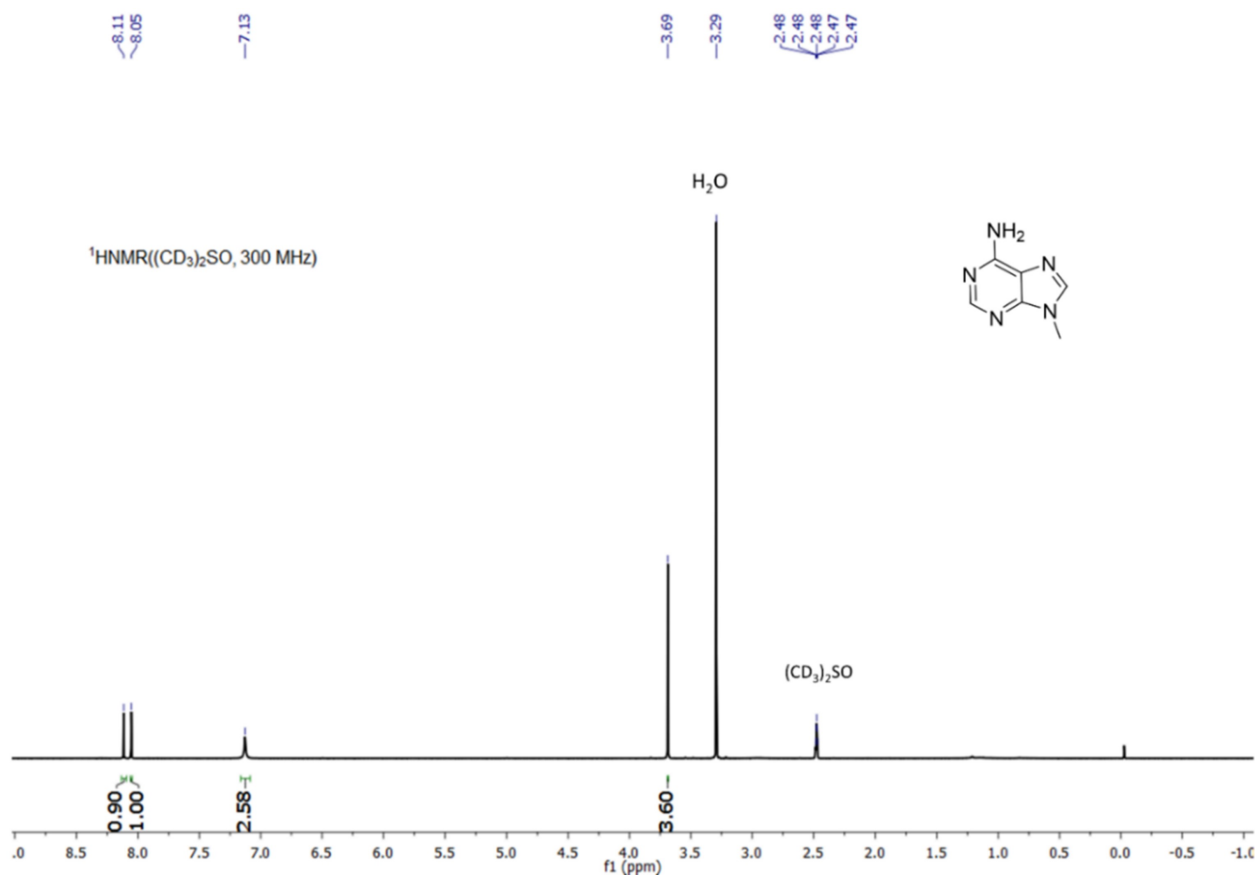
Figure A.7: ^{1}H NMR spectrum of adenine-N9-methyl $((CD_3)_2SO)$, 25 °C.

A.2 Intermediate Small Molecules for Monomer Synthesis
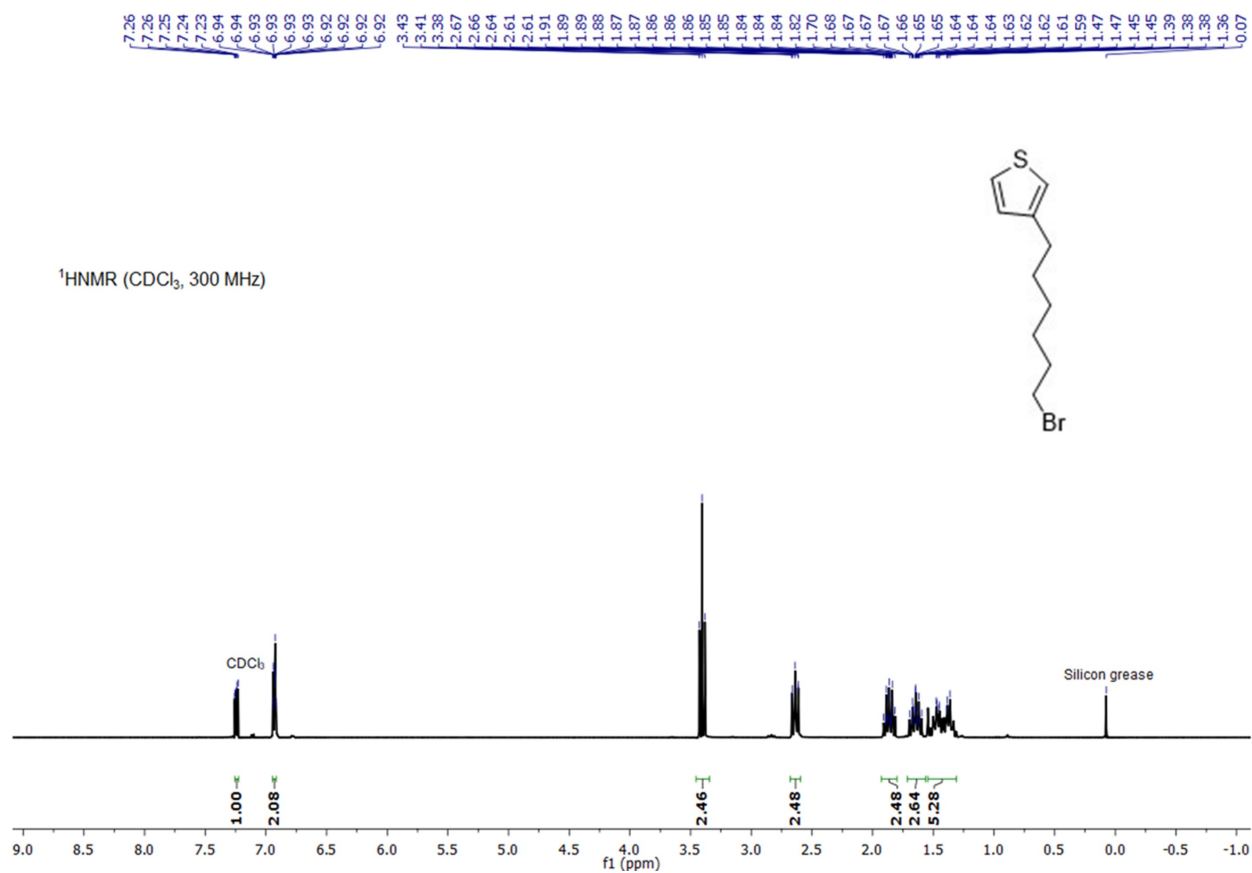
Figure A.8: ^{1}H NMR spectrum of 3-(6-bromohexyl) thiophene (CDCl$_3$, 25 °C).
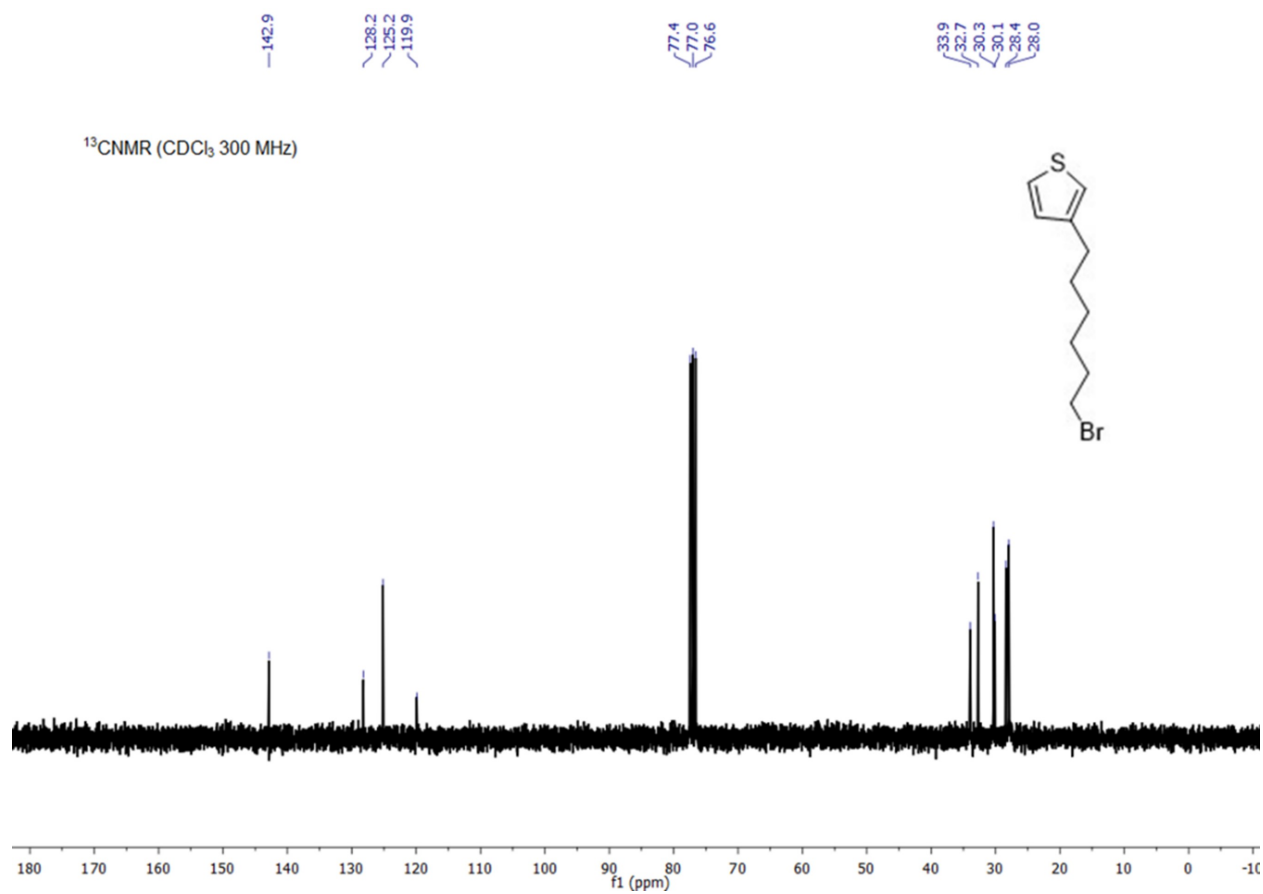
Figure A.9: ^{13}C NMR spectrum of 3-(6-bromohexyl) thiophene (CDCl$_3$, 25 °C).
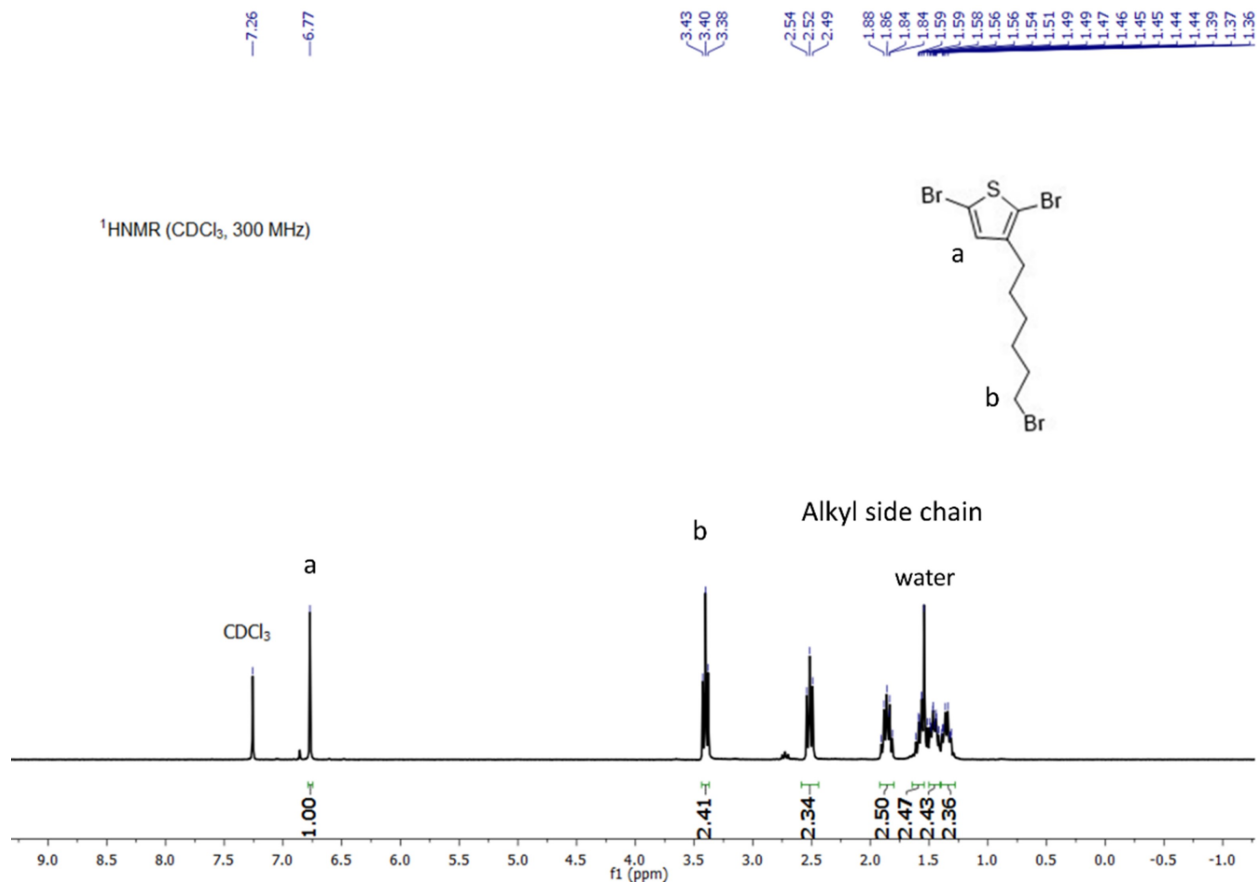
Figure A.10: ^{1}H NMR spectrum of 2,5-dibromo-3-(6-bromohexyl) thiophene (CDCl$_3$, 25 °C).
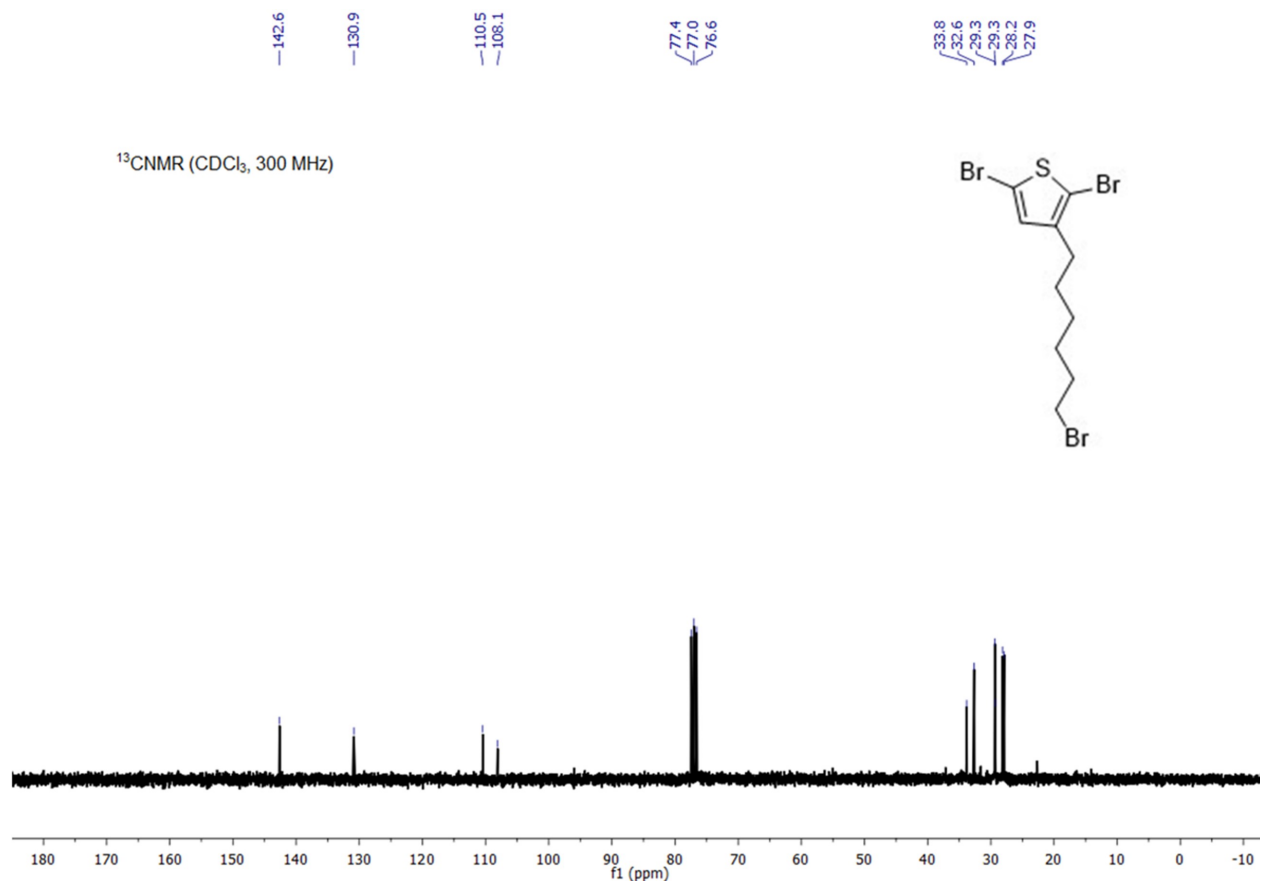
Figure A.11: ^{13}C NMR spectrum of 2,5-dibromo-3-(6-bromohexyl) thiophene (CDCl$_3$, 25 °C).
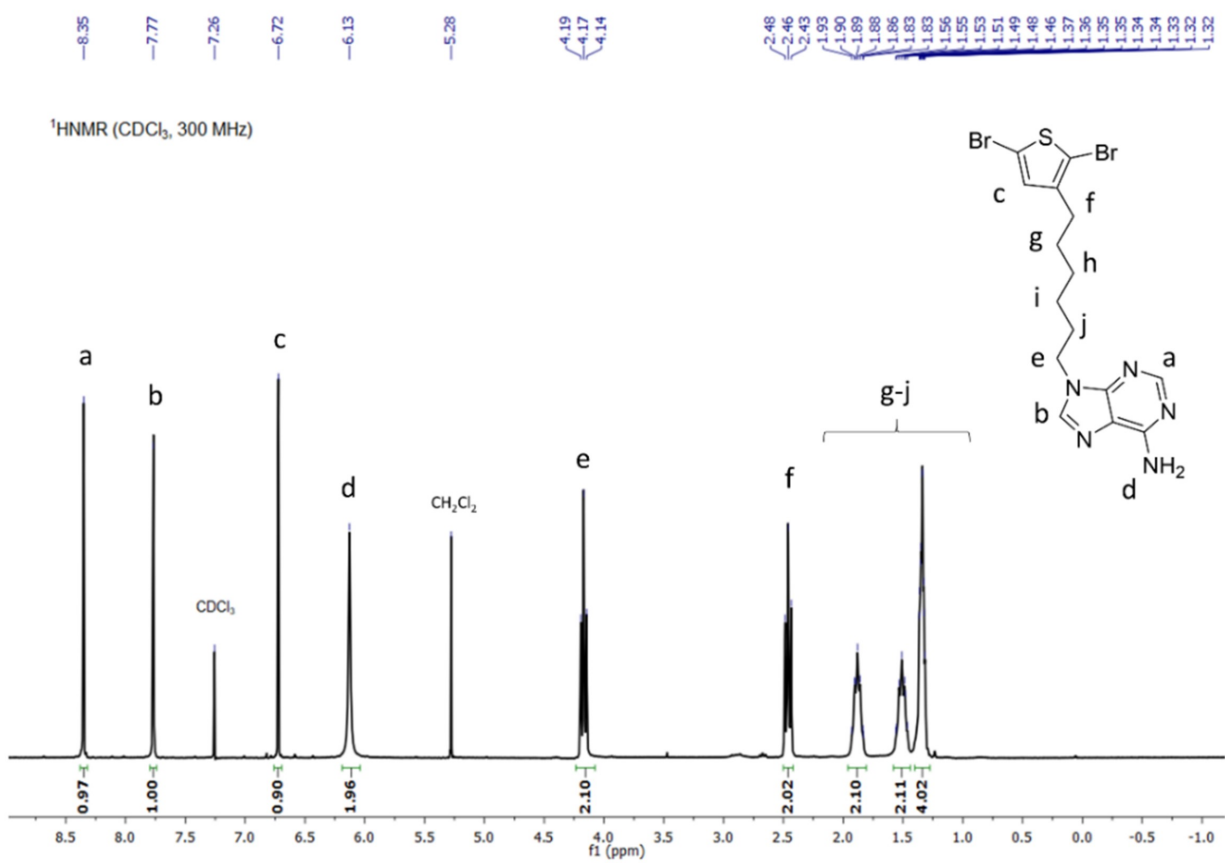
Figure A.12: ^{1}H NMR spectrum of adenine containing dibromo thiophene monomer, $3hT_{Ad}$ (CDCl$_3$, 25 °C).
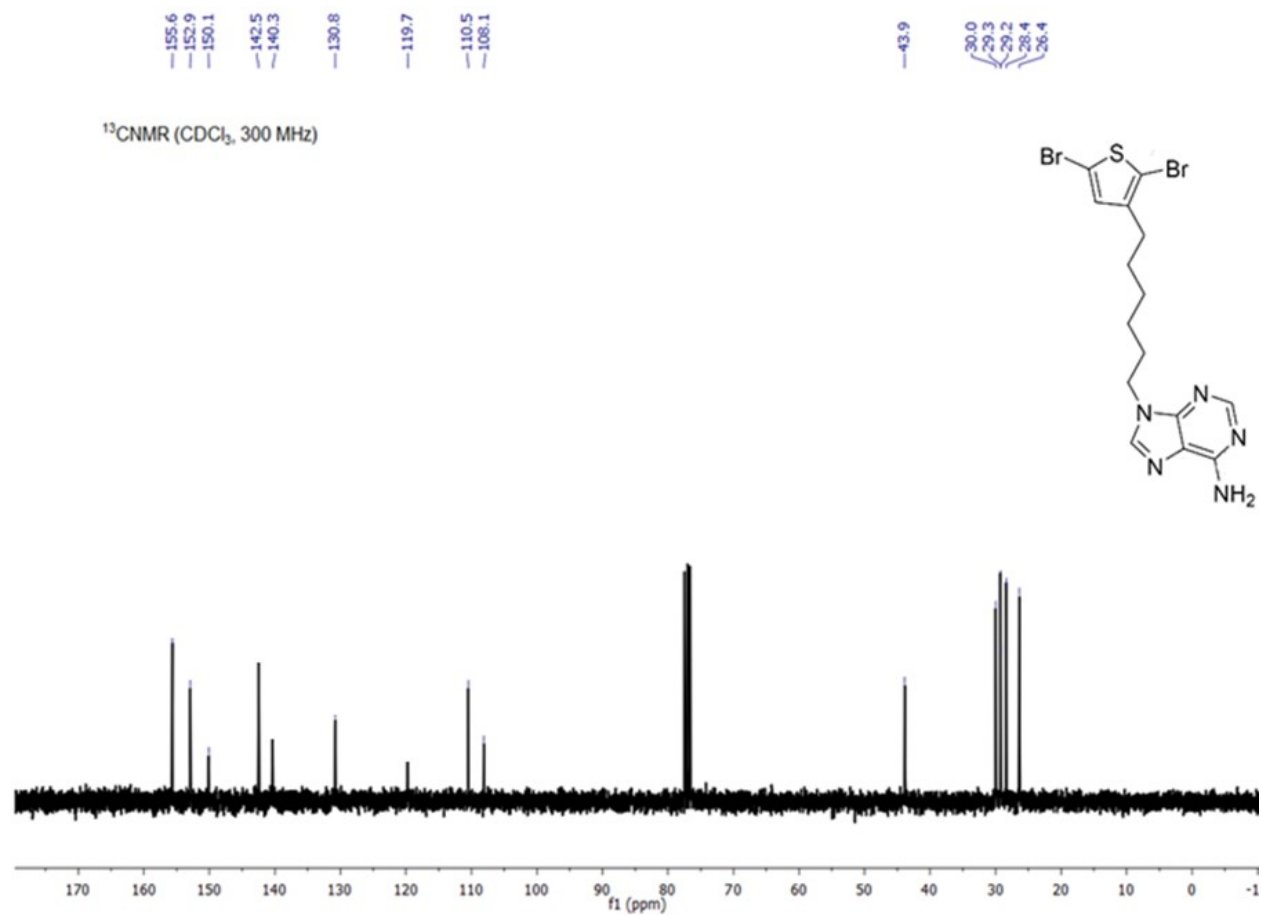
Figure A.13: ^{13}C NMR spectrum of adenine containing dibromo thiophene monomer, 3hT$_{Ad}$ (CDCl$_3$, 25 °C).
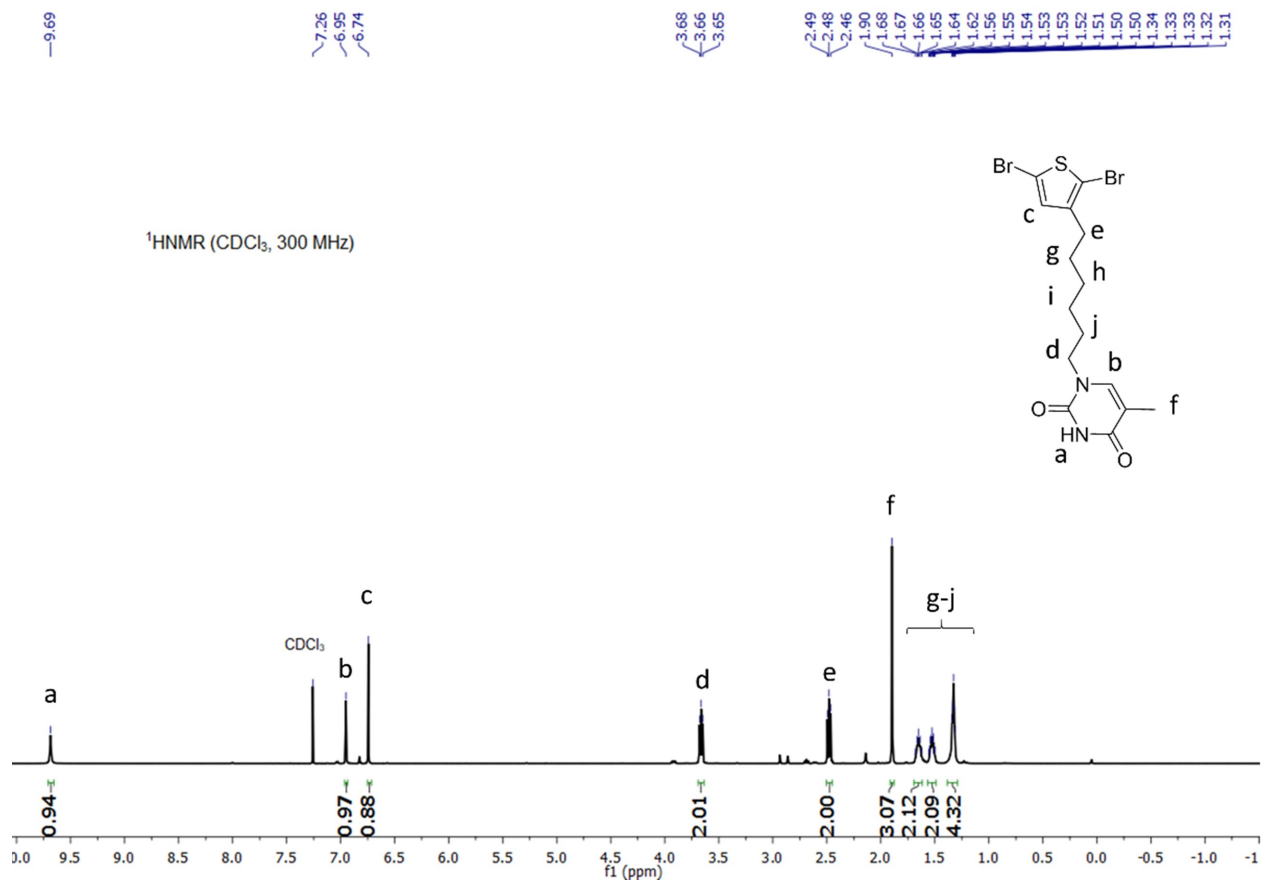
Figure A.14: ^{1}H NMR spectrum of adenine containing dibromo thiophene monomer, $3hT_{Thy}$ (CDCl$_3$, 25 °C).
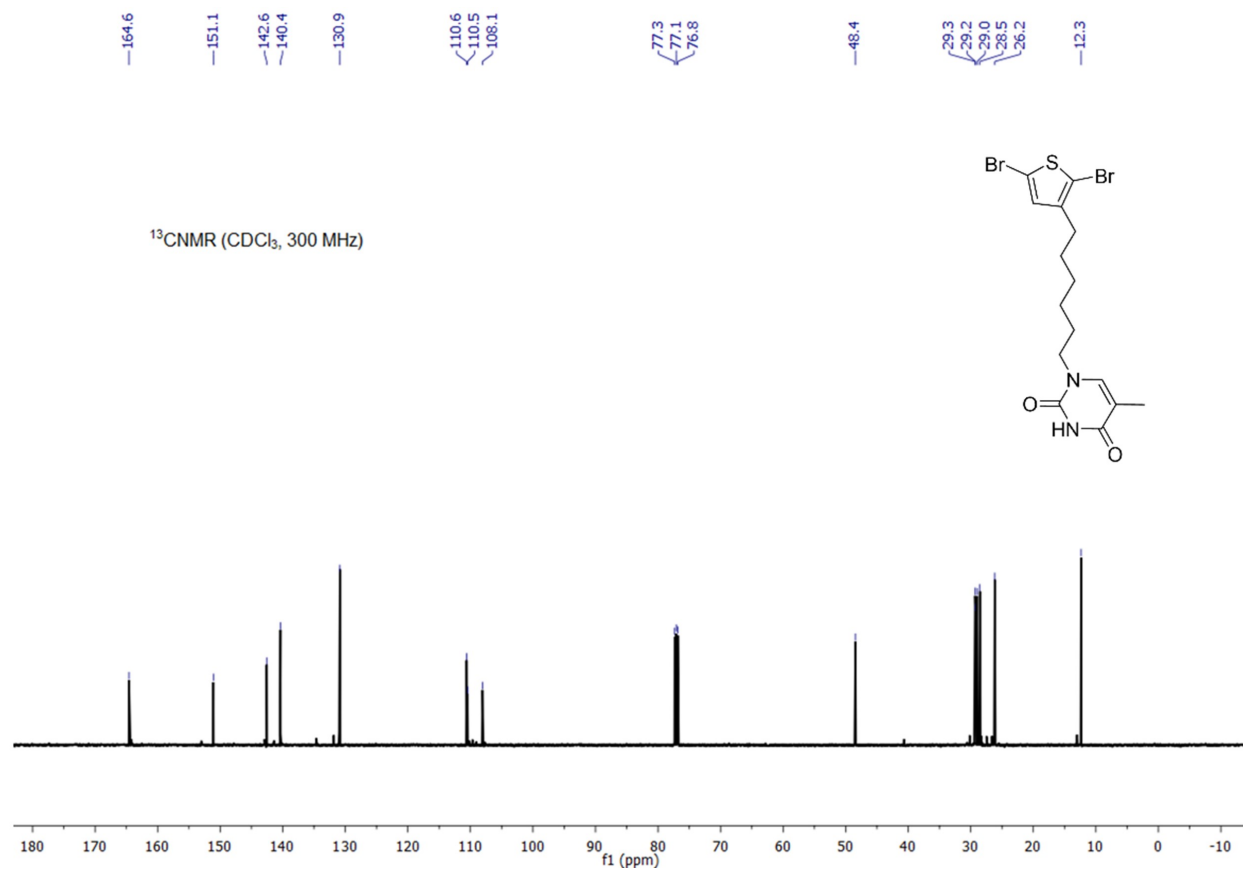
Figure A.15: ^{13}C NMR spectrum of adenine containing dibromo thiophene monomer, $3hT_{Thy}$ (CDCl$_3$, 25 °C).
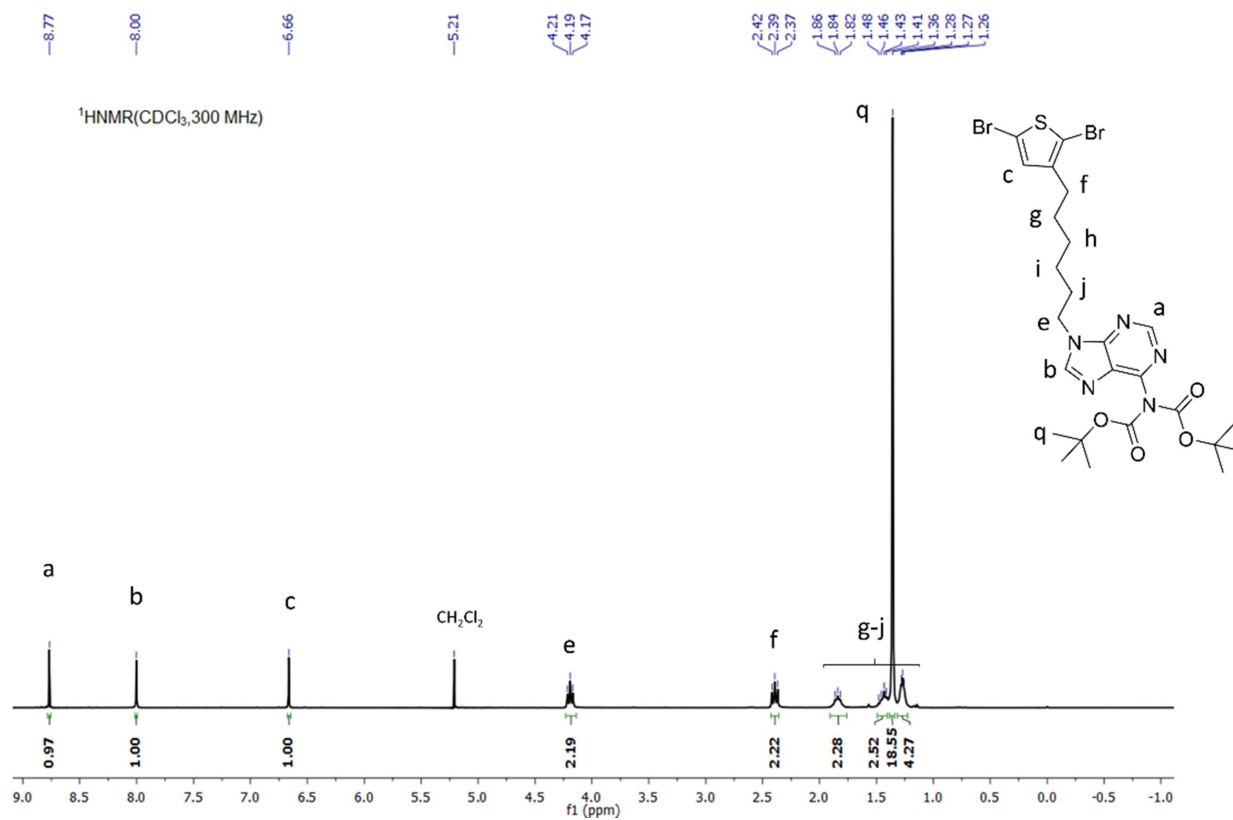
Figure A.16: ^{1}H NMR spectrum of Boc-protected dibromo adenine-containing thiophene monomer, $T_{Ad\text{-}Boc}$ (CDCl$_3$, 25 °C).
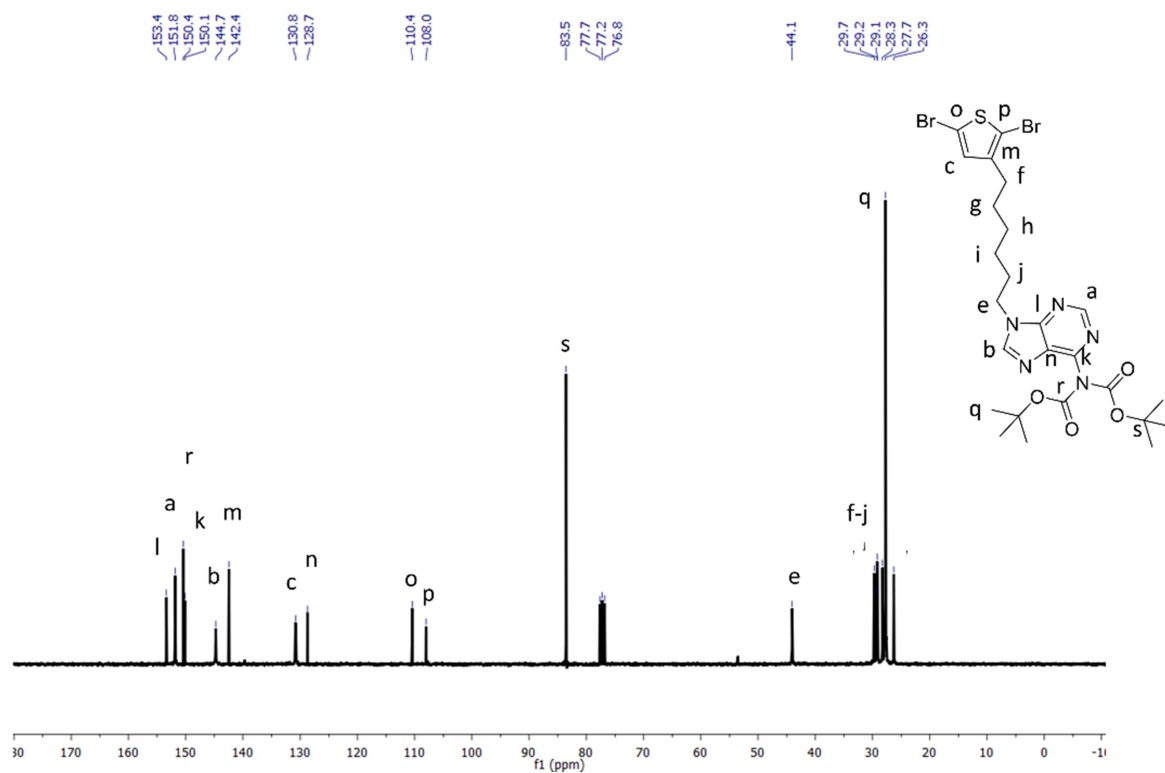
Figure A.17: ^{13}C NMR spectrum of Boc-protected dibromo adenine-containing thiophene monomer, T$_{Ad-Boc}$ (CDCl$_3$, 25 °C).
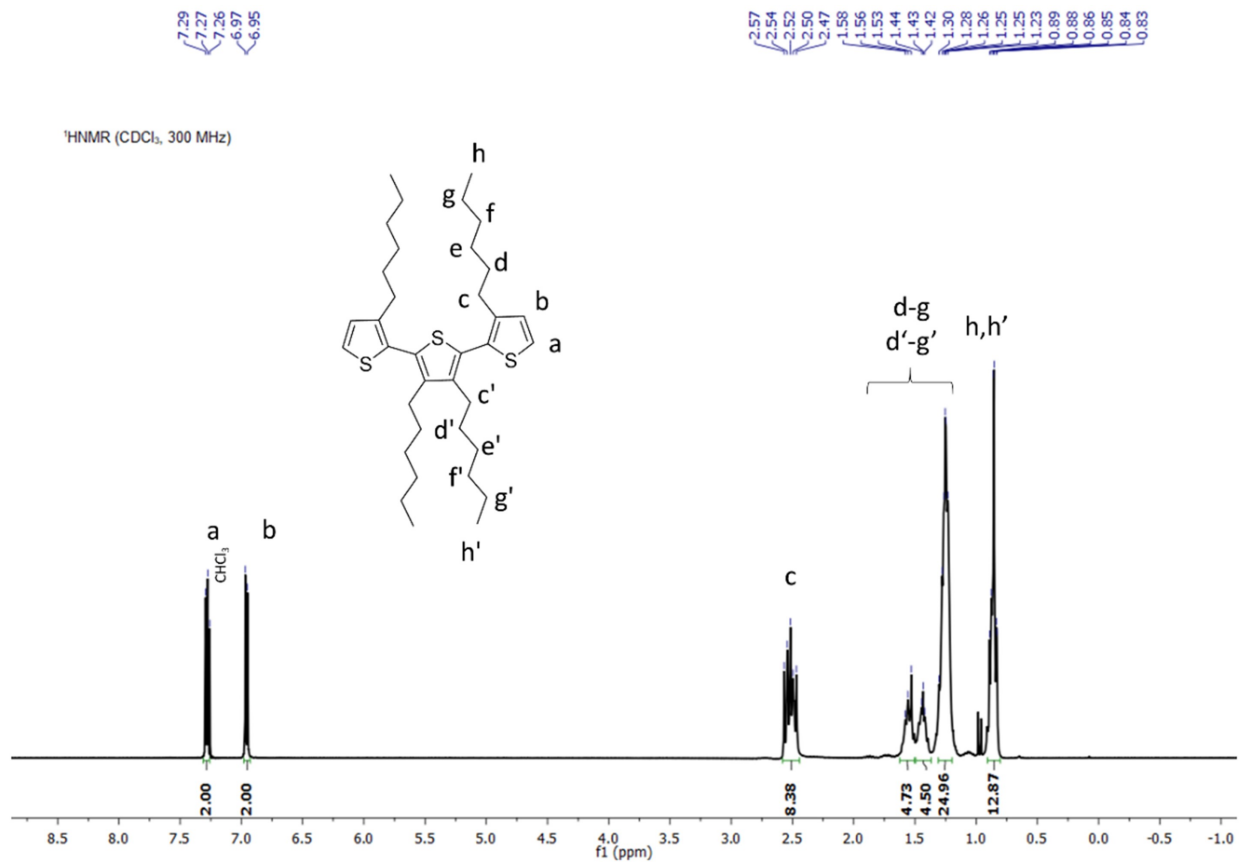
Figure A.18: ^{1}H NMR spectrum of 3,3',3'',4'-tetrahexyl-2,2':5',2''-terthiophene (tT$_{4h}$) (CDCl$_3$, 25 °C).

CNMR (CDCl₃, 300 MHz)
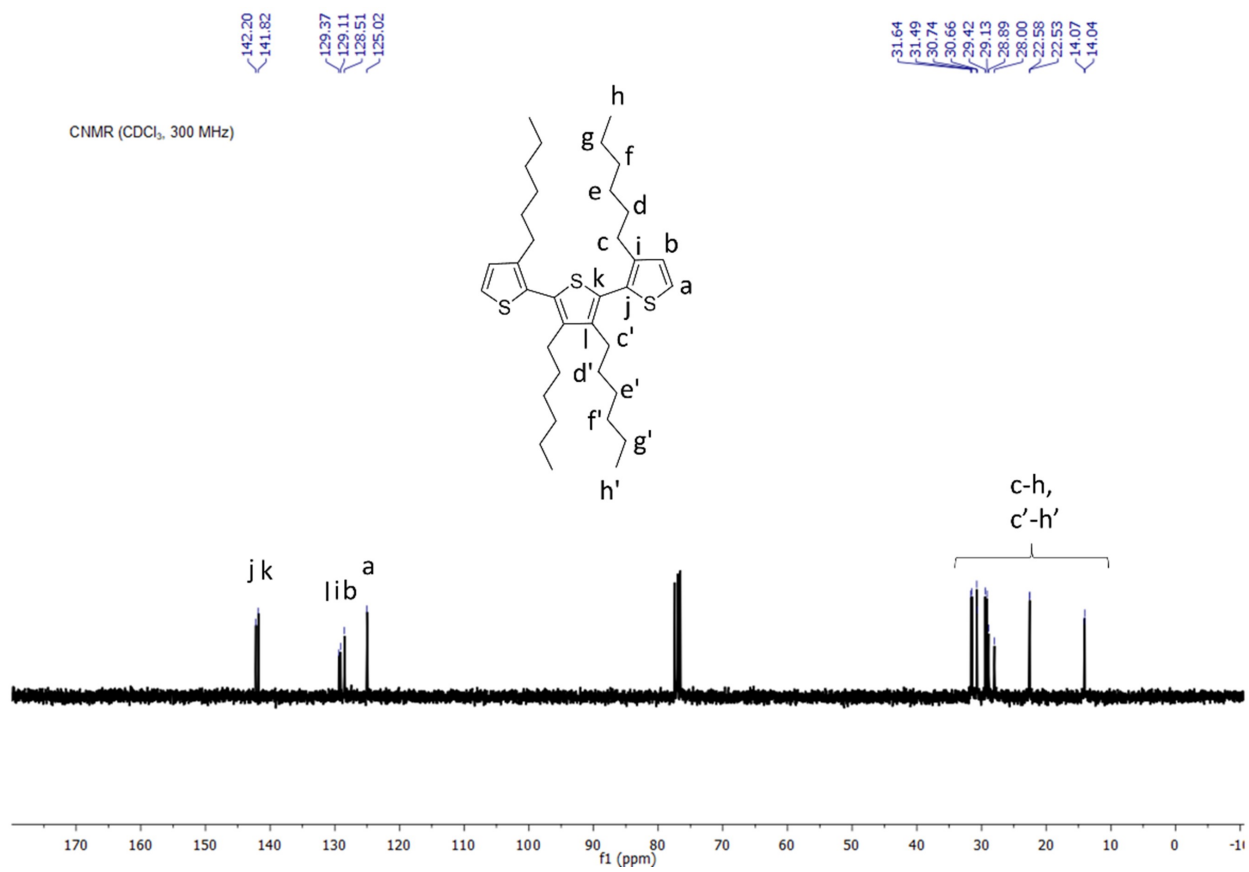
Figure A.19: ^{13}C NMR spectrum of 3,3',3'',4'-tetrahexyl-2,2':5',2''-terthiophene (tT$_{4h}$) (CDCl$_3$, 25 °C).

A.4   Two Dimensional NMR
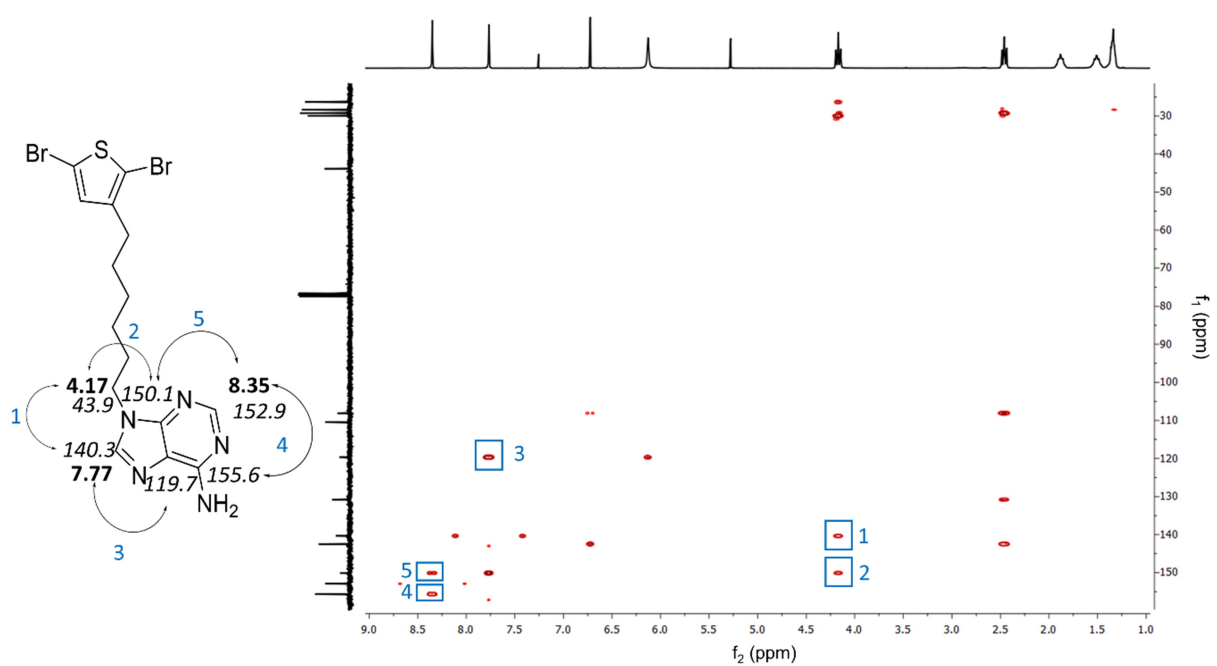
Figure A.20: Important multiple bond correlations from 2D gHMBC NMR spectra of 9-(6-(2,5-dibromothiophen-3-yl)hexyl)-9H-purine-6-amine), which shows corresponding chemical shifts for C-2 and C-8 protons of unprotected adenine and also confirms N-9 attachment (CDCl$_3$, 25 °C).
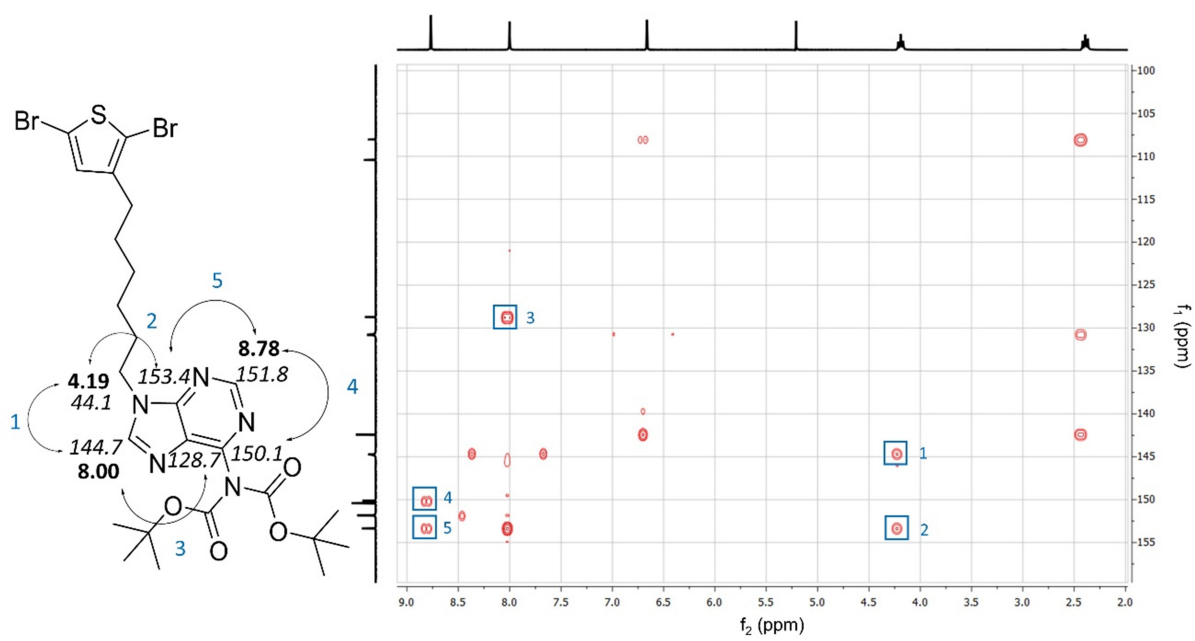
Figure A.21: Important multiple bond correlations from 2D gHMBC NMR spectra of Boc-protected dibromo monomer which shows corresponding chemical shifts for C-2 and C-8 protons of Boc protected adenine (CDCl₃, 25 °C).
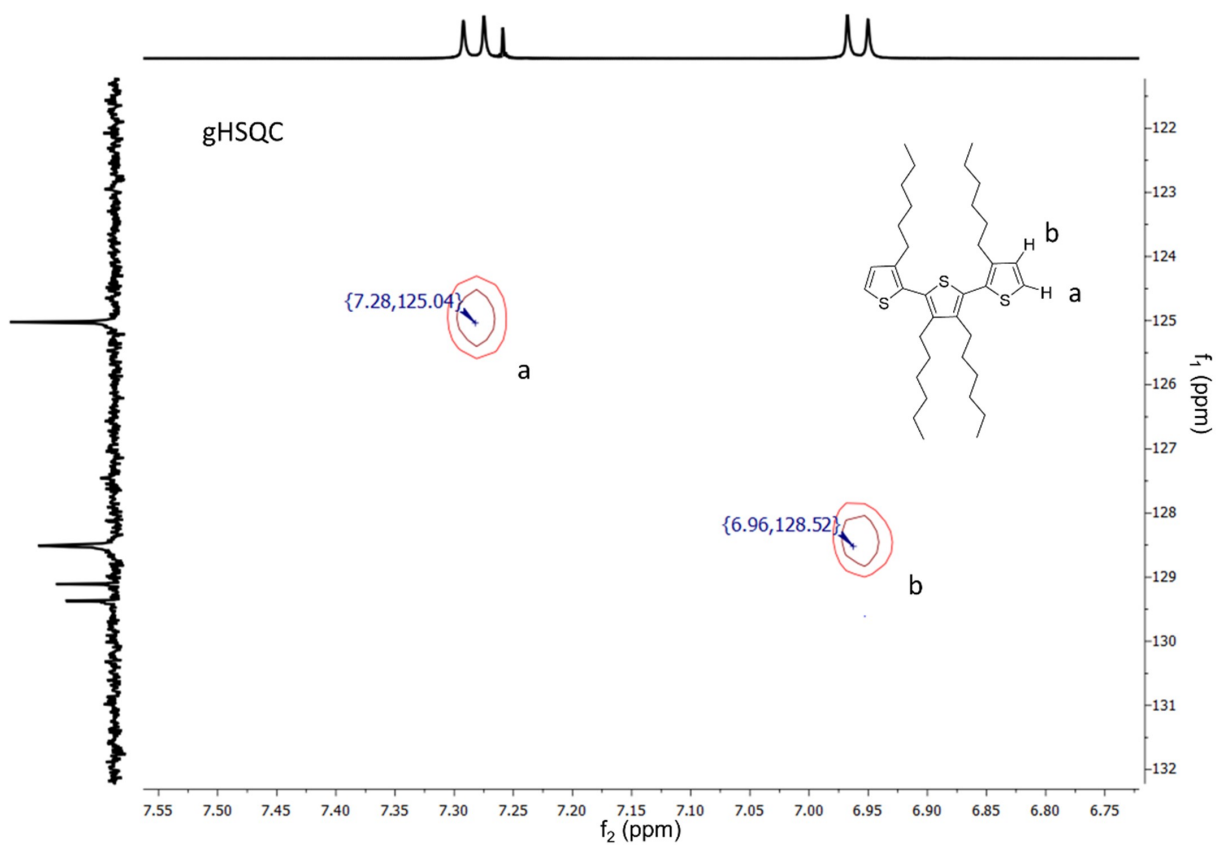
Figure A.22: 2D gHSQC NMR spectra of 3,3',3'',4'-tetrahexyl-2,2':5',2''-terthiophene (tT$_{4h}$) confirms the structure of tT$_{4h}$ monomer (CDCl$_3$, 25 °C).
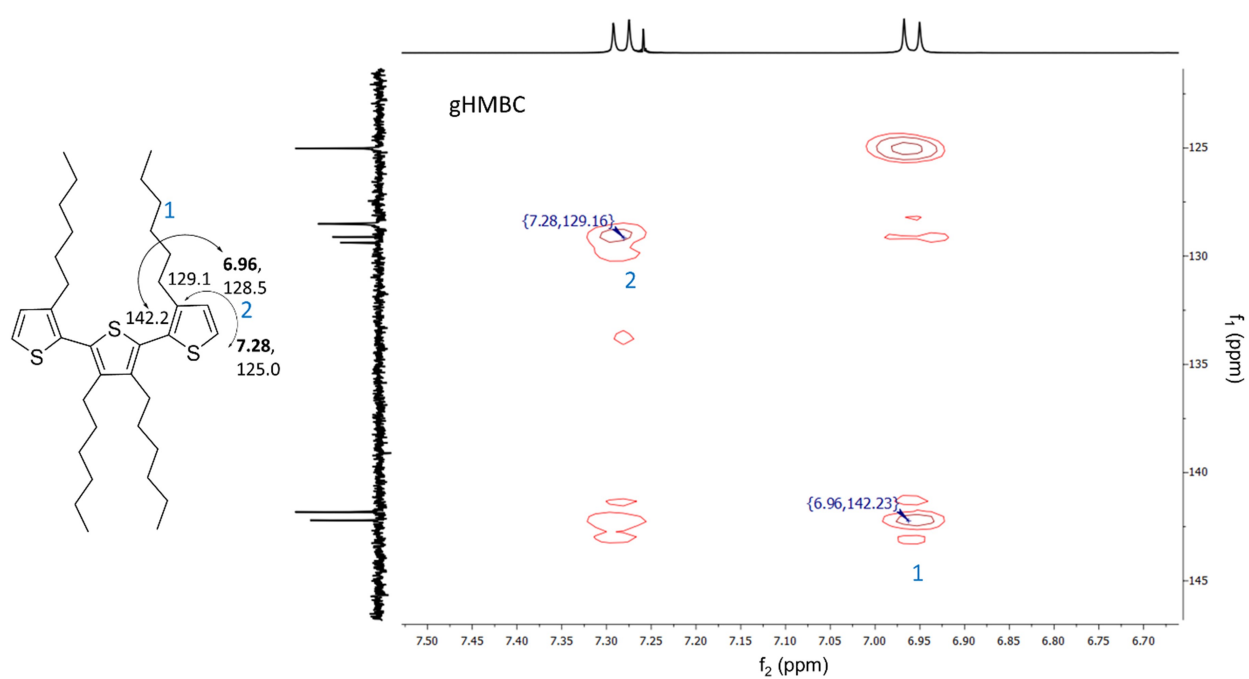
Figure A.23: 2D gHMBC NMR spectra of 3,3',3",4'-tetrahexyl-2,2':5',2"-terthiophene (tT$_{4h}$) confirms the structure of tT$_{4h}$ monomer (CDCl$_3$, 25 °C).

A.5 Polymers
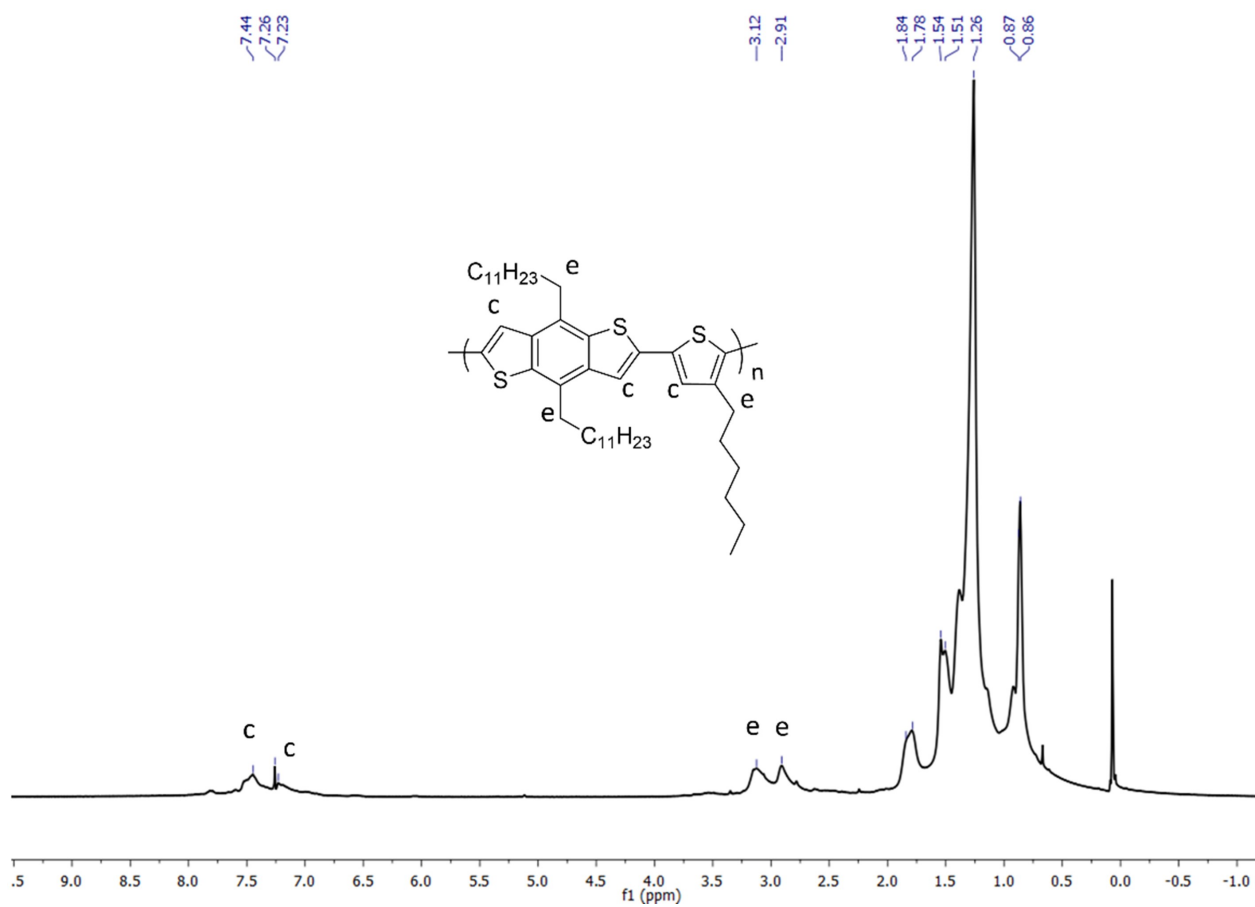
Figure A.24: ^{1}H NMR spectrum of BDT$_d$-3hT (CDCl$_3$, 25 °C).
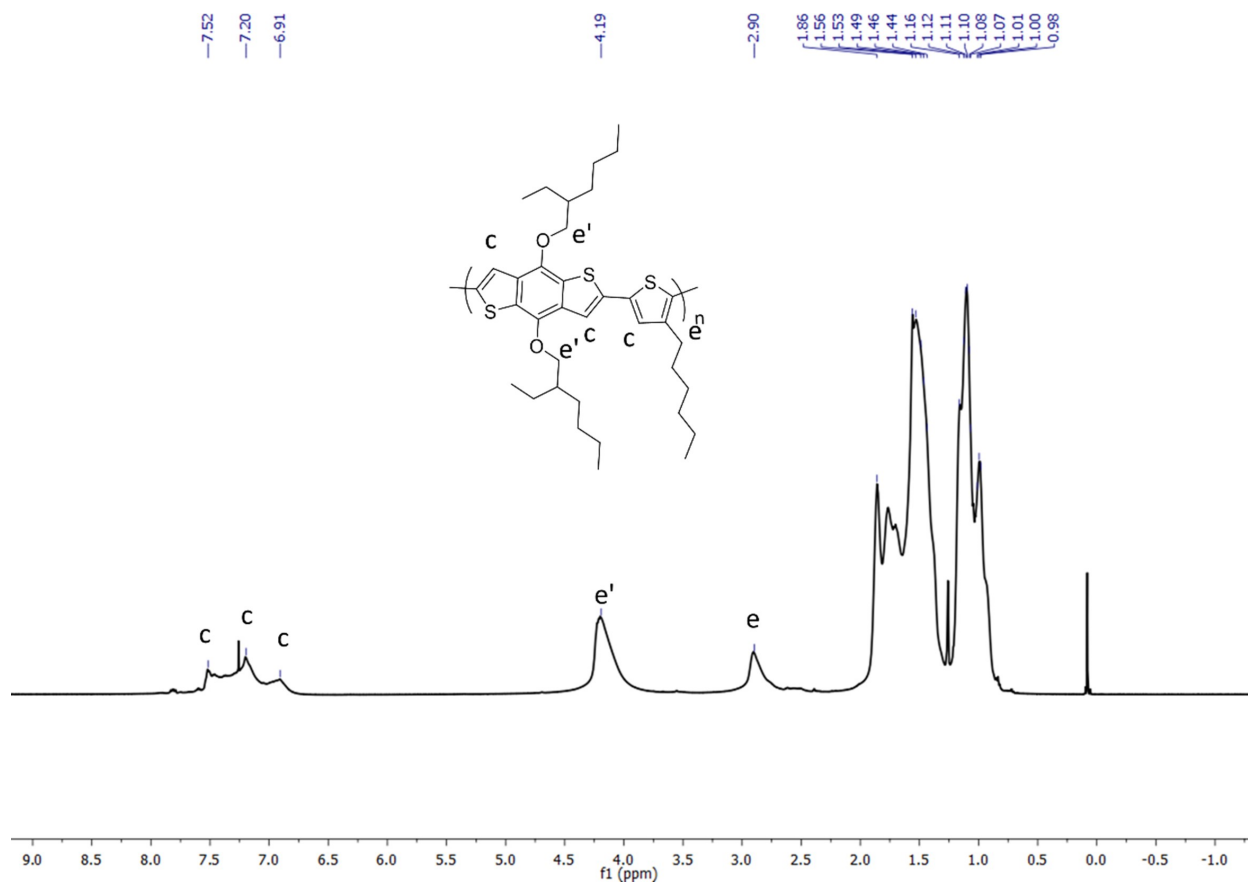
Figure A.25: ^{1}H NMR spectrum of BDT_{eho}-3hT (CDCl$_3$, 25 °C).
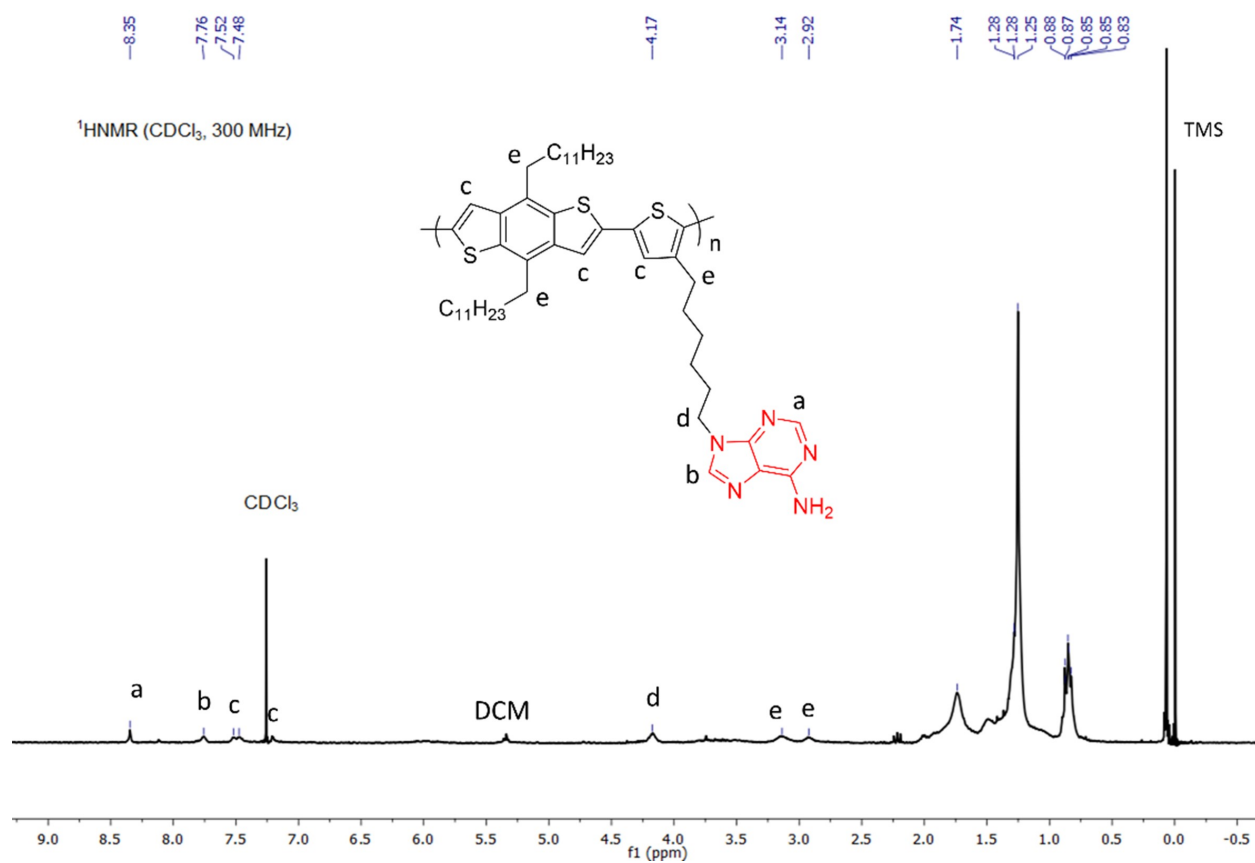
Figure A.26: ^{1}H NMR spectrum of BDT_d-$3hT_{Ad}$ (CDCl$_3$, 25 °C).
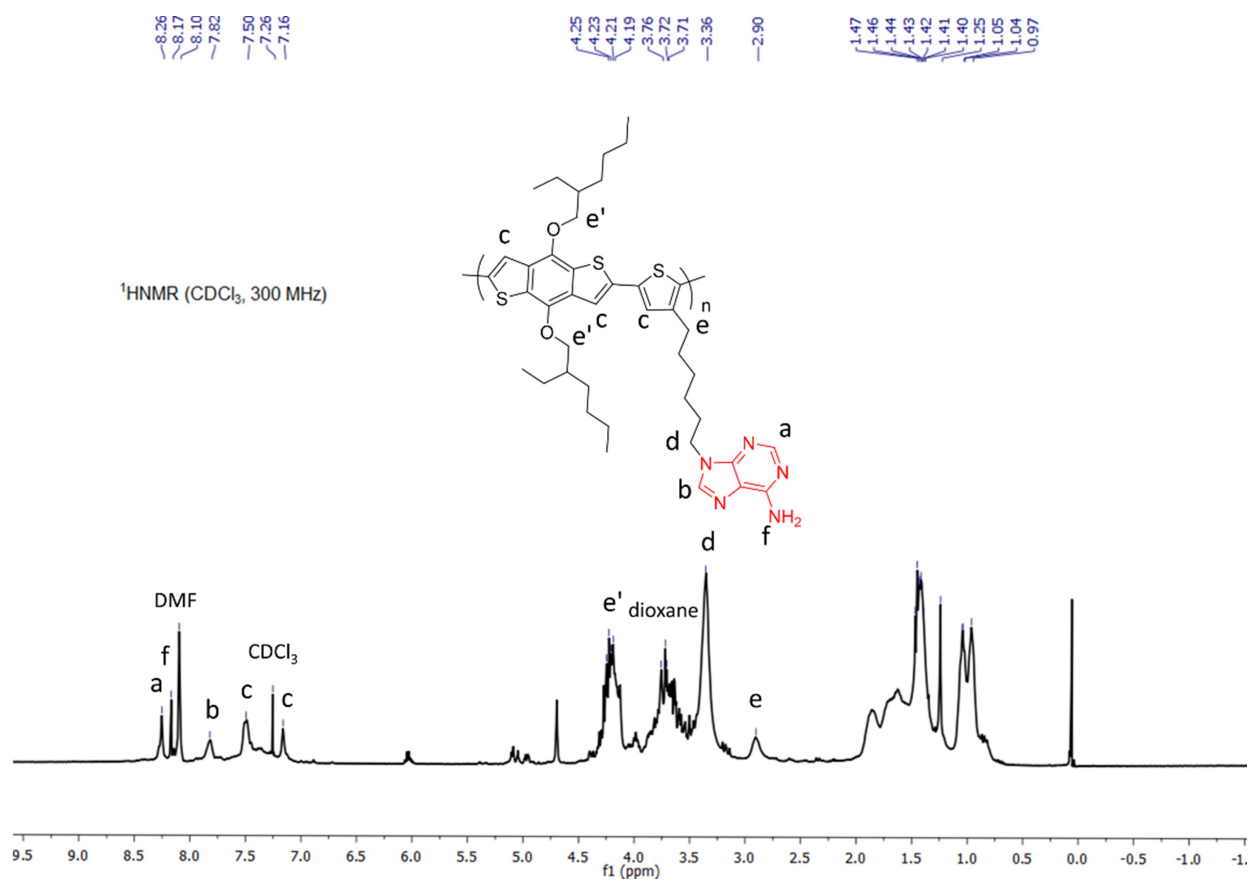
Figure A.27: ^{1}H NMR spectrum of BDT$_{\mathrm{eho}}$-3hT$_{\mathrm{Ad}}$ (CDCl$_3$, 25 °C).

Figure A.28: ^{1}H NMR spectrum of BDT_d-$3hT_{Thy}$ (CDCl$_3$, 25 °C).
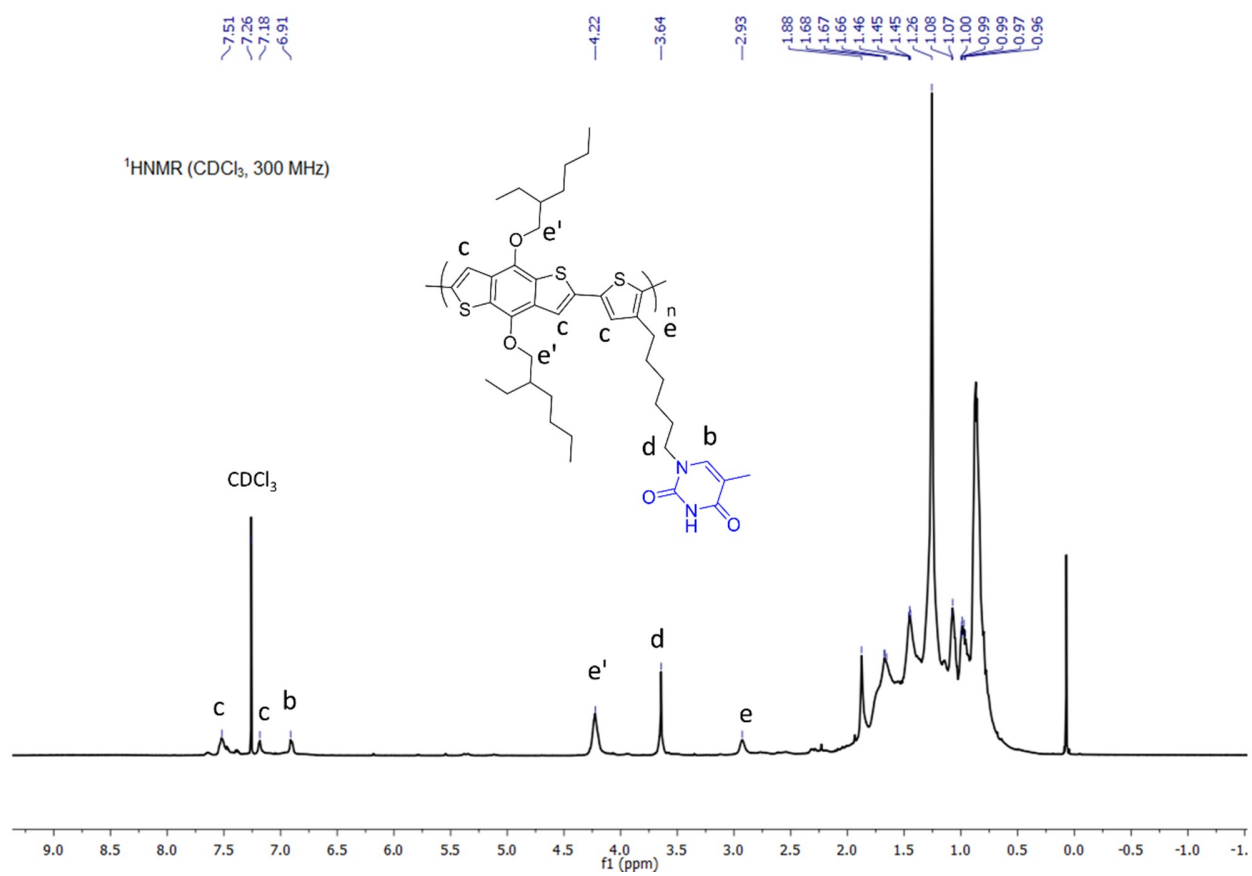
**Figure A.29:** ^{1}H NMR spectrum of BDT_{eho}-$3hT_{Thy}$ (CDCl$_3$, 25 °C).
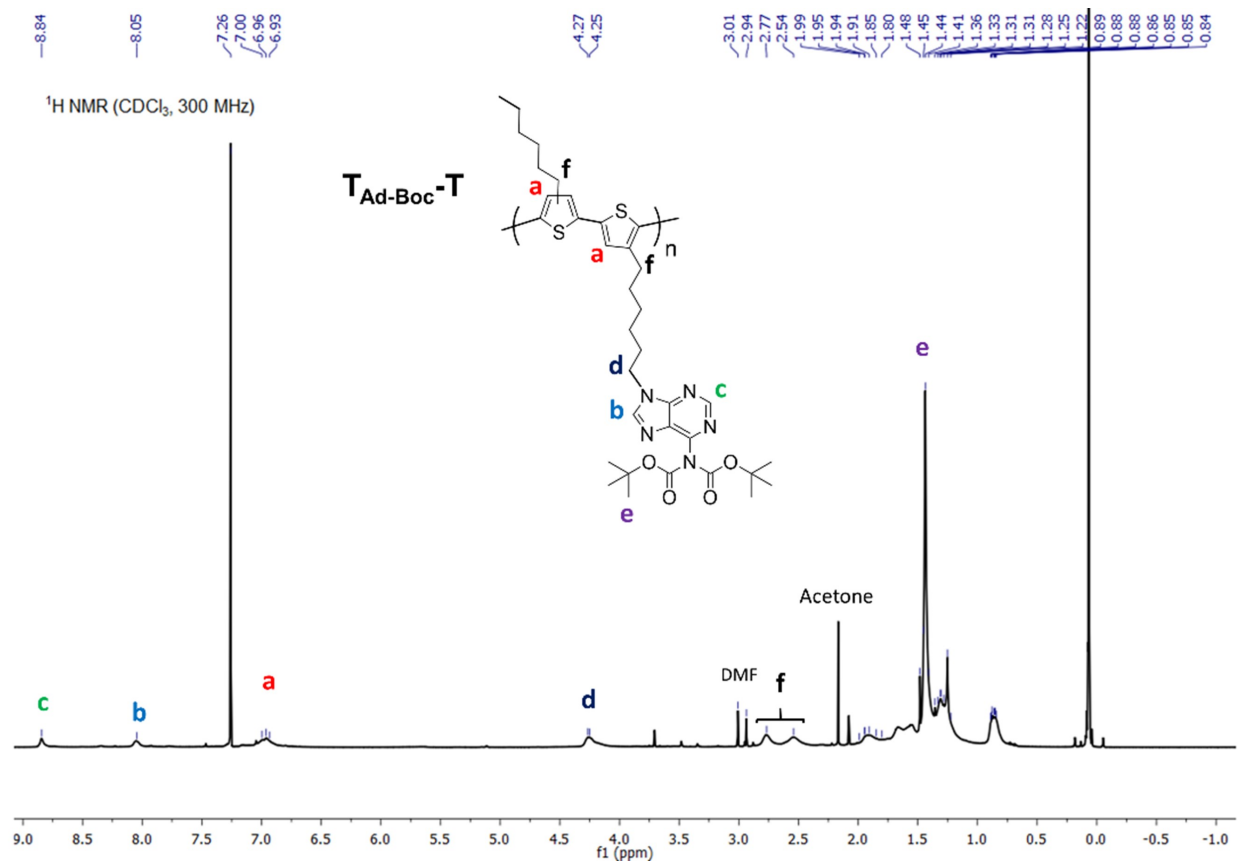
Figure A.30: ^{1}H NMR spectrum of T$_{\text{Ad-Boc}}$-T synthesized via DArP using the amine-protected dibromo monomer (CDCl$_3$, 25 °C).
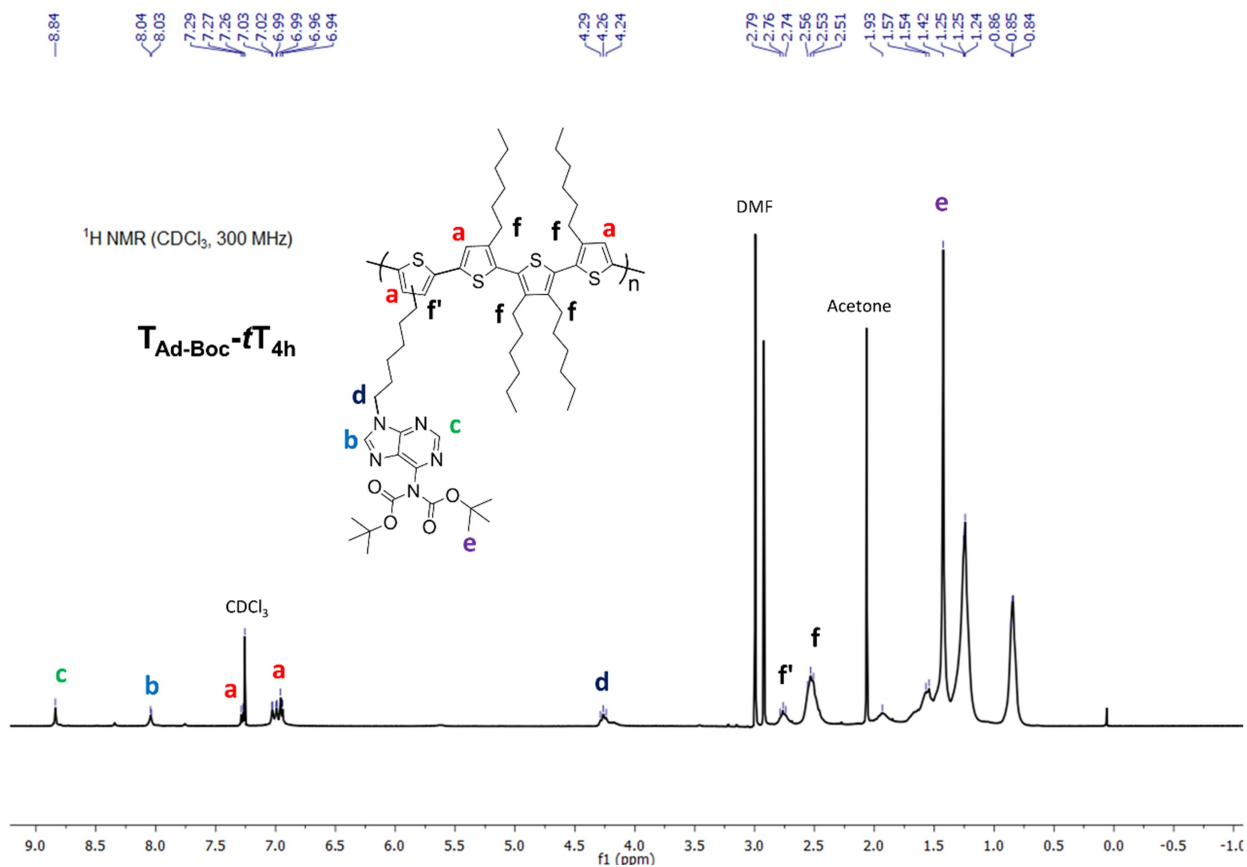
Figure A.31: ^{1}H NMR spectrum of T_{Ad-Boc}-$t$$T_{4h}$ synthesized via DArP using the amine-protected dibromo monomer (CDCl$_3$, 25 °C).
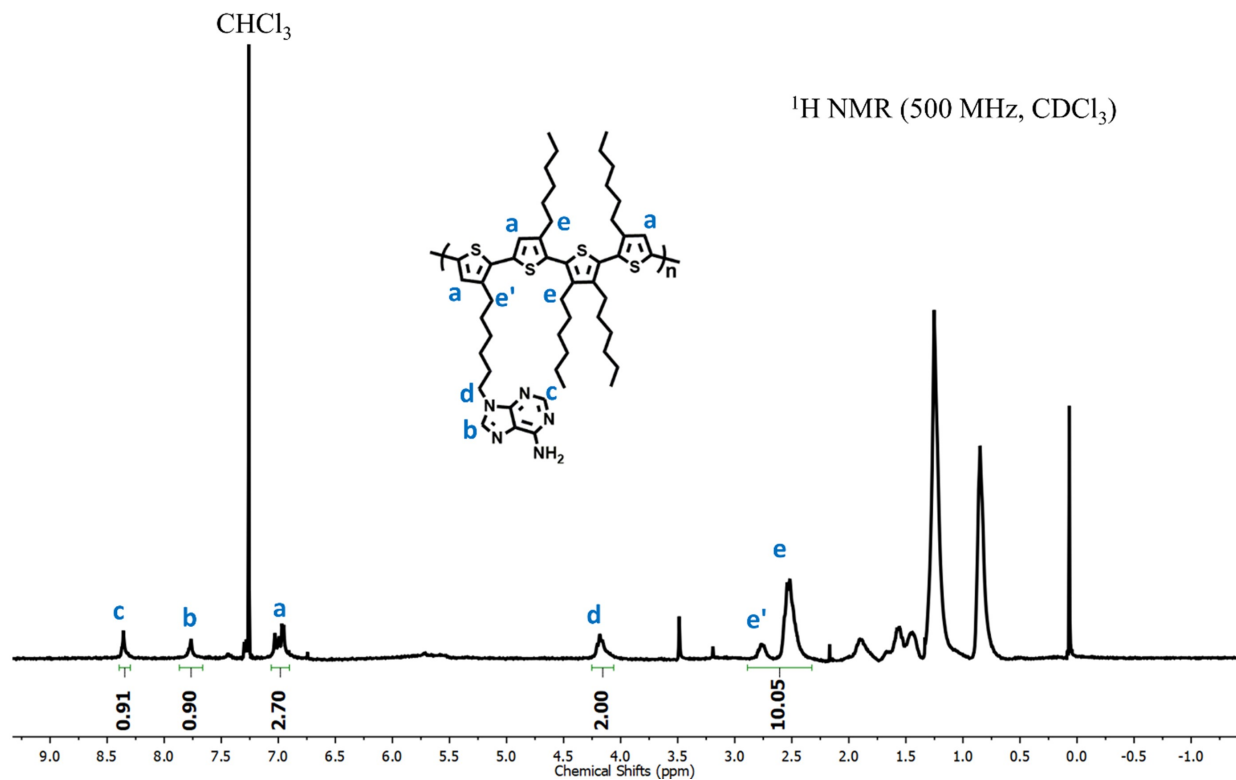
Figure A.32: ¹H NMR spectrum of T_{Ad}-$t$$T_{4h}$ after acid-catalyzed deprotection of the adenine functionality (CDCl$_3$, 25 °C).
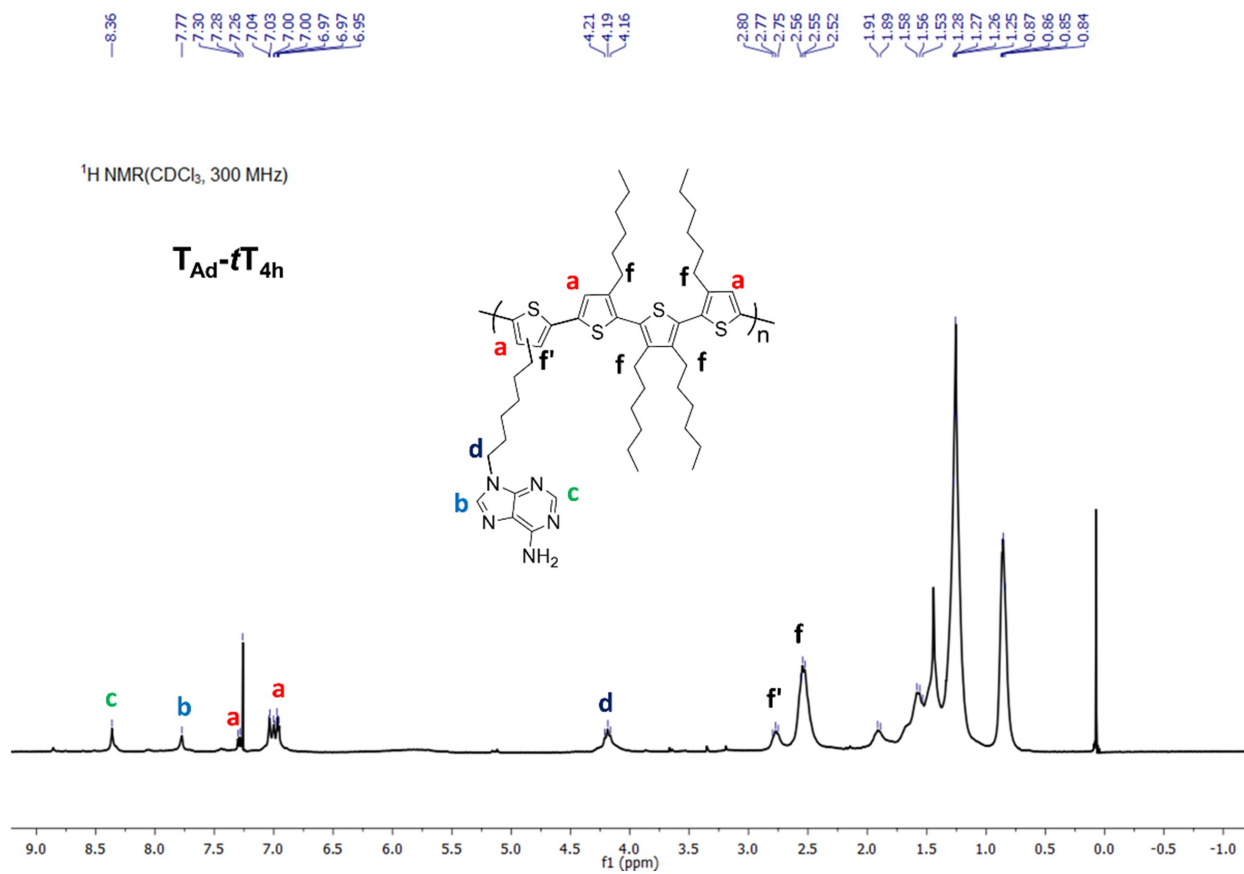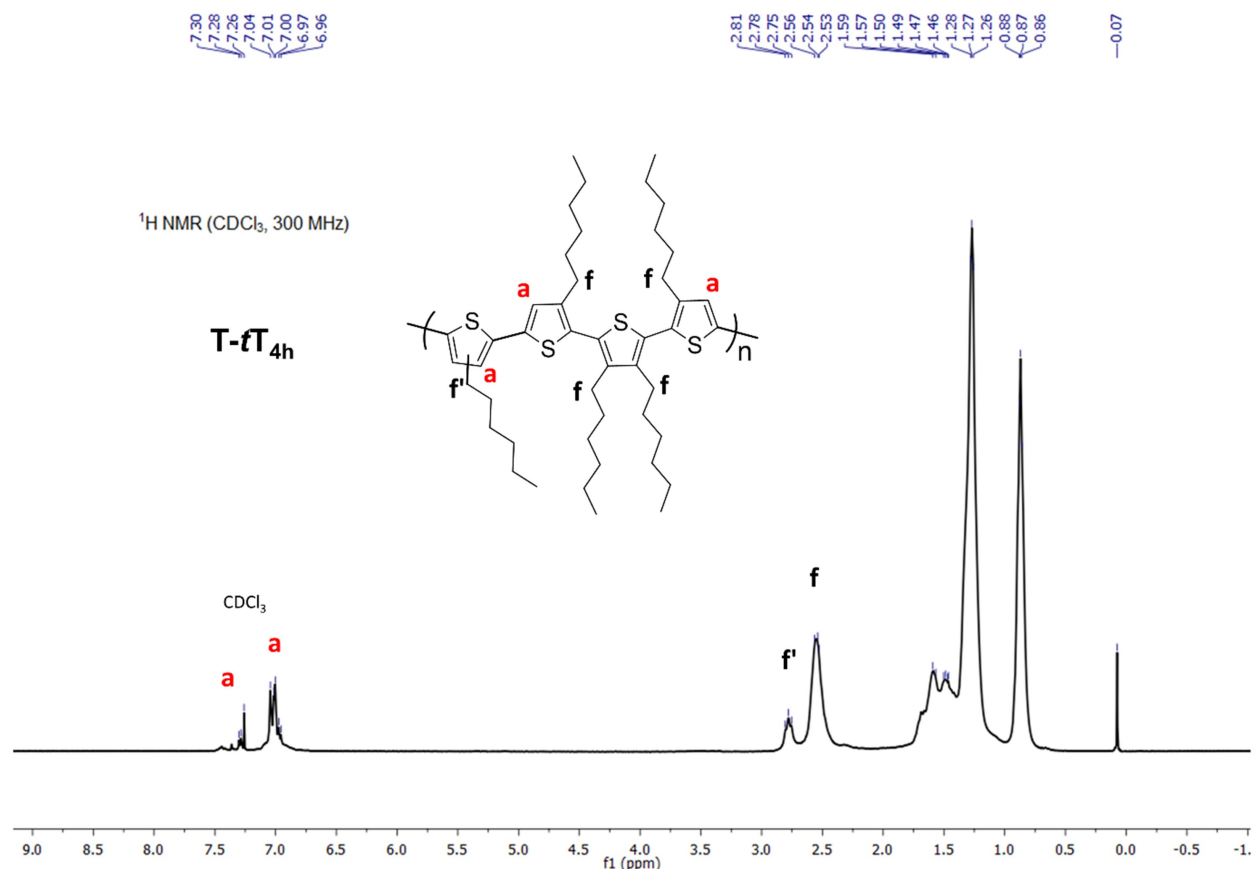
**Figure A.33:** ^{1}H NMR spectrum of T-tT$_{4h}$ synthesized using optimized DArP conditions (CDCl$_3$, 25 °C).

Figure A.34: ^{1}H NMR spectrum of T_{Ad}-$t$$T_{4h}$ synthesized using optimized one-pot approach (CDCl$_3$, 25 °C). The d to (e + e') integral ratio is equal to 2:10 which matches the ideal adenine concentration in the polymer and suggests restricted or untracable amount of homocoupling DArP side reactions. The peak integral ratios in the aromatic region for the c:a or b:a is matching the 1:3 ratio suggesting blocked or minimal beta activation side reactions.

B Monomer Development for Water Solubilization of Conjugated Polymers

B.1 Synthesis Procedure for Thiophene-Based Monomer with Oligo Ether Side Chain Functionality
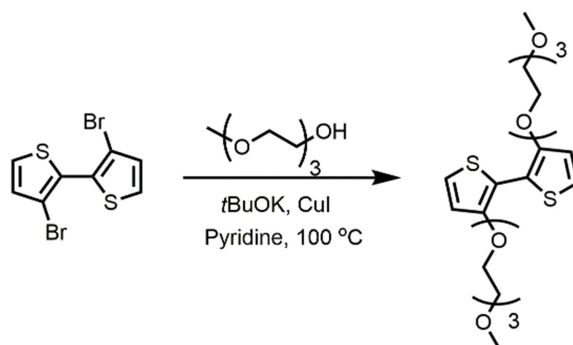

Figure B.1: Reaction conditions for attachment of oligo ether groups to a bithiophene as side chains .

In a dry 150 mL round bottom flask, 3,3'-dibromo-2,2'-bithiophene (648 mg, 2 mmol, 1 equiv.), was added. Copper iodide (38 mg, 0.20 mmol, 0.10 equiv.), potassium tert-butoxide (224 mg, 3 mmol, 1.5 equive.), and triethylene glycol monomethyl ether (639 μL, 656 mg, 4 mmol, 2 equiv.) were also added. Additions were made under positive Argon pressure. 12 mL of pyridine was injected into the round bottom flask, and the reaction mixture was heated to 100 °C and mixed for 24 h. At the end of this time, the mixture was cooled to room temperature and diluted by the addition of 50 mL dichloromethane (DCM). Inorganics were removed by pushing the diluted mixture through silica plug. The crude was concentrated via rotary evaporation and purified via column chromatography, eluting with DCM (with 5 v% MeOH). The desired product was isolated as a pale-yellow oil (64 % yield). ^{1}H NMR (500 MHz, CDCl$_3$), δ (ppm): 7.06 (d, J = 5.6 Hz, 2H), 6.875 (d, J = 5.6 Hz, 2H), 4.24 (t, J = 4.9 Hz, 4H), 3.89 (t, J = 4.9 Hz, 4H), 3.77 – 3.74 (m, 4H), 3.68 – 3.73 (m, 8H), 3.55 – 3.52 (m, 4H), 3.36 (s, 6H). ^{13}C NMR (300 MHz, CDCl$_3$) δ (ppm): 151.7, 121.9, 116.6, 114.7, 71.9, 71.4, 70.9, 70.7, 70.5, 70.0, 59.0.
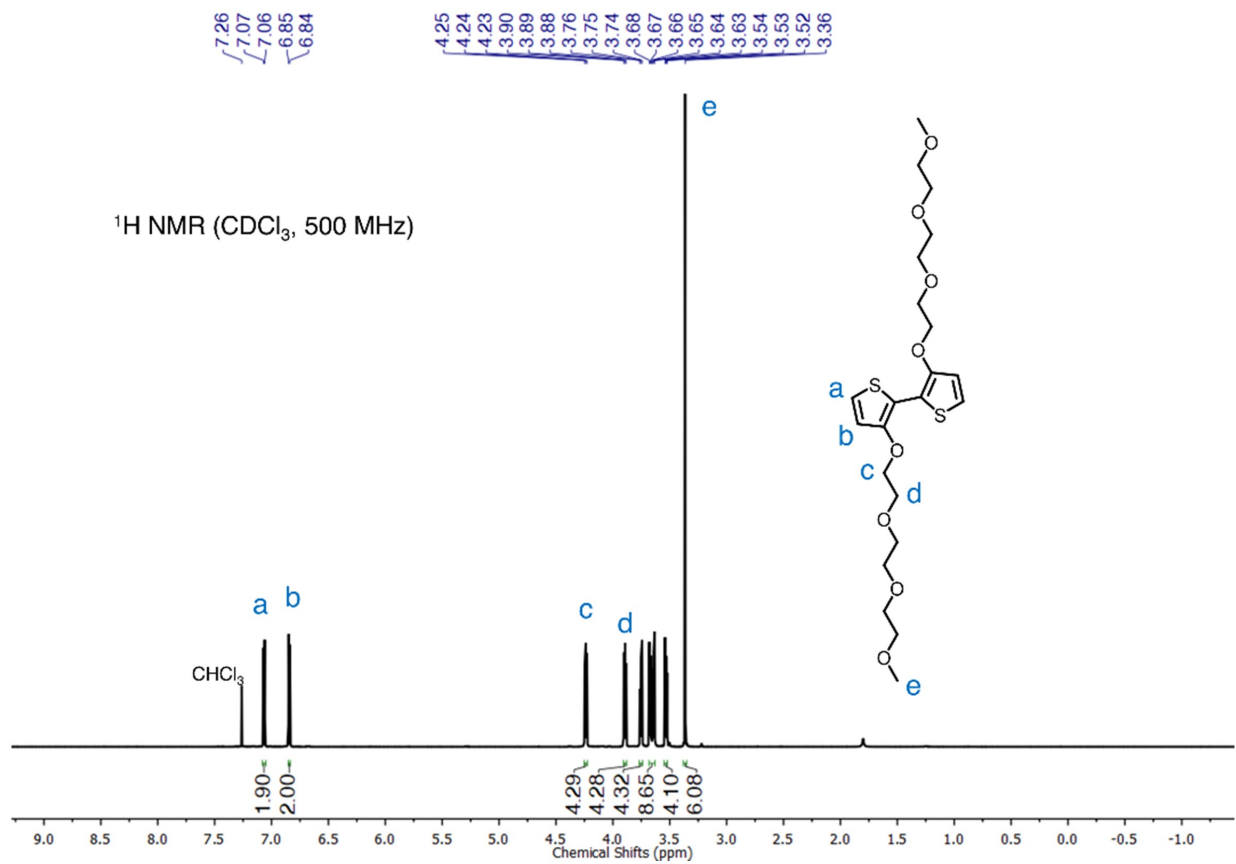
Figure B.2: ^{1}H NMR spectrum of of 3,3'-bis(methyl ether triethylene glycol)-2,2'-bithiophene (CDCl$_3$, 25 °C).
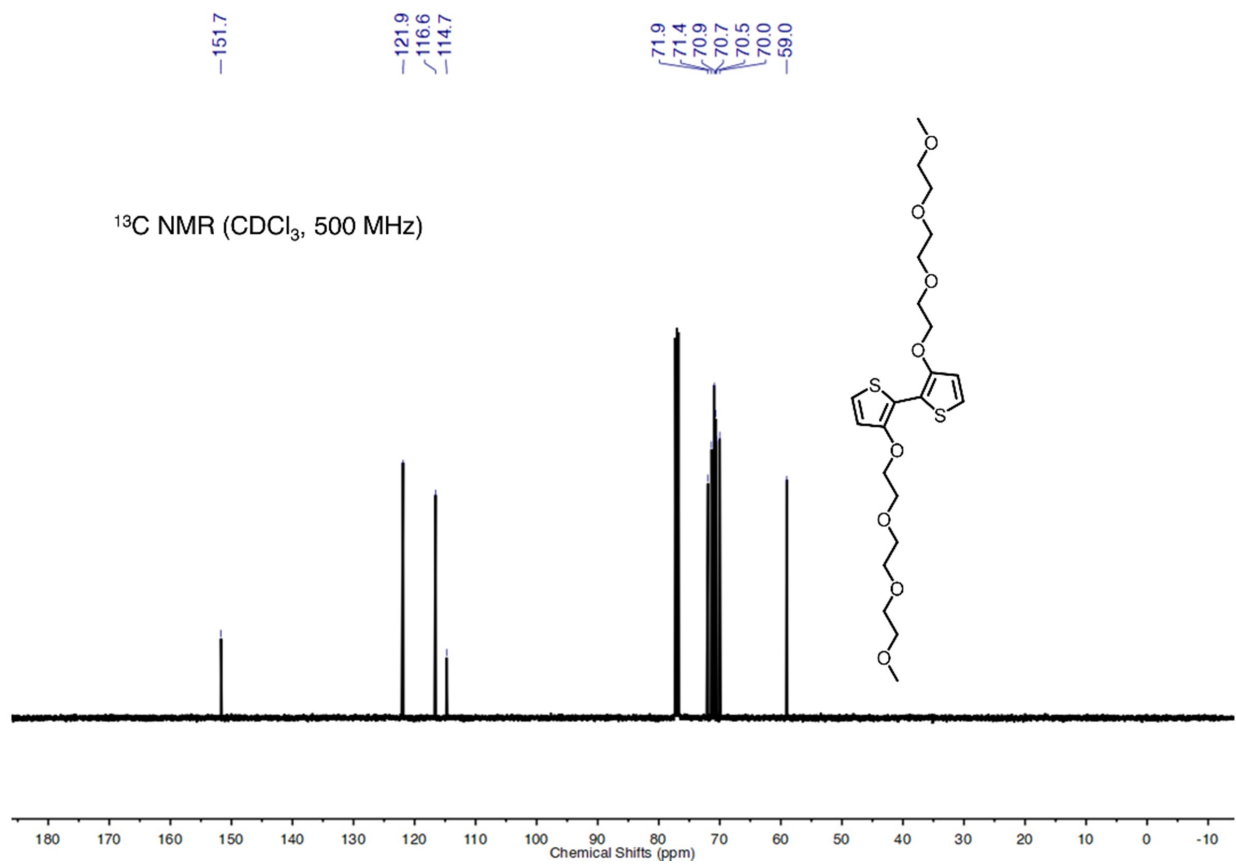
Figure B.3: ^{13}C NMR spectrum of of 3,3'-bis(methyl ether triethylene glycol)-2,2'-bithiophene (CDCl$_3$, 25 °C).

Vita

Sina Sabury was born and raised in Zanjan, Tehran, Iran. Sina won silver medal of national chemistry Olympiad in high school. After graduating in 2008, Sina attended Amirkabir University of Technology in Tehran, Iran studying polymer science and engineering for Bachelor of Science. He continued his academic path and earned Master of Science and Engineering from Amirkabir University of Technology in polymer science and engineering. Sina enrolled at the University of Tennessee-Knoxville to major in polymer chemistry. He joined the research group of Prof. S. Michael Kilbey II, where his research involved the design, synthesis and development of structure-property relationships for side chain functionalized conjugated polymers.